# Mathematical models for perceived roughness of three-dimensional surface textures

Stefano Padilla

Thesis submitted
for the
Degree of Doctor of Philosophy

Heriot-Watt University
School of Mathematical and Computer Sciences
May 2008

# THE ABSTRACT

This thesis reports and discusses results from a new methodology for investigating the visually perceived properties of surfaces; by doing so, it also discovers a measurement or estimator for perceived roughness of *$1/F^{\beta}$ noise surfaces*.

Advanced computer graphics were used to model natural looking surfaces (*$1/F^{\beta}$ noise surfaces*). These were generated and animated in real-time to enable observers to manipulate dynamically the parameters of the rendered surfaces. A method of adjustment was then employed to investigate the effects of changing the parameters on perceived roughness. From psychophysical experiments, it was found that the two most important parameters related to perceived roughness were the magnitude roll-off factor ($\beta$) and RMS height ($\sigma$) for this kind of surfaces.

From the results of various extra experiments, an estimation method for perceived roughness was developed; this was inspired by common frequency-channel models. The final optimized model or estimator for perceived roughness in *$1/F^{\beta}$ noise surfaces* found was based on a *FRF* model. In this estimator, the first filter has a shape similar to a gaussian function and the *RF* part is a simple variance estimator. By comparing the results of the estimator with the observed data, it is possible to conclude that the estimator accurately represents perceived roughness for *$1/F^{\beta}$ noise surfaces.*

**DEDICATED TO**

**MOM AND DAD**

# ACKNOWLEDGEMENTS

I would especially like to thank both of my supervisor, Professor Mike Chantler and Dr. Patrick Green. Thanks Mike for all your support, ideas, discussions, time and for explaining me so patiently the hard topics. Thanks Patrick for all your ideas about experiments, checking this thesis and papers, support and for explaining me the world of psychophysics.

Special thanks to Dr. Ondřej Drbohlav for double-checking my experimental data and explaining me some statistics and model fitting methods.

I will also like to thank Andy Spence, Khemraj Emrith, Kevin McMahon and Jiři Filip for their help and lunchtime discussions. Also thanks to the members of the department for their help in small but essential problems and tasks.

Finally, I will like to express my lasting gratitude to my mom, dad and my brother Martin for their everyday support and enthusiasm.

ACADEMIC REGISTRY
**Research Thesis Submission**

| | | | |
|---|---|---|---|
| Name: | | | |
| School/PGI: | | | |
| Version: *(i.e. First, Resubmission, Final)* | | Degree Sought: | |

## Declaration

In accordance with the appropriate regulations I hereby submit my thesis and I declare that:

1) the thesis embodies the results of my own work and has been composed by myself
2) where appropriate, I have made acknowledgement of the work of others and have made reference to work carried out in collaboration with other persons
3) the thesis is the correct version of the thesis for submission*.
4) my thesis for the award referred to, deposited in the Heriot-Watt University Library, should be made available for loan or photocopying, subject to such conditions as the Librarian may require
5) I understand that as a student of the University I am required to abide by the Regulations of the University and to conform to its discipline.

* *Please note that it is the responsibility of the candidate to ensure that the correct version of the thesis is submitted.*

| | | | |
|---|---|---|---|
| Signature of Candidate: | | Date: | |

## Submission

| | |
|---|---|
| Submitted By *(name in capitals)*: | |
| Signature of Individual Submitting: | |
| Date Submitted: | |

## For Completion in Academic Registry

| | | | |
|---|---|---|---|
| Received in the Academic Registry by *(name in capitals)*: | | | |
| *Method of Submission*<br>*(Handed in to Academic Registry; posted through internal/external mail)*: | | | |
| Signature: | | Date: | |

# TABLE OF CONTENTS

**THE ABSTRACT** ..... **II**

**DEDICATED TO** ..... **III**

**ACKNOWLEDGEMENTS** ..... **IV**

**TABLE OF CONTENTS** ..... **VI**

**LIST OF FIGURES** ..... **IX**

**LIST OF TABLES** ..... **XIII**

**LIST OF SYMBOLS, TERMS AND ABBREVIATIONS** ..... **XIV**

**CHAPTER 1 INTRODUCTION** ..... **1**

1.1 Motivation and goals ..... 1

1.2 Scope of the work ..... 2

1.3 Original contributions ..... 3

1.4 Organization of this thesis ..... 3

**CHAPTER 2 ROUGHNESS AND SURFACES** ..... **5**

2.1 The dimensions of natural textured surfaces ..... 5

2.2 Physical measurements of roughness ..... 8

2.3 Related studies in the perception of roughness ..... 12

2.4 Summary and Discussion ..... 15

**CHAPTER 3 A GENERAL METHODOLOGY** ..... **17**

3.1 Illuminant and viewpoint position ..... 17

3.2 Natural synthetic stimuli ..... 20

3.3 Comparing psychophysical methods ..... 23

3.4 Summary and Discussion ..... 25

**CHAPTER 4 MODELLING THE STIMULI** ..... **26**

4.1 $1/F^{\beta}$ noise surfaces ..... 26

4.2 Construction of the stimuli ..... 29

4.2.1 Light and reflectance ..... 30

4.2.2 Geometry, occlusions, silhouette and edges ..... 32

4.2.3 Cast shadows ..... 36
4.2.4 Stimuli stand ..... 39
4.3 Animating the stimuli ..... 40
4.4 Summary and Discussion ..... 43

**CHAPTER 5 EXPERIMENTAL SETUP ..... 45**
5.1 Constrain environment ..... 45
5.2 Tools ..... 47
5.2.1 Displays ..... 47
5.2.2 Software ..... 49
5.2.3 Hardware ..... 50
5.3 LCD Monitor calibration ..... 50
5.4 Summary and Discussion ..... 53

**CHAPTER 6 ROUGHNESS IN 1/F$^B$ SURFACES ..... 54**
6.1 The effect of varying RMS roughness ($\sigma$) on perceived roughness ..... 54
6.2 The effect of varying magnitude roll-off factor ($\beta$) on perceived roughness ..... 57
6.3 The effect of random phase on perceived roughness ..... 58
6.4 Contours of constant perceived roughness in ($\beta$, $\sigma$) space ..... 61
6.5 Summary and Discussion ..... 66

**CHAPTER 7 A MODEL BASED ON THE HUMAN VISION ..... 67**
7.1 A plausible measurement model ..... 67
7.2 Optimization of $F_1$ ..... 70
7.3 Fitting the models to the data ..... 71
7.3.1 The box filter ..... 71
7.3.2 The power function filter ..... 73
7.4 A filter based on the human vision system ..... 76
7.5 Summary and Discussion ..... 80

**CHAPTER 8 TESTING THE MODELS USING NARROW-BAND SPECTRA SURFACES ..... 83**
8.1 New stimuli based on spatial frequency channels ..... 83
8.2 Relationship between frequencies and perceived roughness ..... 87
8.2.1 Exploring mid-range frequencies ..... 87
8.2.2 Exploring high-range frequencies ..... 90
8.3 Modelling perceived roughness including the frequency bands experiments. ..... 93
8.3.1 Roughness estimator using a gaussian function for $F_1$ ..... 93
8.3.2 Roughness estimator using a power function for $F_1$ ..... 100
8.4 Improving further the model ..... 106
8.5 Summary and Discussion ..... 111

**CHAPTER 9 SCALING THE PROPOSED MODEL ..... 113**

9.1 Perceptual scaling in between iso-roughness lines ..... 113
9.2 The mid-point experiment ..... 115
9.3 Adding units to the model ..... 118
9.4 The optimal model for perceived roughness of $1/F^{\beta}$ surfaces ..... 121
9.5 Summary and Discussion ..... 122

**CHAPTER 10 SUMMARY AND CONCLUSIONS ..... 124**
10.1 Summary ..... 124
10.2 Discussion and future work ..... 127
10.3 Final conclusions ..... 128

**THE APPENDICES ..... 129**

**THE BIBLIOGRAPHY ..... 167**

# LIST OF FIGURES

*Figure 1-1: Photograph of a real texture on the left and on the right its shape. Please notice that one can perceive various characteristics from these samples.* ..... 2
*Figure 2-1: Three different surface profiles with the same $R_a$ value.* ..... 10
*Figure 3-1: The effect of varying illumination conditions on the same surface is shown above. The light is position on top in the first surface, in the middle for the second surface and on the right for the last surface.* ..... 18
*Figure 3-2: Illustration of the bas-relief ambiguity with two cylinders of equal height viewed from above. Because the elevation of the light source is lower for the cylinder on the left, it appears to be taller than the cylinder on the right.* ..... 19
*Figure 3-3: illustration of three textures using dots, lines and Ls, Ts and Xs.* ..... 21
*Figure 3-4: Example of two simple synthetic images constructed with gaussians.* ..... 22
*Figure 3-5: On the left a wireframe illustration of a $1/F^{\beta}$ noise surface whilst on the right a different surface fully rendered.* ..... 23
*Figure 4-1: Graphical demonstration of H(f) in the frequency domain, left for 1D whilst right for 2D ($\beta$ = 2.0).* ..... 27
*Figure 4-2: two surfaces with different random phase values $\theta$.* ..... 27
*Figure 4-3: The top row represents the effects of varying $\sigma$, whilst the bottom row illustrates the effect of changing $\beta$.* ..... 28
*Figure 4-4: On the left a simple height map whilst on the right the three-dimensional surface.* ..... 29
*Figure 4-5: A sample surfaces in fronto-planar view using per-pixel illumination illustrated with three different illuminant positions.* ..... 31
*Figure 4-6: Example of a surface rendered in three different viewpoints with reflectance only. This surface lack silhouettes and occlusions when not taking into account structure or geometry.* ..... 32
*Figure 4-7: Parallax mapping example. Note the lack of edges, artefacts at the bottom and lack of cast shadows.* ..... 33
*Figure 4-8: Relief mapping example, note the cast shadows and improvement in artefacts but lack of edge or silhouettes.* ..... 34
*Figure 4-9: Mesh on the left is loaded into video memory then is per-vertex displaced by a height map in real-time.* ..... 36
*Figure 4-10: Example of a simple polygon displacement, on the left a normally displaced polygon. Note how these appear very smooth. On the right, the correct shape of the sample.* ..... 36
*Figure 4-11: illustration of the shadow mapping method.* ..... 38
*Figure 4-12: On the left the stand shape as a height map and on the right the final rendering of the stimuli.* ..... 39
*Figure 4-13: Illustration of an arcball interface.* ..... 40

*Figure 4-14: The angle between the surface normal and the light position and the percentage of time each observer spent comparing the two surfaces.* ..... 41
*Figure 4-15: The average of the preferred view for all the seven observers and a fitting gaussian function to the average of these results.* ..... 42
*Figure 4-16: Movement path of the animation for later experiments.* ..... 43
*Figure 4-17: Rotation of the surface normal as seen from the light position.* ..... 43
*Figure 5-1: Illustration of the experimental setup.* ..... 46
*Figure 5-2: On the left, an un-calibrated linear gamma and on the right a calibrated one.* ..... 51
*Figure 5-3: Luminance across the screen from an un-calibrated display.* ..... 52
*Figure 6-1: Demonstrates three surfaces with similar β {1.8} and θ {23} but different σ {0.6, 1.0 and 1.2}.* ..... 55
*Figure 6-2: Perceived roughness increases with σ.* ..... 56
*Figure 6-3: Demonstrates three surfaces with similar σ {1.2} and θ {23} but different β {1.8, 2.0 and 2.2}.* ..... 57
*Figure 6-4: Perceived roughness decreases with magnitude roll-off factor (β).* ..... 58
*Figure 6-5: Demonstrating four surface the same σ {1.0 cm} and β {2.0} values but different random phase seed {5, 25, 42 and 62}.* ..... 58
*Figure 6-6: Demonstration of the pair sets for the phase relationship experiment.* ..... 59
*Figure 6-7: Values of RMS roughness of adjustable surfaces set by individual observers when matching five different fixed surface RMS roughnesses (horizontal axis) and with five different combinations of random phase (symbols shown in key).* ..... 60
*Figure 6-8: Demonstration of the method used to obtain the contour lines.* ..... 62
*Figure 6-9: Errors from the pilot experiment to test the limits of the actual experiment.* ..... 63
*Figure 6-10: Individual results for surface matches in (β-σ) space.* ..... 63
*Figure 6-11: Roughness contour lines for the (β, σ) space. Error bars are standard errors of the mean RMS roughness values set over all trials at each combination of values.* ..... 64
*Figure 6-12: Roughness contour lines in (β, log σ) space.* ..... 65
*Figure 6-13: Slopes of the iso-roughness lines obtained from individual observers.* ..... 65
*Figure 7-1: The FRF (filter-rectify-filter) framework.* ..... 68
*Figure 7-2: Effects of varying the parameters $F_p$ and $F_c$ of the box filter* ..... 72
*Figure 7-3: Objective function $\varepsilon_t$ as a function of the box filter parameters, dashed lines indicate where the parameters $f_p$ and $f_p$ intersect or are too small to form a band pass filter (< 1 cycle/degree).* ..... 72
*Figure 7-4: Iso-roughness lines predicted by the optimised box filter model, compared to the experimental data.* ..... 73
*Figure 7-5: Effects of varying the parameters p and $F_c$ of the power function filter.* ..... 74
*Figure 7-6: Objective function $\varepsilon_t$ as a function of the power filter parameters.* ..... 74
*Figure 7-7: Iso-roughness lines predicted by the optimised power function filter, compared to the experimental data.* ..... 75
*Figure 7-8: Plots of all filter functions when optimizing the error.* ..... 76
*Figure 7-9: Spatial frequency channels approximations re-plotted from Wilson's data (Wilson, McFarlane, & Phillips, 1983) as gaussian functions to make them more parsimonious.* ..... 77
*Figure 7-10: Effects of varying the parameters μ and $\sigma_g$ of the Gaussian filter.* ..... 78

*Figure 7-11: Objective function $\varepsilon_t$ as a function of the Gaussian filter parameters.* ..... *78*
*Figure 7-12: Iso-roughness lines predicted by the optimised gaussian filter model, compared to the experimental data.* ..... *79*
*Figure 7-13: Final Gaussian Fit.* ..... *80*
*Figure 8-1: Frequency bands used to construct the new stimuli.* ..... *85*
*Figure 8-2: Demonstration of the band stimuli with and without the base (one to two cycles per stimuli width).* ..... *86*
*Figure 8-3: Demonstration of each gaussian frequency band independently (from left to right: $F_{b1} = 1.0$, $F_{b2} = 0.25$ and $F_{b3} = 0.125$).* ..... *87*
*Figure 8-4: Individual data for the experiment on mid-range frequencies.* ..... *89*
*Figure 8-5: Median observations and iso-roughness lines in the space $[F_{b1}, F_{b2}]$.* ..... *89*
*Figure 8-6: Individual data for the experiment on high-range frequencies.* ..... *91*
*Figure 8-7: Median observations and iso-roughness lines in the space $[F_{b2}, F_{b3}]$.* ..... *91*
*Figure 8-8: Iso-roughness lines in decades from the experiment in section 8-2.* ..... *92*
*Figure 8-9: Iso-roughness contour lines for the experiment in section 8-3.* ..... *93*
*Figure 8-10: Optimization of the parameters of the gaussian function with the $[F_{b1}, F_{b2}]$ bands.* ..... *96*
*Figure 8-11: Optimization of the parameters of the gaussian function with the $[F_{b2}, F_{b3}]$ bands.* ..... *96*
*Figure 8-12: Optimized parameters with all the experiments in chapter eight using a gaussian function.* *97*
*Figure 8-13: Demonstration of the optimized parameters for the gaussian function for each experiment and the total optimization by assigning equal weights to each experiment.* ..... *98*
*Figure 8-14: Fit of the model compared to the iso-roughness lines from chapter six when weighting each optimized parameter from the three experiments equally (unbroken lines are the model's output).* *99*
*Figure 8-15: Fit of the model compared to the iso-roughness lines from $[F_{b1}, F_{b2}]$ when weighting each optimized parameter from the three experiments equally (unbroken lines are the models output).* . *99*
*Figure 8-16: Fit of the model compared to the iso-roughness lines from $[F_{b2}, F_{b3}]$ when weighting each optimize parameter from the three experiments equally (unbroken lines are the models output).* . *100*
*Figure 8-17: Optimization of the parameters of the power function for the $[F_{b1}, F_{b2}]$ iso-roughness lines.* ..... *101*
*Figure 8-18: Optimization of the parameters of the power function for the $[F_{b2}, F_{b3}]$ iso-roughness lines.* ..... *102*
*Figure 8-19: Optimization of the parameters of the power function for the combined experiments.* ..... *102*
*Figure 8-20: Demonstration of the optimized parameters for the power function for each experiment and the total optimization when assigning equal weights to each experiment.* ..... *103*
*Figure 8-21: Fit of the model compared to the iso-roughness lines from chapter six when weighting each optimized parameter from the three experiments equally.* ..... *104*
*Figure 8-22: Fit of the model compared to the iso-roughness lines from $[F_{b1}, F_{b2}]$ when weighting each optimized parameter from the three experiments equally.* ..... *104*
*Figure 8-23: Fit of the model compared to the iso-roughness lines from $[F_{b2}, F_{b3}]$ when weighting each optimized parameter from the three experiments equally.* ..... *105*
*Figure 8-24: $m_c$ and $c_c$ parameters influencing the variable gaussian.* ..... *107*
*Figure 8-25: optimizing the $F_p$ value for the variable gaussian.* ..... *107*

*Figure 8-26: Optimization of the $m_c$ and $c_c$ parameters of the variable gaussian using all the three previous experiments. (Minima from left to right $O_{pl}$, $O_p$, $O_{ph}$)* ..... *108*
*Figure 8-27: Three optimizations for the variable gaussians were they were match by multiplying a factor to them. Please notice that the variable function can be multiplied by any factor, as a result the plot for the line can go even further than plotted here.* ..... *109*
*Figure 8-28: Iso-roughness lines from Chapter 6 compared to the predicted model using a variable gaussian with optimized parameters*..... *110*
*Figure 8-29: Iso-roughness lines from [$F_{b1}$, $F_{b2}$] compared to the predicted model.* ..... *110*
*Figure 8-30: Iso-roughness lines from [$F_{b2}$, $F_{b3}$] compared to the predicted model.* ..... *111*
*Figure 9-1: Demonstration of the stimuli for the mid-point experiment, where the surfaces in the sides are the samples, whilst the middle surface is the adjustable one.*..... *115*
*Figure 9-2: Observation for each trial of the ten observers of the lower and middle iso-roughness reference.*..... *116*
*Figure 9-3: Observation for each trial of the ten observers of the lower and top iso-roughness reference.* ..... *117*
*Figure 9-4: Observation for each trial of the ten observers of the middle and top iso-roughness reference.* ..... *117*
*Figure 9-5: Medians from the results in the mid-point experiment.*..... *118*
*Figure 9-6: Mapping the un-scaled estimator to the scaled one for just one pair of reference surfaces*. *119*
*Figure 9-7: Scaling the estimator with a polynomial function.*..... *121*
*Figure 9-8: Mapping perceived roughness in the [β, σ] space.* ..... *122*

# LIST OF TABLES

*Table 2-1: Example table of the many terms used to describe the perceptual dimensions of surface textures where similar terms where group by the author to demonstrate they interlay in their description. ..... 7*

*Table 2-2: Summary of the amplitude parameters (peak and valley) as defined in the international standard EN ISO 4287:1998. ..... 9*

*Table 2-3: Summary of the amplitude parameters (average of ordinates) as defined in the international standard EN ISO 4287:1998. ..... 10*

*Table 2-4: Summary of the spacing parameters as defined in the international standard EN ISO 4287:1998. ..... 11*

*Table 2-5: Summary of the hybrid parameters as defined in the international standard EN ISO 4287:1998. ..... 11*

*Table 2-6: Summary of the curved and related parameters as defined in the international standard EN ISO 4287:1998. ..... 11*

*Table 5-1: Comparing CRTs and flat panels displays. ..... 48*

*Table 5-2: Table of the NEC monitor specifications. ..... 49*

*Table 5-3: A compilation of all the error when calibrating the gamma in percentage. ..... 51*

*Table 5-4: A compilation of all the error when calibrating the gamma in percentage. ..... 52*

*Table 7-1: Short summary of all the filters, the minimum error and the optimum parameter values. ..... 76*

*Table 7-2: Summary of all the filter functions and their errors. ..... 81*

*Table 8-1: Parameters for each of the iso-roughness lines using every single experiment and all of them. ..... 105*

*Table 8-2: Optimized parameter values for the variable gaussian using the three experiments. ..... 108*

# LIST OF SYMBOLS, TERMS AND ABBREVIATIONS

| Symbols | Description |
|---|---|
| * | Convolution operator |
| a | Squared parameter value from the polynomial function |
| $\beta$ | Magnitude roll-off factor |
| $\beta_{ref}$ | Magnitude roll-off factor for the reference surface |
| $\beta_{adj}$ | Magnitude roll-off factor for the adjustable surface |
| $b$ | Parameter value from the polynomial function |
| $b_c$ | Equal to $-m_c$ |
| $c$ | Intersection parameter value from the polynomial function |
| $c_c$ | Changes high-end of the variable gaussian |
| $\varepsilon$ | Objective function or error measure |
| $\varepsilon_t$ | Total error measurement |
| $\xi_{pr}$ | Perceptual Roughness |
| $\xi_{spr}$ | Scaled perceptual Roughness |
| $f_f$ | Cyclic frequency |
| $f_p$ | Start frequency |
| $f_c$ | Cut off frequency |
| $FRF$ | Back pocket model |
| $F$ | Filter from FRF model |
| $F_1$ | First filter from the FRF model |
| $F_2$ | Second filter from the FRF model |
| $f_1(x, y)$ | First filter of the FRF model in the spatial domain |
| $F_1(u, v)$ | First filter of the FRF model in the frequency domain |
| $F_{b1}$ | Magnitude of the first gaussian frequency band |
| $F_{b2}$ | Magnitude of the second gaussian frequency band |
| $F_{b3}$ | Magnitude of the third gaussian frequency band |
| $H$ | Representation of the top surface ($\xi_{spr}$) |
| $h$ | Representation of the top surface ($\xi_{pr}$) |
| $K$ | Gain used in the box filter |
| $k$ | Variable to normalize the gaussian function filter |
| $K_c$ | Normalizing variable for variable gaussian filter |
| $L$ | Representation of the bottom surface ($\xi_{spr}$) |
| $l$ | Representation of the bottom surface ($\xi_{pr}$) |
| $m_c$ | Changes low-end of variable gaussian |
| $\mu$ | Mean value used in the gaussian function |
| $\mu\sigma$ | Mean used for the RMS roughness calculations |

| | |
|---|---|
| $\mu_{b1}$ | Mean used for the first gaussian frequency band |
| $\mu_{b2}$ | Mean used for the second gaussian frequency band |
| $\mu_{b3}$ | Mean used for the third gaussian frequency band |
| $P$ | Representation of surface in the scaling |
| $p$ | Weight power variable used in the power function filter |
| $R$ | Rectifying stage from the FRF model |
| $R_p$ | Maximum profile peak height |
| $R_v$ | Maximum profile valley depth |
| $R_z$ | Maximum height of profile |
| $R_c$ | Mean height of profile elements |
| $R_t$ | Total height of profile |
| $R_a$ | Arithmetical mean deviation of the assessed profile |
| $R_q$ | Root mean square deviation of the assessed profile |
| $R_{sk}$ | Skewness of the assessed profile |
| $R_{ku}$ | Kurtosis of the assessed profile |
| $RS_m$ | Mean width of the profile elements |
| $R\Delta_m$ | Root mean square slope of the assessed profile |
| $Rmr(c)$ | Material ratio of the profile |
| $Rdc$ | Profile section height difference |
| $Rmr$ | Relative material ratio |
| $\sigma$ | RMS roughness or $R_q$ |
| $\sigma_{ref}$ | RMS roughness for the reference surface |
| $\sigma_{adj}$ | RMS roughness for the adjustable surface |
| $\sigma_g$ | Standard deviation used in the gaussian function |
| $\sigma_b$ | Standard deviation used in the gaussian frequency bands |
| $S(u, v)$ | Surface height in the frequency domain |
| $s(x, y)$ | Surface height in the spatial domain |
| $\theta$ | Random phase |
| $\theta_{ref}$ | Random phase for the reference surface |
| $\theta_{adj}$ | Random phase for the adjustable surface |
| $\theta_f$ | Angle function |
| W | Waviness |
| Z(x) | Profile height |

| Terms | Description |
|---|---|
| *$1/F^{\beta}$ noise surfaces* | Type of textured surface |
| *20/20 vision* | Visual acuity measurement |
| *Adjustable surface* | Variable surface used in the method of adjustment |
| *Back pocket model* | Landy's reference to the FRF model |
| *Box filter* | Type of filter shape used as $F_1$ |
| *Brodatz* | Photographic album used for the study of textures |
| *Category scaling* | Psychophysical method |
| *Contours* | Lines with similar characteristics or values |
| *Fractals* | Different types of surfaces |
| *Frequency band surface model* | Type of textured surface, also known as narrow band spectra model |
| *Gaussian filter* | Type of filter shape used as $F_1$ |
| *Gaussian frequency bands* | Bands used for the new stimuli in chapter 8 |
| *High-range frequencies* | Frequencies from 7.0 cpd to 30 cpd |
| *Iso-roughness lines* | Lines of perceived roughness with equal values |
| *Least square fitting* | Mathematical fitting method |
| *MATLAB* | Software tool |
| *Method of adjustment* | Psychophysical method |
| *Mid-range frequencies* | Frequencies from 0.8 cpd to 7.0 cpd |
| *Narrow band spectra model* | Type of textured surface, also known as frequency band surface model |
| *Perceived Roughness* | How surfaces would feel if touched |
| *Power filter* | Type of filter shape used as $F_1$ |
| *Random phase seed* | Seed is taken from MATLAB |
| *Reference surface* | Invariable surface used in the method of adjustment |
| *RMS Roughness* | Physical measurement $R_q$ |
| *Surface* | Three dimensional |
| *Unitless* | Without a defined unit |
| *Variable gaussian filter* | Type of filter shape used as $F_1$ |
| *Waviness* | Characteristic of a surface |

| Abbreviations | Description |
|---|---|
| *cpd* | Cycles per degree |
| *CRT* | Cathode ray tube screen |
| *CSF* | Contrast Sensitivity Function |
| *DFT* | Discreet Fourier transform |
| *HVS* | Human vision system |
| *ISO* | International organization for standardization |
| *LCD* | Liquid crystal display |
| *MDS* | Multidimensional scaling |
| *RMS* | Root mean square |
| *SA I* | Class of tactile receptor |
| *TFT* | Thin film transistor also known as TFT-LCD as this is also a type of LCD |
| $V_1$ | Primary visual cortex |
| *Var* | Mathematical variance |
| *cpi* | Cycles per image width |

# CHAPTER 1

# INTRODUCTION

This thesis is concerned with the measurement of the perceived roughness of one particular class of textured surfaces, those with a *$1/F^{\beta}$ noise* surface height spectrum. In this chapter, the motivation and goals will be explained in *section 1.1*, the scope and limitations of the work will be described in *section 1.2*, followed by the main contributions in *section 1.3*, finishing with the organization of the thesis as a whole in *section 1.4*.

## 1.1 Motivation and goals

Surface characteristics like roughness, directionality, hardness, waviness, etc are readily used by humans in a daily basis. In certain circumstances, statistical measurements of physical descriptions of the surfaces are assumed to be equivalent to their perceived characteristics like for example perceived roughness and RMS roughness, but it is not known whether these measurements actually match how humans perceive surfaces, they can make mathematical sense and yet be illogical in nature to humans. For that reason, the motivation of this work is to find a measurement based on the human visual system that will be more in-tune with the perception of surface characteristics by humans.

The first main goal of this thesis is to find a surface characteristic to analyse, as one can enumerate hundreds or even thousands of characteristics (as for example looking at the surfaces in *Figure 1-1*), and researching all of them would be an impossible task for the author alone. The second goal is to find a general methodology for measuring the perception of surface characteristics, with this methodology it will be possible to realize my main goal of discovering the perceived measurement for the chosen characteristic, and to further research in the area of perception generally.

Once the surface characteristic is chosen, it would be possible, with further research, to apply this measurement in many other research areas where material characteristics are important (see Adelson (2001)) such as:

- quality control,
- 'human like' sample retrieval,
- perceptual scaling or morphing,
- visualizations,
- product evaluation,
- and product development.

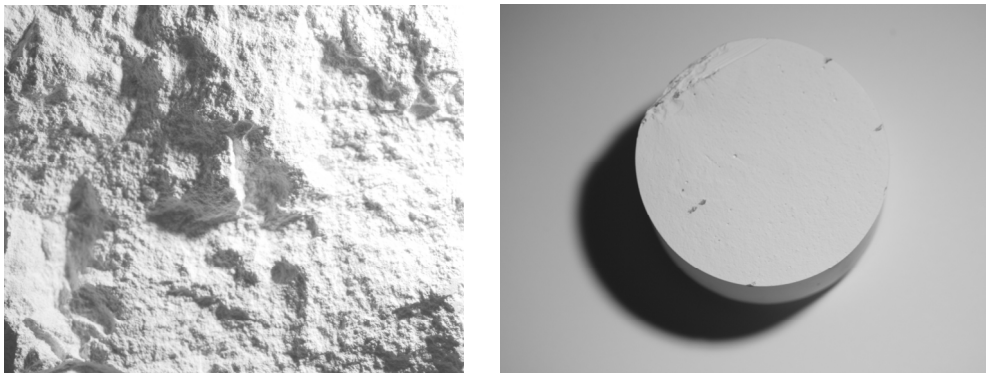

**Figure 1-1: Photograph of a real texture on the left and on the right its shape. Please notice that one can perceive various characteristics from these samples.**

## 1.2 Scope of the work

As previously discussed, it would be impossible to research every single surface characteristic. Therefore, this thesis will only investigate for the visual perception of *roughness* in surfaces; the argument for choosing this surface characteristic is located in *Chapter 2*. Furthermore, because of the wide variety of textured surfaces, the results will only represent synthetic surfaces that are isotropic in nature, in particular $1/F^{\beta}$ *noise surfaces*.

In addition, the stimuli will be free of distractions, colour or any other influencing parameters that can change the surfaces' perceived roughness; none of these extra parameters will be explored in this thesis. The stimuli will also be free of

*microstructure*, to avoid problems with the light model as described in *Chapter 4*. Other smaller limitations and assumptions will be discussed in each of the chapters as they appear.

## 1.3 Original contributions

This thesis contains four main contributions to the field of visual perception of surfaces:

1. As described in *Chapters 4* and *5*, a new way of presenting the stimuli not by just using images but by constructing complex real-time morphable three-dimensional surfaces using advanced computer graphics was developed. These were animated so as to simulate inspection of a real surface by turning it under a light source, so enhancing the depth information available to observers from transformations in the pattern of shading in the rendered image.

2. A perceptual space to describe perceived roughness in terms of two parameters of *$1/F^{\beta}$ noise surfaces* was discovered in *Chapter 6*; this space is very important as it can be used to further the research on the perception of these surfaces.

3. The main contribution of this thesis is the model for perceived roughness in *$1/F^{\beta}$ noise surfaces* based on the human visual system as described in *Chapters 7*, *8* and *9*.

4. The methodology used for deriving this model of perceived roughness, which can be used again for further perceived characteristics.

The combined result of all these contributions makes it possible to develop the methodology and the measurement for visual perceived roughness of *$1/F^{\beta}$ noise surfaces*.

## 1.4 Organization of this thesis

This thesis is subdivided in two main groups of chapters. The first group compromises *Chapters 2* to *5,* and discusses the reasons why roughness was chosen as the research characteristic, why the model for the stimuli was chosen, how it was constructed and

finally the general methodology used. The second part of the thesis, *Chapters 6* to *10*, describes the development of the model for perceived roughness, and the parameters of the model.

Hence, *Chapter 2* provides a short summary of the dimensions of textures and the reasoning for choosing roughness as the surface characteristic for analysis. It also provides a short summary of the current physical and perceptual measurements in the literature. *Chapter 3* discusses the selection of *$1/F^{\beta}$ noise surfaces* as the stimuli, the implications of factors like viewpoint, light, and finishes with a summary of common psychophysical methods for the study of perception.

Having decided on the stimuli, then *Chapter 4* describes the construction of the stimuli and the method of presenting them to the observers. This chapter also describes the general animation (motion) and viewpoint of the stimuli; also, it describes how this motion was obtained. *Chapter 5* explains how the experiments were setup and it also explains the tools used to realize them.

After describing the general methodology and stimuli, *Chapter 6* uses them to discover how the parameters of the stimuli relate to perceived roughness; *Chapter 7* proposes models and estimators to account for the observations whilst C*hapter 8* introduces a new type of test surface for use in experiments to disambiguate the best fitting model. The final model is scaled in *Chapter 9*, followed by the conclusions of the thesis as a whole in *Chapter 10.*

# CHAPTER 2

# ROUGHNESS AND SURFACES

Textured surfaces have many characteristics that are used by humans to judge objects. For example, one might use the surface texture of a fruit to help decide whether it belongs to a familiar edible category or not. In everyday language, humans express judgements of textured surfaces in terms of many properties such as fineness, regularity, roughness, coarseness, etc. However, it is unknown if perceived properties can be associated with physical properties of surfaces or if they can be modelled based on knowledge of the human visual system.

This chapter is subdivided into five sections. S*ection 2.1* describes why roughness was chosen as the perceptual characteristic to be analysed, followed by *Section 2.2* enumerating physical measurements for roughness. *Section 2.3* describes literature about perceived roughness in touch, vision and related studies. This chapter will finish with a short discussion of chapter as a whole and the main conclusions from it in *Section 2.4*.

## 2.1 The dimensions of natural textured surfaces

The objective of this section is to find a common and starting perceptual property to study. Therefore, the first step was to find about perceptual properties and textured surfaces, either in two-dimensional images or in three-dimensional samples.

Many methods have been used to determine the mapping between physical and perceived properties of surfaces textures. Tamura, Mori and Yamawaka's (1978) psychophysical study of textures is the first one that tried to determine this mapping. In order to identify features of textures that approximate to human visual perception, they asked 48 human observers to judge the similarities of texture pairs from 16 pictures (images) from the *Brodatz* album (1966). Tamura et al used six features: *coarseness*, *contrast*, *directionality*, *line/blob likeness*, *regularity* and *roughness*; unfortunately,

these features were chosen without any previous psychophysical experimentation. As a result, all these characteristics can be researched. However, they did not specify a common main characteristic as none is more heavily weighted than the other one. The main contribution from Tamura et al was that they helped start the research into surface texture dimensions.

Adamasun and King (1989) also conducted experiments similar to Tamura and measured similarity judgements according to five visual properties of two-dimensional textures: *coarseness*, *contrast*, *busyness*, *complexity* and *strength* of texture. They devised computational approximations for each of these properties and claimed that there is a high correspondence between their computational measurements and the human rankings of 88 subjects using the same property.

Although these authors found correlations between machine and human rankings, they used descriptive terms that are not always spontaneously used by humans. As a result, the observers might have been implicitly prompted to look for texture properties corresponding to those that the algorithms were designed to measure.

Rao and Lohse (1993a) (1993b) (1996) overcame this problem by using free sorting tasks. They asked 20 subjects to sort 56 Brodatz textures into as many groups as the subjects wished such that the textures in each group were perceptually similar. A multidimensional scaling (MDS) method was later used to derive a perceptual space; in their findings, they correlated a three-dimensional space to the visual properties of *repetitiveness*, *orientation* and *complexity*.

Long and Leow (2001) used a free sorting task to discover the perceptual space. In their experiment, 60 subjects and 50 Brodatz textures were used. They concluded that there is a four-dimensional space but they did not assign names to this, but instead linked the model into a computational space and later into other models like neural networks (Long and Leow, 2002).

Many other experiments have attempted to discover a standard set of predefined dimensions for textured surfaces (Harvey and Gervais, 1981) (Copeland and Trivedi, 1996) (Vanrell and Vitria, 1997) (Payne, Hepplewhite and Stonham, 1999) (Wu,

Manjunanth, Newsam and Shin, 1999) (Payne, Hepplewhite and Stonham, 2000) ( Abbadeni, Ziou and Wang, 2000a) (Abbadeni, Ziou and Wang, 2000b) (Gurnsey and Fleet, 2001) (Payne and Stonham, 2001) (Bittiato, Gallo and Nicotra, 2003) (Fujii, Suji and Ando, 2003) (Ontrup, Ritter and Werseing, 2004) (Geusebroek and Smeulders, 2005). However, there are differences between the studies in the number and nature of the dimensions obtained, suggesting that MDS methods do not identify stable perceived properties of image textures.

In addition, Heaps and Handel (1999) conducted experiments similar to those of Rao and Lohse (1996) using natural textures and their main conclusion was that perceived roughness might be context dependent, therefore it might be impossible to search for a standard set of dimensions. This also does not imply human use these characteristics as perceptual dimensions or that there exist linguistic terms for relating characteristics to the human mind as noted by Petrou, Talebpour and Kadyrov (2007).

| **Similar terms** | | | |
|---|---|---|---|
| | **Group 1** | **Group 2** | **Group 3** |
| **Term 1** | Contrast | Directionality | Complexity |
| **Term 2** | Coarseness | Line | Blob |
| **Term 3** | Roughness | Stringy | Regularity |
| **Term 4** | Hardness | Waviness | Busyness |

**Table 2-1: Example table of the many terms used to describe the perceptual dimensions of surface textures where similar terms where group by the author to demonstrate they interlay in their description.**

As described in *Table 2-1*, many terms frequently appear in the description of the perceptual dimensions. These terms can be easily grouped into many subcategories; this is possible because many of the experiments used images as stimuli and by changing the physical properties of the surface, it is possible to change many related visual terms. For example, by changing the roughness of a surface its contrast and complexity and other terms will also change. Therefore, to avoid repeated or derivate terms the main perceptual characteristic to be researched was not only searched from visual studies but also from tactile ones.

Tactile perceptual spaces were researched by Hollins, Dacremont, Valentin and Giboreau (1993). They concluded that there is a perceptual tactile space consisting of three-dimensions; these are *rough/smooth*, *soft/hard* and *sticky/slippery*. Also Picard, Dacremont, Valentin, Giboreau (2003) concluded that there are three dimensions; these are *hardness/relief*, *soft/harsh* and *thin/thick*. Picard et al also investigated the frequency with which different terms are used when describing textures, and found that after *soft*, *warm*, and *harsh*, the main identifying characteristic is roughness (partly concluded also by Bhusham, Rao and Lohse's texture lexicon (1997)).

If one removes the qualitative terms from the tactile perceptual spaces, adds the most common visual characteristics and by knowing that there is partial perceptual equivalence between vision and touch in texture information as described by Picard (2006), then it is possible to distinguish *roughness* as the most used term to identify a characteristic from surface textures, as roughness is:

*i.* the most used linguistic term to describe surface characteristics,
*ii.* the most relevant tactile dimension, and
*iii.* the most common visual term when classifying textured surfaces.

As a result, I will conclude that roughness is the best starting perceptual characteristic to be investigated in the human perception of textured surface characteristics, followed by either *directionality* or *coarseness*.

## 2.2 Physical measurements of roughness

Many of the physical surface roughness measurements in widespread use today can be traced to the first half of the 20 century where a stylus is moved across a surface and its vertical deflection is recorded. From this stylus technique, hundreds of parameters or measurements can be calculated but only sixteen parameters are defined in the international standard for surface texture parameters (ISO 4287:1998), the most commonly used parameters in relationship to roughness are *Ra*, *Rq* and *Rz*.

These sixteen parameters are divided into five sections of parameters:

a. amplitude parameters (peak and valley), as described in *Table 2-2*;
b. amplitude parameters (average of ordinates) , as described in *Table 2-3*;

c. spacing parameters, as described in *Table 2-4*;
d. hybrid parameters, as described in *Table 2-5*
e. curves and related parameters, as described in *Table 2-6*.

| Parameter | Name | Description |
|---|---|---|
| $R_p$ | *Maximum profile peak height* | The largest peak height within a sampling length |
| $R_v$ | *Maximum profile valley depth* | The largest depth within a sampling length |
| $R_z$ | *Maximum height of profile* | The sum of the height of the largest peak height and the largest depth within a sampling length |
| $R_c$ | *Mean height of profile elements* | The mean value of the height within a sampling length |
| $R_t$ | *Total height of profile* | The sum of the height of the largest profile peak height and the largest profile depth within the evaluation length |

**Table 2-2: Summary of the amplitude parameters (peak and valley) as defined in the international standard EN ISO 4287:1998.**

The amplitude parameters using peak and valleys only account for the variations at random locations. For this reason, these parameters will serve little purpose in finding the perceived roughness of a textured surface. However, these are more suitable for identifying defects or anomalies in surfaces.

The amplitude parameters using ordinates are more likely to be linked to perceived roughness as they take into account the statistical appearance of the surface as a whole. From these parameters, $R_a$ is the most widely used parameter but this only measures the arithmetic mean from the surfaces which is insufficient to describe or differentiate the surface appearance as demonstrated in *Figure 2-1* where the three profiles have the same $R_a$ value. For this reason, this parameter will not be considered any further to be used in this thesis.

| Parameter | Name | Formula | Description |
|---|---|---|---|

| | | | |
|---|---|---|---|
| $R_a$ | Arithmetical mean deviation of the assessed profile | $\frac{1}{l}\int_0^l \lvert Z(x)\rvert \, dx$ | The arithmetic mean of the absolute ordinate values Z(x) within a sampling length ($l$). |
| $R_q$ | Root mean square deviation of the assessed profile | $\sqrt{\frac{1}{l}\int_0^l \lvert Z^2(x)\rvert \, dx}$ | The root mean square value of the ordinate values Z(x) within a sampling length ($l$). |
| $R_{sk}$ | Skewness of the assessed profile | $\frac{1}{{R_q}^3}\left[\frac{1}{lr}\int_0^{lr} Z^3(x)\, dx\right]$ | The quotient of the mean cube value of Z(x) and the cube of $R_q$ within a sampling length |
| $R_{ku}$ | Kurtosis of the assessed profile | $\frac{1}{{R_q}^4}\left[\frac{1}{lr}\int_0^{lr} Z^4(x)\, dx\right]$ | The quotient of the mean cube value of Z(x) and the forth power of $R_q$ within a sampling length |

**Table 2-3: Summary of the amplitude parameters (average of ordinates) as defined in the international standard EN ISO 4287:1998.**

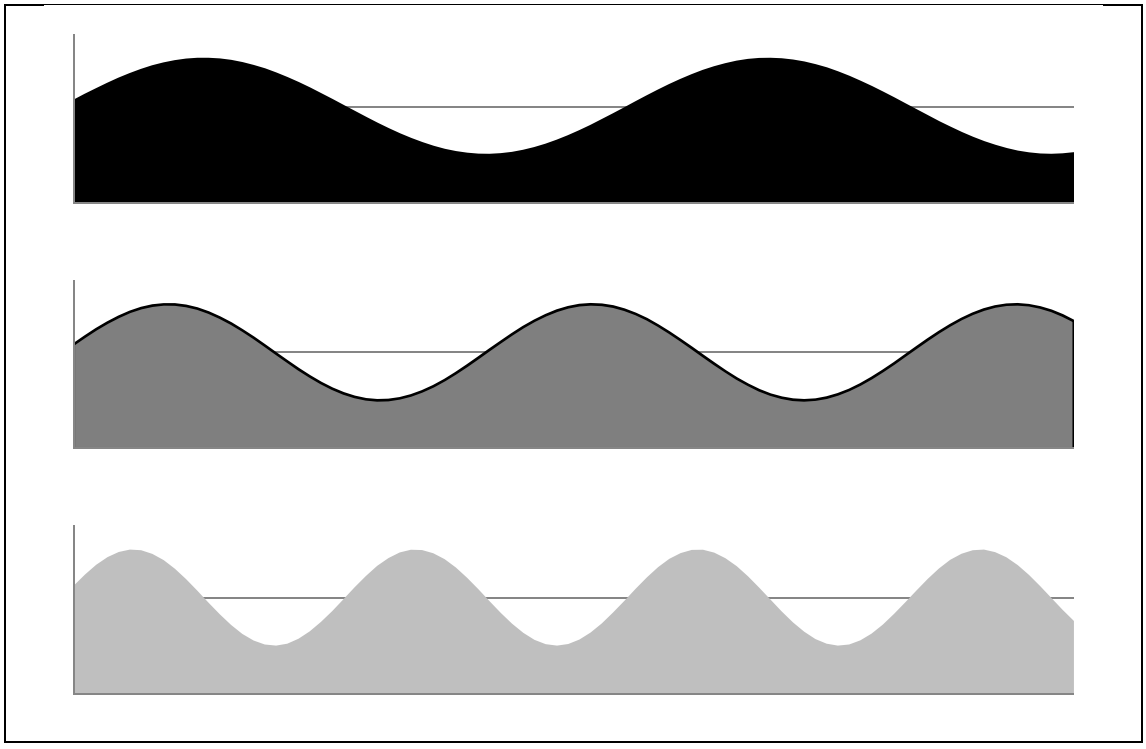

**Figure 2-1: Three different surface profiles with the same $R_a$ value.**

| Parameter | Name | Formula | Description |
|---|---|---|---|
| $RS_m$ | Mean width of the | $\frac{1}{m}\sum_{i=1}^{m} Xs_i$ | The mean of the profile element |

| | | | |
|---|---|---|---|
| | profile elements | | widths *Xs* within a sampling length |

**Table 2-4: Summary of the spacing parameters as defined in the international standard EN ISO 4287:1998.**

| Parameter | Name | Description |
|---|---|---|
| $R\Delta_m$ | Root mean square slope of the assessed profile | The root means square of the ordinate slopes dZ / dX, within a sampling length. |

**Table 2-5: Summary of the hybrid parameters as defined in the international standard EN ISO 4287:1998.**

| Parameter | Name | Description |
|---|---|---|
| ***Rmr(c)*** | Material ratio of the profile | Ratio of the material length of the profile elements at a given level c to the evaluation length. |
| ***Abbot Firestone Curve*** | Material ratio curve of the profile | The curve representing the material ratio of the profile as a function of level. |
| ***Rdc*** | Profile section height difference | Vertical distance between two section levels of given material ratio. |
| ***Rmr*** | Relative material ratio | The material ratio determined at a profile section level, related to a reference. |
| | Profile height amplitude curve | The sample probability density function of the ordinate Z(x) within the evaluation length. |

**Table 2-6: Summary of the curved and related parameters as defined in the international standard EN ISO 4287:1998.**

The spacing, hybrid, curved and related parameters will not be used as some of these are defined only over an evaluation length or they can be represented statistically by simpler parameters (like $R_q$). More information about all the parameters can be found in the international standards (ISO 4287, 1997) (ISO 4287, 1998) (ISO 4288, 1998) (ISO 11562, 1998) (ISO 12085, 1998) (ISO 2632/2, 1985) (BS 1134-1, 1988) (BS EN 623-4, 2004).

Therefore, the most suitable physical parameters to consider as a base for perceived roughness are $R_q$, $R_{sk}$, and $R_{ku,}$ as all of these are statistical measurements that take into

account the surface as whole. From these, $R_q$ (RMS deviation) is the easiest to calculate and the most used in calculations and the most used also in instruments from the three. As a result, this thesis will focus only on $R_q$.

Note that the international standard stipulates that the value of $R_q$ must be calculated without surface waviness ($W$), but unfortunately, it does not specify this waviness measure. For that reason, values of $W$ will not be considered in our calculations of $R_q$.

$R_q$ is defined using or in term of the profile for a surface; its definition for a three dimensional surface has not yet been approved but its mention in the standard proposal N756 (ISO RC 213 Workgroup 16, 2005). The definition of the RMS roughness for three-dimensional surfaces ($R_q$ or $\sigma$) used in this thesis is described in *Equation 2-1*. Where Z(x, y) represents the height at a point (x, y) in the surface and $\mu\sigma = \frac{1}{MN}\sum_{i=0}^{M-1}\sum_{j=0}^{N-1} Z(x_i, y_j)$.

$$\sigma = \sqrt{\frac{1}{MN}\sum_{i=0}^{M-1}\sum_{j=0}^{N-1}\left[Z(x_i, y_j) - \mu\sigma\right]^2} \qquad \textbf{(2.1)}$$

There are many other three dimensional measurements and techniques (like fractals) to assess physical surface roughness but none of these will be used as we can define roughness just with $R_a$ (Blunt and Jiang, 2003) (Schmahling, Hamprecht and Hoffmann, 2006) (Jahn and Truckenbroth, 2003) (Hyslip and Vallejo, 1997).

## 2.3 Related studies in the perception of roughness

This section will summarise studies in relationship with the perception of roughness by touch, vision or both. Many more studies related to roughness and other perception mechanisms like sound and taste can be found but they will not be discussed as its very difficult to relate them to this work (Shirado and Maeno, 2005) (Douiri, Khoudeir and Olivier, 2001) (Engelena, Wijka, Van der Biltb, Janssena and Bosma, 2005). This section will first summarize the perception of roughness by touch, then by haptic touch

or by imagining touching surface. It will then summarize studies of touch and vision combined, finishing with studies in the visual perception (or appearance) of roughness in surfaces.

There have been many studies of touch perception (active and passive). For briefness, only those concerned with the estimation or discrimination of roughness in surfaces will be discussed.

The skin of the fingers has four classes of receptors; the structure and function of these are fully described by Phillips, Johansson and Johnson (1992). One hypothesis of tactile perception is *Katz's hypothesis*, were vibration cues are used for fine textures and spatial cues are used for coarse textures. Experiments by Hollis and Risner (2002) concluded that spatial cues are perceptible down to a spacing of 0.1 mm between elements, and that movement was required for elements below 0.1 mm. This claim is also supported by neurophysiological experiments by Yashida, Gibb, Dorsch, Hsiao and Johnson (2001) were they concluded that spatial variation in SA I receptors is the only neural measurement that correlates with perceived roughness in fine textures (0.1mm to 2.0mm). Bensmaia and Hollins (2003) suggest that the roughness of finer textures (< 0.2mm) is determined by the power of the vibrations caused by the scanning with a finger, weighted by the sensitivity of the Pacinian receptors.

In further studies of tactile perception, Meftah, Belingard and Chapman (2000) used a passive presentation in their experiments and varied the spatial period of dot patterns. They concluded that perceived roughness increases approximately linearly with spatial period (in the direction of the surface motion) over the range 1.5mm to 8.5mm. They also concluded that scanning speed had no effect on perceived roughness. However Casio and Sathian (2001) concluded that temporal cues also affect perceived roughness, as they could prove that changing either the inter-element spacing or the element width had a systematic effect on perceived roughness. It was also found by Gamzu and Ahissar (2001) that temporal cues are essential for texture exploration.

Smith, Chapman, Deslandes, Langlais and Thibodeau (2002) followed Meftah et al's experiments by looking for correlations between subjective roughness estimates and measurements of the forces exerted on a surface by a moving finger. They found a

strong correlation between roughness and the RMS variation of the force rate during a single stroke. Finally Gibson and Craig (2002) concluded that measurements of tactile sensitivity using gratings and orientation (square wave gratings presented at different orientations) are consistent and valid measurements of spatial acuity. Whilst measurements of tactile sensitivity using smooth and grooves (smooth domed contactor or equal-width grooves and ridges) are inconsistent with previous results. Gibson et al suggest that spatial and intensive factors are both involved in the tactile perception of perceived roughness.

The previous experiments on tactile perception of surface roughness can be related to visual perception of surfaces as discussed by Lederman and Abbott (1981) who concluded that subjects performed texture identification with comparable accuracy and precision whether using touch, vision or both together. In later work, Lederman proposes a *modality appropriateness* interpretation of inter-sensory integration, according to which subjects weight differently the input of touch and vision depending on the task. For example, there was a greater emphasis on tactile perception when judging roughness whilst there was a greater emphasis on visual perception when judging spatial cues (Lederman, Thorne and Jones, 1986).

Evidence for *modality appropriateness* implies that tactile and visual perception of roughness are not entirely similar (Picard, 2006), and this is shown in experiments on the weighting of the two senses using real surfaces or haptically displayed ones (Weiskopt and Ertl, 2003) (Ballesteros, Reales, de Leon and Garcia, 2005). For that reason, the following discussion will concentrate on the visual appearance of surface roughness only.

There is little work related to the visual perception of roughness. Most is related to the perception of roughness in just one type of surface, for example in paper (Beland and Bennet, 2000), paintings (Cai and Siegel, 2002), textiles (Lee and Sato, 2001), paint and steel (Scheers, Vermeulen, De Mare and Meseure, 1998), and carpet (Pourdeyhimi and Sobu, 1993)

Unfortunately, none of these studies advances me to a general model for how roughness is perceived in surfaces. As a possible source of evidence on which to base a more

general model of visual perception of texture, I will next consider the literature concerning the workings of the human visual system, especially V1 mechanisms (Olshausen, 2005).

Landy and Graham (2004) provide a short summary of the most important studies in texture discrimination and edge detection. Perception in vision consists of a series of spatial frequency channels and filters. The first order spatial frequency channels have been extensively studied, for example, the contrast sensitivity function is viewed as an envelope of narrow band spatial and frequency tuned mechanism (Campbell and Robson, 1968). Whilst second order processes in vision vary, the most used model is the "back-pocket model" as this is usually used routinely to make sense of results as discussed by Landy and Oruc (2002). This model will be used for the experiments in this thesis, as described in *Chapter 7*.

Finally Ho, Landy and Maloney (2006) also investigated the stability of judgements of roughness when the illumination was changed, the effects of viewpoint (Ho, Landy and Maloney, 2007) and the effect of gloss (Ho, Landy and Maloney). These studies are discussed extensively in later chapters.

## 2.4 Summary and Discussion

Roughness was found to be an important perceptual dimension from visual, tactile and linguistic studies, and will therefore be the research topic for this thesis. There are many physical measurements for roughness but RMS roughness ($R_q$ or $\sigma$) will be used, as it the simplest possible measurement that describes surfaces as a whole in a statistical manner.

From the literature, it was found that there are many studies in the area of tactile perception of roughness. These show that the minimum spatial resolution is 0.1 mm and values below this are perceived using vibrations instead. These can be related to visual perceived roughness, but not fully, as there are studies that prove that humans weight differently vision and touch depending on the task (*modality appropriateness*), suggesting that perception in vision and touch are not entirely similar.

Studies in the visual perception are scarce therefore in the next chapter a novel methodology will be proposed to facilitate the study of surface characteristics.

# CHAPTER 3

# A GENERAL METHODOLOGY

The studies and methods reviewed so far all share an important limitation, they work with single still images of textured surfaces, or synthetic images derived from them, and not with the surfaces themselves. Furthermore, these images have been obtained under arbitrary and unspecified illumination therefore these will contain ambiguities about surface relief and reflectance that cannot be resolved, as in a natural situation, by altering the relative orientation of the surface and the illuminant position.

As a result, this chapter will discuss techniques to address these limitations. It will also describe a novel methodology later used in *Chapter 6* to discover how roughness is perceived in textured surfaces.

This chapter is divided in four sections, the first one will discuss how changes in illuminant and viewpoint affect perceived roughness (*Section 3.1*), followed by *Section 3.2* summarizing the different kinds of stimuli found in previous studies, whilst *Section 3.3* will summarize different psychophysical methods that can be used for the general methodology when experimenting in this thesis. The chapter will end with a short summary (*Section 3.4*).

## 3.1 Illuminant and viewpoint position

Illuminant and viewpoint position play an important role in perception as changing the illuminant position affects the statistics of the surface whilst changing the viewpoint solves ambiguities. The first part of this section will talk about the illuminant position whilst the second half will discuss viewpoint and perception.

By looking at the example in *Figure 3-1,* it is possible to notice that the appearance of the same surface differs when changing the illuminant position; Chantler showed that variation in illumination conditions adversely affected classification performance (Chantler, 1995).

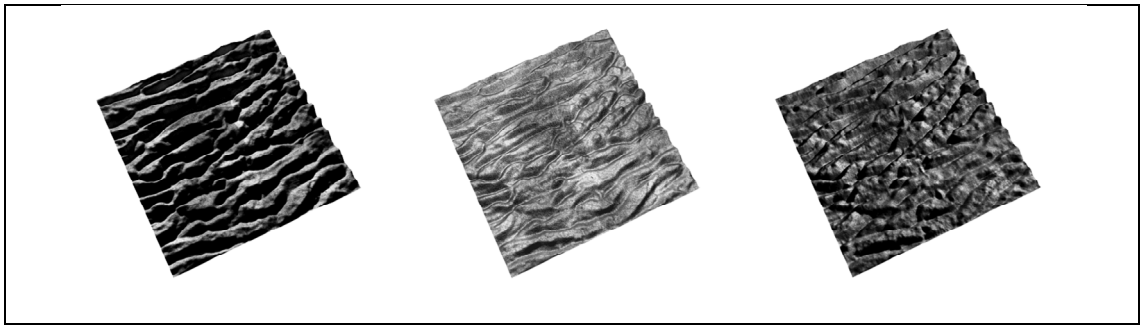

**Figure 3-1: The effect of varying illumination conditions on the same surface is shown above. The light is position on top in the first surface, in the middle for the second surface and on the right for the last surface.**

A way of overcoming this problem is to use sets of photographs obtained under multiple precisely controlled illumination conditions, such as the image database used by Dana, Nayar, Ginneken and Koenderink (1997). Histogram models (Dana and Nayar, 1998) (van Ginneken, Koenderink and Dana, 1999) and correlation models (Dana and Nayar, 1998) for the textures in this database exist which explain the variations in the illumination conditions and texture.

With the help of this method of using images with controlled illumination conditions, Koenderink (2003) (Koenderink, Van Doorn and Pont, 2004) proved with psychophysical experiments that humans can judge the direction of illumination from image textures, therefore confirming the effectiveness of the method and overcoming the uncontrolled light problem.

In addition, to solve this problem it is also possible to create models of surfaces that are rendered graphically under specified illuminations. This second method offers the advantages of speed and flexibility, but the quality of the model for the surface and its renderings must be on a par with real samples.

Ho, Landy and Maloney (2006) used this approach to investigate the stability of judgements of roughness when the illumination direction was changed. They used surface models made up of irregular arrays of triangular faces, varying the mean height of the facets to create surfaces of different roughness. Observers were able to judge relative roughness of images presented in pairs, but not to compensate fully for

variations in the elevation of the light source (50 to 70 degrees), perceiving greater roughness with decreasing elevation.

The method used in this thesis will be to create models of surfaces that are rendered under specified illuminations, but these surfaces will also be animated in real time as if they were handled in a natural manner. This *natural animation* will have a constant illuminant position, similar to the static position of the sun, whilst the rotation will be similar to an observer picking up an object and wobbling it to perceive more accurately its characteristics. At the same time, by rotating the surface, the depth perception of the rendered surface is solved by the motion as described by Anderson and Brodley (1998) in their studies, and by Ichikawa, Nishida and Ono (2004).

Viewpoint and lighting ambiguities are also solved by adding motion to the surfaces. These ambiguities are:

1. *Generalized bas-relief ambiguity* (GBR), produced when the observers' viewpoint is fixed and the light is changed. Just consider a set of images produced with the same viewpoint but under all possible light positions, the ambiguity is produced when an object with different shape produces the same image as another object because the position of its illuminant has changed (Belhumeur, Kriegman and Yuille, 1999), an example is shown in *Figure 3-2*.

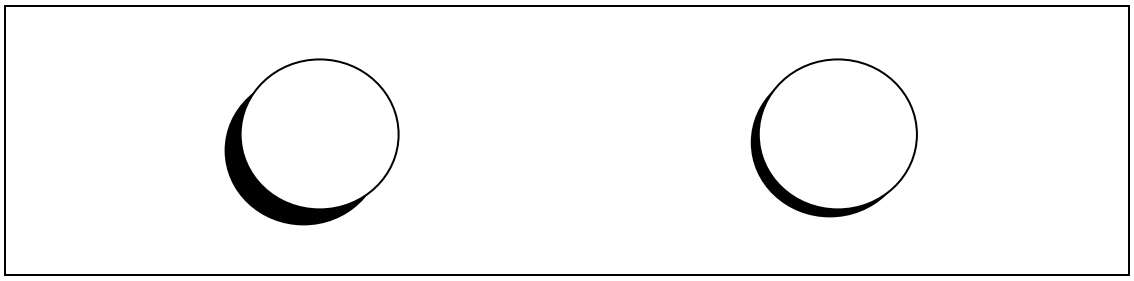

**Figure 3-2: Illustration of the bas-relief ambiguity with two cylinders of equal height viewed from above. Because the elevation of the light source is lower for the cylinder on the left, it appears to be taller than the cylinder on the right.**

2. Viewpoint-lighting ambiguity (KGBR) is similar to the bas-relief ambiguity but here viewpoint is also considered to produce similar sets of images (Yuille, Coughlan and Konishi, 2003).

Solving viewpoint and light ambiguities is possible by humans because we can retrieve three-dimensional shape from motion or from binocular disparity. The capacity to extract shape or structure from motion is also known as *motion parallax* (Gibson, Gibson, Smith and Flock, 1959) or the *kinetic depth effect* (Koenderink, 1986). It was proven by Dijkstra, Cornilleau-Peres, Gielen and Droulez (1995) that it is possible to detect shape from small field stimuli (< 8 degrees) better when using either head translation or object rotation than when using object translation only.

Summarizing, the general method for this thesis will create models of surfaces that are rendered graphically under specified illuminations; these will be animated by rotating the surfaces to solve illuminant location problems, light and viewpoint ambiguities. The construction details of the surfaces and animation are further detailed in *Chapter 4*. The next section will describe the stimuli previously used in studies and the reasoning behind using natural surfaces for the stimuli in this thesis.

## 3.2 Natural synthetic stimuli

Stimuli for psychophysical experimentation of textures or surface textures can be separated into five categories:

1. *Synthetic textures involving texture elements*. These include dots, line segment, figure-like Ls, Ts and Xs, as illustrated in *Figure 3-3*. This use of randomly placed elements was developed by Julesz (1987) in his definition of textons, and also later used by Malik and Perona (1990) in their studies. This type of stimulus will not be used because it does not resemble surfaces found in nature.

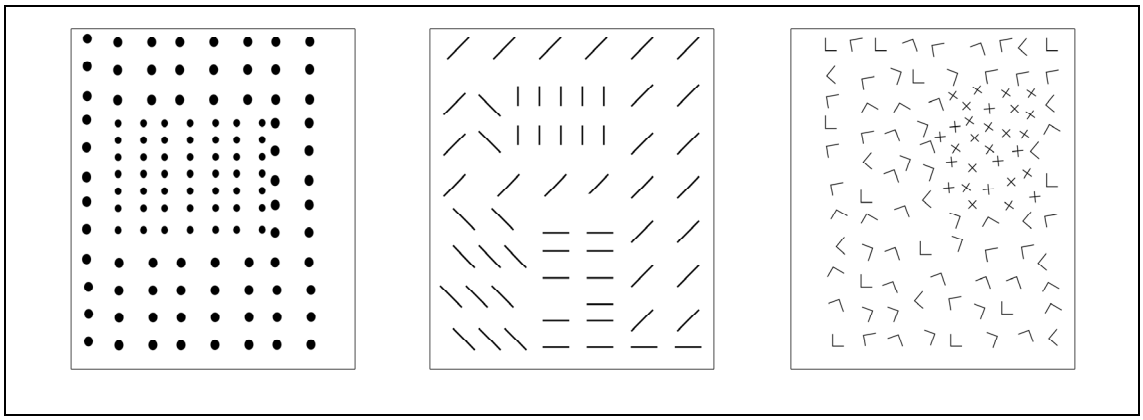

**Figure 3-3: illustration of three textures using dots, lines and Ls, Ts and Xs.**

2. *Natural images of textured surfaces*. These will not be used in this thesis, because their parameters (e.g. RMS roughness) cannot be controlled, and the illumination must be controlled for every image as previously described. There are many studies in perception using natural images (e.g. Leung and Malik (2001)); the studies related to roughness perception are described throughout this thesis.

3. *Synthetic images*. These are created synthetically but resemble images of real textured surfaces closely enough to engage the same perceptual mechanism (see *Figure 3-4*). An example of the applications of these surfaces is described in Balas (2006) who tested the effects on observers of artificial images produced using a texture synthesis algorithm (Portilla and Simoncelli, 2000) that resembled images of real textured surfaces. Another example is Gurnsey and Fleet's study (2001) using stimuli composed of band-pass images produced by filtering a single sample gaussian noise with an isotropic filter. These surfaces will not be used as they do not convey depth information, do not have a natural appearance and do not account for illumination.

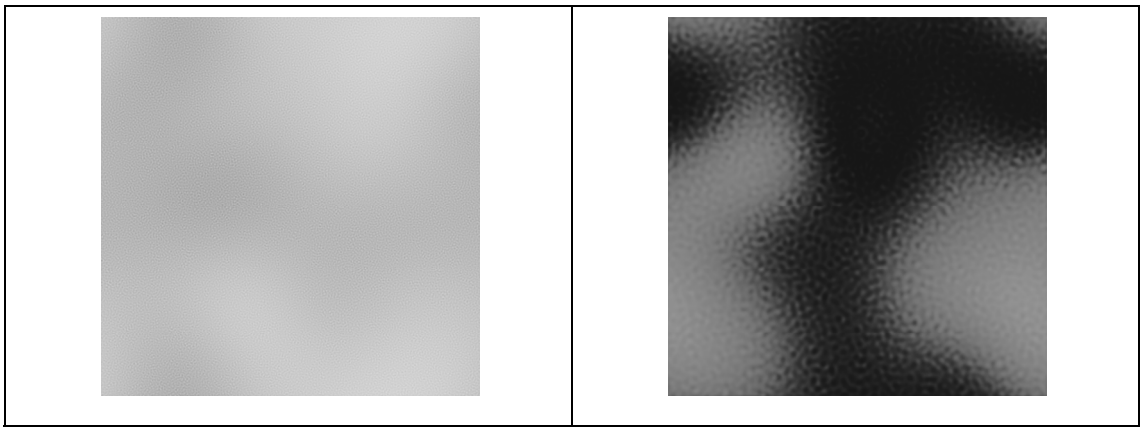

**Figure 3-4: Example of two simple synthetic images constructed with gaussians.**

4. *Geometrical surfaces*. These are created by grooves, cavities, elevations or any other geometrical modulation of the surface height. Ho, Landy and Maloney use surfaces composed of randomly oriented Lambertian facets to discover how viewpoint (2007) and direction of illumination (2006) affect roughness. Other studies include surfaces composed of v-shaped cavities (e.g. Torrance and Sparrow (1967)).

5. *Natural synthetic surfaces*. These surfaces look like samples found in the real world (see *Figure 3-5*). Therefore, observers can interpret them more consistently, making psychophysical measures based on them more reliable. The most common natural synthetic surfaces are fractal surfaces as described by Russ (1994).

As discussed previously, natural synthetic surfaces are the surfaces best suited for the experiments in this thesis. The type of surfaces used will be *$1/F^{\beta}$ noise surface*s as they have the advantages of possessing a natural appearance and they are isotropic in nature. A full description of the construction and mathematical model of these *$1/F^{\beta}$ noise surface*s is located in *Chapter 4*.

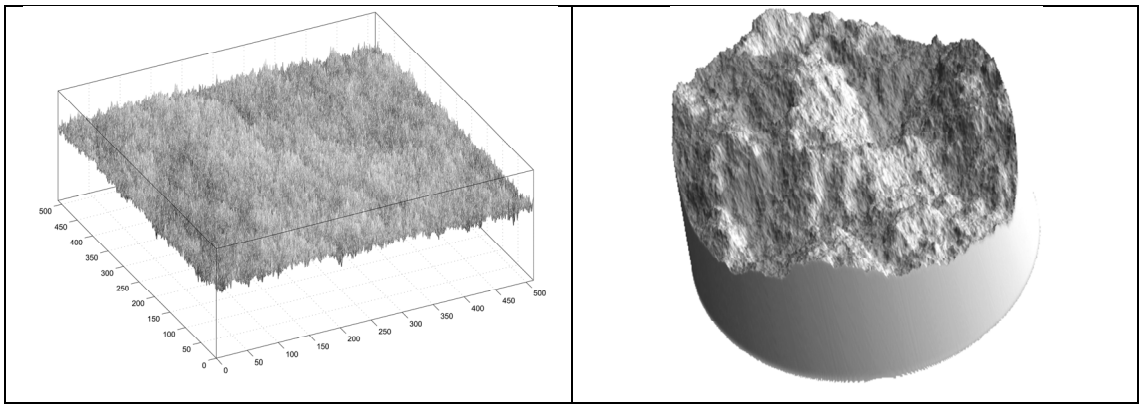


**Figure 3-5: On the left a wireframe illustration of a $1/F^{\beta}$ noise surface whilst on the right a different surface fully rendered.**

## 3.3 Comparing psychophysical methods

Finding a well-suited method to obtain information about perceived roughness from the observers is the last step to finish the methodology to be used later on in the experiments. To do this, a short summary about common psychophysical methods will precede the discussion about the method selected; further information about each method can be found in Ehrenstein and Ehrenstein (1999) chapter about psychophysical methods.

Psychophysical methods enable the researcher to determine the relationship between perceptual experience and physical stimuli. They include:

- The *pairwise comparison* method presents stimuli in pairs to an observer, who judges which of each pair is greater in some respect, such as roughness. This method produces reliable results but is time consuming. In our case, this method would be impractical to implement due to the number of stimuli and the added time of pairwise comparing stimuli with an animation (e.g. a five-second animation).

- The *method of adjustment* lets the observer adjust the stimulus until it becomes just noticeable, or until it just matches another, standard stimulus. This method provides the added advantage of speed and flexibility as it is possible to choose the adjustable parameter from the generated stimuli.

- The *method of limits* presents changes in the stimuli in discrete steps until a response is recorded. This method is also more time consuming than the method of adjustment, and for that reason it will not be used.

- The *method of constant stimuli* presents a set of stimuli in random order to the observer, who reports whether or not each stimulus was detected, or whether it was greater or less than a comparison stimulus in some respect. This method will not be used, as it is more time-consuming than the method of adjustment.

- The method of *adaptive testing* is used to keep the test stimuli as close as possible to the threshold by adjusting the stimuli. The *staircase method* is such an adaptive method. Although this method reduces the time by reducing the number of stimuli, it is still more time consuming than the method of adjustment.

- The *category scaling* method consists of sorting a set of stimuli in correct order of intensity. This method is quite useful to recognize in which direction a parameter influences perception. There are further similar methods to calculate numerical magnitudes but these will not be used, as the thresholds of roughness are unknown.

- *Other methods* including force-choice, signal detection, chronometric, comparative psychophysics, reflex, stimulus associated operant conditioning and cross modality methods will not be discussed, as they are difficult to implement for the investigation of perceived roughness (Ehrenstein, et al., 1999).

As previously described, only two methods will be used in this thesis

1. *Category scaling* will be used in *Chapter 6* to determine how parameters of the surface influence perceived roughness.
2. The *method of adjustment* will be used in *Chapters 6* and *8*. Although it is possible to use pairwise comparison, as proven by Ho, Landy and Maloney (2007), it is impractical for our experiments due to the added length of using stimuli with animation. As a result, the method of adjustment provides added speed and more flexibility.

The performance of the *method of adjustment* was calculated in later experiments and the results of the performance is described in *Appendix 3-A*. As a result, it will be used for the methodology proposed in this chapter.

Please note that it can be argued that the ability of the observers' to detect explicitly the equivalence in roughness between two surfaces may not reflect the true sensitivity of the perceptual system to differences in surface roughness, different methods (e.g. RTs, EEG, functional imaging, error rates, etc) might show if the psychometric experiments were correct but this are outside the scope of this thesis.

## 3.4 Summary and Discussion

In this chapter, a general methodology was proposed which consists of four main parts:

*i.* To create models of surfaces rendered under specified illuminations so that surface characteristics can be perceived independently of illumination direction;

*ii.* Add motion (rotation) to the stimuli which will help in the perception of depth and at the same time avoid illumination and viewpoint ambiguities;

*iii.* Use natural looking stimuli models to try to avoid biasing the experiments towards specific mathematical models;

*iv.* Use the *method of adjustment* to measure human perception of roughness in the surfaces.

Points (*i*) and (*iii*) will be discussed in the next chapter, where the model of the surfaces will be explained in its entirety, followed by how the animation (*ii*) was developed. Later in *chapter 6*, the method of adjustment (*iv*) will be used to discover how the surface parameters influence perceived roughness.

# CHAPTER 4

# MODELLING THE STIMULI

In this chapter, the general methodology described in the *Chapter 3* will be extended to describe the stimuli (*$1/F^{\beta}$ noise surface*) for the experiments in perceived roughness. These surfaces will be discussed in full depth, were a general mathematical description for them will be formulated also the three-dimensional construction (including rendering) of the model will be described, including general algorithms and techniques. Finally, the animation method will be illustrated.

The chapter is structured as follows, s*ection 4.1* will discuss the general model for *$1/F^{\beta}$ noise surface* were the influence of all the parameters will be illustrated; *section 4.2* will follow by describing how the surfaces were rendered in three-dimensions whilst *section 4.3* will discuss the animation of the stimuli. A final section (*section 4.4*) will summarize the chapter as a whole and will discuss the general conclusions about the stimuli.

## 4.1 $1/F^{\beta}$ noise surfaces

As previously explained in the methodology chapter, *$1/F^{\beta}$ noise surfaces* are perfect for the experimentation as they congregate these essential characteristics:

- they look natural by simple inspection;
- they are parsimonious (i.e. have a low number of parameters);
- their structure is isotropic in nature, and
- they are modelled easily in the frequency domain which helps when experimenting with frequency models related to the human vision system.

The *$1/F^{\beta}$ noise surfaces* are generated by producing a height map with a magnitude spectrum H($f$) scaled with spatial frequency as shown in *equation 4.1*, where $\beta$ is the *roll-off factor* of the surface height magnitude spectrum (or the inverse of its slope in

log H and log *f* coordinates, as shown in *Figure 4-1*), $\sigma$ is the RMS height of the surface and N($\beta$) is a normalizing factor.

$$\mathrm{H}(f) = \frac{\sigma}{\mathrm{N}(\beta)} f^{-\beta} \tag{4.1}$$

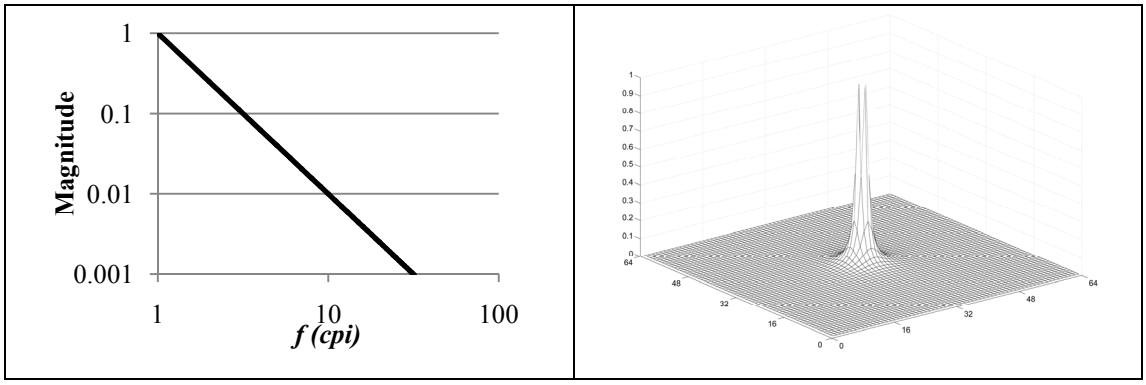


**Figure 4-1: Graphical demonstration of H(*f*) in the frequency domain, left for 1D whilst right for 2D ($\beta$ = 2.0).**

The height maps have a random-phase (see *Figure 4-2*), the $\theta$ symbol will describe the phase of the stimuli and any numerical value next to it will correspond to the random seed used with the Matlab random number generator. The code for generating $\theta$ is located in *Appendix 4-A* whilst the code to generate the magnitude in the frequency domain is located in *Appendix 4-B*. Therefore, the reader can accurately reconstruct any surface height map from this thesis.

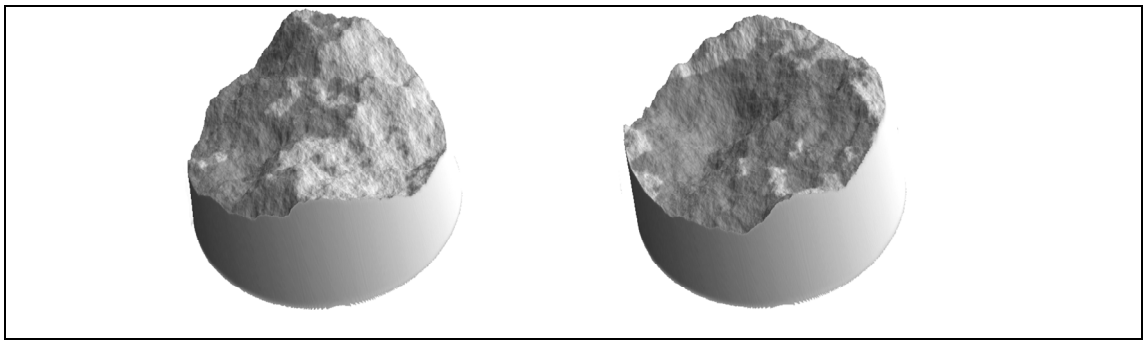

**Figure 4-2: two surfaces with different random phase values $\theta$.**

The N($\beta$) value is relative to the roll-off factor, these values can be obtained with Parseval's theorem (*Appendix 7-A*) or by changing the actual stimuli from frequency domain to spatial domain or vice versa. The actual value of each of the N($\beta$) values is enumerated in *Appendix 4-C*.

The magnitude spectrum for the height map H($f$) was sampled at 256 cycles per image width (*cpi*) as this is the minimum resolution which renders all the frequencies necessaries to cover human vision acuity (0.1 cpd to 30 cpd), as described by Campbell and Robson (1968).

The effects of varying the two parameters of the height magnitude spectrum, the RMS height ($\sigma$) and the roll-off factor ($\beta$) are illustrated for three-dimensional rendered examples of the surfaces in *Figure 4-3*.

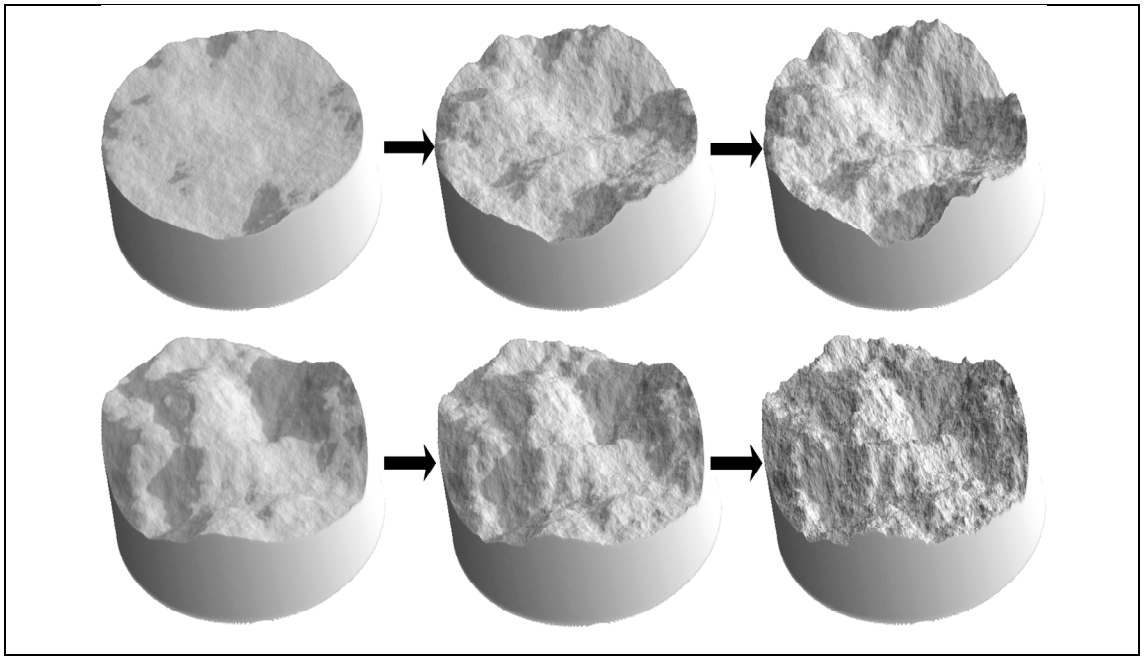

**Figure 4-3: The top row represents the effects of varying $\sigma$, whilst the bottom row illustrates the effect of changing $\beta$.**

As illustrated previously, the final renderings are full three-dimensional surfaces, these were produced from the height maps calculated using *Formula 4-1* (code *Appendix 4-D*). The next section will fully describe how the surfaces were transformed from simple height maps to full three-dimensional surfaces.

## 4.2 Construction of the stimuli

There are many techniques to convert a height map to three-dimensional surfaces (see *Figure 4-4)*; these have advantages and disadvantages in their implementations and their rendering quality. As a result, to facilitate the description of the models I will divide this section into four parts: reflectance, geometry, cast shadows and the stand shape.

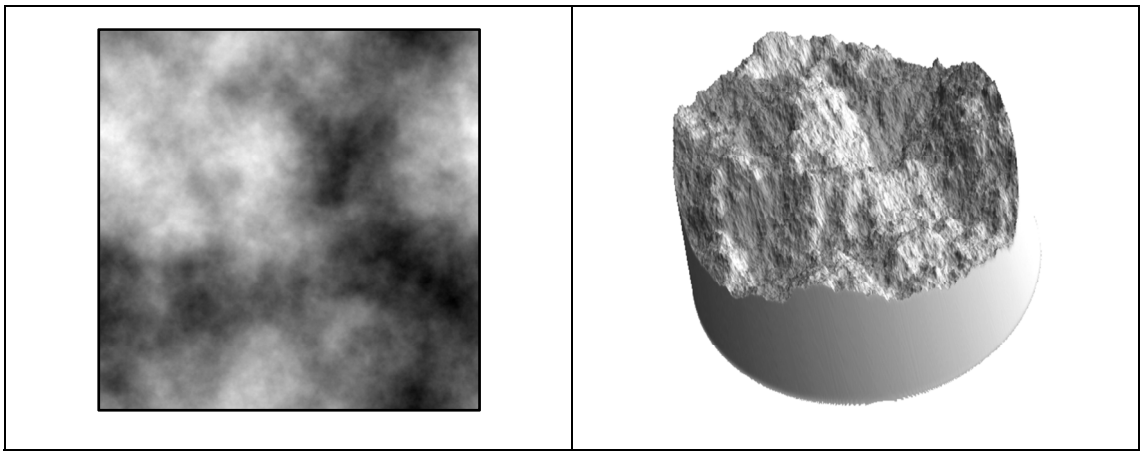

**Figure 4-4: On the left a simple height map whilst on the right the three-dimensional surface.**

The indirect light caused from the surface inter-reflections was not rendered, as it is impossible to realize them for real-time animations with the current hardware. Fortunately, research has demonstrated that inter-reflexions can facilitate the judgements of lightness (Gilchrist and Jacobsen, 1984) and surface contact (Madison, 2001) but these do not provide additional information for the perception of the three-dimensional surface shape as described by Liu and Todd (2004).

The lightness of the surface is pre-determined by the *albedo* of the surface material. In optics, the reflectance is the amount of incident radiation reflected by a surface whilst the *albedo* of a surface is the extent to which the surface itself reflects light back. Therefore, the albedo depends in the material properties and not in its geometry. For the stimuli in the experiments, the albedo is set to 0.60 or 60% to emulate lightness similar to a rock material and this is a little bit brighter than soil or sand (0.40). Unit albedo was found to be too bright for the stimuli, for example an albedo near its unit value is bright snow with an albedo around 0.90 (Ress, 1990).

### *4.2.1 Light and reflectance*

To represent the reflectance many methods or formulas exist, the most important are:

- *Lambert model*, which states that the radiation reflected, is proportional to the cosine between the observer's line of sight and the surface normal. This model was first published by Johann Heinrich Lambert in his Photometria book (1760). This model has been widely used in psychophysical experiments and computer graphics since them, Koenderink, Van Doorn and Pont (2003) discuss Lambert's law and perception in extend in his published work about the perception of light position. The Lambert model can be formulated as described in *formula 4-2* in its modern form (Kilgard, 2000), where $I_{amb}$ is the intensity of the ambient, $K_{dif}$ is the albedo of the surface, L is the light vector and N is the surface normal vector.

$$I_{lambert} = I_{amb} + k_{dif} \cdot \max(0, \mathrm{L} \circ \mathrm{N}) \quad \textbf{(4.2)}$$

- *Blinn model* is an empirical model extending the Lambertian's one to account for specularities in the surface. This model was first described by James Blinn (1977) and it is shown in *formula 4.3* where *V* is the view vector, *H* is the half vector between the light and view vectors and *SH* is the shininess factor. This model will not be used as our surfaces have only diffuse reflectance and specularities were not used to avoid confusing the observers.

$$I_{Blinn} = I_{amb} + k_{dif} \cdot \max(0, \mathrm{L} \circ \mathrm{N}) + k_{spec} \cdot \mathrm{I_{spec}} \cdot \max(0, \mathrm{H} \circ \mathrm{N})^{SH} \quad \textbf{(4.3)}$$

- *Phong model* was the first model to account for specularities in the surfaces, this is another empirical model and it was designed by Bui Toung Phong (1975), this model is also not used, as it is similar to the Blinn model.

- *Ray tracing models* are based on the idea to follow the rays of light from the eye position onwards; these models produce correct reflections and refractions for the surface but cannot be rendered in real-time. Wald, Friedrick and Marmitt

(2005) manage to render a surface with shadows (640x480 pixels) at just 0.3 frames per second but this is too slow for the animations in the experiments, as a result, ray-tracing methods cannot be used for the stimuli.

- *Global illumination models* take also into account indirect lighting, these are very accurate and can calculate the ambient intensity, but they are also very difficult to implement in real-time (Wald, Kollig and Benthin, 2002) (Benthin, Wald and Slusallek, 2003).

In summary, the most suitable reflectance model for the experiments is the Lambert model as it has the advantage of being accurate and fast. The other models are either too slow for the animations of the surface in real time or are not relevant to this study.

I would like to clarify that the surfaces for the stimuli used do not have microstructure as the resolution used for these texture pixel match the displays and each face is considered as a perfect diffuse with an albedo. Therefore, the surfaces have a Lambertian behaviour because they are free of scaling and resolution problems. An example of non-Lambertian behaviour caused by resolution is Opik's (1924) classical description of the reflectance of the moon. Any models that incorporate microstructure into them will not be used because of the perfect resolution of the surfaces used in this thesis; an example of this unused model is the Oren and Nayar model (1994).

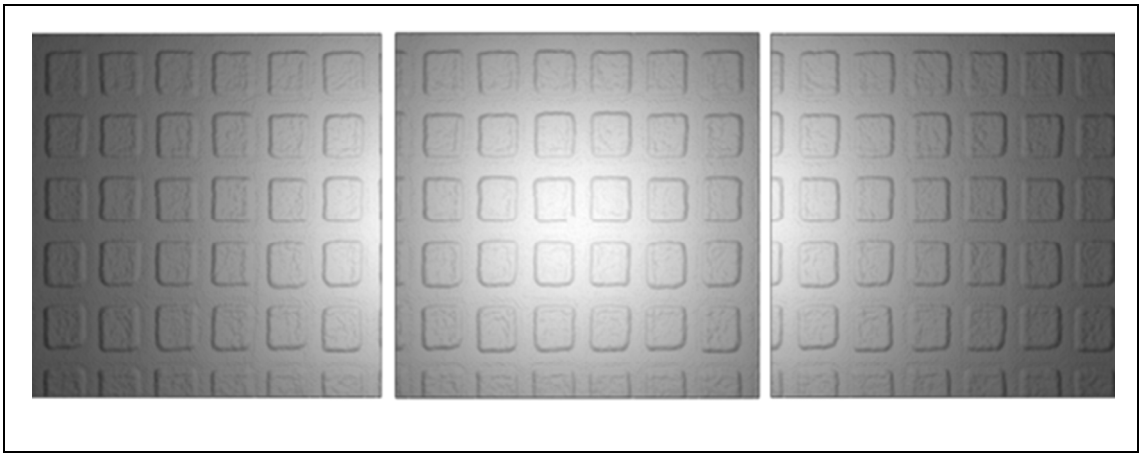

**Figure 4-5: A sample surfaces in fronto-planar view using per-pixel illumination illustrated with three different illuminant positions.**

The surfaces are per-pixel illuminated; with this method, the light can be applied to every pixel to avoid resolution errors. In addition, this method produces better results than the normally used per-vertex illumination, which produces unrealistic effects in surfaces (Shreiner, 2003). An example of this per-pixel illumination is shown in *Figure 4-5*.

However, lighting does not constitute a complete surface; a method for displaying the surface geometry is also necessary. Otherwise, the result would look correct in fronto-planar view but it would lack occlusions and edge in other views (e.g. profile). The technique of only illuminating the surface is called per-pixel bump mapping (Blinn, 1978) and its disadvantages can be observed in *Figure 4-6* when the surface is rotated.

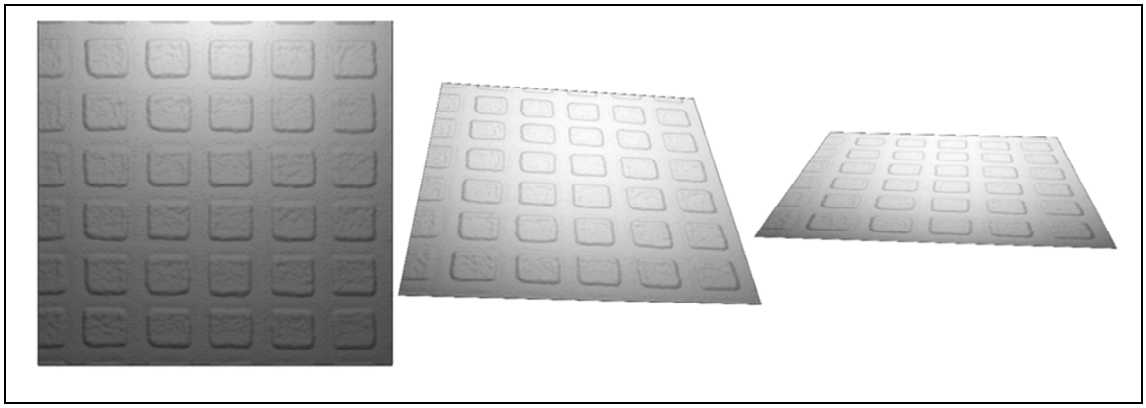

**Figure 4-6: Example of a surface rendered in three different viewpoints with reflectance only. This surface lack silhouettes and occlusions when not taking into account structure or geometry.**

### *4.2.2 Geometry, occlusions, silhouette and edges*

There are two ways of displaying correctly the effect of geometry in surfaces; these are by either displacing each of the pixels to their correct position in a plane or by tessellating the plane or displacing each vertex correctly. The first technique is commonly referred as *per-pixel displacement* whilst the second one is called *per-vertex displacement*.

Per-pixel displacement mapping has the advantages of reducing the amount of vertex transformations in hardware and the amount of memory needed for the vertices. The most important and relevant per-pixel displacement techniques are:

- *Parallax mapping* which was introduced by Kaneko et al (2001) in computer graphics were each pixel is offset in the (u, v) coordinates to represent correctly occlusions. The disadvantages of this method are the estimation artefacts, resolution problems and lack of cast shadows as shown in *Figure 4-7*.

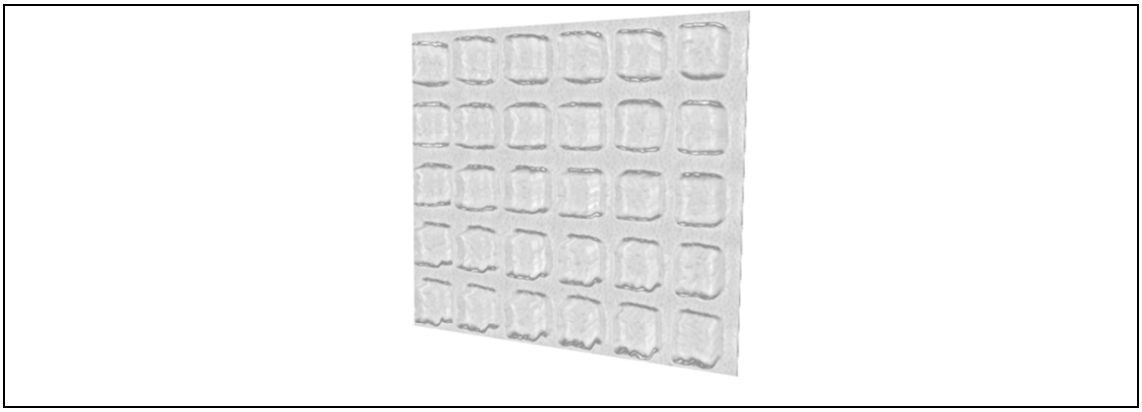

**Figure 4-7: Parallax mapping example. Note the lack of edges, artefacts at the bottom and lack of cast shadows.**

- *Horizon mapping* improves on parallax mapping by encoding the height at each point of the surface, its drawbacks are that it requires eight times the texture memory and the edges are still missing (Sloan and Cohen, 2000).

- *Ray tracing* implementations, these are more sophisticated and include casting a ray to displace correctly geometry as presented by Policarpo, Oliveira and Comba (2005) in their work about *relief mapping* as demonstrated in *Figure 4-8*. Alternatively, another example is *per-pixel displacement mapping with distance functions* by Donnelly (2005). Both of these suffer from approximation errors and lack of edges and silhouette.

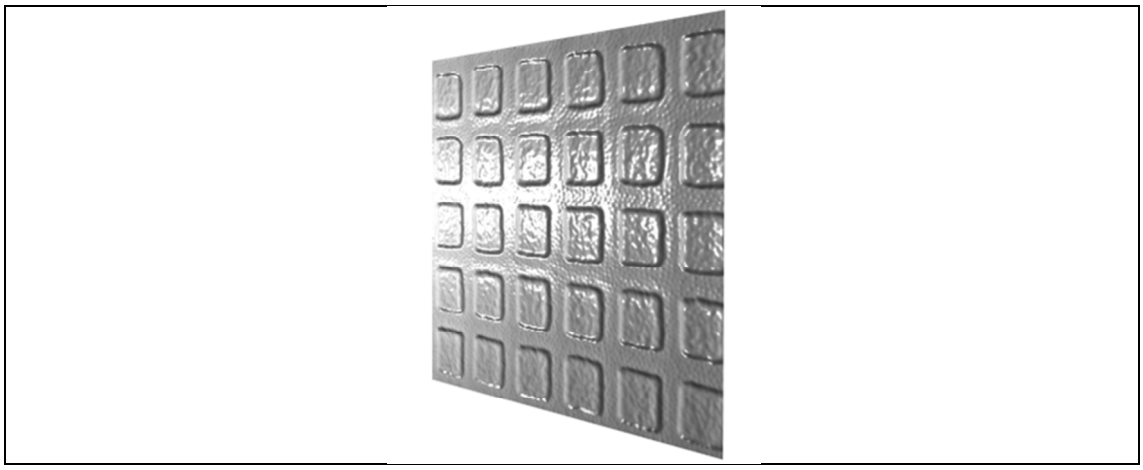

**Figure 4-8: Relief mapping example, note the cast shadows and improvement in artefacts but lack of edge or silhouettes.**

- Approximations errors were reduced by Oliveira and Policarpo (2005) in their newest work, and they also emulated silhouettes and edges by displacing inwards pixels and not filling holes. Although this technique produces all the necessary geometry elements in the surface, it is slow and still suffers from approximations caused by the tracing of the ray. A similar method is the one described by Hirche, Ehlert Guthe and Doggett (2004).

- Finally *view-dependent displacement mapping* invented by L. Wang, X. Wang, Tong, Lin, Hu, Guo and Shum (2003) allows for the efficient rendering of self-shadows, occlusions and silhouettes by performing its calculations in screen-space. This method was later extended by Wang, Tong, Lin, Hu, Guo and Shum (2004) to fix minor problems and allow the rendering of closed geometry, they called it *generalized displacement mapping*. Although this method produces a very realistic and correct geometry, it will not be implemented for the experiments as this algorithm is patented and it requires also a great amount of texture memory.

As summarized previously, per-pixel displacement suffers from three main problems:

1. the real-time methods lack edges and silhouettes,
2. the ray tracing algorithms have approximation errors, and
3. few render cast-shadows at the same time.

Because the experiments need to be as accurate as possible, then approximation errors also need to be minimised; it is crucial for the perception of roughness that the stimuli are complete, including silhouettes and edges as it is unknown if observers use these to judge roughness. Cast shadows are necessary as these help human perceived better shape as described by Liu and Todd (2004).

For those reasons, per-vertex displacement will be used to render the stimuli in the experiments as with this method all the disadvantages of per-pixel displacement are solved. Robert Cook (1984) was the first to introduce this method, this type of displacement has been used in passive renderers over the last few years as it produces excellent results. The disadvantage of using this method is that it needs a huge amount of memory and bandwidth to save all the vertices geometry and transformations.

There have been studies to optimize the tessellation of the displacement maps to save vertices, like the work from Moule and McCool (2002) were they optimize meshes by doing a view-dependent tessellation. Alternatively, Lee, Moreton and Hoppe (2000) describe a method to optimize the displacement in their work referred as *displaced subdivision surfaces*. However because in the stimuli only surfaces are used, then it is possible to optimize differently the displacement for only the experiments in this thesis.

To achieve maximum output speed, first a planar mesh is cached in the video card memory, as seen in the left side of *Figure 4-9*; this mesh will be process in strips, as it allows a more optimal concurrent processing in the video card as detailed in the NVIDIA programming guide (NVIDIA, 2005). Then each pixel will be displaced matching its position to the height map as detailed by Gerasimov, Randima and Green (2005). Finally, to avoid exceeding the video memory, the pre-displaced mesh is instantiated twice, therefore the height map is the only element of the surface that changes for each trial in the experiments.

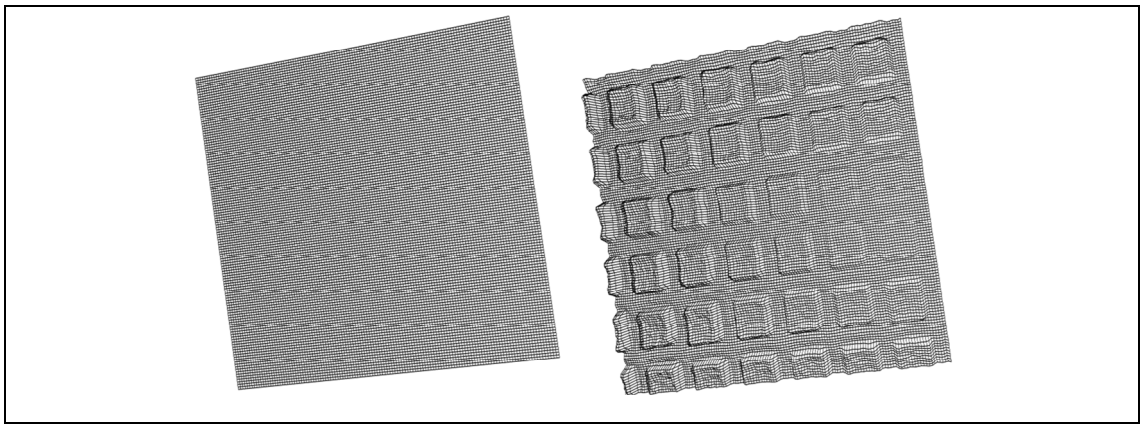

**Figure 4-9: Mesh on the left is loaded into video memory then is per-vertex displaced by a height map in real-time.**

The height of the displaced mesh can be varied by programming the offset for each vertex in the graphics card. However, this method it is not suitable when displacing the surfaces with very large magnitudes as the frequencies (specially >128 cycles per image width) are stretched too much and form patches that are perceived as being very smooth because they constitute just displaced geometry (see *Figure 4-10*).

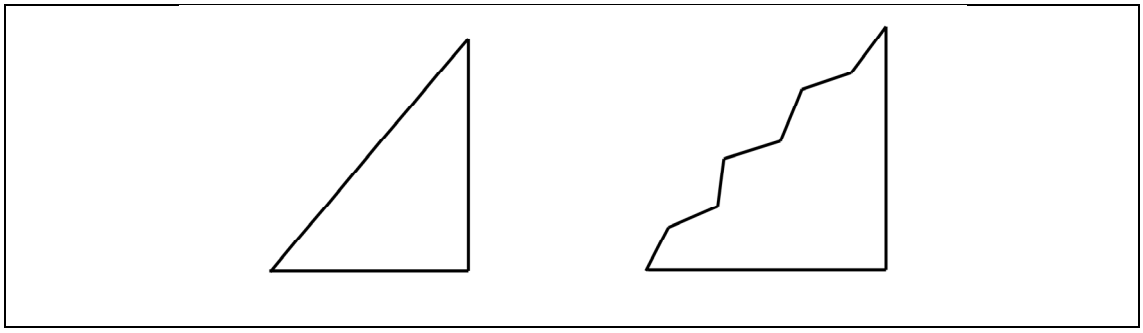

**Figure 4-10: Example of a simple polygon displacement, on the left a normally displaced polygon. Note how these appear very smooth. On the right, the correct shape of the sample.**

The final surface mesh consisted of a quarter of a million polygons, fully illuminated and with variable height, can be rendered interactively at least 60 times per second. However, it still lacks cast shadows, therefore in the next sub-section these will be added to the model.

### *4.2.3 Cast shadows*

Excluding ray tracers, there are two main ideas for constructing real-time cast shadows:

1. *Shadow volumes*, this is an object space approach. These methods use complex and expensive calculations to render the shadows, these also use large amounts of fillrate (Wimmer, Scheerzer and Purgathofer, 2004) but they deliver high precision shadows. These algorithms cannot be implemented for the surface rendering as they only calculate shadows from one object cast into a second one (or a surface) and not to itself (Crow, 1977).

2. S*hadow mappin*g, are simple methods where the calculations are done in scene geometry, therefore all light shadows are calculated in one extra pass (object-cast and self-cast shadows). The drawback of these methods is that they suffer from aliasing artefacts as these use an image space approach (Lipp, 2005).

Shadow volume techniques cannot be used because of the high count of polygons per surfaces (quarter of a million) and the inability of this to produce self-cast shadows.

The shadow mapping algorithm used to render the cast shadows in the surfaces consist of the following steps (as illustrated in *Figure 4-11*):

1. The scene is rendered, as seen from the light position, in a shadow map image ($depth_{shadow}$) where every pixel depth from the shadow plane is stored using the z-buffer of the scene.
2. The scene is rendered from the view position and stored in $perspective_{view}$, this view is changed to $depth_{view}$ by first multiplying it by the inverse model view matrix (world space), then transforming it to a shadow plane projection, later normalizing it to device coordinates (NDC) and scaled to [0,1] and finally applying a perspective division. Everitt, Rege and Cebenoya (2002) discusses thoroughly the matrices calculation and implementation for this step.
3. The two depths are then compared so if $depth_{view} > depth_{shadow}$ then the pixel P lies in shadows otherwise the Lambertian reflectance is applied.

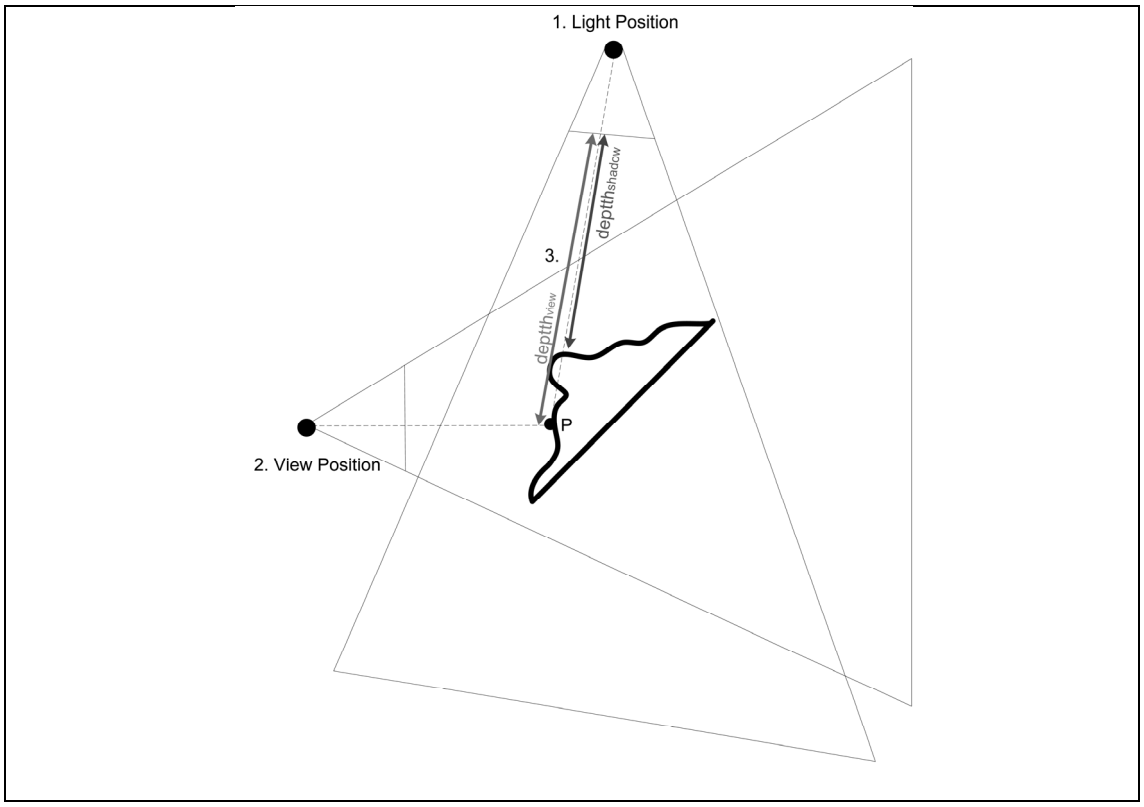


**Figure 4-11: illustration of the shadow mapping method.**

Unfortunately, two kinds of artefacts occur when using the shadow mapping technique as this is an image space approach. The first artefact known as perspective aliasing or projective aliasing is caused by the discrete nature of the depth maps where aliasing exists when the two planes do not match in pixel size (Wimmer, Scheerze and Purgathofer, 2004). The second kind of artefact is known as surface moiré or incorrect self-shadowing and it is produced by the quantized depths, because these have finite precision (Willians, 1978).

To fix some of the aliasing effects, first both of the depth maps were over-sampled at four times (4096x4096) the normal screen resolution (Fernando, Fernandez, Bala and Greenberg, 2001). Second, the depth maps from the light position were rendered twice, front and back faces (Weiskopt and Ertl, 2003). Finally, the z-values of depth maps were changed from logarithmic scale to linear scale (Brabec, Annen and Seidel, 2003).

The cast-shadows in the surfaces were also softened using a 3x3 pixel gaussian blur to give them a more natural look and feel, as soft-shadows are impossible to implement in real-time for the surfaces (Hasenfratx, Lapierre and Holschuch, 2003).

Due to hardware limitations, algorithms that are more complex were not implemented, like for example: perspective shadow maps (Stamminger and Drettakis, 2002) (Kozlov, 2004), light space perspective shadow maps (Wimmer, Scheerze and Purgathofer, 2004), variance shadow maps (Donnelly and Lauritzen, 2006), trapezoidal shadow maps (Martinand Tan, 2004) or convolution shadow maps (Annen, Mertens, Bakaert, Siedel and Kautz, 2007).

### *4.2.4 Stimuli stand*

Finally, to avoid biasing the observers with any edges in the stimuli mesh and to achieve a more 'real sample' appearance; the final meshes were cropped with a circular circumference to produce a stand. These can be observed in *Figure 7-12*; this stand had a height of 2.5cm.

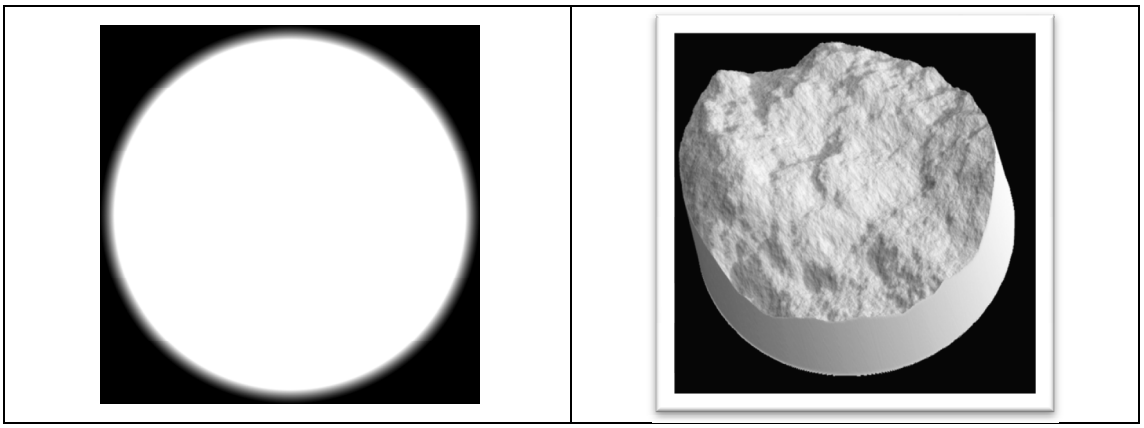

**Figure 4-12: On the left the stand shape as a height map and on the right the final rendering of the stimuli.**

As described previously, the stimuli will be rendered with Lambertian shading, where per-vertex displacement mapping is used to render correctly the geometry and the cast shadows are calculated using shadow mapping techniques. Due to limitations in hardware, better cast-shadows and inter-reflections were not implemented but I am confident this method produces the best possible tradeoffs between having an interactive stimuli and quality. The next section will describe how the animation was developed.

## 4.3 Animating the stimuli

As described in the previous chapter, the stimuli are animated to avoid light and viewpoint ambiguities and at the same time allow depth perception. An experiment was designed first to discover how subjects manipulate the motion of surfaces.

Before the experiment could be realized, a method was needed so observers could manipulate the surfaces. A mouse or keyboard interface was chosen instead of specialised hardware as most subjects use them every day. Four usable interfaces exist that can use the keyboard and mouse to rotate the surfaces:

1. *Euler angles* (also known as yaw, pitch and roll); the advantage is that subjects are familiar with them. However, the limitation is that the interface produces the 'gimbal lock' problem where one rotational gimbal cannot compensate for rotations in that direction anymore therefore not all the viewpoints can be specified.
2. *Vector roll*, this was popularized by OpenGL and their GLRotate function where the subject chooses a roll angle and an X, Y, Z-axis. This interface can describe any viewpoint but it is very unintuitive.
3. *ArcBall* using quaternions allows the description of a three-dimensional viewpoint by wrapping a ball sphere around the object (see *Figure 4-13*). This interface was first implemented by Ken Shoemake (1985) and the benefits are that the interface is very intuitive and any viewpoint can be fully described.

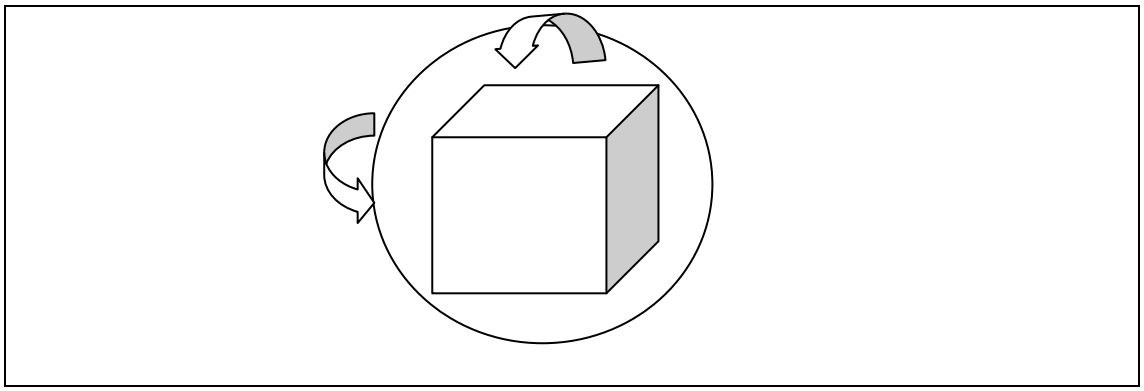

**Figure 4-13: Illustration of an arcball interface.**

4. *Elevation and azimuth*, this is where the subjects specify both parameters. The advantages are that is very intuitive and the parameters do not interact between

each other, the disadvantages are that it is not possible to specify all of the viewpoints.

From the four interfaces, the ArcBall was chosen as it can specify all the viewpoints and it is very intuitive; this was also concluded by Hinckley, Tullio, Pausch, Proffitt and Kassell (1997). They also found in their usability studies that the ArcBall had an accuracy of 5.1 degrees.

As mentioned earlier, an experiment was developed to discover the preferred viewpoint when judging surfaces; this will later be used for the animations of the stimuli. In this experiment, two surfaces where rendered at the same time, with different $\beta$ {1.8, 2.2} and $\sigma$ {0.8cm, 1.2 cm} and $\theta$ {1, 2} values. The observers were then asked to annotate which surface felt rougher if touched; the subjects had an ArcBall interface to rotate the surface and were not time constrained when making their decisions. All rotations were saved at each frame and the experiment was setup as described in *Chapter 5*.

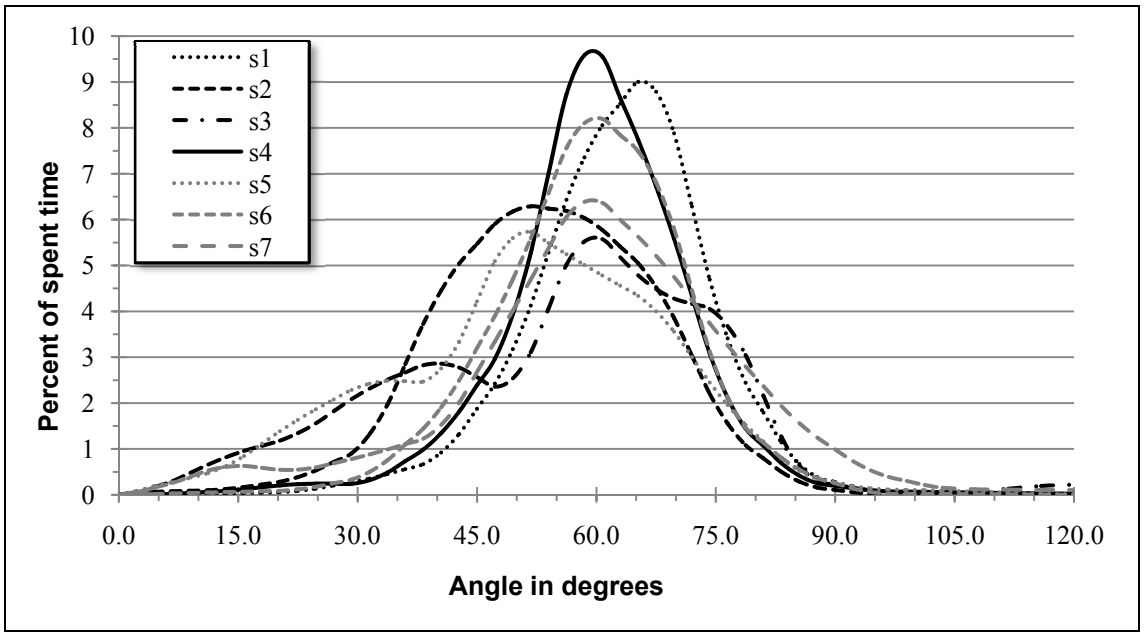


**Figure 4-14: The angle between the surface normal and the light position and the percentage of time each observer spent comparing the two surfaces.**

Seven observers took part in the experiment; the results show no preference to any specific slant, tilt or rotation. However, there is a clear indication that observers preferred to have an angle between the surface normal and the light of about 60 degrees

as show on *Figure 4-14* for each observer (values described in *Appendix 4-E*) and *Figure 4-15* for all the observers. A gaussian function was fit to the average of the results to show that the observations follow this function, which has a centre or mean of 60 degrees and a variance of 8 degrees.

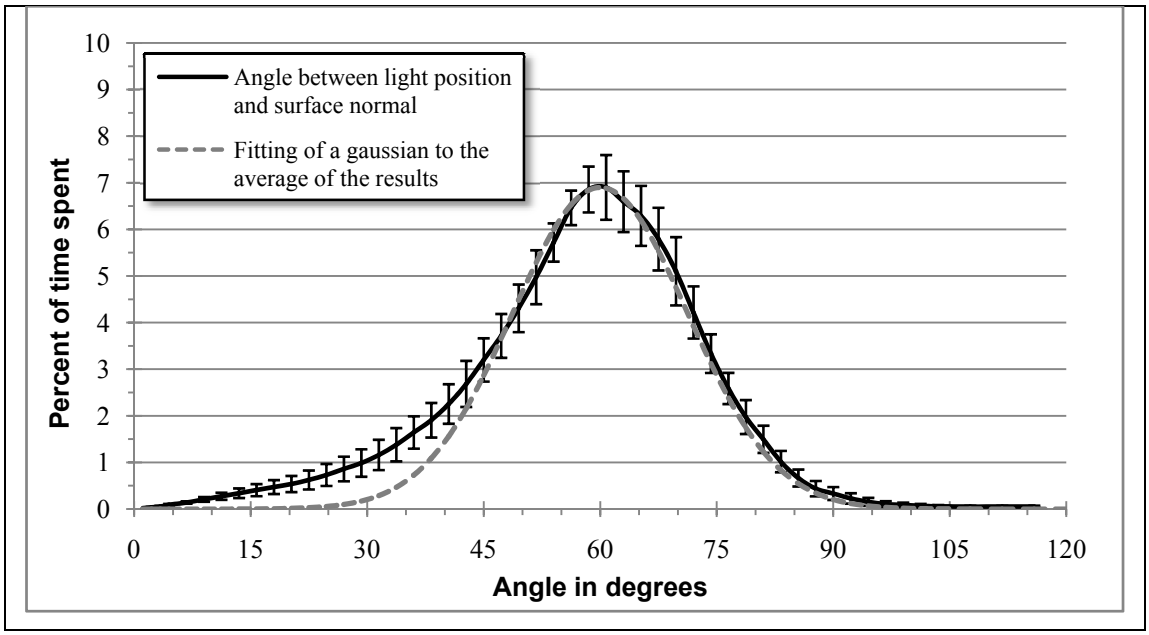


**Figure 4-15: The average of the preferred view for all the seven observers and a fitting gaussian function to the average of these results.**

It was also noticed from the experiment data, that the observers wobble the surfaces, as they would do if they had the real samples. For that reason, an animation was developed which encapsulates the preferred viewing angle and the wobbling motion. This was done by selecting a section of the saved animation which had both of the previous attributes (angle and wobble). The final animation to be used in the next experiments is illustrated in *Figure 4-16* for the angle between the surface and the light. *Figure 4-17* illustrates the three-dimensional rotation of the surface as seen from the light position to the surface normal.

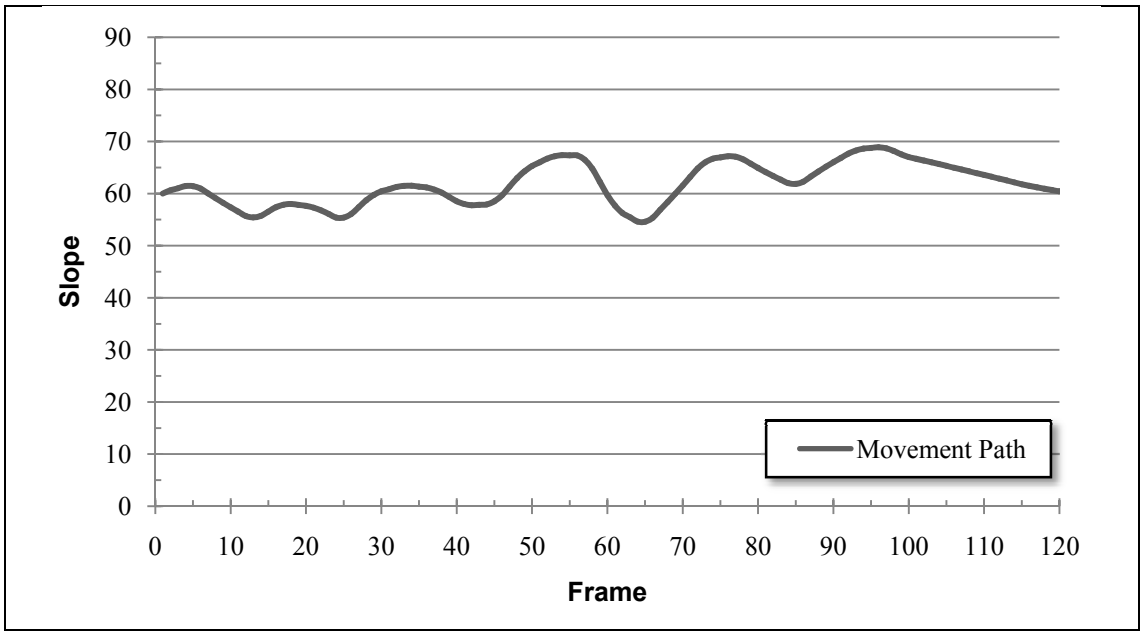


**Figure 4-16: Movement path of the animation for later experiments.**

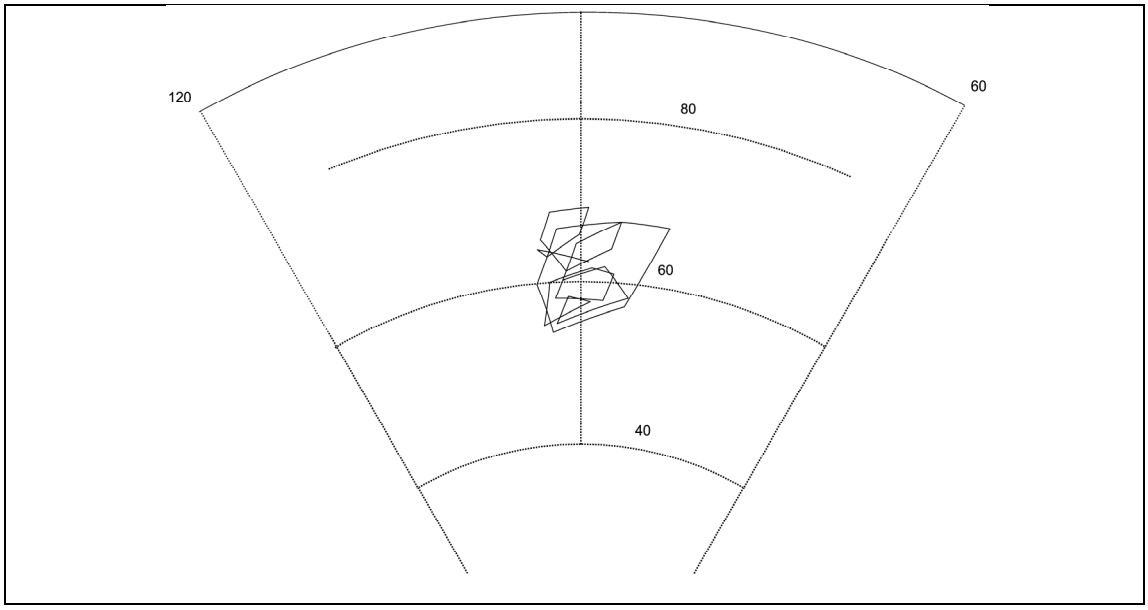


**Figure 4-17: Rotation of the surface normal as seen from the light position.**

## 4.4 Summary and Discussion

This chapter discusses and summarizes how *$1/F^{\beta}$ noise surfaces* were constructed. It starts by giving the general mathematical formula for the surfaces and then it illustrates how each parameter changes roughness.

In its second part, it discusses the general construction and rendering of the *$1/F^{\beta}$ noise surfaces*, including a short summary of the related algorithms for reflections, geometry representation and cast shadows. It concludes that the best way of rendering the surfaces is a trade-off between accuracy and quality, where the surfaces have perfect illumination and geometry but cast shadows and inter-reflections can be improved in the future. The final render uses per-pixel Lambertian illumination with per-vertex displacement mapping to represent the geometry and cast shadows produced using shadow mapping techniques.

Finally, the last section describes the animation and it discusses also that this was developed from a simple experiment, where it was found that observers like to judge surfaces when viewed at a 60-degree angle between the light position and the surface normal. In addition, a wobbling motion around this angle was also identified from the observers' judgements.

In the next chapter, the experimental setup will be discussed where the environment, tools and calibrations will be described.

# CHAPTER 5

# EXPERIMENTAL SETUP

Previously the experimental method and stimuli construction were discussed; in this chapter I will discuss the experimental constraint, tools and calibration methods for the experiments to be used in following chapters. The discussion that will take place in this chapter is necessary as any un-calibrated tool or external distracters can cause unsuspected errors in the psychophysical experiments. The goal was to design and build a controlled environment free of all possible distractions to obtain the most reliable observations; also all equipment was calibrated and set appropriately for each experiment.

This chapter is divided into four sections, where *Section 5.1* discusses the design and construction of the controlled environment, *Section 5.2* argues the use of the tools for the experimental setup, *Section 5.3* discussed the monitor calibration methods. *Section 5.4* presents a summary of the chapter as a whole.

## 5.1 Constrain environment

First, the observers' visual acuity was tested for 20/20 vision (maximum resolution of 30 cycles per degree), a well lit *Snellen chart* was used to test each subject. Although this chart is well known for its designs flaws (Thomson, 2005) specially when observers read part of the characters in a line, but in the experiment each volunteer accurately read all characters from the 20/20 line, therefore the Snellen charts were still used to measure visual acuity.

Knowing that every subject could observe up to 30 cycles per degree allows calculating the distance from the subjects' eyes to the screen. To follow the 'natural approach', the distance would have to be as if the observer was naturally holding the surface, this *arms' length* distance is around 30 cm for a flexed arm or around 60 cm for a stretched one (own measurements). To achieve this distance with a resolution of 30 cycles per

degree, the display would need to have a minimum resolution of 300 pixels per inch (also known as dpi – dots per inch) at 60cm or 600 pixels per inch at 30 cm. However, these resolutions are not currently available for commercial monitors therefore the distance between the subject and the display was increased to an unnatural distance but at this distance the subjects were able to perceive the full range of visual frequencies

As a result, a monitor with high resolution but small screen size was used to minimize the distance of the observer to the display. As later described in *section 5.2* a 20-inch monitor with a UGA resolution (1200x1600) was chosen, this display has a pixel size of 0.255mm (100 dpi). To display a maximum resolution of 30 cycles per degree the observer was positioned at 87.74 cm away from the display, the observer's head was fixed at this distance for all the experiments using a chin rest.

The surface width and length was chosen so it would include displaying frequencies up to the biggest frequency range of 0.11 cpd as described by Campbell and Robson (1968). Therefore, surfaces had a maximum resolution of 512 cycles per image width and a size of 13.056cm as so to display frequencies with a minimum resolution of 0.1 cpd and a maximum resolution of 30 cycles per degree.

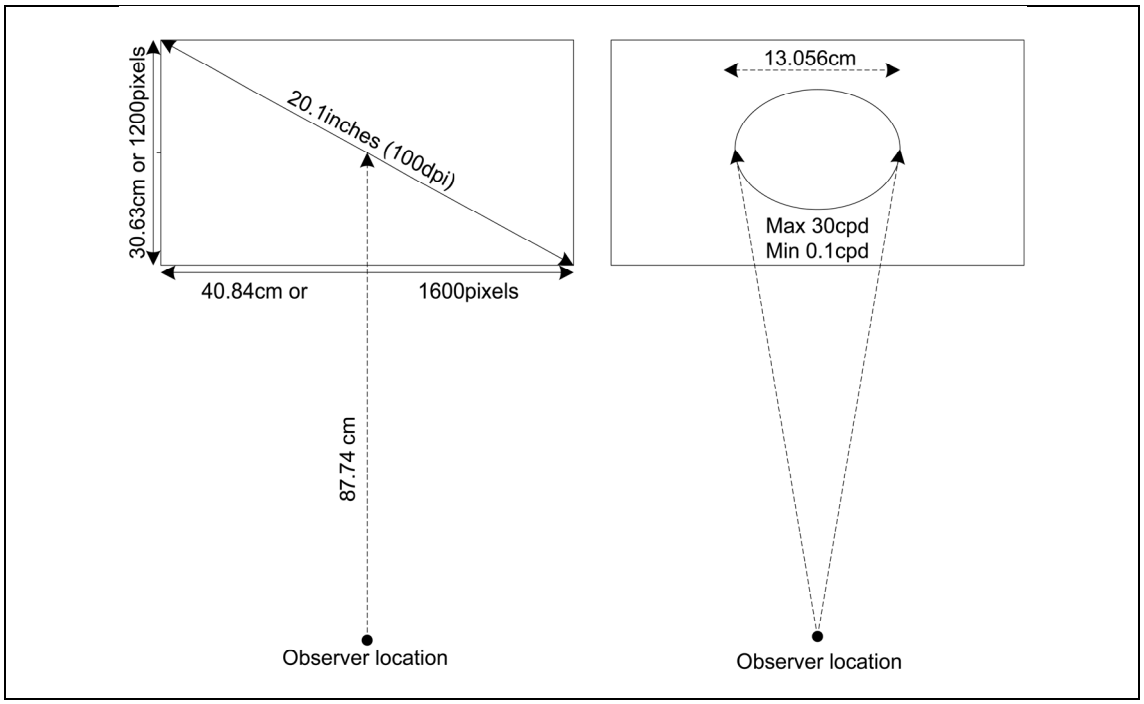


**Figure 5-1: Illustration of the experimental setup.**

The surfaces' rendering had correct perspective (surface displayed at 87.7 cm), also the surfaces had a maximum luminance of 100 cd/m$^2$ including compensating for the ambient light of the room. The room had a normal indirect daylight to avoid alienating observers and avoid observers' contrast perception being adjusted throughout the experiment length (as normally happens when a person enters a dark cinema).

A short summary of the experimental setup is illustrated in *Figure 5-1*. In the next section a discussion about the chosen tool will follow.

## 5.2 Tools

The tools section is divided in three parts: displays, software and hardware. These groups were chosen only to facilitate the organization of this section.

### *5.2.1 Displays*

The representations (renderings) of the stimuli must be as close as possible to the actual real sample to avoid, or at least reduce, the insertion of errors in the observations. If no precautions are taken then the errors will later affect the calculations of the perceptual model; for that reason, this section will discuss the latest display technology for the experiments.

There are many technologies available for displaying images; these include and are not limited to CRTs, LCDs/TFTs, projectors, DLPs, etc. Although it is possible to build the experiments using any of these technologies only CRTs and LCDs/TFTs will be discussed here, as these two are the most viable solutions and they offer the best performance in terms of image quality and colour reproduction.

For many years CRTs have been the facto display technology for psychophysical experimentation, CRT technologies are very mature and they have become common tools in laboratories where they are systematically used, errors and calibrations procedures are also well documented for CRTs. However, for our experiments flat panel

LCDs/TFTs displays are used; the main reasons for choosing flat panels technologies instead of CRTs are:

1. The *spatial modulation transfer function* (MTF) of flat panel display is superior to the MTF of CRTs. As reported in monitor calibration studies (Blume, Steven, Ho, Stevens, Abileah, Robinson, Roehrig, Fan, Chawla and Ghandi, 2003) the maximum MTF for a flat panel display is around 0.90 whilst for any CRT this figure varies dramatically from 0.07 to around 0.50 depending on the display manufacturer. This is the main reason flat panels were chosen instead of CRTs, is that CRTs would have undermined high frequencies in the surface stimuli therefore pre-biasing the observers' judgements and consequentially miscalculating any frequency-weighted model.
2. The *gamma correction* in flat panels has been known for being arduous to achieve, but with modern hardware spectrometers (see *Section 5.2.3*) and better calibration software, this is no longer the case. At the same time modern flat panel displays' look up tables have more resolution (8-bits, 10bits or 12bits per colour) making the task of gamma calibration more accurate and less time-consuming.
3. The *luminance uniformity* was fixed using a related method to Blume et al and the uniformity of the luminance across the screen in the flat panel displays was found to be better than the one of CRTs.

| CRT | Flat Panel |
|---|---|
| Corrections must be done to obtain accurate geometry but errors are still introduced | The geometry is perfect as the array of pixels in perfectly aligned |
| Not uniform sharpness across the screen | Sharpness is uniform across the screen |
| Good contrast ratio | Contrast ratios are not as good as CRTs currently but these can be improved in controlled environments |
| Perfect black is achievable | Lowest black is around 1cd/$m^2$ |
| Reflections can be reduced using a dark room | Reflections can be reduce too with a dark room |
| Contrast ratio is independent of the viewing angle | Contrast changes with view angle but this is not crucial as observers' view is fixed and in a frontal planar view |

**Table 5-1: Comparing CRTs and flat panels displays.**

Other important factors when comparing CRTs with flat panel displays are described in *Table 5-1*. All these extra features in flat panels add a strong support for using this instead of CRTs for the experiments.

The monitor chosen for the experiments was the NEC MultiSync LCD (LCD2090UXi), this has an A-TW-IPS (in-plane switching) panel manufacture, which offers more improvements in comparison to normal LCDs like improved viewing angle, better colour reproduction at the cost of speed, 10-bit look up tables, more natural whites, increased gamut, increased contrast ratio and support for true 8-bit colour without dithering methods.

| Specifications | NEC MultiSync LCD2090UXi |
|---|---|
| **Panel** | A-TW-IPS TFT |
| **Screen size** | 51.0 cm (20.1 inches) |
| **Input** | DVI-D |
| **Response time** | 8 ms (gray to gray) |
| **Pixel pitch** | 0.255 |
| **Viewing angle** | 178 degrees horizontal / 178 degrees vertical |
| **Contrast ratio** | 700:1 |
| **Brightness** | 280cd/$m^2$ |
| **Frequency** | 85 Hz |
| **Resolution** | 1600 x 1200 pixels |

**Table 5-2: Table of the NEC monitor specifications.**

Due to the panel manufacture, this NEC monitor is perfectly suited for the psychophysical experiments, as this fixes most of the deficiencies of LCD panel like contrast, view angle and colour reproduction. In Section 5.3, it is demonstrated how the monitors were calibrated for the experiments.

### *5.2.2 Software*

For constructing the stimuli Matlab (www.mathworks.com) was used; the code of the program can be found in the *Appendix 4*. Matlab was also used to optimize the model for perceived roughness as described in *Chapters 7*, *8* and *9*.

For displaying the surfaces, OpenGL 2.0 (www.opengl.com) was used to render the surfaces as described in *Chapter 4*. The interface was programmed in C++ to add speed, the Microsoft .NET framework 2.0 (msdn.microsoft.com/netframework) was used to parse external strings and XML models and finally the DEVIL image library (openil.sourceforge.net) was used to interface the height maps from Matlab to the rendering program.

### *5.2.3 Hardware*

To restrict the head movement from the observers an UHCOTECH Headspot was used, this is a general-purpose observer-positioning device that attaches to any desk. It can be height adjusted depending on the viewer; it is made of aluminium alloy and finished in "optical" black.

For the interface between the observer and the program a standard keyboard was used, where only the space bar was used to register when the surfaces matched in roughness, as for the adjustment of the surface parameters (up and down) (or the movement of the ArcBall) a standard optical mouse was used.

To render the surfaces two NVIDIA 7900 cards were used, connected to a dual core AMD X2 3500+ machine with enough ram. The final rendering speed was 15 frames per second for the experiments with adjustable surfaces and 24 frames for the experiments with fixed parameters.

Finally, to calibrate the monitors a Gretag-Macbeth Eye-One Pro spectrometer and a Cannon 350D D-SLR camera were used. The calibration methods are further described in the next section.

## 5.3 LCD Monitor calibration

The monitors need to be calibrated to avoid errors in the observations as described by Roehrig, Chawla, Krupinski, Fan and Gandhi (2004). The monitors were calibrated to

display a linear gamma with a white balance similar to the sun colour (chromaticities set to x=0.3233 and y=0.3326) (5750 Kelvin) and a luminance of 100cd/cm$^2$.

As seen in *Figure 5-2,* the gamma differs greatly from an un-calibrated display (left one) to a one that has been calibrated (right one). An Eye-One Pro spectrometer was used to calibrate the gamma and colour, the resulting errors in calibration are shown in *Table 5-3*.

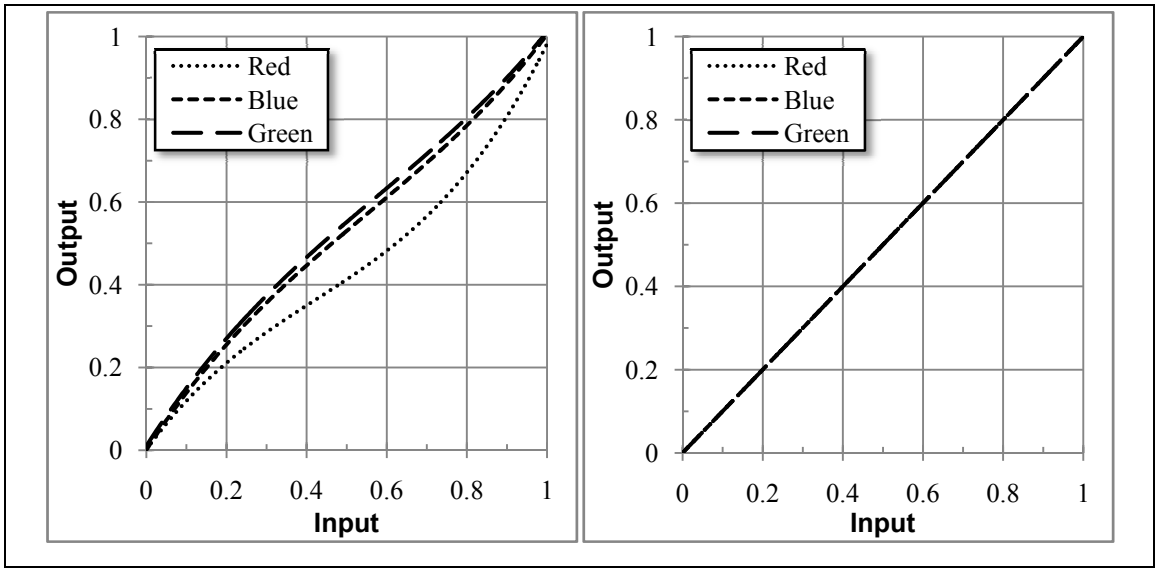


**Figure 5-2: On the left, an un-calibrated linear gamma and on the right a calibrated one.**

| | Average Error | Maximum Error |
|---|---|---|
| **Monitor 1 Red** | 1.09% | 2.35% |
| **Monitor 1 Green** | 1.29% | 2.74% |
| **Monitor 1 Blue** | 1.12% | 2.35% |
| **Monitor 2 Red** | 0.30% | 0.78% |
| **Monitor 2 Green** | 0.54% | 1.37% |
| **Monitor 2 Blue** | 0.24% | 0.78% |

**Table 5-3: A compilation of all the error when calibrating the gamma in percentage.**

To calibrate the luminance across the screen a digital SLR camera was used to take pictures of the screen as described by Blume et al (2003); later these pictures were transformed to compensate for the display variations, to apply the compensation to the

screen luminance, the renderings were altered per-pixel using a soften version of the compensation images. *Figure 5-3* shows an image of the screen variations in luminance before being calibrated and *Table 5-4* describes the errors in the display.

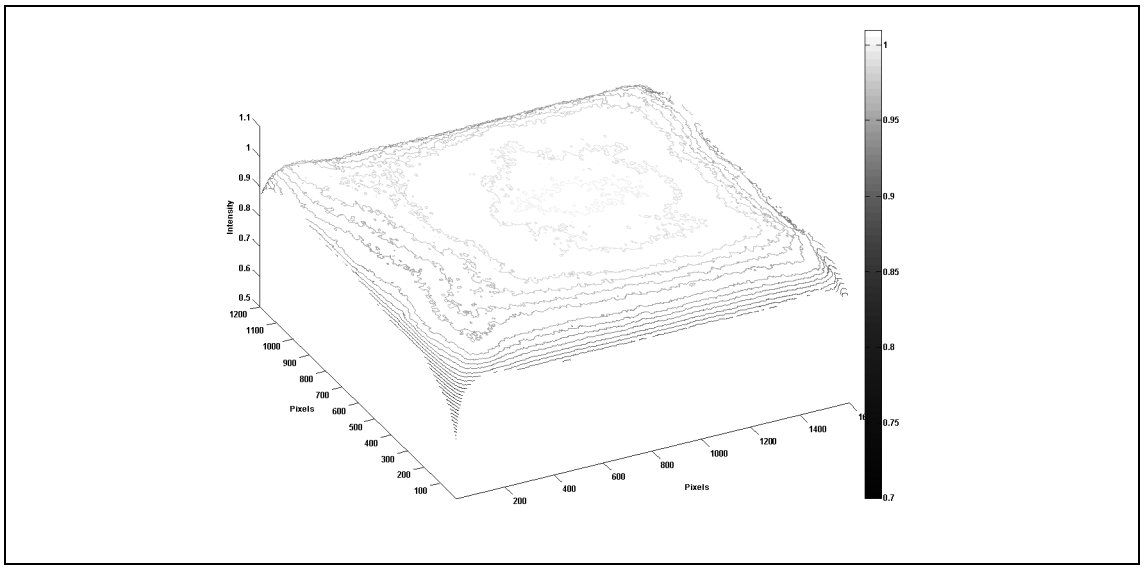


**Figure 5-3: Luminance across the screen from an un-calibrated display.**

| Monitor | Luminance $cd/cm_2$ | Border Screen | Border Texture | Centre | Border Texture | Border Screen |
|---|---|---|---|---|---|---|
| **One** | *100* | 1.71 | 0.40 | 0.03 | 0.07 | 1.13 |
| | *75* | 1.08 | 0.12 | 0.06 | 0.13 | 0.16 |
| | *50* | 0.97 | 0.40 | 0.00 | 0.13 | 0.07 |
| | *25* | 0.13 | 0.32 | 0.08 | 0.27 | 0.19 |
| **Two** | *100* | 1.47 | 0.18 | 0.03 | 0.02 | 1.15 |
| | *75* | 1.02 | 0.06 | 0.10 | 0.18 | 0.73 |
| | *50* | 0.67 | 0.13 | 0.01 | 0.16 | 0.61 |
| | *25* | 0.11 | 0.13 | 0.03 | 0.11 | 0.40 |

**Table 5-4: A compilation of all the error when calibrating the gamma in percentage.**

The maximum total variation across luminance and gamma across the surfaces in monitor one was 5% and 3% for monitor two, which shows that these methods for monitor calibration of LCDs produce excellent calibrations.

## 5.4 Summary and Discussion

In this chapter, the display technologies were described and it was argued that LCDs are the best choice for displays for the experiments. In addition, the tools were described and the method of calibration was also explained, including the final errors (maximum 5% error) for the calibration. In the next section, perceived roughness in *$1/F^{\beta}$ noise surfaces* will be studied.

# CHAPTER 6

# ROUGHNESS IN $1/F^B$ SURFACES

The main objective of this thesis is to develop a measurement model for perceived roughness of *$1/F^\beta$ noise* surfaces. These surfaces were chosen because they look natural, are isotropic, and are fully described by three parameters ($\sigma$, $\beta$ and $\theta$). This chapter's aim is to carry out a first investigation into the way in which these parameters affect perceived roughness. Thus its goals are:

1. to discover whether or not each of these parameters independently affects perceived roughness, and
2. to investigate how the parameters that do affect roughness interact with each other.

The work is organised as follows: the independent investigations of $\sigma$, $\beta$ and $\theta$ are described in *Sections 6.1, 6.2* and 6.3 respectively, while *Section 6.4* reports on the combined effect of varying both $\sigma$ and $\beta$.

## 6.1 The effect of varying RMS roughness ($\sigma$) on perceived roughness

As discussed in *chapter two*, the classical roughness definition is *root mean square roughness* (*RMS* or $\sigma$). By observation, one can discern that changes in $\sigma$ do affect perceived roughness (e.g. Figure *6-1*). This relationship is investigated further here.

*RMS roughness* affects several cues that could be used to estimate surface characteristics, for example the height profile, shadows produced by the peaks, occlusions from neighbouring slopes, global luminance, shading of the surface, etc. To the author's knowledge, no single cue has been discovered which correlates with perceived roughness. However, Ho, Maloney and Landy (2007) (2008) proposed a model of perceived roughness comprising a linear combination of quantifiable visual cues.

In contrast, we directly investigate the influence that measurable surface parameters have on perceived roughness, and in this section, we investigate the affect of varying $\sigma$ while holding $\beta$ and $\theta$ constant (as shown in *Figure 6-1* below).

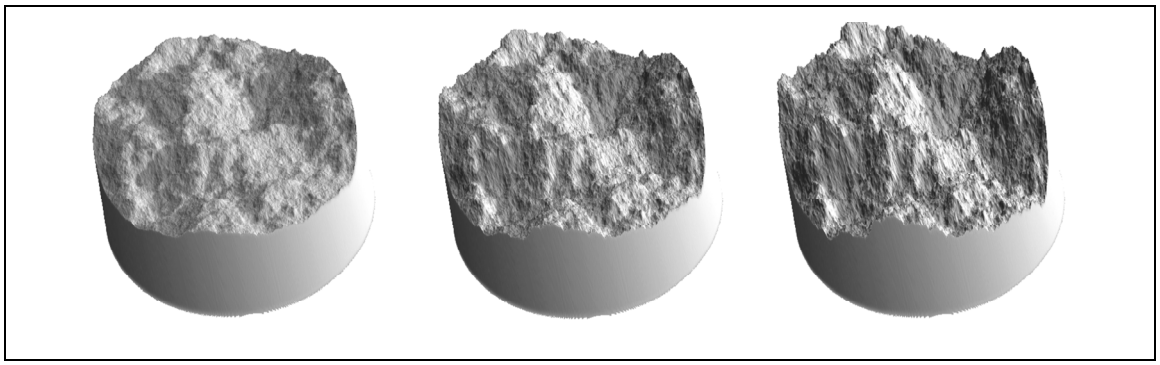

**Figure 6-1: Demonstrates three surfaces with similar $\beta$ {1.8} and $\theta$ {23} but different $\sigma$ {0.6, 1.0 and 1.2}.**

A $\sigma$ of zero produces planar (completely smooth) surfaces. We argue therefore that *human observers will perceive surfaces with larger values of σ as being perceptually rougher*.

To test this hypothesis a simple experiment was designed in which three non-naïve observers were asked to compare three surfaces and to order them according to their perceived roughness. Each surface had a *different* $\sigma$ but the values $\beta$ and $\theta$ were kept constant. All ten possible combinations of three surfaces chosen from five samples {σ = 0.6, 0.8, 1.0, 1.2 and 1.4 cm} were presented. $\beta$ was kept at 1.8 and $\theta$ at a constant random seed {25}. The experiment was repeated for a $\beta$ of 2.2 and a $\theta$ of 30. In total, each observer ordered twenty-five triples (including five training trials). *Appendix 6-A* shows the order in which the surfaces were presented and the detail information of the characteristics of the stimuli in each trial.

There were no time restrictions placed on the observers and they were able to manipulate the orientation of the sample textures while the light position was kept constant as explained in *Chapter 4*. This low number of observers and the reduced control over external variables were appropriate for this pilot experiment.

*Category scaling* was used to determine the perceived rank order of the roughness of the surfaces. The *scale* of the magnitude of the perceptual roughness was not investigated at this stage.

The procedure used to rank the surfaces was as follows. The surface of any triple that was perceived to be the most rough was assigned +1; the smoothest surface was assigned -1 while the intermediate was assigned the value of 0. All values assigned to a surface where totalled and an offset of 10 added (purely for display purposes). The resulting bar chart is shown in *Figure 6-2*. It is important to note that the numbers on the perceptual ranking axis indicate purely an *ordinal* relationship. For full details of the results, see *Appendix 6-B*.

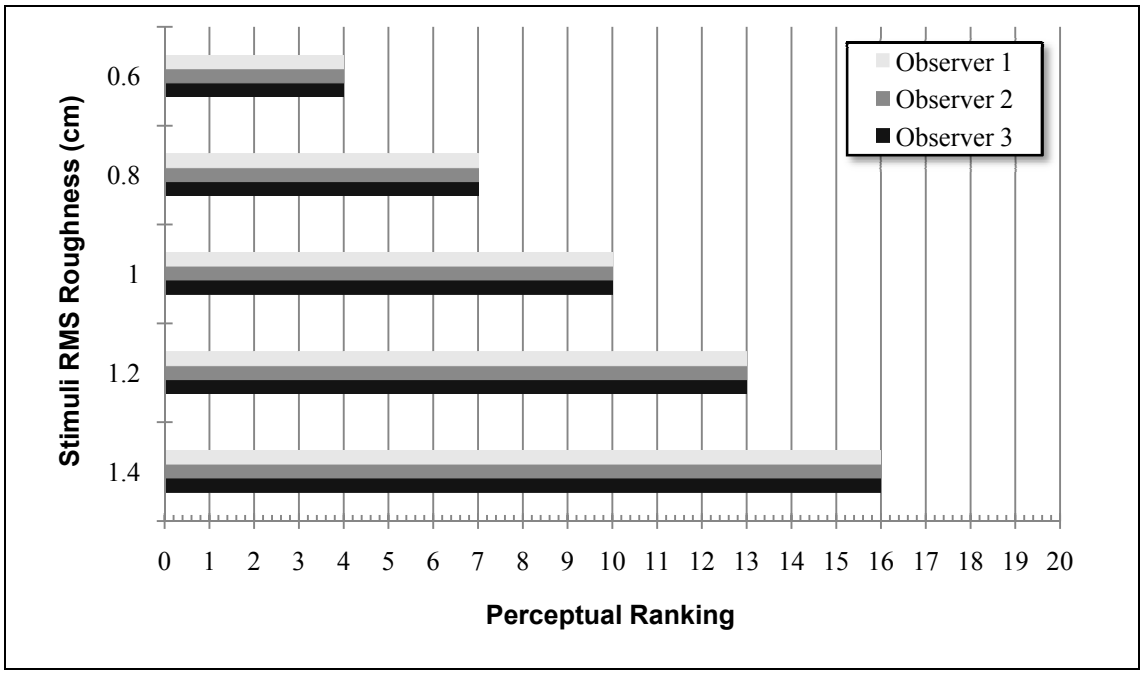


**Figure 6-2: Perceived roughness increases with $\sigma$.**

The results of this experiment confirm that perceived roughness does increase with the increasing $\sigma$ and it also established a range of values of this parameter over which observers make consistent roughness judgements. Values of $\sigma$ outside this range yield surfaces that do not appear natural, and are either almost flat or extremely *"mountainous"*. In the next section, we investigate the effect of changes in the parameter $\beta$ on roughness judgements.

## 6.2 The effect of varying magnitude roll-off factor ($\beta$) on perceived roughness

Recall from *Chapter 4* that varying $\beta$ changes the weight (variance) of different frequencies within a surface's height spectrum. In particular, for a fixed RMS roughness, reducing $\beta$ increases the variance of the higher frequencies at the expense of the lower frequencies. Furthermore, it is well known that increasing the power of higher frequencies increases the perceived roughness of the surface when sensed using touch (Meftah, Belingard and Chapman, 2000) (Yoshida, 2001) (Smith, 2002) (Gibson and Craig, 2002). Consequently, we formulate the following hypothesis for this section: *if $\beta$ is related to perceived roughness, then observers will perceive surfaces with smaller $\beta$ as being rougher.*

The methodology used for this experiment is similar to the one used in the previous section. *Category scaling* was used to rank different surfaces, however, this time $\beta$ was varied while $\sigma$ and $\theta$ were held constant at 0.8 cm and 20 respectively (see *Figure 6-3*). The three observers from the first experiment were asked to order all combinations of three from six surfaces {$\beta$ = 1.7, 1.8, 1.9, 2.0, 2.1 and 2.2}. A second trial was performed using a $\sigma$ of 1.2 cm and $\theta$ of 35. In total, each observer ordered forty-five triples (which included five training triples, see *Appendix 6-C* for detail description of the stimuli and trials). Otherwise, the conditions were the same as for the previous experiment.

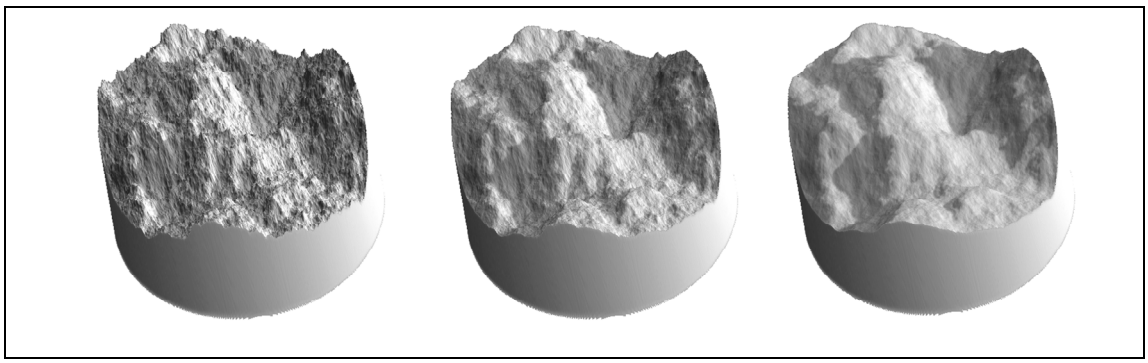

**Figure 6-3: Demonstrates three surfaces with similar $\sigma$ {1.2} and $\theta$ {23} but different $\beta$ {1.8, 2.0 and 2.2}.**

Ranks were assigned to surfaces as before and the results are shown in *Figure 6-4*. This shows that there is a clear relationship between $\beta$ and perceived roughness, and validates the hypothesis that observers perceive surfaces with higher $\beta$ values as being

smoother and surfaces with lower $\beta$ values as being rougher (the actual observations are detailed in *Appendix 6-D*).

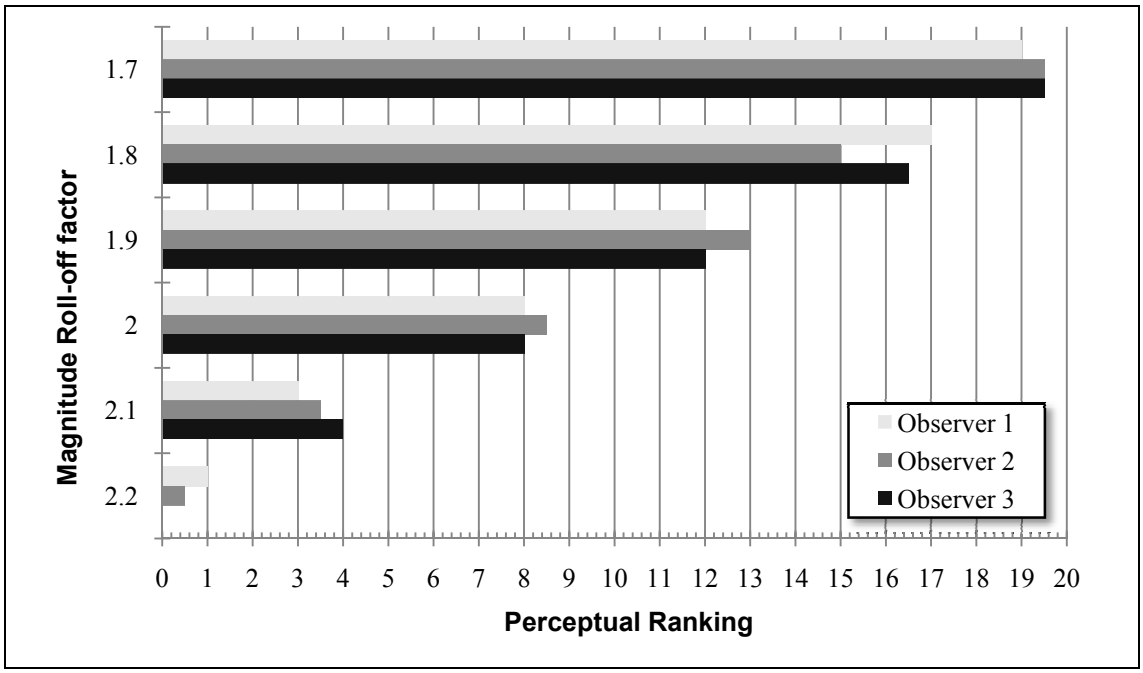


**Figure 6-4: Perceived roughness decreases with magnitude roll-off factor ($\beta$).**

## 6.3 The effect of random phase on perceived roughness

The surfaces used in the experiments were constructed using random values for their phase magnitudes as described in C*hapter 4*. Although it is known that the random phases produce surfaces with similar appearance (Russ, 1994), it is not known if the perceived roughness is affected by the seed of the phase (see *Figure 6-5*).

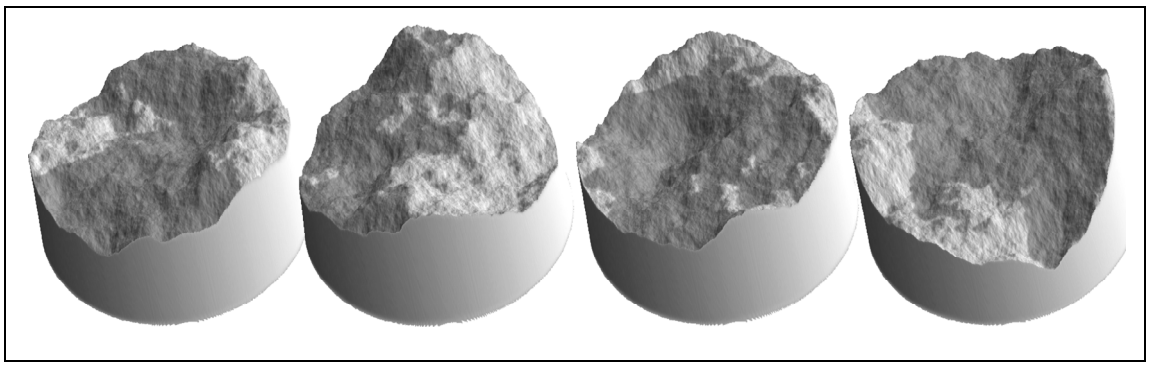

**Figure 6-5: Demonstrating four surface the same $\sigma$ {1.0 cm} and $\beta$ {2.0} values but different random phase seed {5, 25, 42 and 62}.**

Phase controls the relative positions of the sinusoidal basis functions that when added together produce an instance of a surface. It does not affect the variance of the surface or the shape of the power spectrum. The most obvious assumption to make therefore is that the particular assignment of random phase does not affect perceived roughness. Thus, the hypothesis to be tested here is *if the seed of θ is not related to perceived roughness, then observers will perceive surfaces with different seeds of θ, but having the same σ and β, as having similar roughness*.

To validate this hypothesis a new experiment was constructed. Ten naïve observers were asked to match the roughness of pairs of surfaces using the *method of adjustment* (previously explained in C*hapter 4*). Each pair comprised a "*reference surface"* and an "*adjustable surface*" generated using different seeds but with the same value of $\beta$ {2.0}. The RMS roughness of the *reference surface* was chosen from $\sigma$ = 0.4, 0.6, 0.8, 1.0, and 1.2 while that of the *adjustable surface* was initialised to a random $\sigma$. Both surfaces where presented simultaneously to the observers, during which time the orientation of both surfaces followed a predetermined motion (described in *Chapter 5*). The observers were asked to adjust the RMS roughness of the adjustable surface until its perceived roughness matched that of the reference surface (this concept is depicted in *Figure 6-6*). Details of each trial and the characteristic of the stimuli are listed in *Appendix 6-E*.

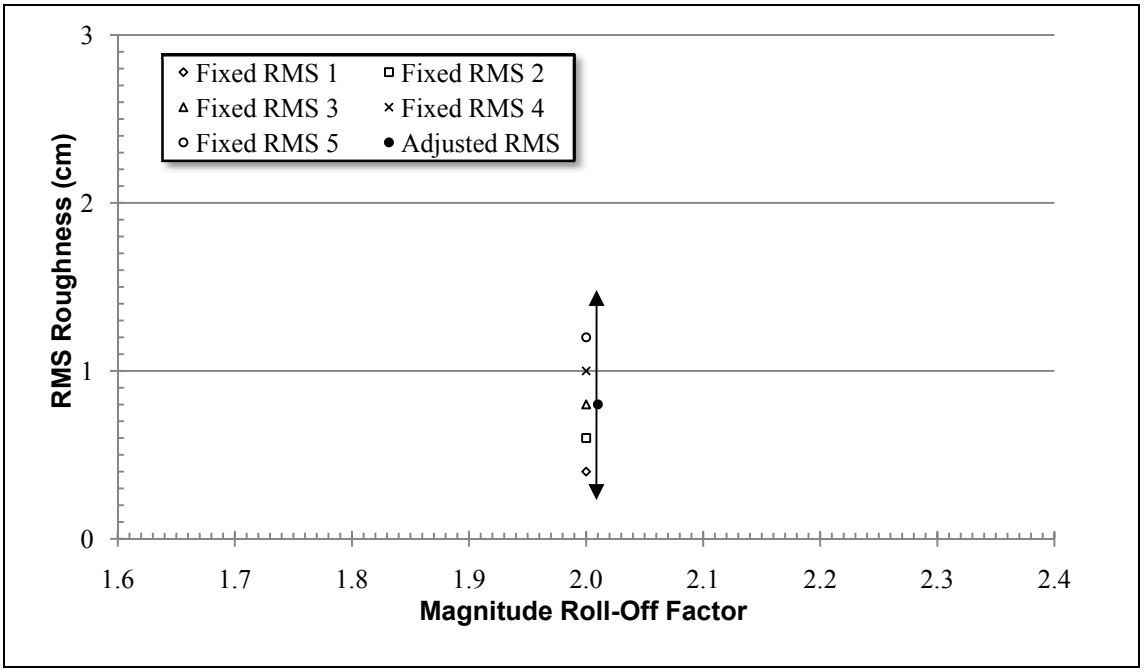


**Figure 6-6: Demonstration of the pair sets for the phase relationship experiment.**

By obtaining the median of the observations (last column of *Appendix 6-F*) it is possible to obtain ten 'observations' for each of the five $\sigma$ values {0.4, 0.6, 0.8, 1.0, and 1.2cm}. Furthermore, from the results it is possible to obtain the variation in perceived roughness for the five pairs of random $\theta$ for each of the five $\sigma_{ref}$ values. The scatter plot shown in *Figure 6-7* compiles all the values from the ten observers, it also illustrates the spread in observations. The actual observation values are given in *Appendix 6-F*.

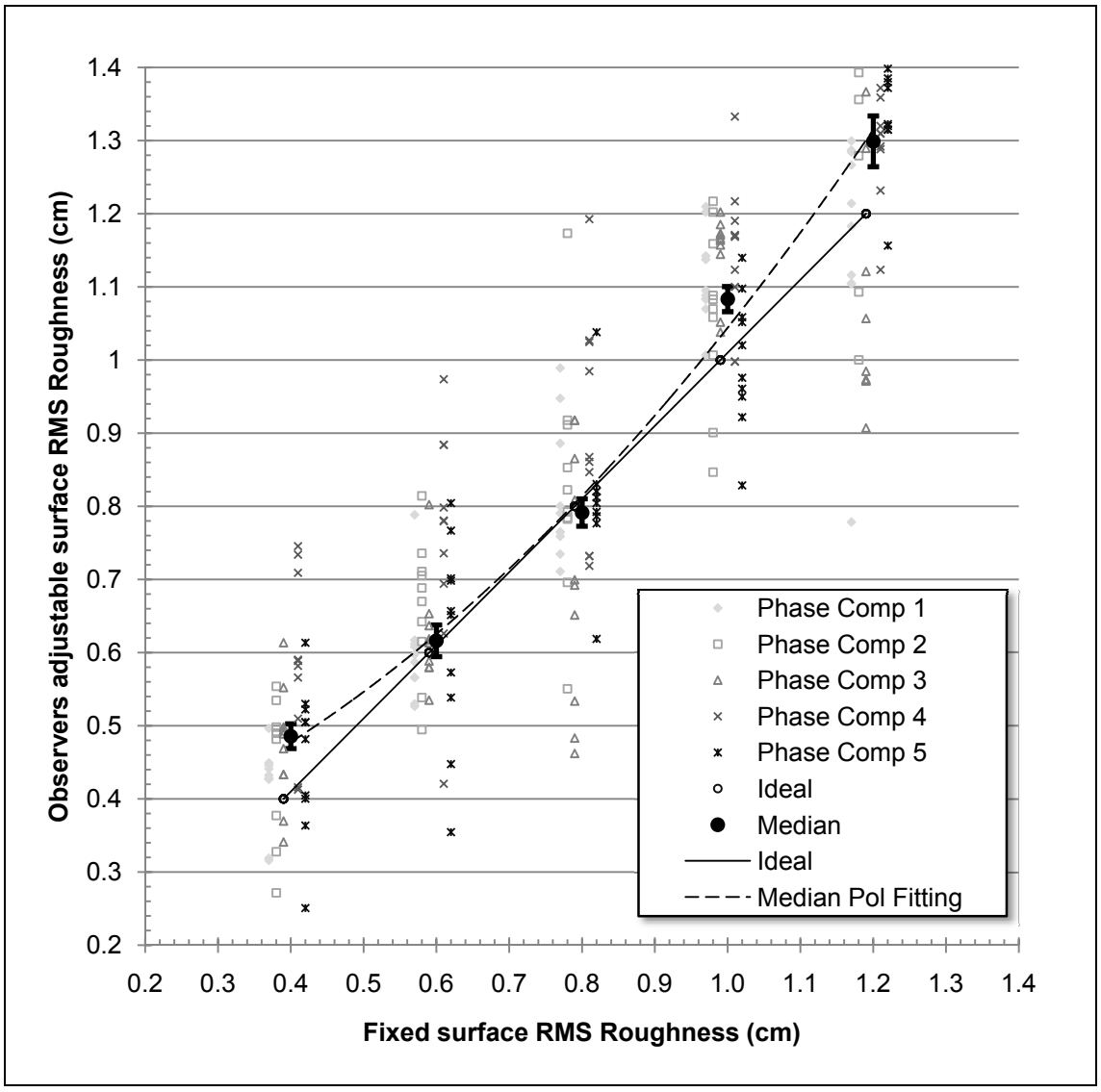


**Figure 6-7: Values of RMS roughness of adjustable surfaces set by individual observers when matching five different fixed surface RMS roughnesses (horizontal axis) and with five different combinations of random phase (symbols shown in key).**

*Figure 6-7* shows that the seed of the phase ($\theta$) does not significantly affect the perceived roughness of a surface. The largest discrepancy occurs when the random

phase generation significantly changes the relative position of the lowest frequency Fourier components (1 cycle per image width) of the two surfaces. This substantially changes the average viewing angle of surface detail (see the last two surfaces of *Figure 6-5*).

Despite this, the overall results, shown in *Figure 6-5,* support the hypothesis that *the seed used for random generation of the phase spectrum does not change perceived roughness*.

## 6.4 Contours of constant perceived roughness in ($\beta$, $\sigma$) space

The previous sections have shown that the perceived roughness of a *1/F$^{\beta}$ noise surface* is not affected by variation of the seed used to randomise its phase ($\theta$) but is affected by independent variation of RMS roughness ($\sigma$) or roll-off factor ($\beta$). Hence, the goal of this section is to investigate *simultaneous* variation of $\sigma$ and $\beta$. This is done by determining lines (contours) of constant perceived roughness in the ($\beta$, $\sigma$) space.

The experimental procedure followed is described below and illustrated in *Figure 6-8*. The procedure is:

1. generate a reference surface with a predefined RMS roughness ($\sigma_{ref}$), and a roll-off factor $\beta_{ref} = 2.0$;
2. generate an adjustable surface with a different roll-off factor ($\beta_{adj}$) and a random RMS roughness ($\sigma_{adj}$);
3. present both surfaces to the observer during which time the orientations of both surfaces follow a predefined motion (described in *Chapter 4*);
4. ask observers to adjust the RMS roughness ($\sigma_{adj}$) of the adjustable surface until its perceived roughness matches that of the reference surface;
5. choose a new value of $\beta_{adj}$ for the adjustable surface and repeat steps 1-4 for the set of possible $\beta_{adj}$;
6. choose a new value of $\sigma_{ref}$ for the reference surface and repeat steps 1-5 for the set of $\sigma_{ref}$.

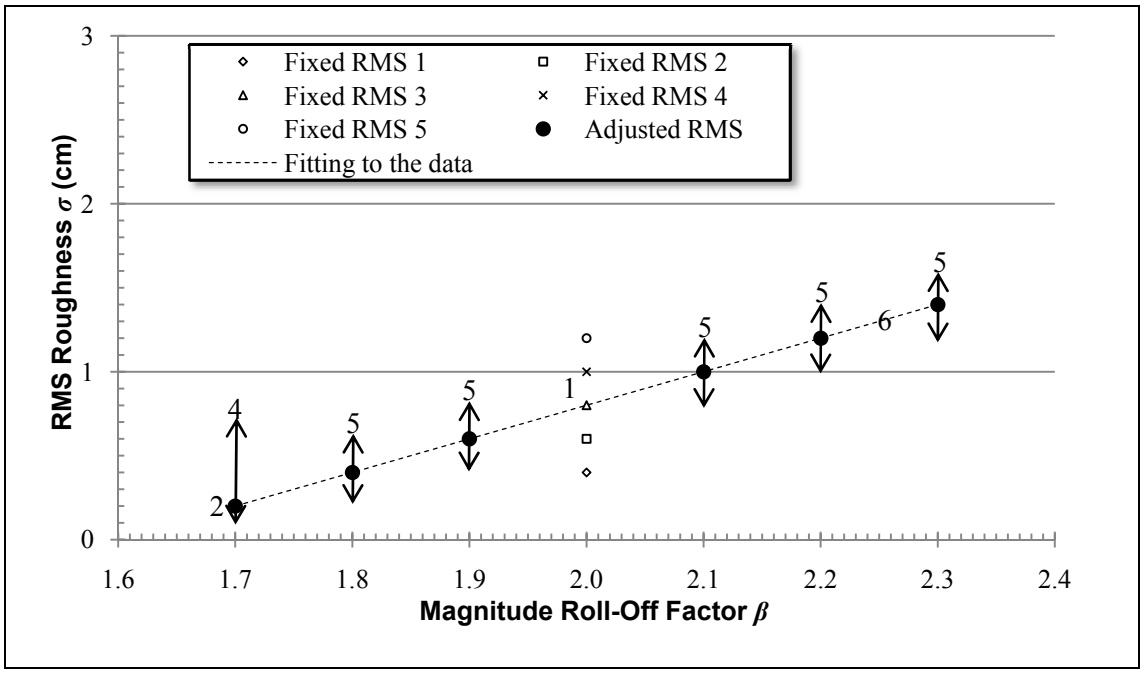


**Figure 6-8: Demonstration of the method used to obtain the contour lines.**

A pilot study was performed initially with five non-naïve observers in order to establish reasonable bounds for the ($\beta$, $\sigma$) space. From this experiment, it was noted that surfaces with roll-off factors between 1.7 and 2.4 appeared the most realistic and natural, and that ones outside these values were judged by observers either as being too synthetic or as impossible to match with the reference surfaces. Similarly, RMS roughness values greater than 3.0 cm where described as unrealistic and produced large variations in observers (this is likely to be because displacement mapping does not tessellate the sides of the slopes with high magnitudes and low frequencies as explained in *Chapter 4*). *Figure 6-9* shows the errors produced by the pilot experiment when extreme values of $\beta$ were used.

Thus the sampling chosen for the ($\beta$,$\sigma$) space used for the full version of this experiment (which used ten naïve observers) was:

- seven values for the roll-off factor ($\beta_{adj}$ = 1.7, 1.8, 1.9, 2.0, 2.1, 2.2, 2.3); and
- five RMS roughness values ($\sigma_{ref}$ = 0.4, 0.6, 0.8, 1.0, 1.2 cm).

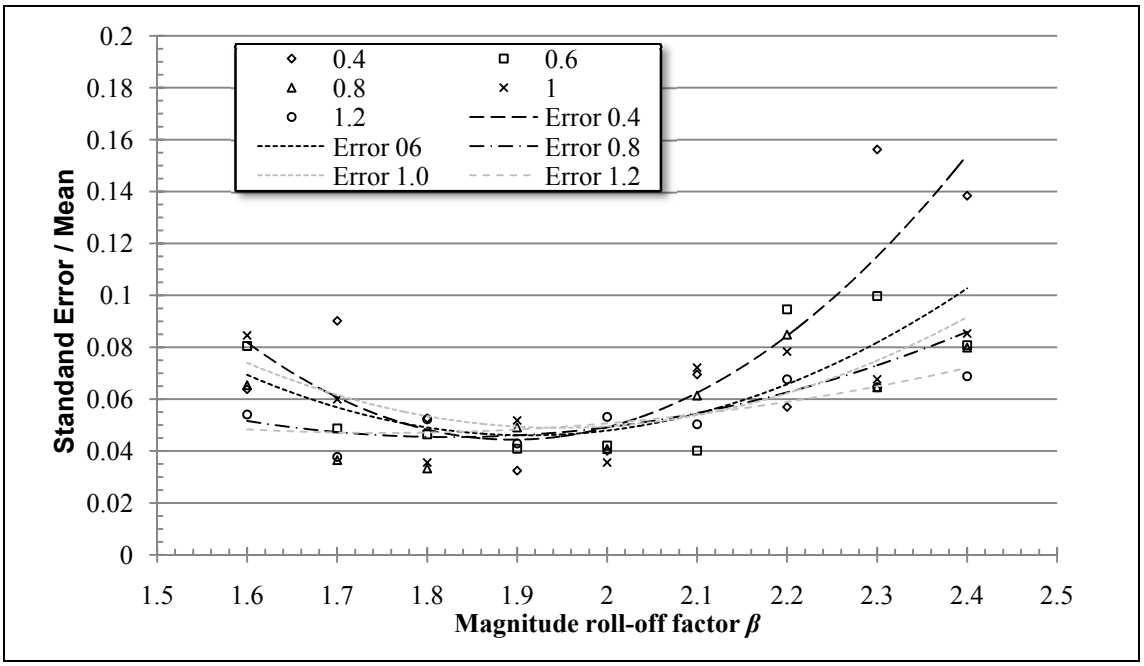


**Figure 6-9: Errors from the pilot experiment to test the limits of the actual experiment.**

In total, each observer matched thirty-five surface pairs (seven values of $\beta_{adj}$ times five values of $\sigma_{ref}$) but to add robustness to the results, each observer repeated the experiment *two more times* with different random phase seed values. In total one hundred and five observations were collected per observer (excluding five practice observations). The complete description of the experiment is given in *Appendix 6-G*.

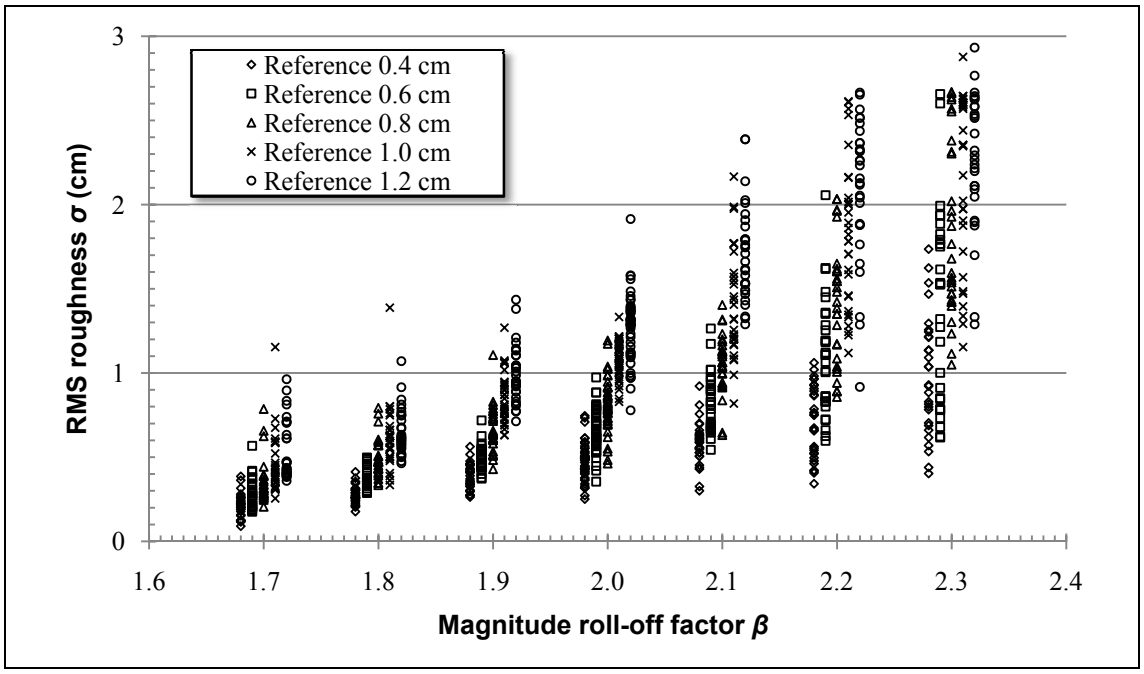


**Figure 6-10: Individual results for surface matches in (*β*-*σ*) space.**

The detailed results are provided in *Appendix 6-H* and shown in *Figure 6-10*, where there is a statistical significance between $\beta$ and $\sigma$ ($p < 0.00001$ for both samples calculated using analysis of variance). These data theoretically contain only five unique values of *perceived roughness* (as observers matched all surfaces to one of five reference values of ($\beta_{ref}$, $\sigma_{ref}$)). Thus, we should be able to draw five lines of *constant* perceived roughness (*iso-roughness lines*) through *Figure 6-10* that will account for all the data.

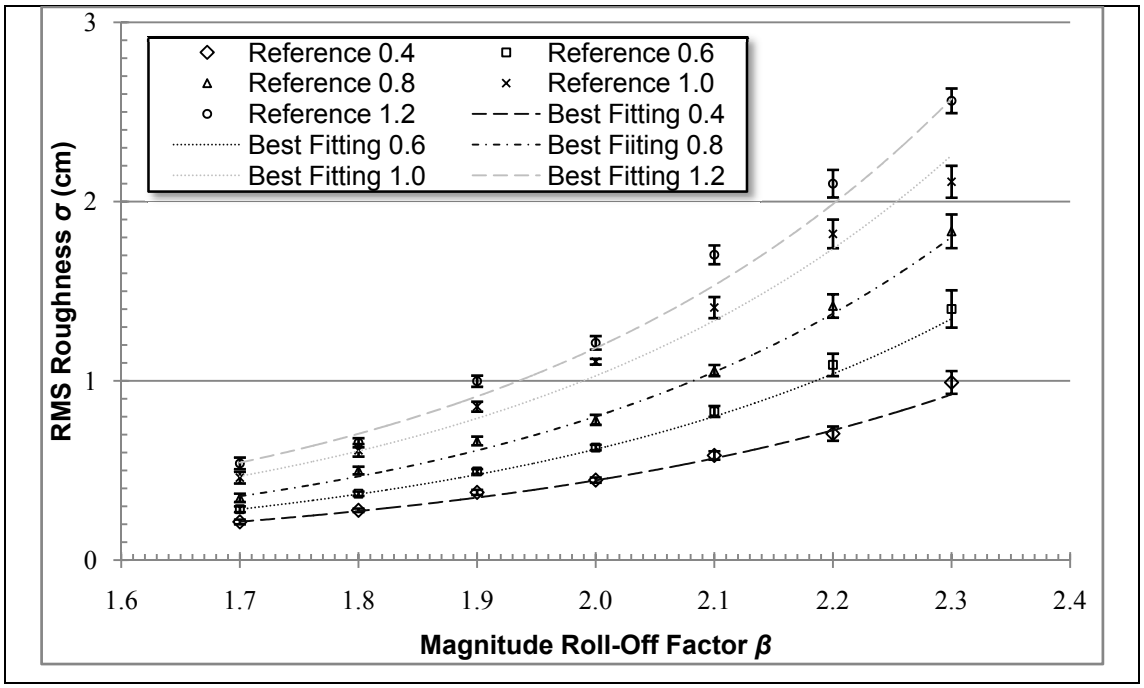


**Figure 6-11: Roughness contour lines for the ($\beta$, $\sigma$) space. Error bars are standard errors of the mean RMS roughness values set over all trials at each combination of values.**

*Figure 6-11* shows these *iso-roughness lines* derived by minimising the least-squares error of a quadratic fit to each of the five data sets (statistical significance and error values are detailed in *Appendix 6-I* and *Appendix 6-J*). Notice that none of these lines crosses each other and that none of the error bars intersects each other too.

By changing the scale of the RMS roughness axis to use $log(\sigma)$ it is possible to simplify the presentation of these data further. *Figure 6-12* shows the results of fitting straight lines in this new axis space. It clearly indicates that the contours of constant perceived roughness follow a *linear relationship between log(σ) and β*.

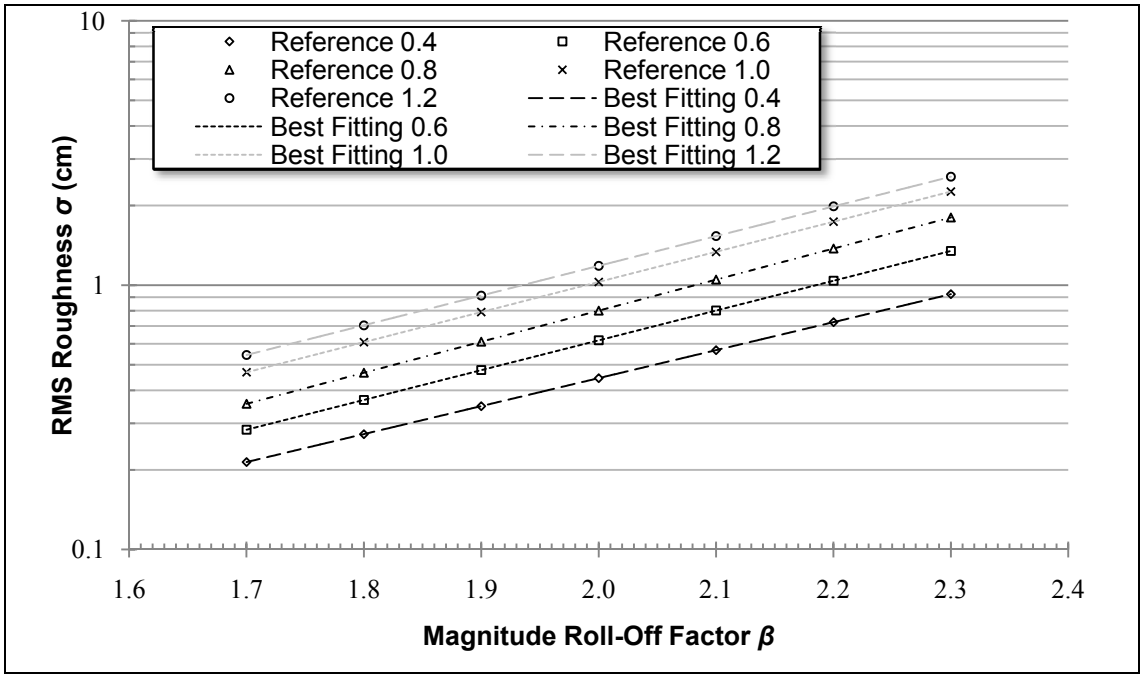


**Figure 6-12: Roughness contour lines in ($\beta$, log $\sigma$) space.**

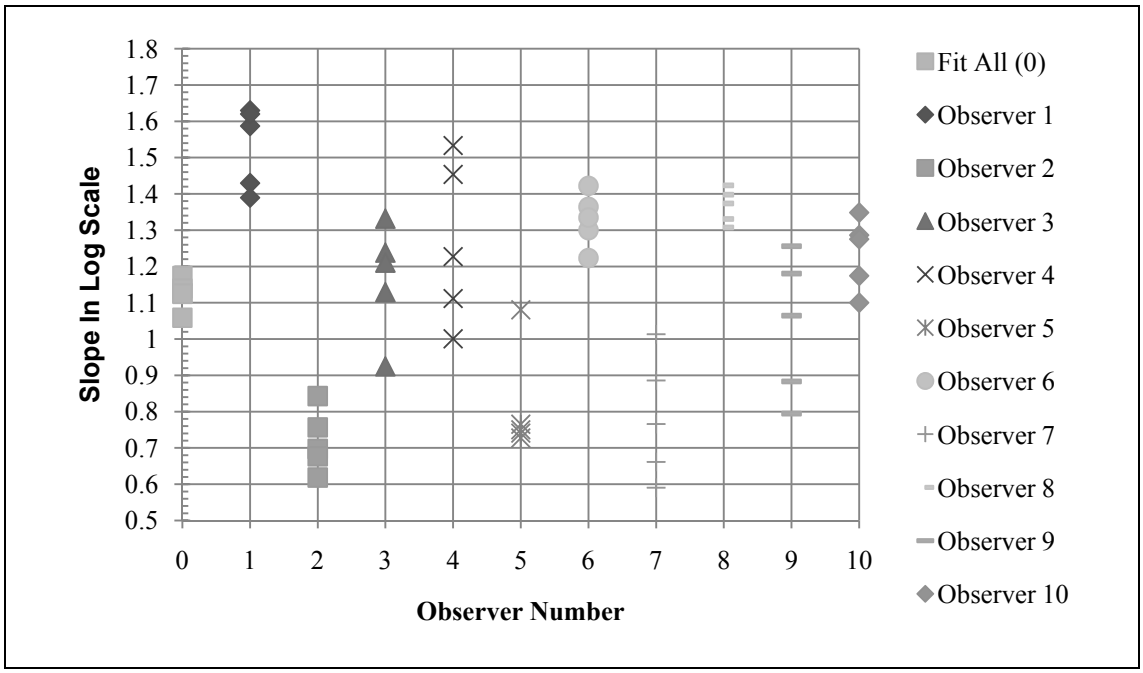


**Figure 6-13: Slopes of the *iso-roughness lines* obtained from individual observers.**

*Figure 6-13* shows the slopes of the five *iso-roughness lines* for each of the individual observers. Note that there is relatively little variation in slopes within observers, implying that individuals' *iso-roughness lines* almost never cross in ($\beta$, log $\sigma$) space, but

there is greater variation between observers. This implies that people vary in the relative weights that they give to the two parameters when they make matches between the perceived roughnesses of surfaces. (Samples of the largest and smallest slope variation are shown in *Appendix 6-K* and *Appendix 6-L* respectively, and the actual slope values are detailed in *Appendix 6-J*). The author did not found any relationship between the obtained data and the variation in slope between observers therefore this is still open discussion and further experimentation is needed.

## 6.5 Summary and Discussion

From the experiments described above it is clear that of the three parameters *($\sigma$, $\beta$* and *random phase seed $\theta$)* used to specify *$1/F^{\beta}$ noise* surfaces only $\sigma$ and $\beta$ affect perceived roughness. That is:

i) increasing RMS roughness ($\sigma$) increases perceived roughness;
ii) decreasing roll-off factor ($\beta$) increases perceived roughness; and
iii) changing the random phase seed ($\theta$) does not affect perceived roughness.

Furthermore, the last experiment has clearly shown that there is a *linear relationship between log $\sigma$ and $\beta$* for lines of constant perceived roughness for *$1/F^{\beta}$ noise* surfaces.

Although, the above results from the experiments show a clear relationship between the surfaces' characteristic and perceived roughness, some factors are still not modelled like prior knowledge, expertise or binocular disparity. We will assume these factors do not contribute or do it insignificantly to the perception in surfaces as observers were chosen to represent a well-balanced population.

Given the above results, it is now possible to propose how a measurement model for perceived roughness might be developed. From (iii) above it is clear that phase spectra have no effect on perceived roughness. Thus, the model can be based on the surface's power (or magnitude) spectrum, and this will be the focus of the next chapter.

# CHAPTER 7

# A MODEL BASED ON THE HUMAN VISION

The goal of this chapter is to develop a model (or estimator) of perceived roughness for *1/F$^{\beta}$ noise* surfaces that is consistent with the data obtained in the preceding chapter. This model should therefore:

1. be able to predict the contours of constant perceived roughness reported in *Section 6.4* and
2. be independent of a surface's phase spectrum.

The second requirement dictates that we use only the surfaces' power (or magnitude) spectra. These data are commonly used in computer vision for classification and segmentation of image texture. The algorithms were originally inspired by the popular frequency channel models of early processing in the human visual cortex, and typically follow an *FRF* (filter-rectify-filter) structure. Hence, this chapter will assess the suitability of a number of different *FRF* models as estimators of perceived roughness.

The chapter is organised in five parts. The first section explains the reasoning behind the proposed models. *Section 7.2* describes the methodology used for fitting these models to the data obtained in the preceding chapter. In *Section 7.3,* two simple models are investigated to determine how consistent they are with observers' data. In *Section 7.4*, a model with a more plausible basis in human vision is fitted to the data. Finally, the results are discussed and a short explanation is given as to why further experiments are necessary.

## 7.1 A plausible measurement model

The form of our model is based on the *FRF* structure that is often used for modelling visual processes. This also known as the *back pocket model* in vision science because Landy et al argue that "it has become the default model that researchers in the field routinely 'pull from their back pocket' to attempt to make sense of texture segregation

results" (Landy and Oruc, 2002). In this framework, the first filter is usually a band pass filter (e.g. a Gabor) which is both orientation and frequency tuned (Landy and Bergen, 1991) (Graham, Sutter and Venkatesan, 1993). However, there is not so much agreement as to the form of the second filter. Some vision scientists argue that it is most likely to be another (lower frequency) band pass filter (Landy and Oruc, 2002) (Dalkin, Willians and Hess, 1999), whilst computer vision researchers often implement it simply as a pooling (or averaging) filter (Randen and Husoy, 1999) (Bovik, Clark and Geisler, 1990). In the latter case, when we define *R* to be a squaring function ($x^2$) the result is a local variance estimator (see *Figure 7-1*).

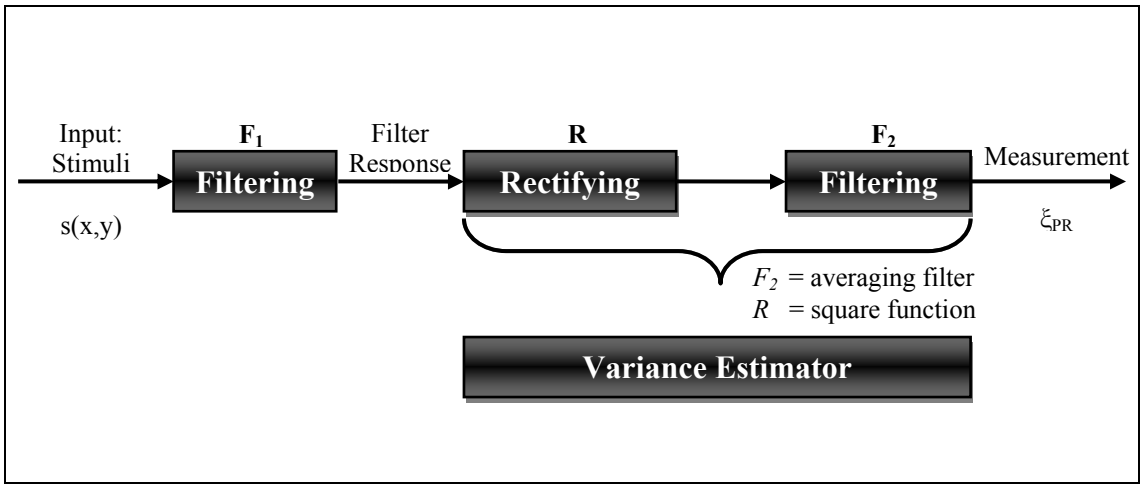


**Figure 7-1: The *FRF* (filter-rectify-filter) framework.**

Normally, *FRF* models are applied directly to image data. Here, however, the algorithm is used in a different context from image texture segregation or classification. As we wish the estimator to be independent of illumination conditions, we apply it *directly* to the *height data,* as it is known that the slant and tilt of the illumination affects the statistics of images as described by Chantler (1995). Thus in the proposed model, the surface height description $s(x,y)$ is directly convolved with the first filter $f_1(x, y)$ and the result passed to the combined *R* $F_2$ stage which performs the variance (Var) estimation as defined in *Equation 7.1*.

$$\xi_{pr} = \mathrm{Var}(\, f_1(x,y) * s(x,y)) \qquad \textbf{(7.1)}$$

Assuming that the signal is *zero-mean* then *Equation 7.1* can be expressed by a simple summation (*Equation 7.2*) and Parseval's theorem (Oppenheim, Schafer and Buck, 1999) can then be used to transform the expression into the *discrete Fourier transform* (*DFT*) domain (*Equation 7.3*)

$$\xi_{pr} = \mathrm{Var}\big(f_1(x,y) * s(x,y)\big) = \sum_{x,y} [f_1(x,y) * s(x,y)]^2 \qquad \textbf{(7.2)}$$

$$\xi_{pr} = \sum_{x,y} [f_1(x,y) * s(x,y)]^2 = \sum_{u,v} F_1(u,v)^2 \cdot S(u,v)^2 \qquad \textbf{(7.3)}$$

$F_1(u, v)$ is the transfer function of the first filter, $S(u, v)$ is the *DFT* of the surface height function and $(u, v)$ are *DFT* Cartesian frequency coordinates. As we have previously defined surface height of the $1/F^{\beta}$ *noise* surfaces as a continuous function of polar coordinates we will express (*Equation 7.3*) in the continuous Fourier polar domain and integrate over the range of frequencies detectable by human vision (*Equation 7.4*).

$$\xi_{pr\theta} = \iint_{f_p}^{f_c} F_1\big(f_f, \theta_f\big)^2 . S\big(f_f, \theta_f\big)^2 \; \mathrm{d}f_f \, \mathrm{d}\theta_f \qquad \textbf{(7.4)}$$

Where $f_f$ is the cyclic frequency, $\theta_f$ is the angle of the basis function, $f_p$ is the starting frequency of 0.11 cpd and $f_c$ is the cut-off frequency of 30 cpd. This formula can be defined in cycles per degree because the experiments have a fixed viewing distance as previously described in *Chapter 5*.

The next section will describe the methodology used to optimise $F_1$, and its parameters, to the iso-roughness data presented in the previous chapter.

## 7.2 Optimization of $F_1$

There are a variety of choices for the form of $F_1$ and the values of its parameters. We therefore require an error measure (*objective function*) that will allow us to optimise these. In the previous chapter we established five *iso-roughness lines* in the ($\beta$, $\sigma$) space (*Figure 6-11*). Seven surfaces, which observers have perceived to have the same roughness, are associated with each of these lines. If an estimator for $\xi_{pr}$ fits these data well, then its output will have the same value for all surfaces associated with a particular *iso-roughness line*. Conversely, if it does not fit the data well, then these values will vary. Thus, one could use the standard deviation of the values of $\xi_{pr}$ obtained for the surfaces associated with one line as the *objective function*. However, the different candidate $F_1$ filters may produce quite different values for their estimates of $\xi_{pr}$ and so we use the normalised standard deviation of the error function over each line (*Equation 7.5*).

$$\varepsilon = \frac{\sqrt{\frac{1}{\mathrm{n}} \cdot \sum_{\mathrm{i}=1}^{\mathrm{n}} \left(\xi_{pr_{\mathrm{i}}} - \overline{\xi_{pr}}\right)^2}}{\frac{1}{\mathrm{n}} \cdot \sum_{\mathrm{i}=1}^{\mathrm{n}} \left(\xi_{pr_{\mathrm{i}}}\right)} \tag{7.5}$$

Note that the values of $\xi_{pr}$ used in evaluating the *objective function* $\varepsilon$ are the medians of the values obtained from the ten observers in the experiment described in *Chapter 6*.
In order to obtain an overall error value ($\varepsilon_t$) the line errors ($\varepsilon$) for all lines are simply summed (*Equation 7.6*).

$$\varepsilon_t = \sum_{\mathrm{i}=1}^{\mathrm{lines}} \varepsilon_i \tag{7.6}$$

As we assume that $F_1$ is circularly symmetric and as the stimuli are isotropic, *Equation 7.7* can be further simplified by performing the calculation over the radial variable $f_r$, i.e. we omit the angular variable ($\theta_f$). This result in *Equation 7.7 below* (please notice that it is assumed that the factor of ($2\pi f$) is already multiplied to the equation, as this is necessary when a circular symmetry was assumed):

$$\xi_{pr} = \int_{f_p}^{f_c} F_1(f_f)^2 \cdot S(f_f)^2 \ \mathrm{d}f_f \qquad \textbf{(7.7)}$$

Thus, *Equation 7.7* provides the objective function that must be minimised in order to optimise the fit of $F_1$ to the psychophysical data. We found no general way of solving *Equation 7.7* and therefore evaluate it numerically using Simpson's rule (Matlab implementation).

In the next subsection, different shapes of $F_1$ will be investigated and their parameters optimised using *Equation 7.6*.

## 7.3 Fitting the models to the data

The criteria used to select candidate models for $F_1$ are that they should be:

1. of a simple form;
2. parsimonious (i.e. have a low number of parameters); and
3. biologically plausible.

The simplest bandpass filter is a *box filter.* While this satisfies criteria one and two, it is arguable whether it meets criterion three, as it requires computation of a global function. However, as it is very easy to calculate we will start with it, and then go on to consider *power* and *gaussian filters*.

### *7.3.1 The box filter*

The *box filter*'s roughness estimator is easily implemented by setting the integration limits in *Equation 7.7* to the desired cut-off frequencies of the filter. The result is *Equation 7.8* ($f_p$ is the start frequency, $f_c$ is the cut out frequency and the gain $K$ is set to one). *Figure 7-2* shows how the filter parameters affect its shape.

$$\xi_{pr} = \int_{f_p}^{f_c} K \cdot S\left(f_f\right)^2 \ \mathrm{d}f_f \qquad \textbf{(7.8)}$$

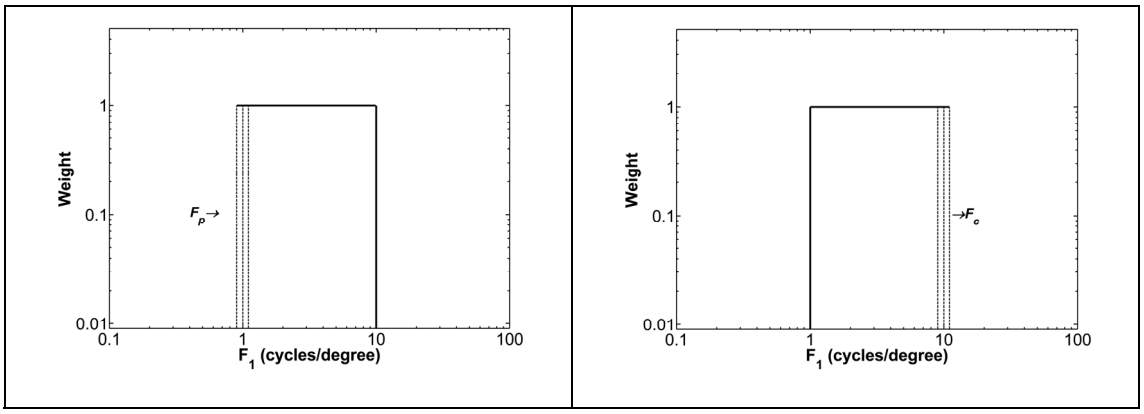


**Figure 7-2: Effects of varying the parameters $F_p$ and $F_c$ of the box filter**

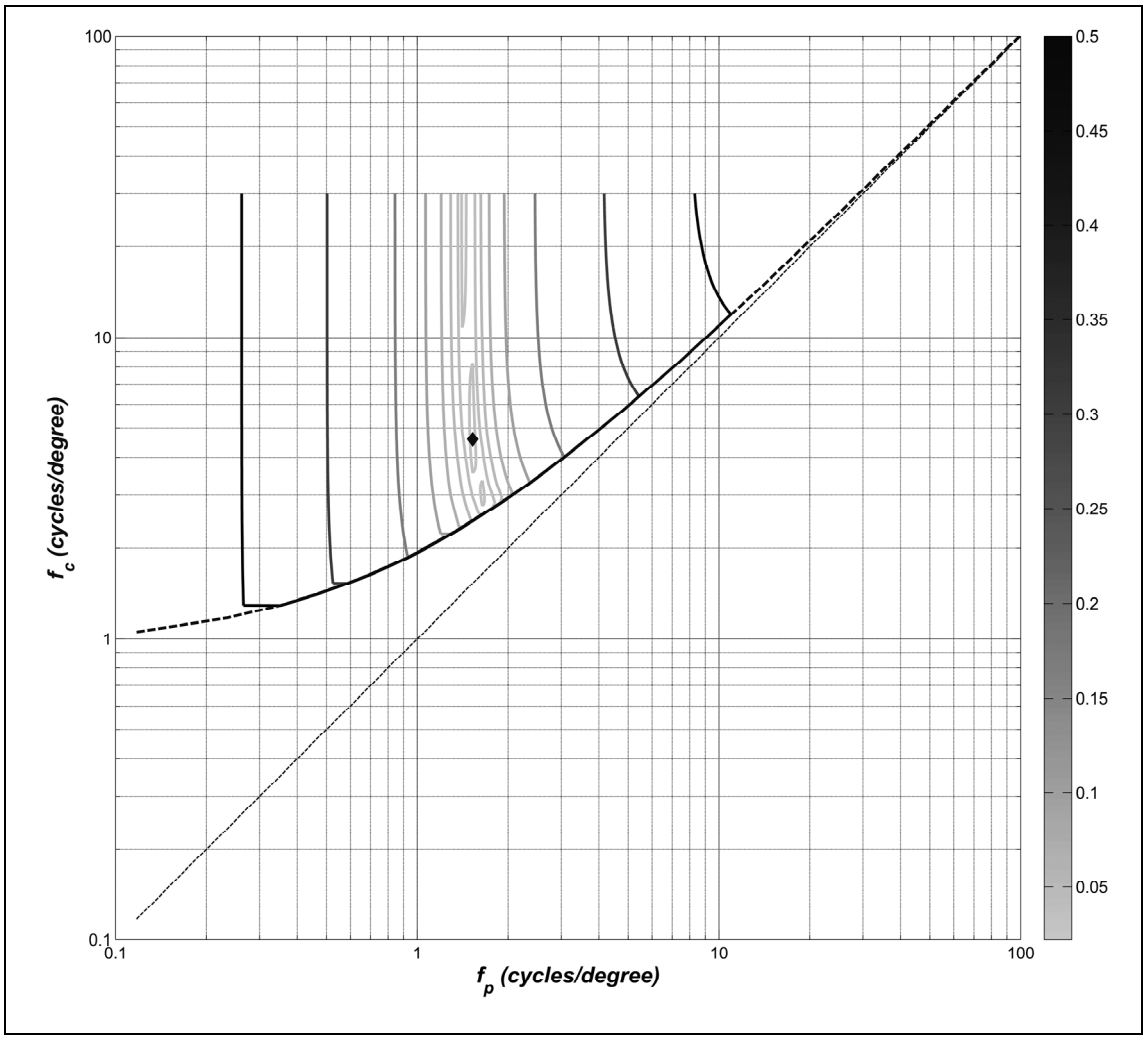


**Figure 7-3: Objective function $\varepsilon_t$ as a function of the box filter parameters, dashed lines indicate where the parameters $f_p$ and $f_p$ intersect or are too small to form a band pass filter (< 1 cycle/degree).**

*Figure 7-3* contains a contour plot of the *objective function* ($\varepsilon_t$) as a function of the two cut-off frequencies of the box-filter. The diamond shape indicates the optimum value of the parameters:

- start frequency ($f_p$) = 1.53 cycles per degree, and
- cut off frequency ($f_c$) = 4.58 cycles per degree.

Note that the error is sensitive to changes in the low frequency cut off but that the same is not the case for the high frequency cut off.

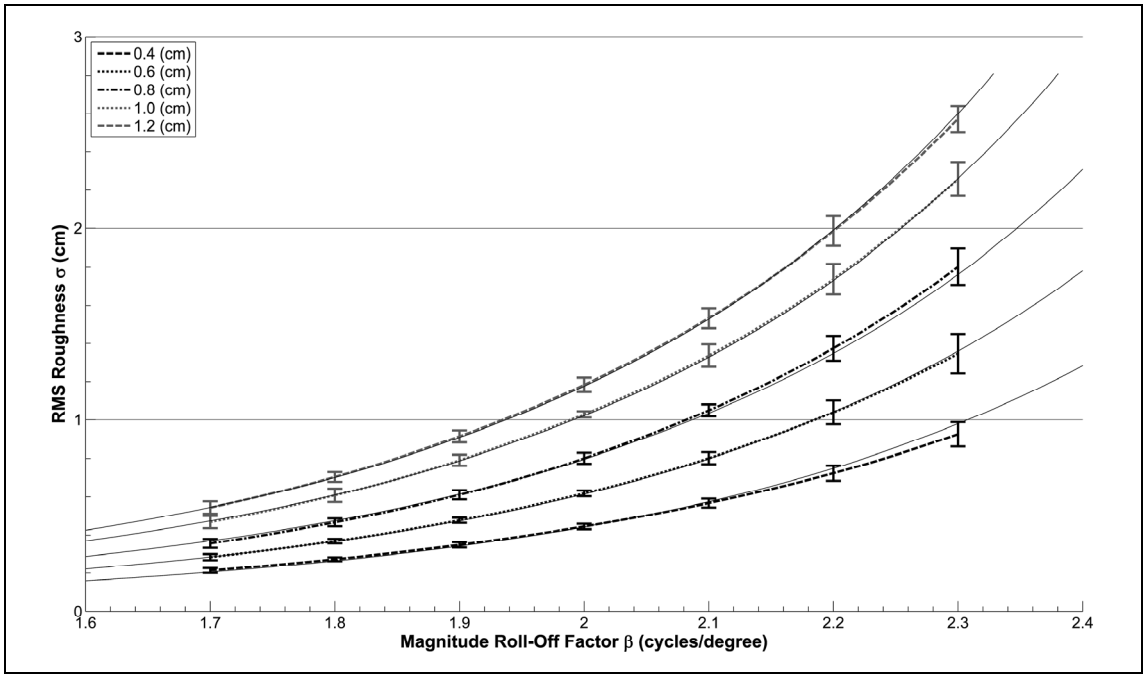


**Figure 7-4:** ***Iso-roughness lines*** **predicted by the optimised** ***box filter*** **model, compared to the experimental data.**

### *7.3.2 The power function filter*

In this function, described in *Equation 7-9*, the weighting of frequencies across the range from $f_p$ to $f_c$ is not constant, as in the *box model*, but varies according to a power law. The high cut off frequency $f_c$ is fixed at 30 cycles per degree, while the low cut off frequency $f_p$ and the power of the weighting function $p$ vary, as illustrated in *Figure 7-5*.

$$\xi_{pr} = \int_{f_p}^{f_c} (f_f - f_p)^p \ . \ S(f_f) \ \mathrm{d}f_f \tag{7.9}$$

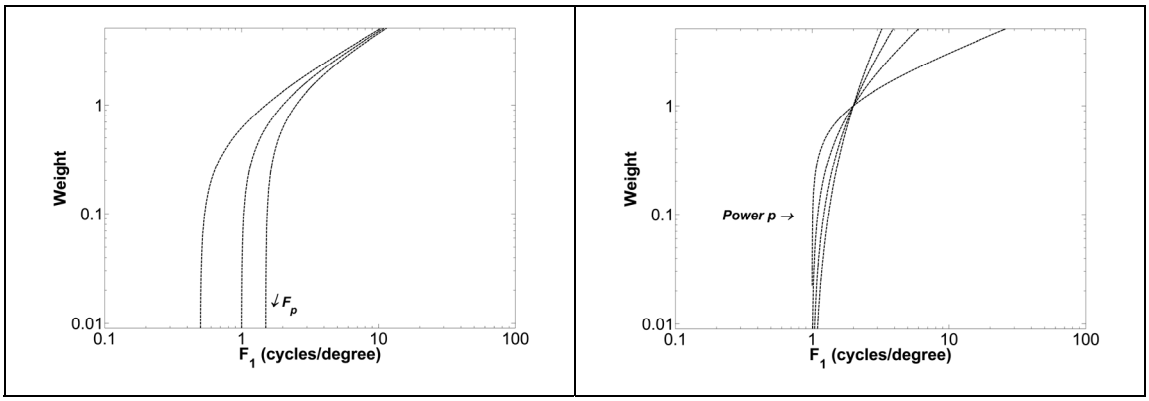


**Figure 7-5: Effects of varying the parameters $p$ and $F_c$ of the power function filter.**

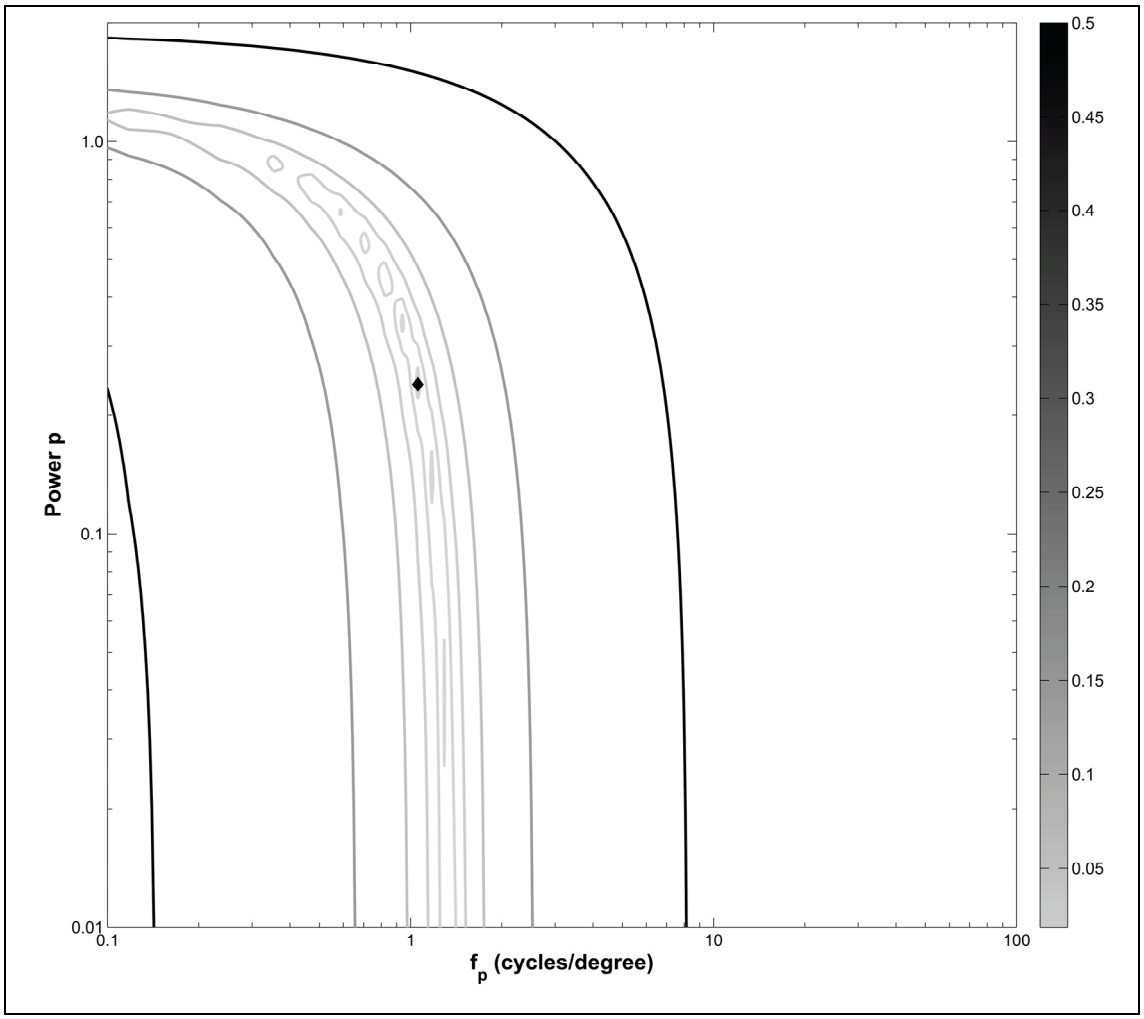


**Figure 7-6: Objective function $\varepsilon_t$ as a function of the power filter parameters.**

The optimized parameters of the *power function filter* when minimizing the error $\varepsilon_t$ are a $p$ value of 0.24 and a low cut off frequency $f_p$ of 1.06 cycles per degree (see *Figure 7-6*) With these parameters, the fit of the model to the experimental data is shown in *Figure 7-7*.

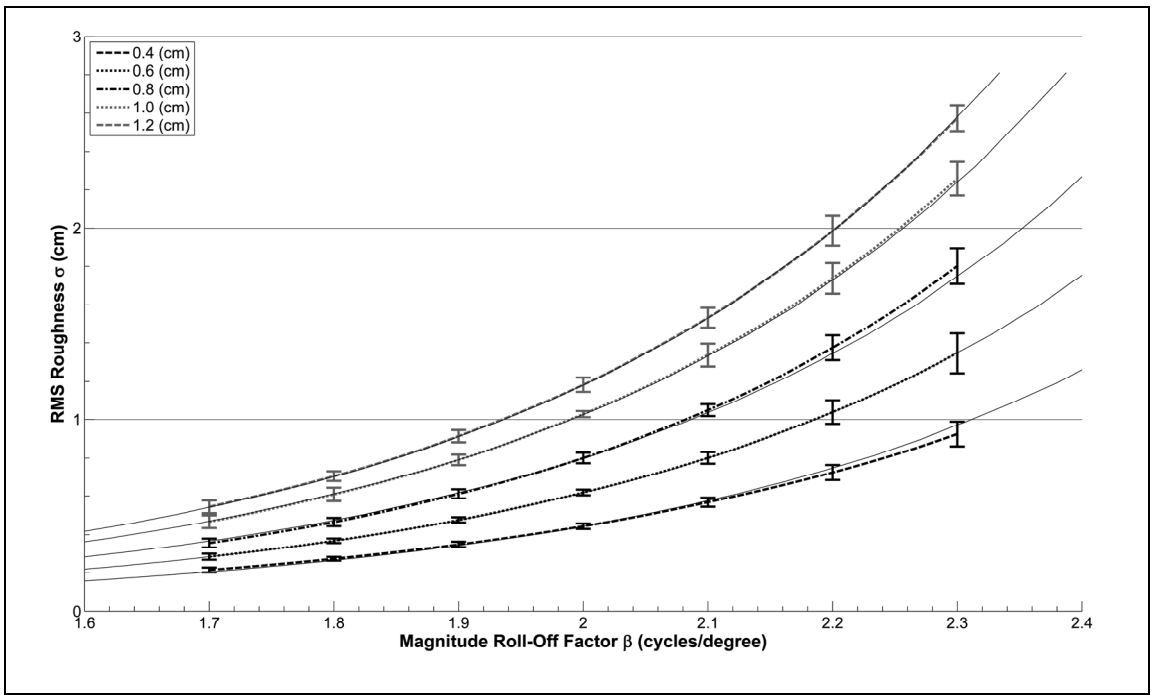


**Figure 7-7:** ***Iso-roughness lines*** **predicted by the optimised** ***power function filter*****, compared to the experimental data.**

*Table 7-1* summarises the formulas and the optimized values for each of the two functions, and shows that the optimized *power filter* achieves a lower error ($\varepsilon_t$ = 0.0187) in matching the experimental data than does the optimized *box filter* ($\varepsilon_t$ = 0.0220). *Figure 7-8* plots each of the filters with their optimized parameters, together with the *contrast sensitivity function* that describes the sensitivity of the human vision system to spatial frequency (Campbell & G, 1968).

| Function | Filter Function | Min Error $\varepsilon_t$ | Optimized Parameters |
|---|---|---|---|
| **Box** | $\xi_{pr} = \int_{f_p}^{f_c} K \,.\, S(f_f)\ \mathrm{d}f_f$ | 0.0220 | $K$ = 1.00, $f_p$ = 1.53 cpd, $f_c$ = 4.58 cpd. |
| **Power** | $\xi_{pr} = \int_{f_p}^{f_c} (f_f - f_p)^p \,.\, \mathrm{S}(f_f)\ \mathrm{d}f_f$ | 0.0187 | $p$ = 0.24, $f_p$ = 1.06 cpd, $f_c$ = 30.00 cpd. |

**Table 7-1: Short summary of all the filters, the minimum error and the optimum parameter values.**

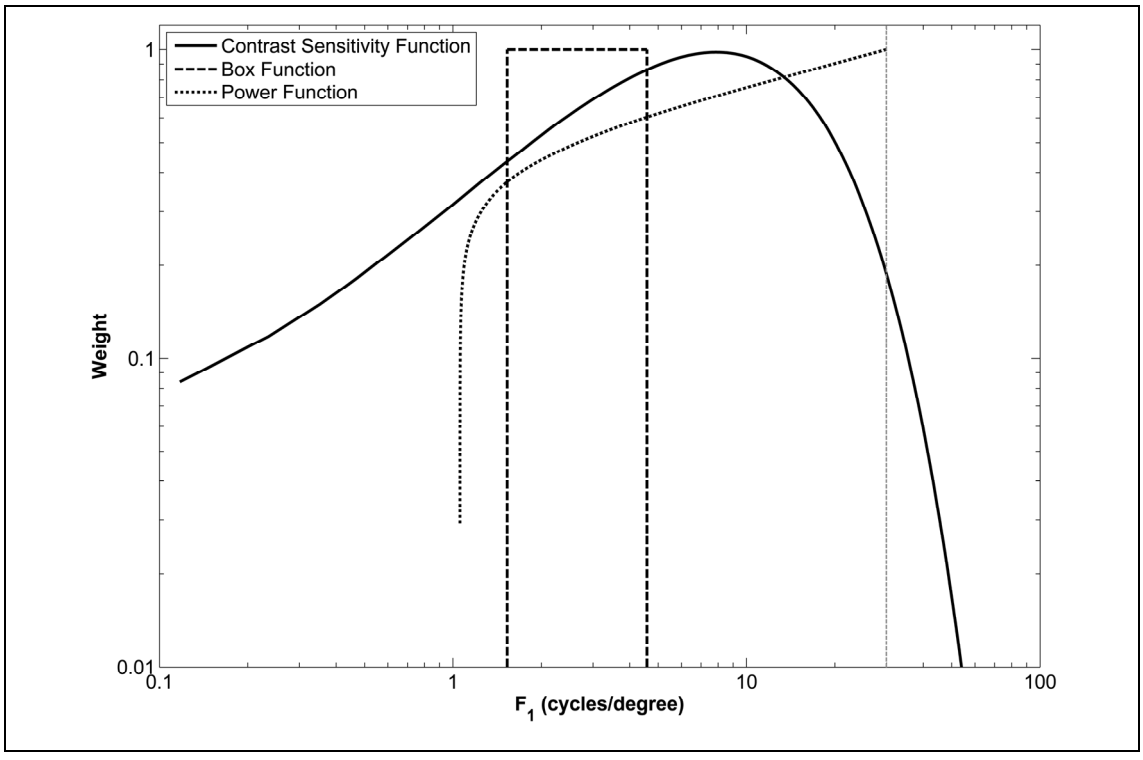


**Figure 7-8: Plots of all filter functions when optimizing the error.**

## 7.4 A filter based on the human vision system

The spatial frequency channels in the human visual pathway are characteristically described in literature as gaussian-like functions (Wilson, McFarlane and Phillips, 1983) (see *Figure 7-9*). A gaussian shape for the filter $F_1$ therefore has greater

biological plausibility than the filters considered so far, as well as being a simple form of a band pass filter.

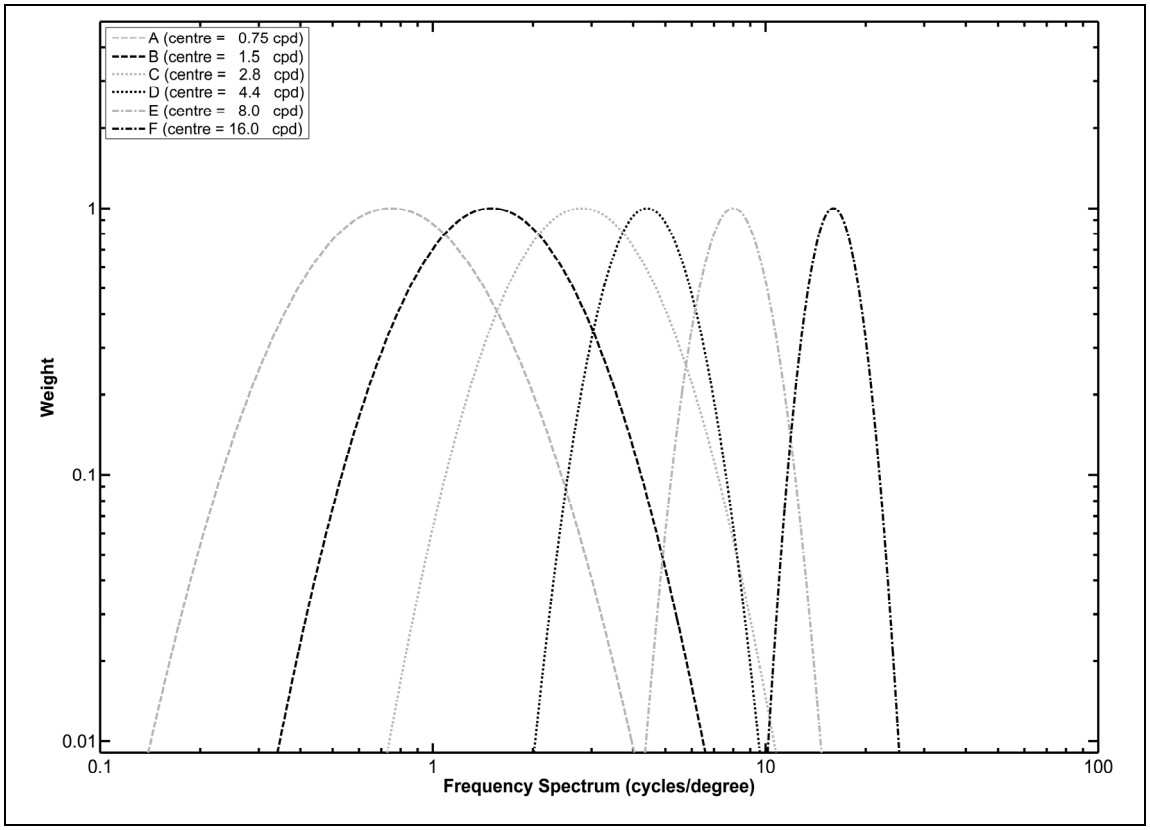


**Figure 7-9: Spatial frequency channels approximations re-plotted from Wilson's data (Wilson, McFarlane, & Phillips, 1983) as gaussian functions to make them more parsimonious.**

The *gaussian function* to be tested against the observed data is described in *Equation 7.10,* where *k* replaces the multiplying variables of a normal gaussian with the inverse of the maximum of the function; as a result, the *gaussian function* is normalized (maximum of one in the peak of the function). $\mu$ and $\sigma_g$ are the mean value and the standard deviation of the *gaussian function*, respectively.

$$\xi_{pr} = \int_{f_p}^{f_c} \mathrm{k} \,.\, \mathrm{e}^{-\frac{\left(\log(f_f) - \log(\mu)\right)^2}{2\sigma_g^2}} \,.\, S_{(f)} \; \mathrm{d}f_f \qquad \textbf{(7.10)}$$

Logarithmic values of these parameters are used in the equation to give the *gaussian function* its distinctive shape in the logarithmic frequency domain, and a closer match to the shapes of the spatial frequency channels in human vision. The effects of varying the

two parameters are illustrated in *Figure 7-10*. Pilot fittings showed that a normal gaussian had a worse fitting than the log gaussian, and so it will not be discussed further.

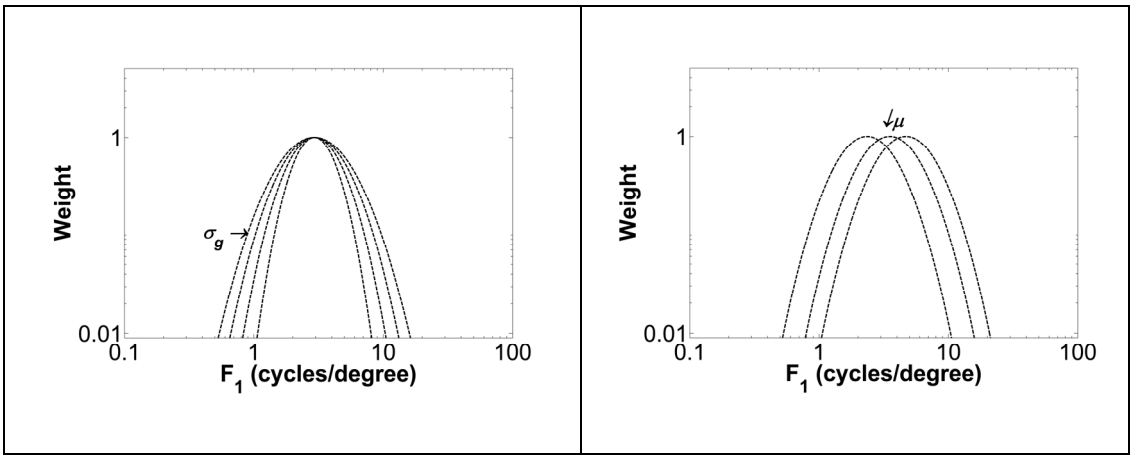


**Figure 7-10: Effects of varying the parameters $\mu$ and $\sigma_g$ of the Gaussian filter.**

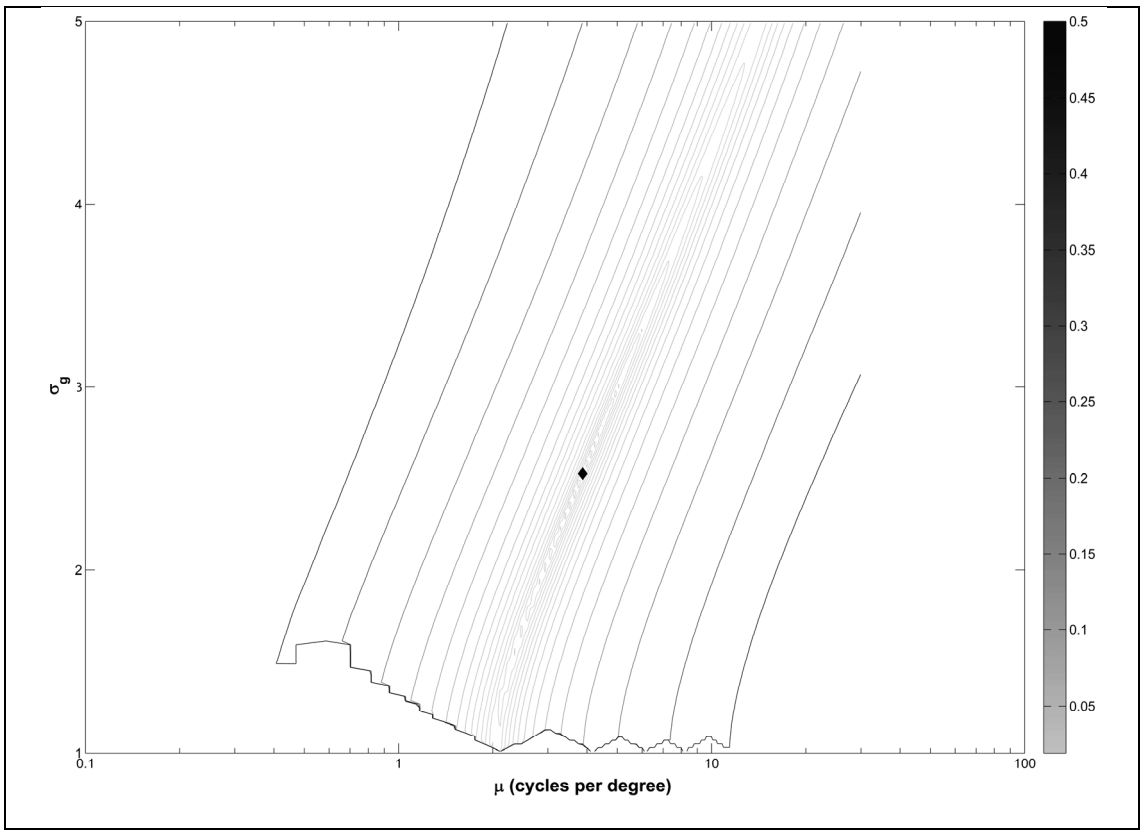


**Figure 7-11: Objective function $\varepsilon_t$ as a function of the Gaussian filter parameters.**

The *gaussian function* as $F_1$ fits the data with a minimum error $\varepsilon_t$ of 0.0189 when the optimum value of $\mu$ is 3.87 cpd and of $\sigma_g$ is 2.53 (see *Figure 7-11*). The fit of the *iso-roughness lines* predicted by the optimized model to the experimental data is shown in *Figure 7-12*.

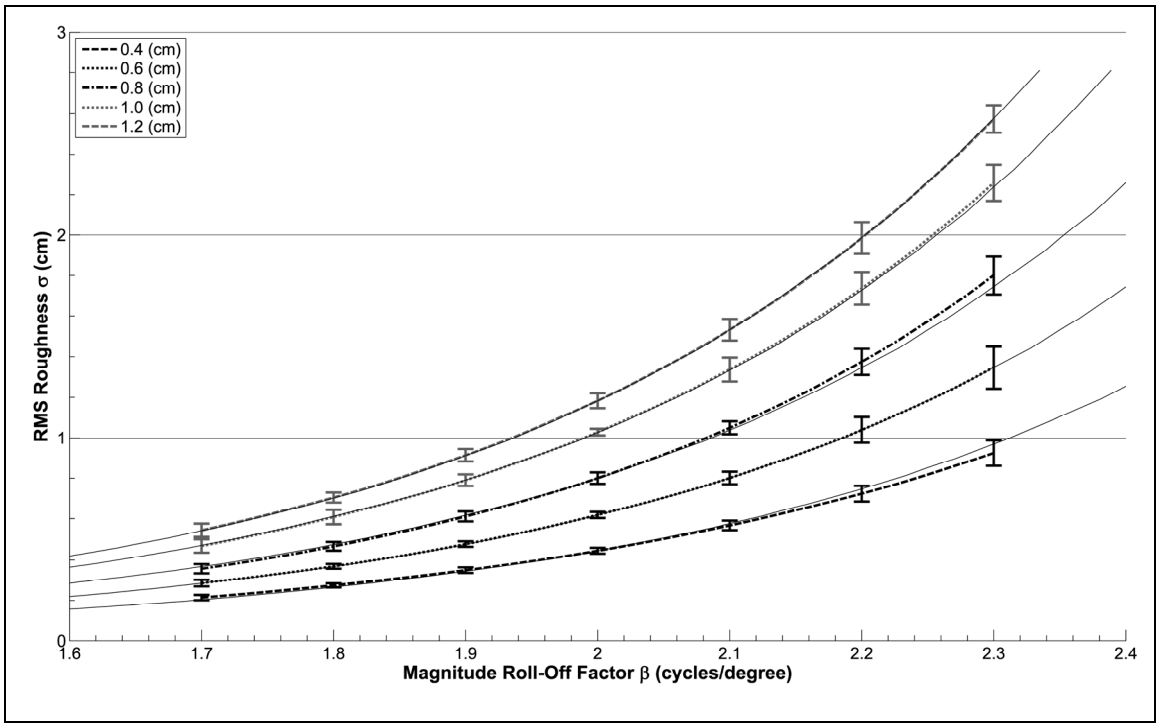


**Figure 7-12: *Iso-roughness lines* predicted by the optimised *gaussian filter* model, compared to the experimental data.**

A plot of the final optimized *gaussian function* is shown in *Figure 7-13,* alongside the contrast sensitivity function. Note that the filter falls well inside the *CSF* and that the centre of the filter is close to that of the *CSF*.

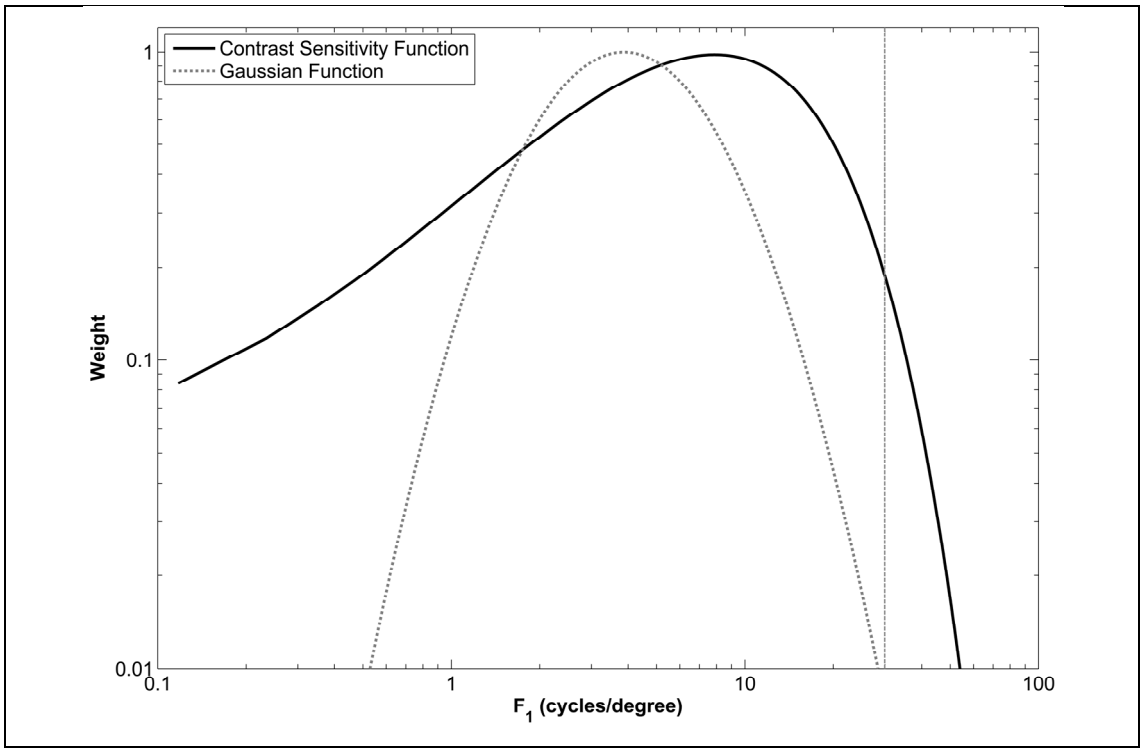


**Figure 7-13: Final Gaussian Fit.**

## 7.5 Summary and Discussion

In this chapter, three *FRF* models of perceived roughness have been developed and tested against the experimental results that define the combinations of the surface parameters $\sigma$ and $\beta$ that give surfaces of equal perceived roughness. Of these, the *power* and *gaussian* models provide a better fit than does the *box* model (see *Tables 7.1* and *7.2*). Other filter shapes were tested in pilot work, but because of the complexity of minimizing more than two parameters, and the unlikelihood of these being natural; these further possibilities are not presented.

The optimised *gaussian filter* does offer two advantages over the *power filter* in terms of its biological plausibility. First, its shape resembles that of the spatial channels that have been identified physiologically and psychophysically in the primate visual pathway. Second, it falls within the human contrast sensitivity function and so does not imply that frequencies outside those detectable by human vision could contribute to the perception of roughness. Even so, experimental evidence is still required to decide conclusively between the two models. Since the *power filter* could be considered as equivalent to a *gaussian* with a centre frequency located above 30 cpd, the critical

difference between them is in the contribution of high frequencies to roughness perception that they imply (compare *Figures 7-8* and *7-13*).

| Function | Filter Function | Min Error $\varepsilon_t$ | Optimized Parameters |
|---|---|---|---|
| **Box** | $\xi_{pr} = \int_{f_p}^{f_c} K \,.\, S(f_f)\ \mathrm{d}f_f$ | **0.0220** | $K$ = 1.00, $f_p$ = 1.53 cpd, $f_c$ = 4.58 cpd. |
| **Power** | $\xi_{pr} = \int_{f_p}^{f_c} (f_f - f_p)^p \,.\, \mathrm{S}(f_f)\ \mathrm{d}f_f$ | **0.0187** | $p$ = 0.24, $f_p$ = 1.06 cpd, $f_c$ = 30.00 cpd. |
| **Gaussian** | $\xi_{pr} = \int_{f_p}^{f_c} \mathrm{k}.\,\mathrm{e}^{\left(-\frac{(\log(f_f)-\log(\mu))^2}{2(\sigma_g)^2}\right)} \,.\, S_{(f_f)}\ \mathrm{d}f_f$ | **0.0189** | k = 1 / max, μ = 3.87 cpd, $\sigma_g$= 2.53 cpd, $f_p$ = 0.01 cpd, $f_c$ = 30.00 cpd. |

**Table 7-2: Summary of all the filter functions and their errors.**

There are two reasons why the $1/F^{\beta}$ *noise* surfaces used in the experiments so far are not suitable to test between these two models. One is the decaying shape of the frequency spectrum of such a surface, in which the magnitudes of high-end frequencies critical for testing between the models are very low relative to those of lower frequencies. As a result, the magnitudes of high frequencies cannot be varied sufficiently for tests between the models without creating large changes in those of low frequencies, which render the surfaces unrealistic. Another reason is the symmetry of the stimuli frequencies, making it possible to compensate with lower frequencies by increasing their weight and decreasing the weight of the high frequencies, or the other way around, therefore making it impossible to determine which is the best fitting filter.

Consequently, in the next chapter, a new kind of stimulus will be presented, where it will be possible to manipulate the magnitudes of high and low frequencies independently. These new stimuli will show which filter provides the best model for perceived roughness.

# CHAPTER 8

## TESTING THE MODELS USING NARROW-BAND SPECTRA SURFACES

The last chapter showed that a *gaussian function* and a *power function* fit the $F_1$ filter (of the *FRF* model of roughness perception) best in comparison to other functions, with closely similar errors. The *gaussian function* had a mean of 3.87 cpd and a standard deviation of 2.53, whilst the *power function* had a power factor equal to 0.24 and a starting cut-off frequency of 1.06 cpd. It is important to notice that the *power function* can also be thought of as a *gaussian function* with a mean greater than 30 cycles per degree (the limit of acuity for observers with 20/20 vision). However, from only the observations in *chapter six*, it is impossible to discern the best fitting model between the *gaussian* and the *power function*.

In this chapter, the construction of new stimuli based on spatial frequency channels will be described. These new stimuli will be used in a set of experiments that will help to discern the best fitting shape for $F_1$ filter. To accomplish this, first the construction of the new stimuli will be examined in *Section 8.1*. In the next (*Section 8.2)*, the *mid-range frequencies* will be explored followed by the *high-range frequencies* and their relationship with perceived roughness. Next in *Section 8.3* both functions will be tested against the new observations from the previous two sections and the *iso-roughness lines* from *chapter six*, followed by *Section 8.4* which will improve the proposed filter by using a function which compromised between shape and parameters. Finishing with a short summary and the conclusions from the chapter as a whole (*Section 8.5*).

### 8.1 New stimuli based on spatial frequency channels

As previously described, it was not possible to distinguish the best fitting filter for $F_1$ between the *gaussian* and the *power function* because two difficulties exist when fitting a function in the $F_1$ filter for the *FRF model* for $1/F^{\beta}$ *noise* surfaces. These two difficulties are produced by the general construction of $1/F^{\beta}$ *noise* surfaces, which suffer from two unwanted characteristics:

a) *Symmetric decay*. In *$1/F^{\beta}$ noise* surfaces magnitude decays symmetrically by the inverse of the frequency to the power of beta (*$1/F^{\beta}$*). Because also the filters are symmetrical, it is possible to compensate for lower frequencies by increasing their weight and decreasing the weight of the high frequencies, or the other way around, therefore making it impossible to determine which is the best fitting filter

b) *Small magnitude in the high frequencies*. The decaying shape of the frequency spectrum of *$1/F^{\beta}$ noise* surfaces produces high-range frequencies that are a hundred times smaller than the magnitude of lower frequencies. Therefore, it reduces the importance of high-range frequencies on the $F_1$ filter and in the model as a whole.

Subsequently a new set of stimuli was constructed, which help the modelling of perceived roughness by exploring how magnitude in bands of frequencies influences perceived roughness. To do this, three main characteristic were required when creating these new stimuli, which are:

1. *Natural looking* surfaces so an observer will not find difficulty matching surfaces;
2. *Isotropic* surfaces, as the 1/f noise surfaces are, and
3. Stimuli that can be tested for roughness at *different frequency* bands.

Although many different surfaces types were considered, the most suitable one that satisfied all of the three characteristics previously described was a surface constructed of *gaussian frequency bands*. This '*frequency bands surface model*' or '*narrow-band spectra surface model*' produces realistically looking surfaces that are also isotropic and the frequency bands' centre, constructed from a *gaussian function*, can be chosen at any frequency to facilitate experimentation with different frequencies.

To get the most realistic feel to the surfaces and to facilitate the experimentation on this surfaces, all the gaussian bands where significantly spaced (10% max overlap), as a result only three *gaussian frequency bands* where used. These three mimic the gaussian approximations of the spatial frequency channels as described by Wilson (1983) and shown in *Figure 8-1*. Only the B, D and F channel approximations were used, as they

do not overlap significantly. Frequency bands below 0.8 cpd will not be tested to avoid puzzling observers between shape and surface texture as it is still unknown the border frequency between an object's shape and its surface's characteristics(Newman, Klatzky, Lederman, & Just, 2005).

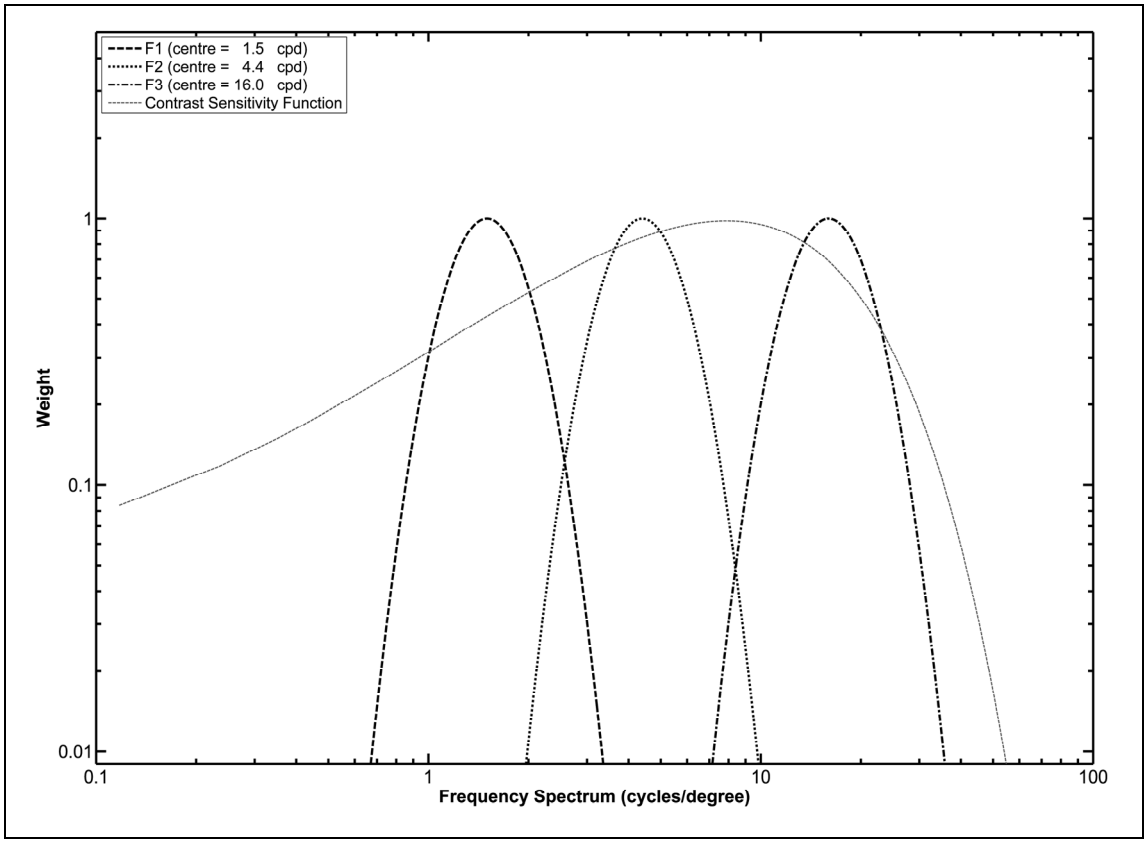


**Figure 8-1: Frequency bands used to construct the new stimuli.**

This *gaussian band surface model* is described in *Formula 8.1* where $S_{gb}$ is the surface in frequency domain, the $F_{b1}$, $F_{b2}$ and $F_{b3}$ values are the magnitudes of the gaussian frequency bands respectively. The $\mu_{b1}$, $\mu_{b2}$ and $\mu_{b3}$ variables correspond to the mean of the logarithmic *gaussian functions* and $\sigma_b$ is the standard deviation of the bands.

$$S_{\mathrm{gb}(f_f,\theta_f)} = F_{b1} \cdot \mathrm{e}^{-\frac{\left(\log\left(X(f_f,\theta_f)\right)-\log(\mu_{b1})\right)^2}{2{\sigma_b}^2}} + F_{b2} \cdot \mathrm{e}^{-\frac{\left(\log\left(X(f_f,\theta_f)\right)-\log(\mu_{b2})\right)^2}{2{\sigma_b}^2}} + \quad \textbf{(8.1)}$$

$$F_{b3} \cdot \mathrm{e}^{-\frac{\left(\log\left(X(f_f, \theta_f)\right) - \log\left(\mu_{b3}\right)\right)^2}{2{\sigma_b}^2}}$$

Although the centres of the three bands used are the same as the approximations of the spatial frequency channels, the standard deviation of each of them was fixed to 1.3. This value was chosen to minimise overlap between bands and at the same time use bands with similar standard deviations but different centres to facilitate the discovery of how frequencies influence perceived roughness.

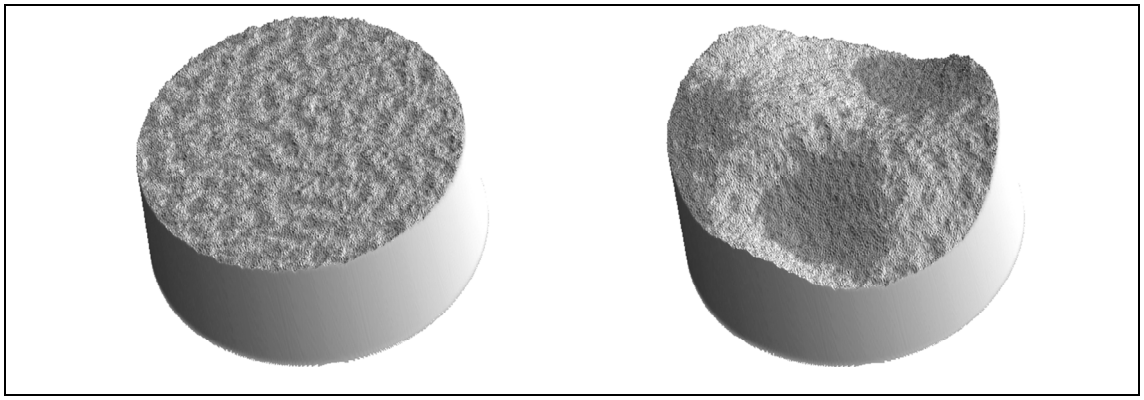

**Figure 8-2: Demonstration of the band stimuli with and without the base (one to two cycles per stimuli width).**

When constructing the stimuli only pairs of adjacent bands were used at a given time to provide the stimuli with its natural feel (more bands give the stimuli a more natural feel), as a result, in the stimuli one band always had a magnitude of zero. In addition, to ensure that occlusions were present and enhance the depth perception by shading, a very low frequency base (0.11 to 0.23 cpd) was used to give the stimuli its characteristic *waviness*, as demonstrated in *Figure 8-2*.

The final stimuli were rendered using the same lighting and construction parameters as previously described in C*hapter 4*, but the frequency profile of the surface was changed to the model of two *gaussian frequency bands* (plus the low-frequency base).

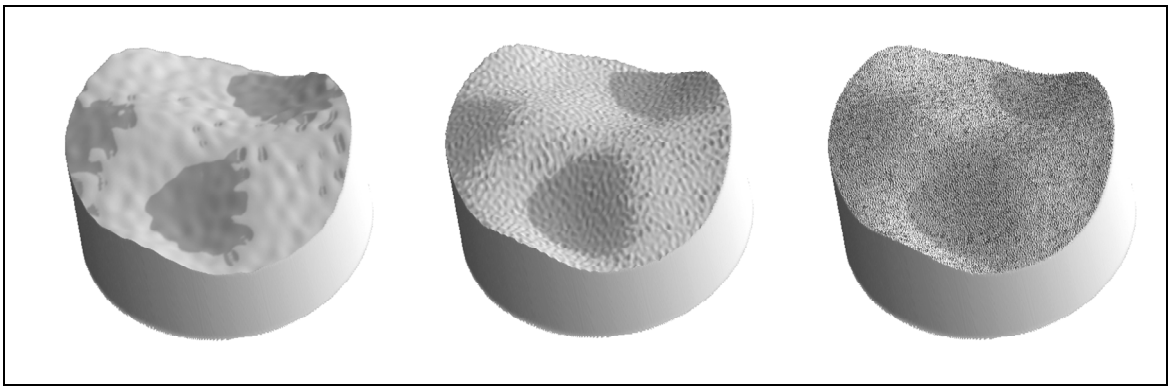

**Figure 8-3: Demonstration of each gaussian frequency band independently (from left to right: $F_{b1}$ = 1.0, $F_{b2}$ = 0.25 and $F_{b3}$ = 0.125).**

## 8.2 Relationship between frequencies and perceived roughness

The next two subsections will explore the connection between the narrow-band spectra surfaces and perceived roughness. To achieve these two new experiments were developed, one for the *mid-range frequency* and one for the *high-range frequencies.*

### *8.2.1 Exploring mid-range frequencies*

In the first experiment, the *mid-range frequencies* will be explored (0.8 cpd to 7.0 cpd). This experiment compromises all of the frequencies that fall underneath the B (centre at 1.5 cycles per degree) and D (centre at 4.4 cycles per degree) gaussian approximations of the spatial frequency channels, as previously described.

The experiment will follow a similar methodology to that described in *Chapter 6*, where contour lines of similar perceived roughness were discovered by comparing two different parameters that influence perceived roughness. For example in the experiment from *Section 6.4*, the two influencing parameters were the $\sigma$ and $\beta$ values. However, for this experiment, the two magnitudes from the gaussian filter bands will be used as influencing parameters ($F_{b1}$ and $F_{b2}$).

The *method of adjustment* was used again to obtain the *iso-roughness lines* between $F_{b1}$ and $F_{b2}$, but this time the observers were adjusting the magnitude of $F_{b2}$ to match a reference surface with fixed parameters. In each trial of this experiment, the observer was asked to match a pair of surfaces, where the *reference surface* always had a

magnitude of $F_{b1}$ {1.0} and a magnitude of $F_{b2}$ {0.25, 0.5 or 1.0}. The *adjustable surface* had a fixed magnitude of $F_{b1}$ {0.25, 0.5, 1.0 or 2.0}, while the magnitude of $F_{b2}$ could be adjusted by the observers.

Observers were presented with a surface pair, the *reference surfaces* and the *adjustable surface* and then observers were asked to adjust the *adjustable surface* until it looked as being similar in perceived roughness to the *reference surface*, again imaging how surfaces would feel if touched. At no point, the observers were aware they were adjusting the magnitude of just one *frequency band* or the inner workings of the adjustment.

Each observer was asked to match in random order twelve surface pairs (i.e. all combinations of three values of $F_{b2}$ in the *reference surface* and four values of $F_{b1}$ in the *adjustable surface*). Each pair was presented three times, with different random $\theta$ (seed values {1, 2 or 3}) to add robustness to the results. In total, each observer had to match by perceived roughness thirty-six surface pairs (plus four practice pairs). The experiment stimuli, trials and characteristics are fully described in *Appendix 8-A*. Ten naïve observers volunteered to take part in the experiment, which used the standard set-up described in *Chapter 5*. Each observer took on average twelve seconds to match a surface pair. The results from all the observers are compiled in *Figure 8-4* and tabulated in *Appendix 8-B*.

*Figure 8-5* shows the median values of $F_{b2}$ for each of the 12 matches, together with the *iso-roughness lines* fitted to the all the observers' data using the *least squares fitting* method, which show that the best fitting line is a polynomial function. It is also possible to discern from *Figure 8-5* that the high frequency band ($F_{b2}$) is much more important to perceived roughness than the lower frequency band ($F_{b1}$), as small changes in $F_{b2}$ influence drastically $F_{b1}$ (also, the two variable samples are statistically relevant as $p < 0.000001$ in both). The parameters of the lines, statistical relevance and fitting error are further detailed in *Appendix 8-C*.

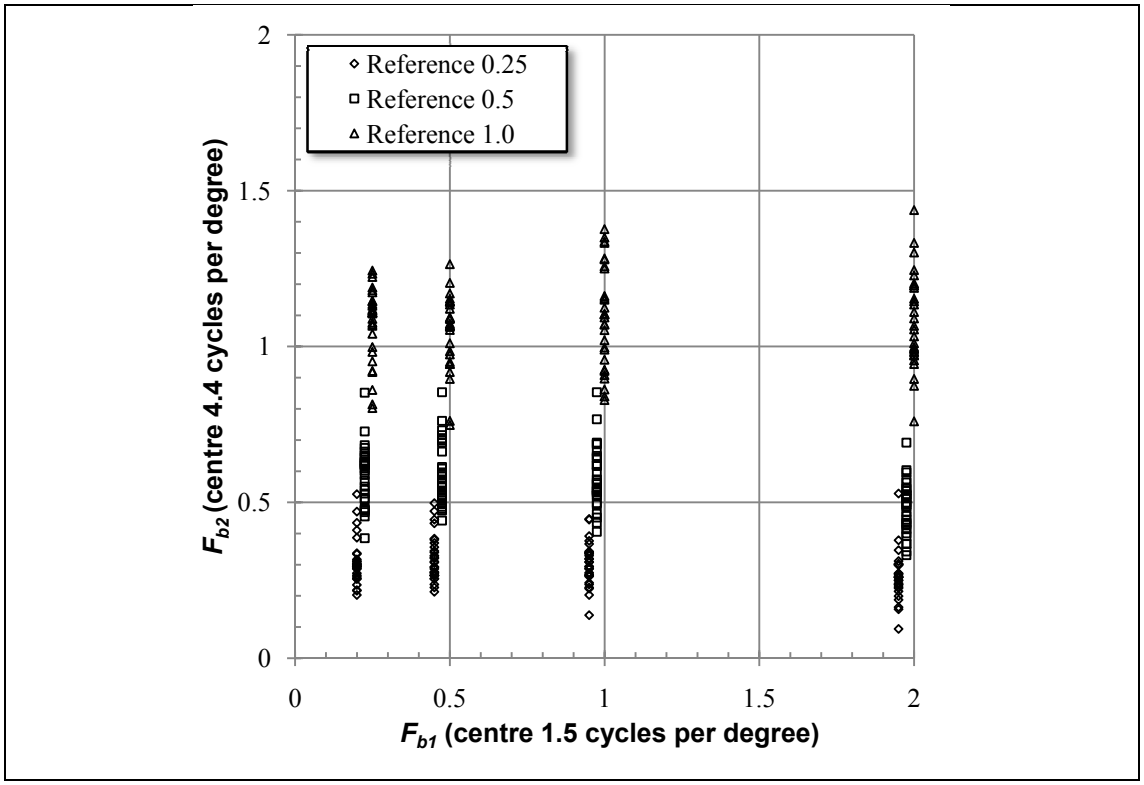


**Figure 8-4: Individual data for the experiment on mid-range frequencies.**

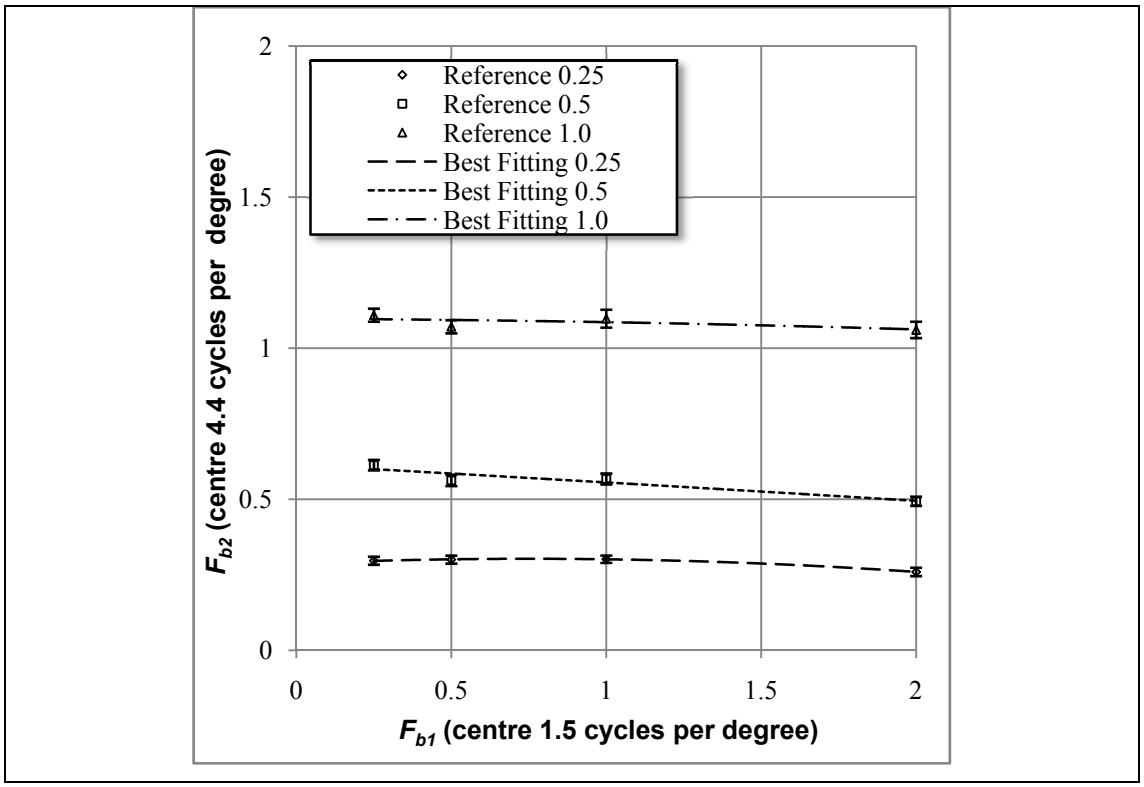


**Figure 8-5: Median observations and *iso-roughness lines* in the space [$F_{b1}$, $F_{b2}$].**

However, we cannot generalize that higher frequencies are more influential in perceiving roughness than lower frequencies, as this might not hold true for frequencies greater than the second *frequency band* (centre at 4.4 cpd). Therefore, in the next section, the effects of the second and third (highest) *gaussian frequency bands* will be explored.

### *8.2.2 Exploring high-range frequencies*

Humans with *20/20* vision are sensitive to frequencies up to 30 cpd, but frequencies above 10 cpd were not tested in the previous experiment. As a result in this section a new experiment is constructed this follows the previous experiment to analyze high frequencies (relationship between the $F_{b2}$ and $F_{b3}$ with centre at 16 cpd and a standard deviation of 1.3 cpd).

The same ten observers as the previous experiment (*Section 8.2*) were asked again to match by perceived roughness a number of surfaces using the *method of adjustment*. Each observer had to match four pair of surfaces where the *reference surface* always had a magnitude of $F_{b2}$ [0.25] and a magnitude $F_{b3}$ [0.25, 0.125 or 0.0625]. The *adjustable surface* had a fixed magnitude of $F_{b2}$ [0.5, 0.25, 0.125 or 0.0625], while the magnitude of $F_{b3}$ could be adjusted by the observers.

In total, each observer had to match thirty-six surface pairs (three value of $F_{b3}$ in the fixed surface times four values of $F_{b2}$ in the adjustable surface times three random phases for robustness) plus four trial pairs. The full description of the experiment is compiled in *Appendix 8-E*, with includes all the characteristics for the stimuli in each trial. The observers took on average 10 seconds to match a surface pair, all the observations are fully described in *Appendix 8-F* and plotted in *Figure 8-6*.

*Figure 8-7* shows the median values of $F_{b2}$ for each of the 12 matches ($p > 0.00001$ for both variables), together with the *iso-roughness lines* fitted to all the observers' data using the *least squares fitting* method. Polynomial lines were found to be the best fit to construct the *iso-roughness lines* from the observers' data, these follow a similar decay as the previous experiment where higher frequencies have a bigger impact on perceived

roughness than the lower frequencies as clearly revealed in *Figure 8-7* and fully described, including statistical analysis in *Appendix 8-D*.

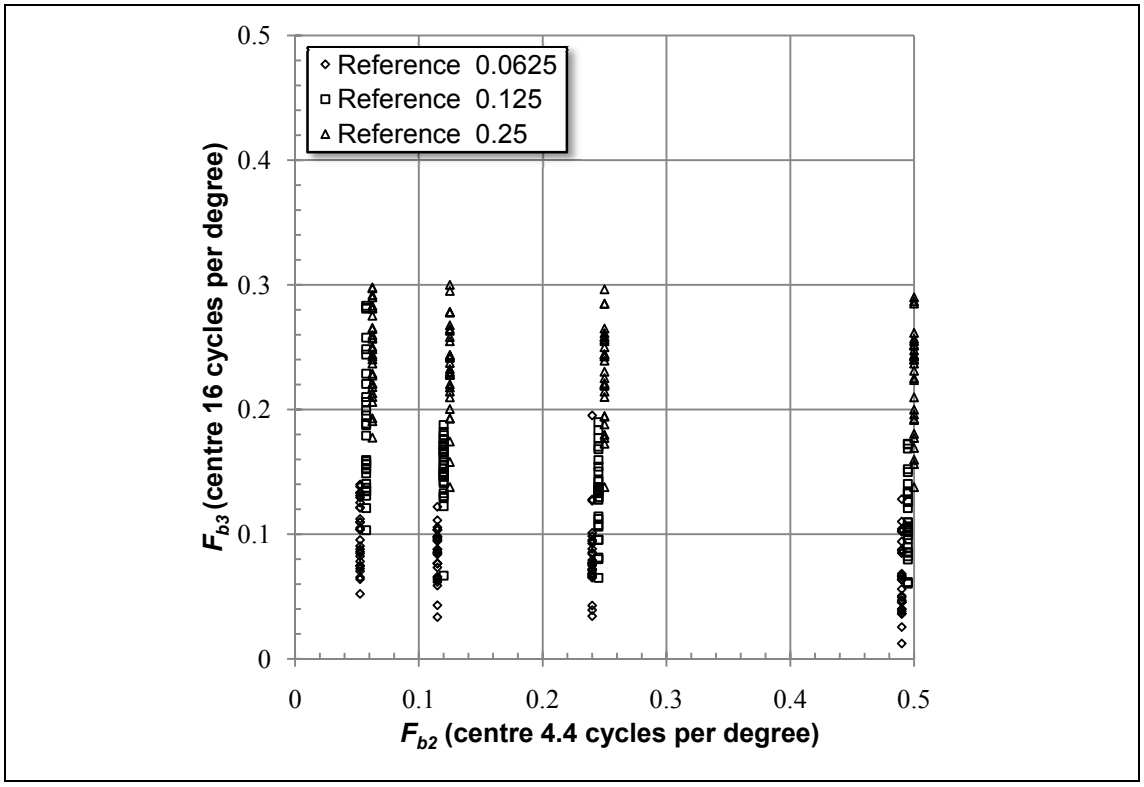


**Figure 8-6: Individual data for the experiment on high-range frequencies.**

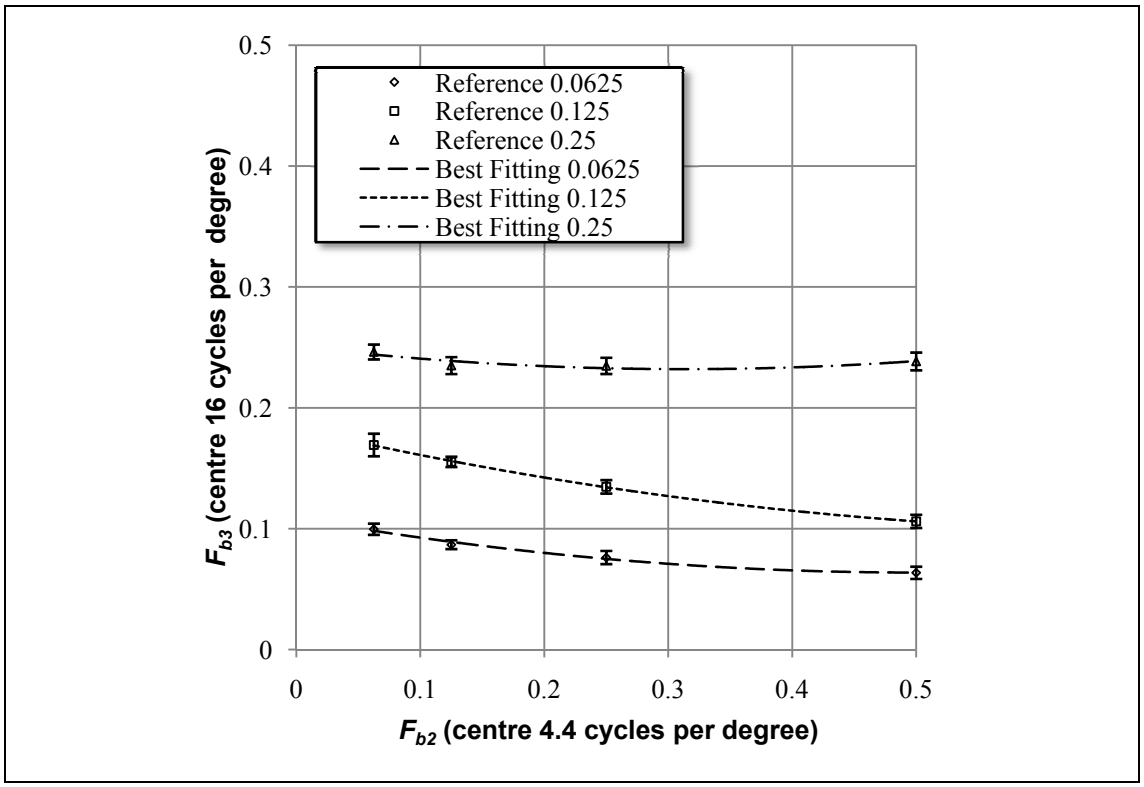


**Figure 8-7: Median observations and *iso-roughness lines* in the space [$F_{b2}$, $F_{b3}$].**

From the last two experiments, it is possible to conclude that higher frequencies are increasingly significant to the perception of roughness, across the range from 0.8 cpd to 30 cpd. It was not possible to test frequency bands higher than 30 cycles per degree because reliable measurements are difficult to obtain due to the limitation in human vision and equipment limitations (resolution, size and modulation transfer function of the displays).

Finally, the results from the previous two experiments were re-plotted in logarithmic scales to demonstrate in similar scales, how different frequencies affect perceived roughness. This are demonstrated in *Figure 8-8* for the [$F_{b1}$, $F_{b2}$] space and *Figure 8-9* for the [$F_{b2}$, $F_{b3}$] space.

These two relationships will be used in the next section to refit a perceptual roughness estimator that takes into account of all frequencies across the range studied, applying similar weight to each experiment.

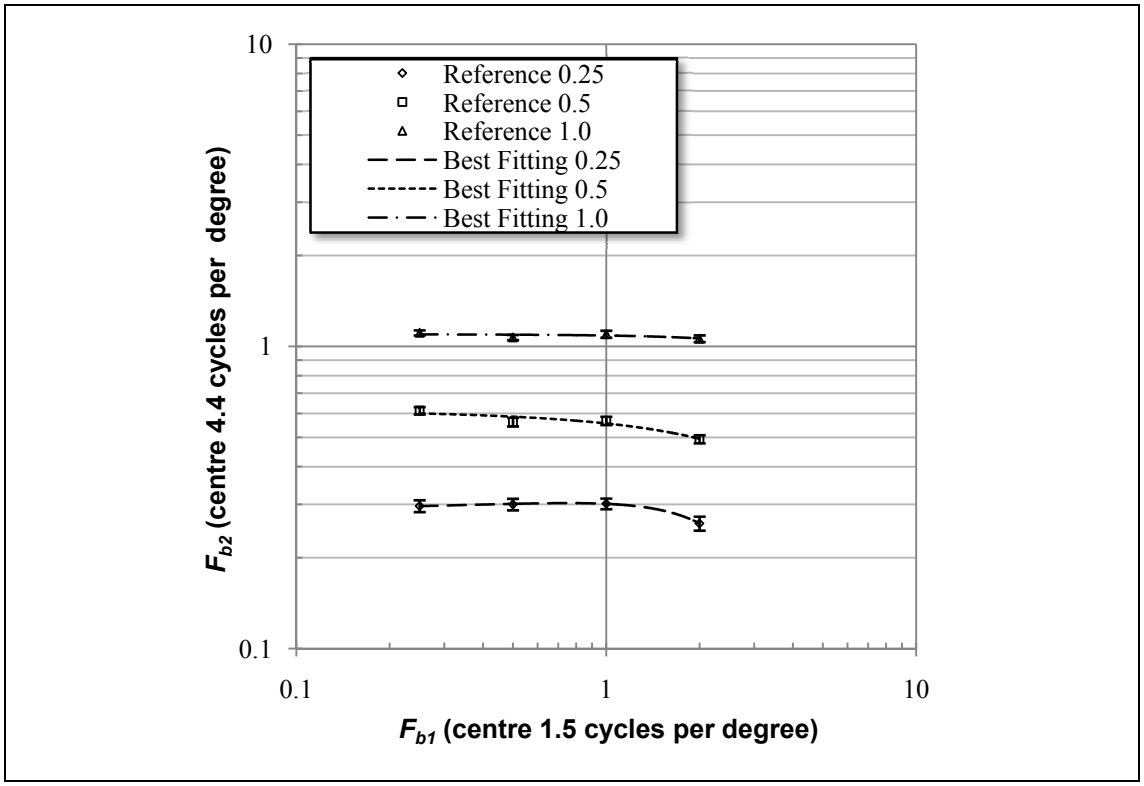


**Figure 8-8: Iso-roughness lines in decades from the experiment in section 8-2.**

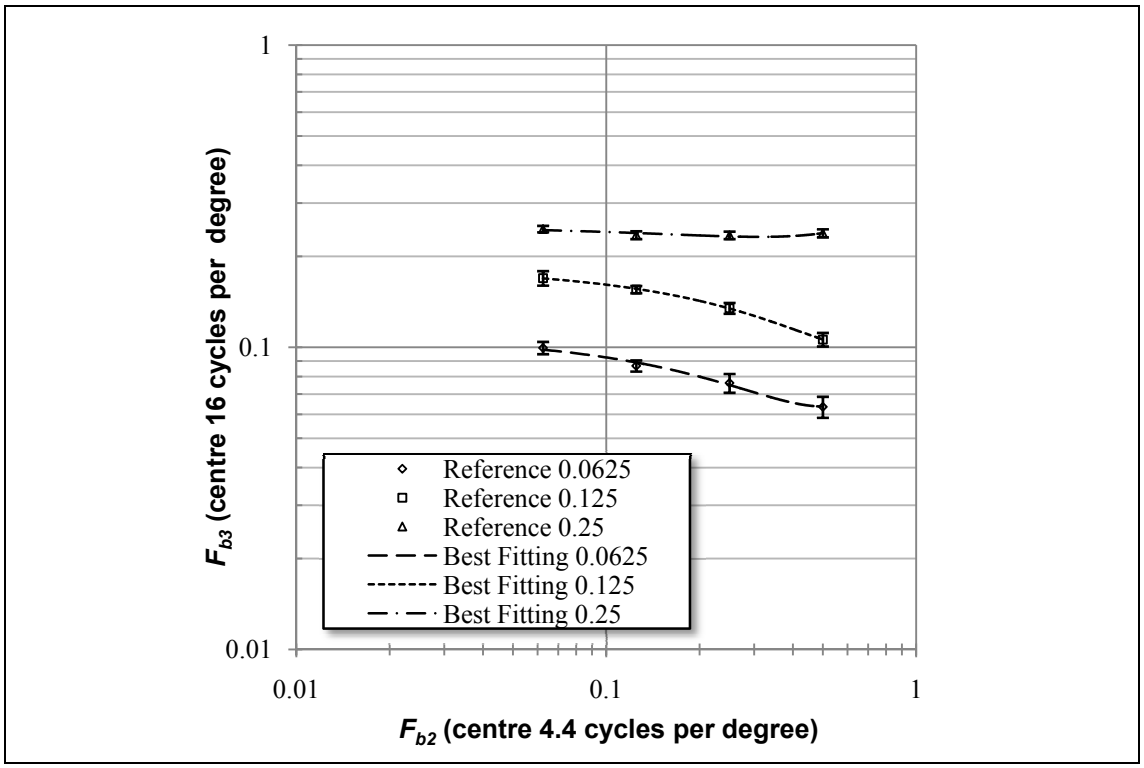


**Figure 8-9: Iso-roughness contour lines for the experiment in section 8-3.**

## 8.3 Modelling perceived roughness including the frequency bands experiments.

As described in *chapter seven*, two functions for the $F_1$ filter of the proposed *FRF* model fit the observed *iso-roughness lines* from *Chapter 6* with the lowest error. These two functions are a *gaussian function* and a *power function*. Unfortunately, it is impossible to differentiate the best fitting function only from the data in *chapter six*. Therefore, these two functions will be tested against the new *iso-roughness lines* discovered from the previous two experiments (*Section 8-2)*.

### *8.3.1 Roughness estimator using a gaussian function for $F_1$*

First, the estimator using a *gaussian function* will be modified to incorporate the two new *iso-roughness line* plots ($F_{b1}$ versus $F_{b2}$ and $F_{b2}$ versus $F_{b3}$). Looking at the results from the previous sections it is possible to appreciate that frequency bands in higher frequencies have more perceptual importance than the band with lower frequencies. Therefore, when fitting a *gaussian function* as the $F_1$ filter this mathematically can only have two forms of parameters:

i. where the centre of the *gaussian function* ($\mu$) is in between two *frequency bands* (in between $F_{b1}$ and $F_{b2}$ or in between $F_{b2}$ and $F_{b3}$) and
ii. where the centre of the *gaussian function* ($\mu$) is above all the *frequency bands* and it can have any width ($\sigma_g$).

The parameters of the *gaussian function* will never be able to fit the model if the centre of the function ($\mu$) is lower than the centre of both of the frequency bands as this is mathematically not possible.

For (*i*), the centre of the *gaussian function* needs to be in between the two *frequency bands* simply because:

a) The lower, less important *frequency band* that is bigger in magnitude (as described in the results from *Section 8.3*) will lie in the raising section of the *gaussian function* therefore this will reduce it.
b) At the same time, the centre and the immediate lowering part of the gaussian will boost the more important, but low in magnitude, high band.

As a result, by having the *gaussian function* in between two of the *frequency bands* it is possible to minimize the error and produce a reliable estimator for perceived roughness.

However, a problem arises when using a *gaussian function* for $F_1$ in between the experiments' three *frequency bands* as the model needs to be fitted to both sets of *iso-roughness lines* (*Section 8.2.1* and *Section 8.2.2*). Therefore, this would imply that it is necessary to have two *gaussian functions* for $F_1$, one in between the *first* and *middle frequency bands* (space [$Fb_1$, $Fb_2$]) and the second one in between the *middle* and *last frequency bands* (space [$Fb_2$, $Fb_3$]), these *gaussian functions* would also need to be of a rather a small width ($\sigma_g < 1.3$).

As a result, the parameters described in (*i*) are mathematically possible but unlikely to be used for the perception of roughness, as $\sigma_g$ is small. Therefore, a more attention will be devoted to a *gaussian function* as described in (*ii*) where the centre is above the experiment's frequency bands (>16 cpd), as it is unlikely the $F_1$ filter is composed of just two gaussian shapes. Nonetheless, the $F_1$ filter might be composed of a number of inter-lapping *gaussian functions*. This will not be tested, as it requires the optimization of a number of gaussians with different weights and parameters for the three

experiments. Furthermore, if the $F_1$ filter is formed by many gaussians then the final optimized function for *F1* can be thought as an estimation of these multiple gaussians.

As for the last form of parameters (*ii*) of the *gaussian function* were the mean is greater than the centre of the frequency bands, then this is mathematically viable (as observed in *Section 8.2*) because:

a) The lower, less important however high in magnitude band is reduced with the starting inclination of the gaussian, whilst
b) The high, more important but low in magnitude band is boosted with the increasing slope of the gaussian.

As the centre of the gaussian needs to exceed the mean of the pairs of bands then it is implied that the centre of the gaussian needs to be greater than the third gaussian band mean frequency (> 16 cpd).

Optimizing the parameters, using the same method as previously described in *chapter seven,* of the *gaussian function* [$\mu$, $\sigma_g$] that give the best fit to the [$F_{b1}$, $F_{b2}$] *iso-roughness lines* yields values of 28.29 cycles per degree and 4.91 cycles per degree respectively (see *figure 8-10*). The mean value is located above the mean of $F_{b3}$ and near the upper-edge of the 20/20 visual range. The parameters of the *gaussian function* that give the best fit to the [$F_{b2}$, $F_{b3}$] *iso-roughness lines* are similar to these values where $\mu$ is 24.65 cycles per degree and $\sigma_g$ is 4.37 cycles per degree (see *Figure 8-11*).

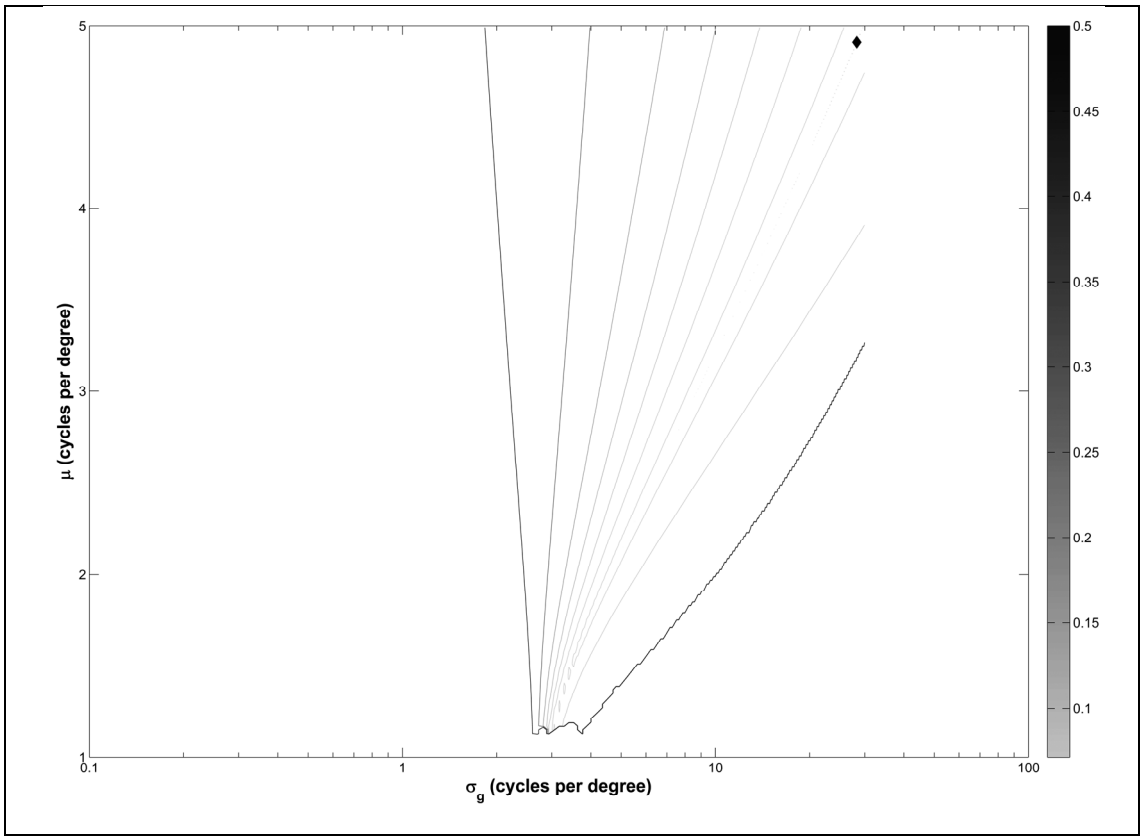


**Figure 8-10: Optimization of the parameters of the *gaussian function* with the [$F_{b1}$, $F_{b2}$] bands.**

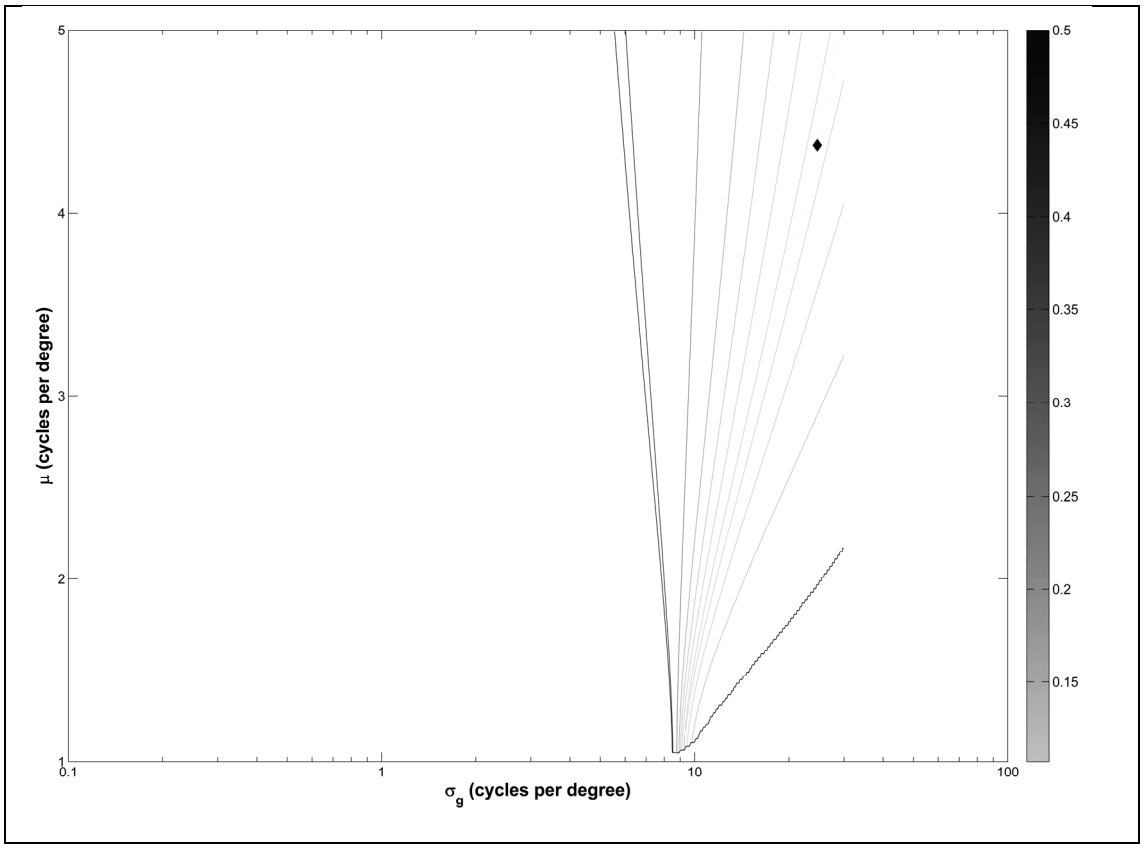


**Figure 8-11: Optimization of the parameters of the *gaussian function* with the [$F_{b2}$, $F_{b3}$] bands.**

Currently, more important than finding the individual optimized parameters of each set of *iso-roughness lines* is to find a solution (of optimized parameters) that minimises the errors $\varepsilon_t$ to the minimum of both. Therefore, a similar weight was assigned to each of the optimized parameters plots and then they were combined together, similar to calculating $\varepsilon_t$ for the six *iso-roughness lines* in *Section 8-2*. The result from these new optimized values shows that the optimized parameters coincide with the upper range of the human visual acuity (30 cpd) as detailed in *Figure 8-12*. The optimized parameters are $\mu$ equal to 30 cycles per degree and $\sigma_g$ equal to 5.0.

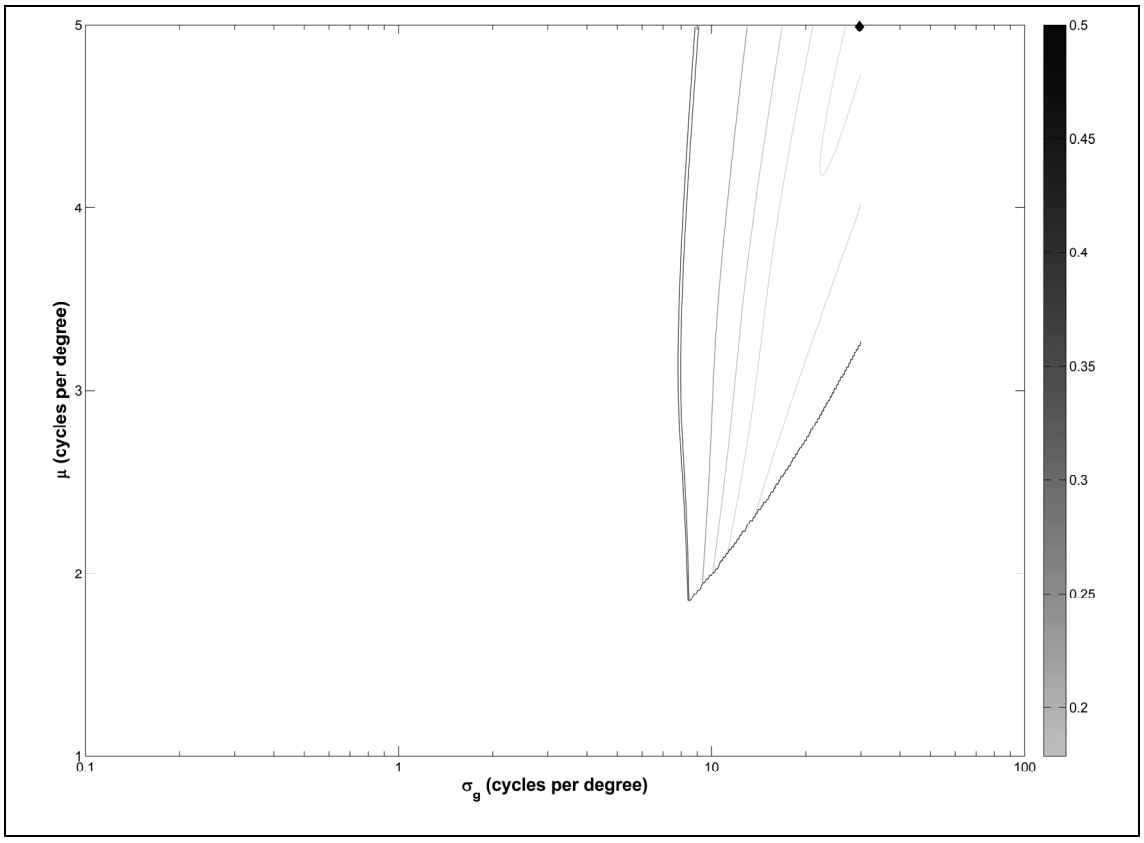


**Figure 8-12: Optimized parameters with all the experiments in *chapter eight* using a *gaussian function*.**

The optimized minimum from the experiments together falls on the edge of the visual range ($\mu$ > 30 cpd), further values were not calculated as with these values the function stops being a *gaussian* and it acts more as a simple slope or *power function*. When comparing this optimization to the ones in *chapter seven* (*Figure 7-11*) it is apparent that the two minima fall at very different points in the parameter space, in particular, the centre of the gaussian lies at approximately 4 cpd when the data from the experiment in *Chapter six* are fitted, but at 30 cpd when the present data are fitted. As a result, if we

sought to get a final optimization for the experiments in *Chapter 6* and *Chapter 8*, the solution is going to be just an approximation of the correct value, as the final optimized parameters would be in between the optimal ones for each experiment.

*Figure 8-13* shows the three possible gaussian shapes of the optimized parameters for each of the experiments and the approximation of the optimized parameters when using all the experiments. In the figure, the *gaussian functions* are represented when:

1. the optimal parameters are from the fit of the *iso-roughness lines* of the experiment in *Chapter 6* [$\sigma$, $\beta$],
2. the parameters are fitted to the *iso-roughness lines* from the [$F_{b1}$, $F_{b2}$] space,
3. the parameters are fitted to the *iso-roughness lines* from the [$F_{b2}$, $F_{b3}$] space and
4. the three sets of data are combined with equal weight.

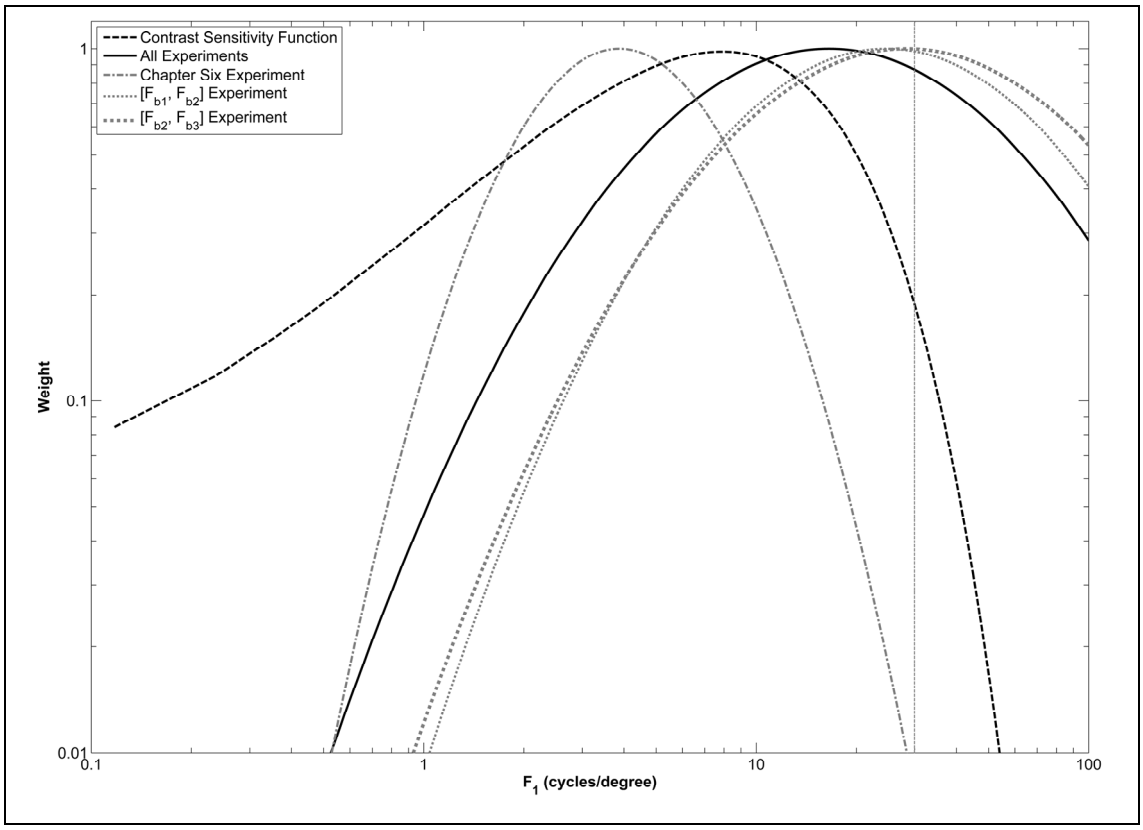


**Figure 8-13: Demonstration of the optimized parameters for the *gaussian function* for each experiment and the total optimization by assigning equal weights to each experiment.**

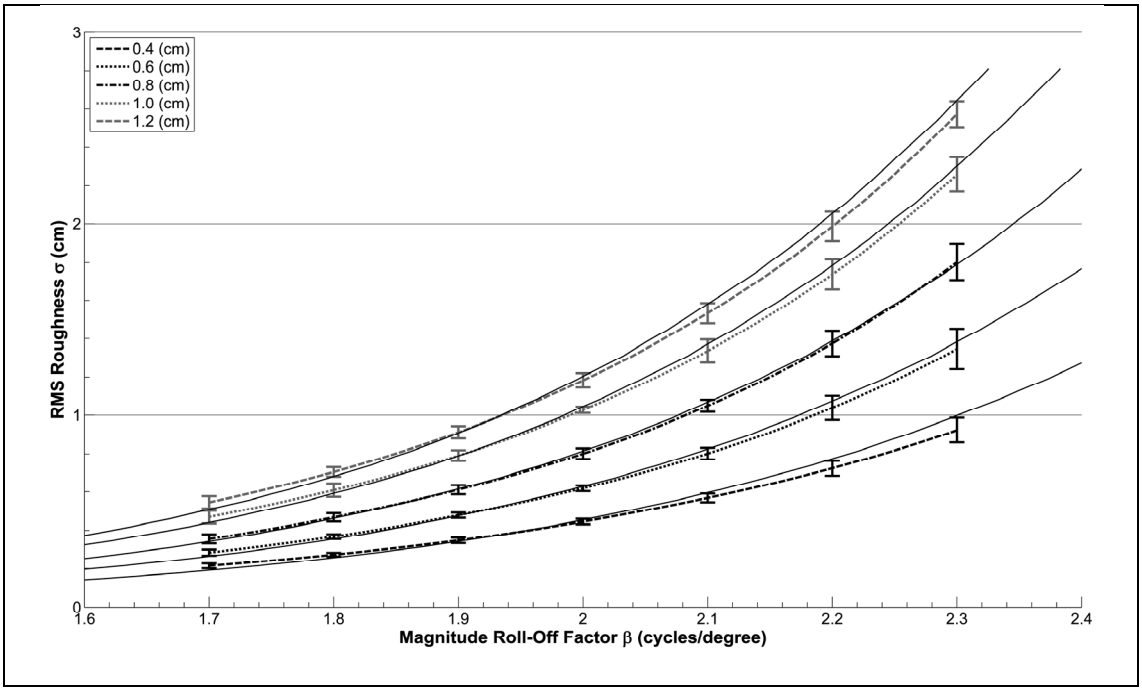


**Figure 8-14: Fit of the model compared to the *iso-roughness lines* from *chapter six* when weighting each optimized parameter from the three experiments equally (unbroken lines are the model's output).**

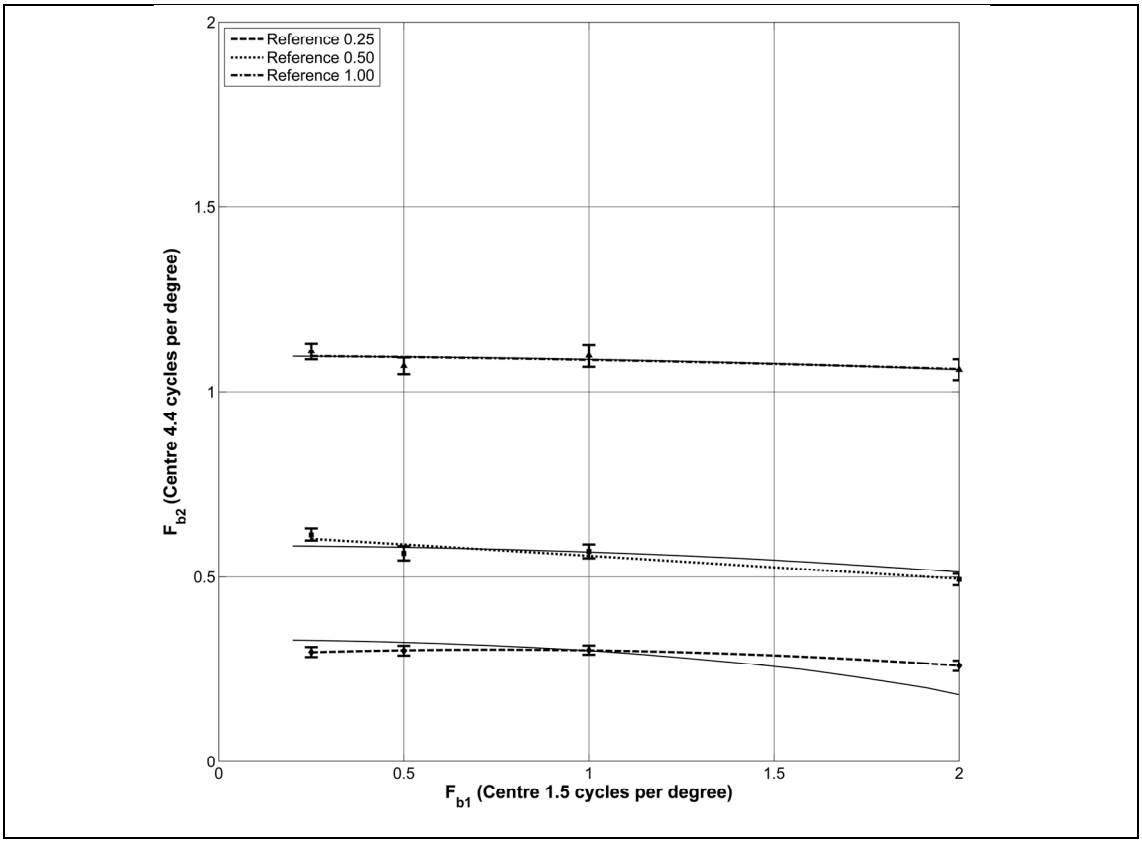


**Figure 8-15: Fit of the model compared to the *iso-roughness lines* from [$F_{b1}$, $F_{b2}$] when weighting each optimized parameter from the three experiments equally (unbroken lines are the models output).**

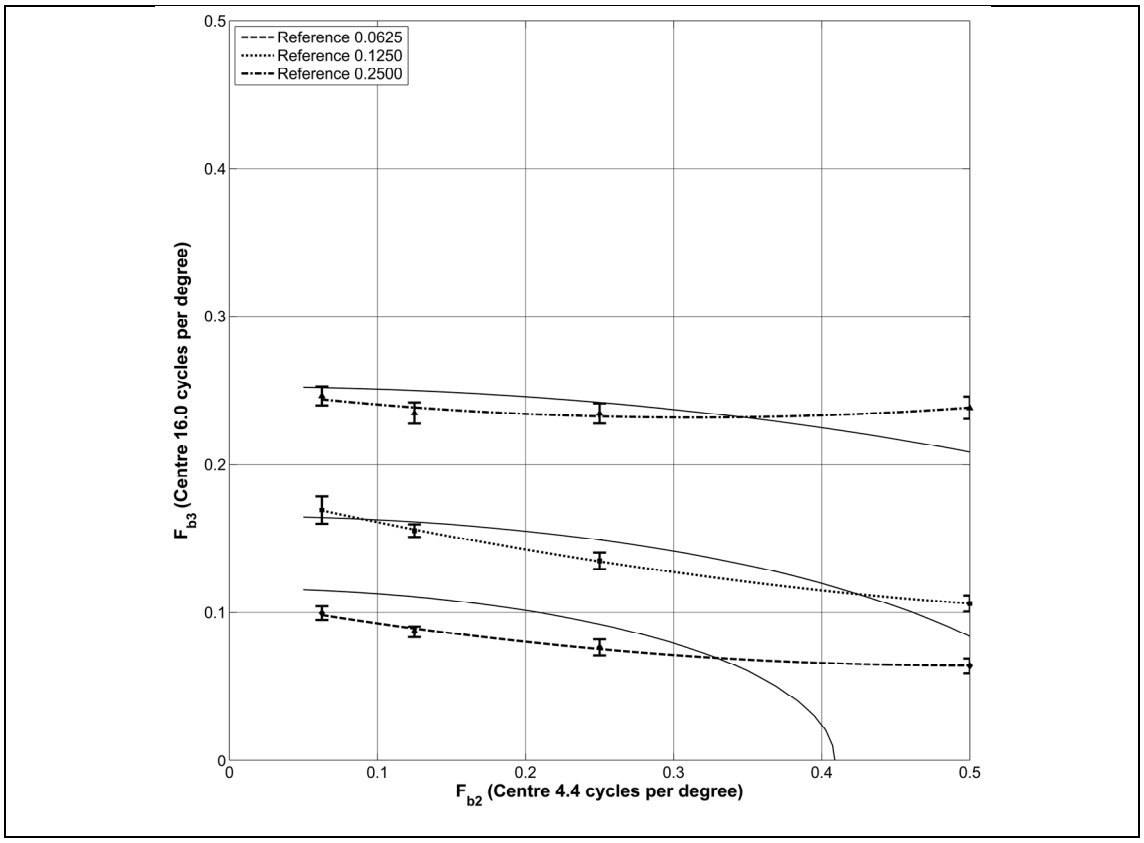


**Figure 8-16: Fit of the model compared to the *iso-roughness lines* from [$F_{b2}$, $F_{b3}$] when weighting each optimize parameter from the three experiments equally (unbroken lines are the models output).**

When the experiments are similarly weighted the results are poor as demonstrated in *Figure 8-14* for the experiment in *Chapter 6*, *Figure 8-15* for the [$F_{b1}$, $F_{b2}$] *iso-roughness lines* and *Figure 8-16* for the [$F_{b2}$, $F_{b3}$] *iso-roughness lines*. *Appendix 8-G* to A*ppendix 8-O* illustrate the fittings when weighting the model at the optimal parameters from each experiment.

Nevertheless, the *gaussian function* was not the only one that fitted with the least error the iso-roughness lines from *Chapter 6*; a *power function* fitted the lines also as described in *chapter seven*, therefore the parameters from the *power function* will be also optimized by the two new experiments.

### *8.3.2 Roughness estimator using a power function for $F_1$*

In this section, the *power function* previously described in *Section 7.3.2* will be optimized again to incorporate the two new experiments from *Section 8.2*. With these

new experiments, the new optimization is going to represent more accurately perceived roughness in most of the frequency spectrum.

The optimizations of the parameters of the *power function* [$f_p$, $p$] that minimize the error $\varepsilon_t$ are shown in *Figure 8-17* and *8-18.* The optimal parameters for the [$F_{b1}$, $F_{b2}$] *iso-roughness lines* are located at a starting frequency $F_p$ of 0.70 cpd and an exponent $p$ of 1.31. As for the optimized parameters for the [$F_{b2}$, $F_{b3}$] *iso-roughness lines* the $F_p$ is at 4.70 cpd and a $p$ of 0.2.

If the two sets of optimized parameters, for the experiments in this chapter, are weighted similarly and the optimal parameter is searched then there is a clear minimum at $F_p$ of 1.41 cpd and a $p$ of 0.78. Unfortunately, this minimum value does correspond to the optimized value from the experiment in *Chapter 6* (*Figure 7-6*). Therefore, the final optimized parameters for the *power functions* are going to be a compromised approximation between experiments as shown in *Figure 8-19*.

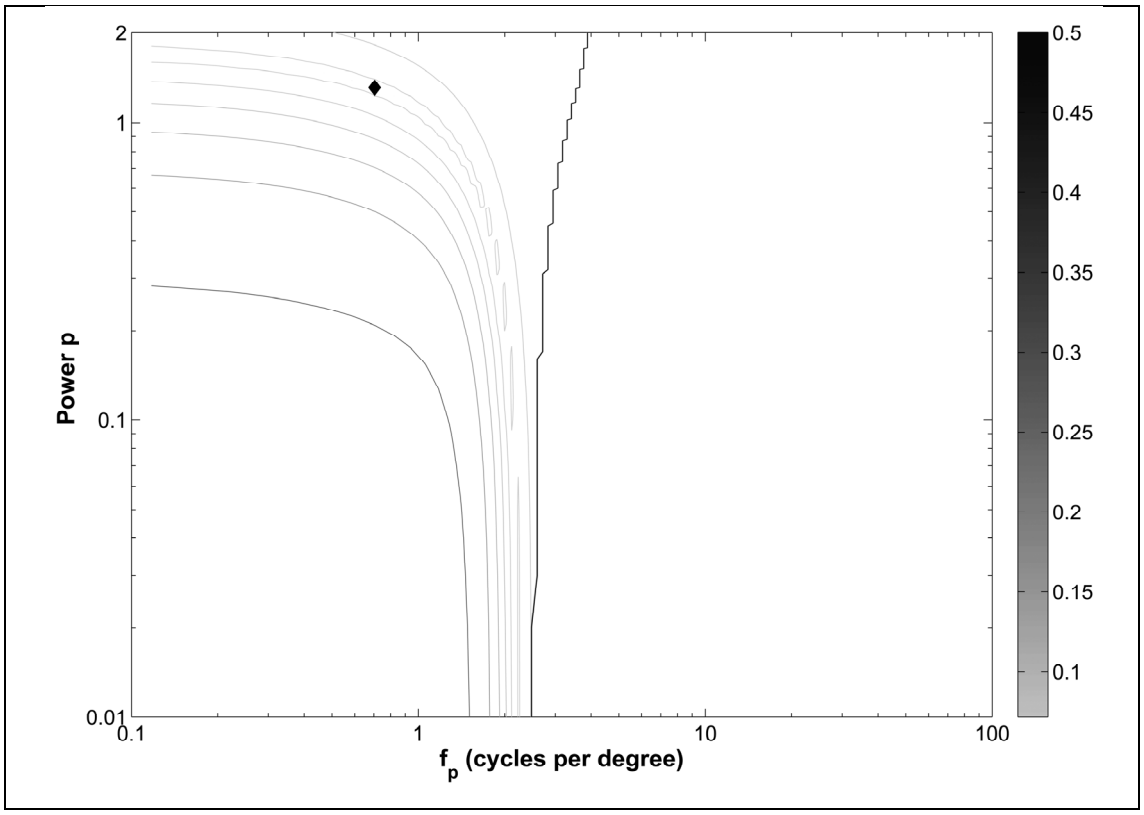


**Figure 8-17: Optimization of the parameters of the *power function* for the [$F_{b1}$, $F_{b2}$] *iso-roughness lines*.**

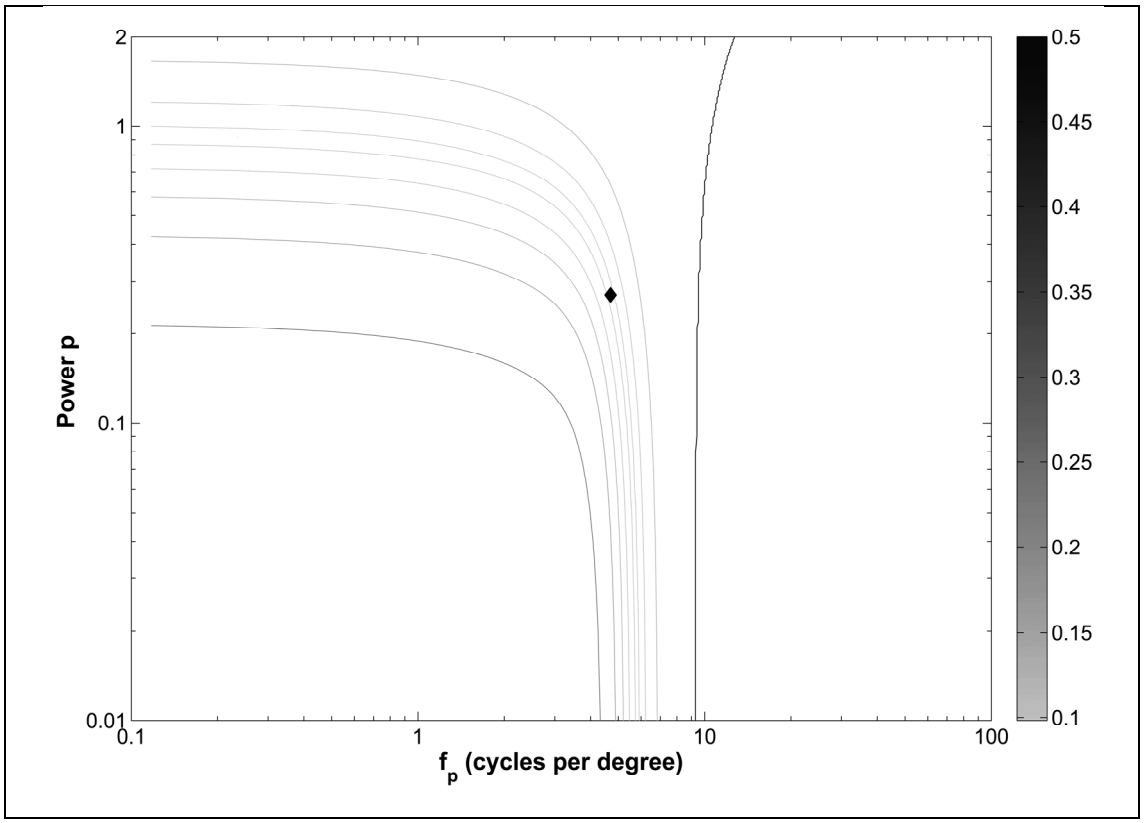


**Figure 8-18: Optimization of the parameters of the *power function* for the [$F_{b2}$, $F_{b3}$] *iso-roughness lines*.**

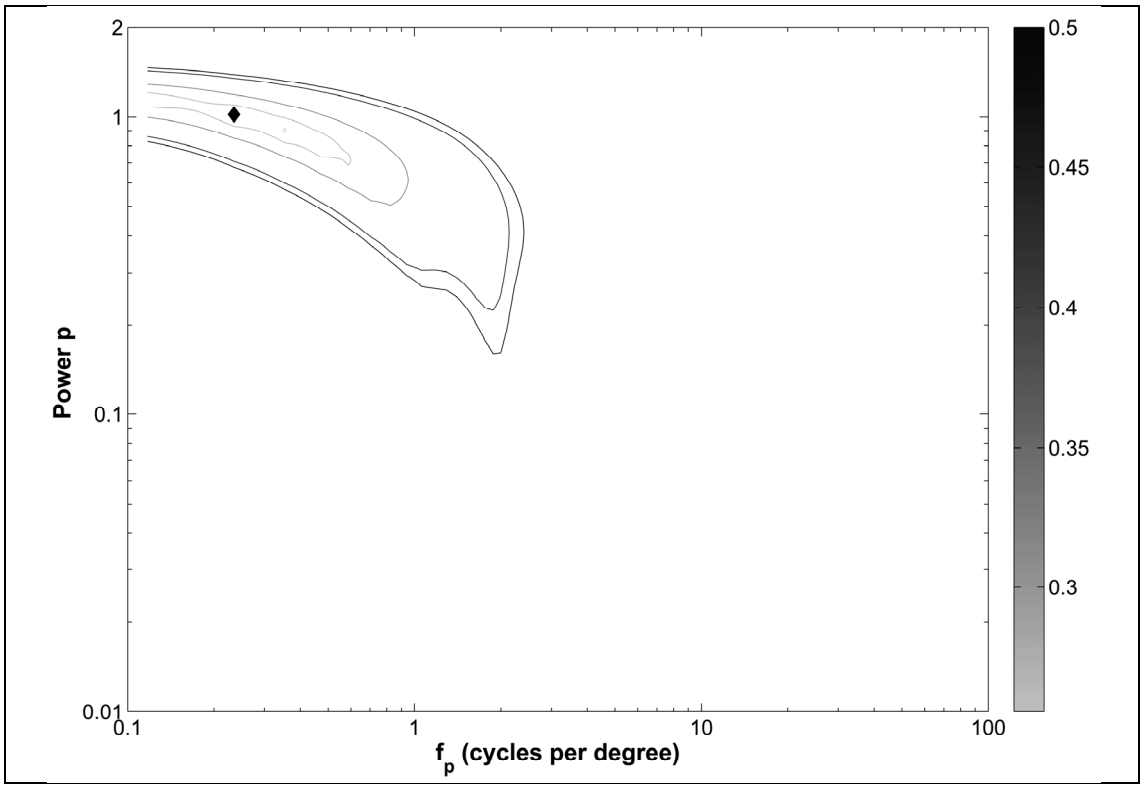


**Figure 8-19: Optimization of the parameters of the *power function* for the combined experiments.**

*Figure 8-20* shows the three possible *power function* shapes of the optimized parameters for each of the experiments and the approximation of the optimized parameters when using all the experiments. Finally, even when the experiments are similarly weighted the results are poor as demonstrated in *Figure 8-21* for the experiment in *Chapter 6*, *figure 8-22* for the [$F_{b1}$, $F_{b2}$] *iso-roughness lines* and *Figure 8-23* for the [$F_{b2}$, $F_{b3}$] *iso-roughness lines*. *Appendix 8-G* to *Appendix 8-X* illustrate the fittings when weighting the model at the optimal parameters from each experiment.

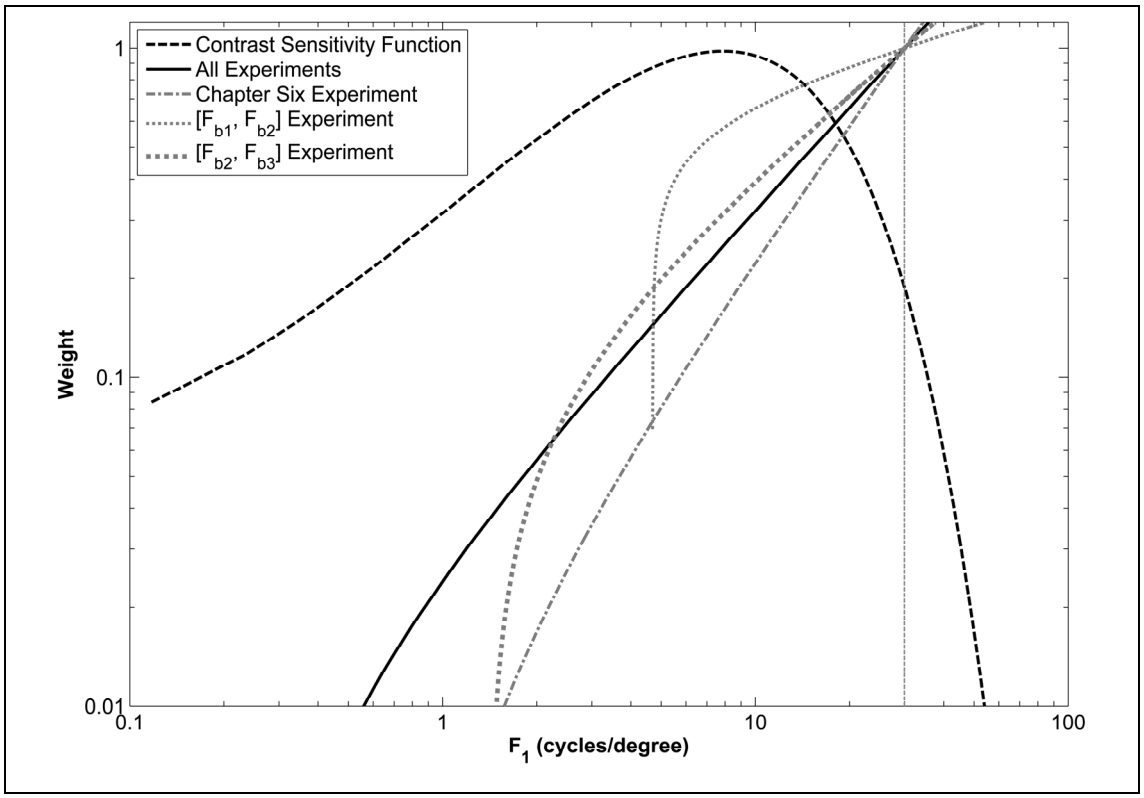


**Figure 8-20: Demonstration of the optimized parameters for the *power function* for each experiment and the total optimization when assigning equal weights to each experiment.**

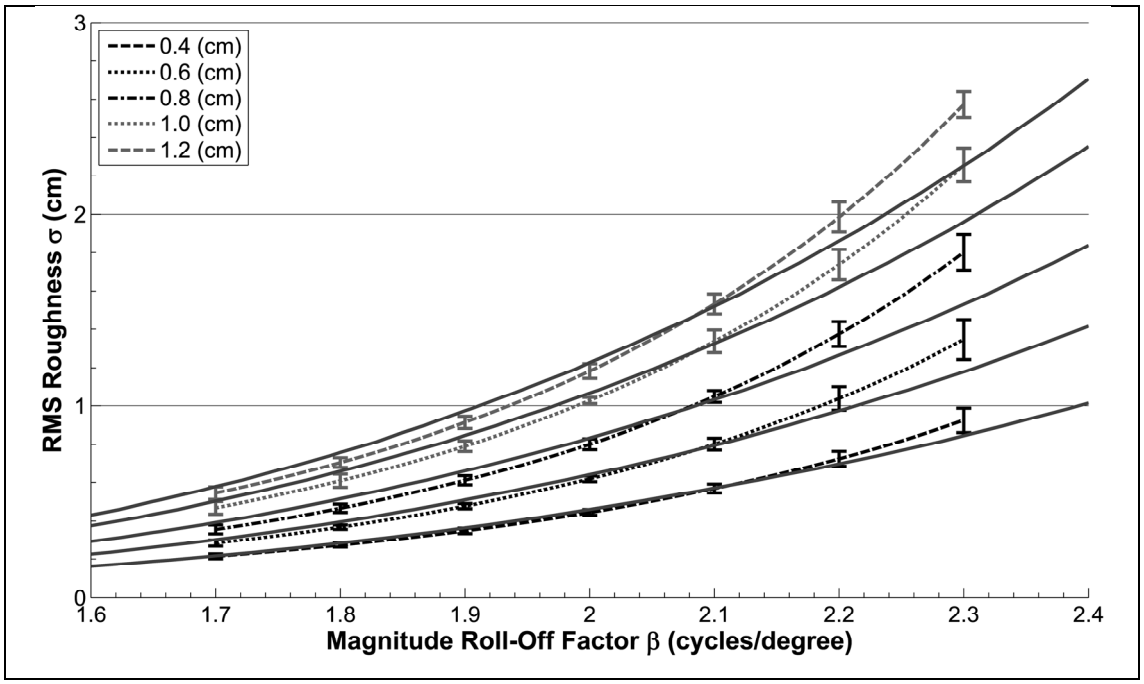


**Figure 8-21: Fit of the model compared to the iso-roughness lines from chapter six when weighting each optimized parameter from the three experiments equally.**

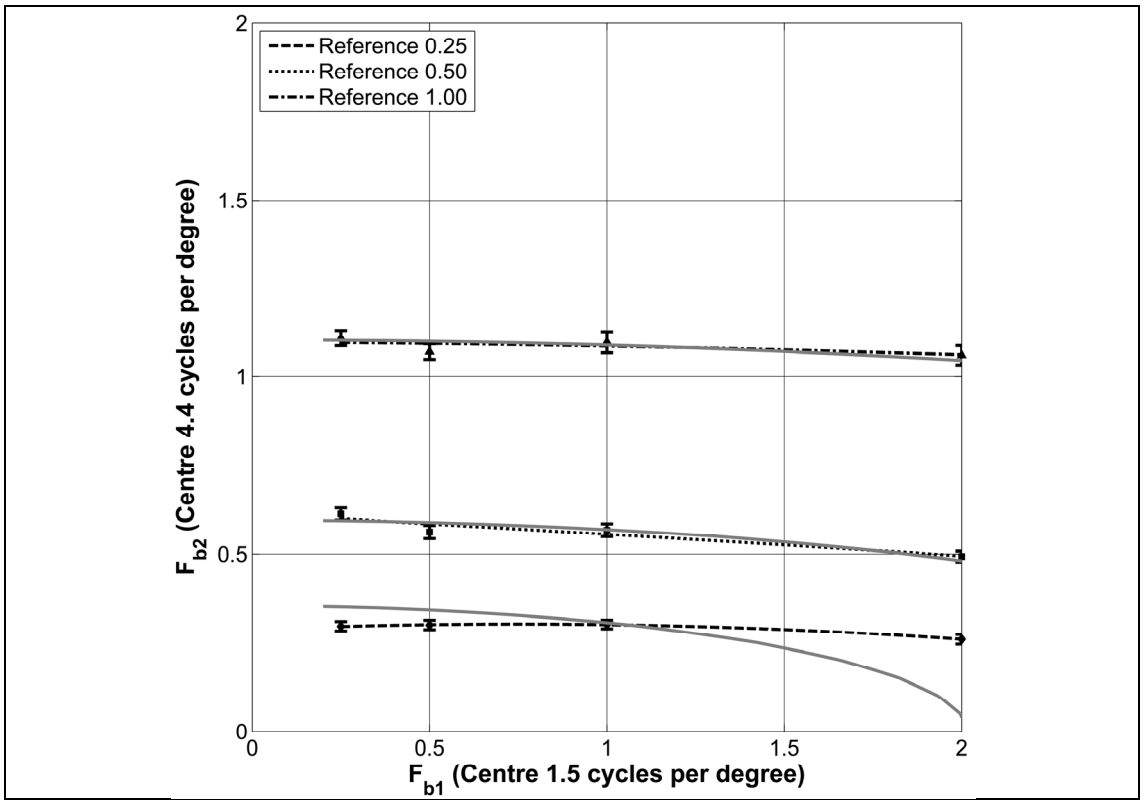


**Figure 8-22: Fit of the model compared to the *iso-roughness lines* from [$F_{b1}$, $F_{b2}$] when weighting each optimized parameter from the three experiments equally.**

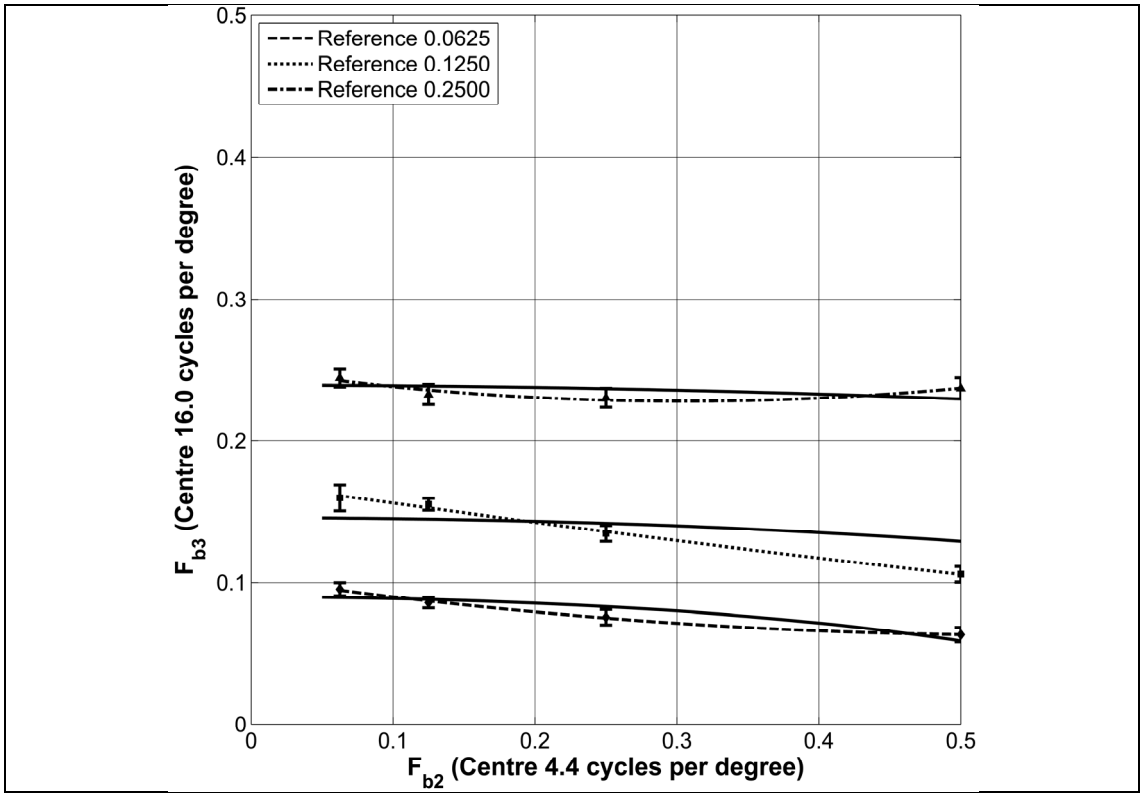


**Figure 8-23: Fit of the model compared to the *iso-roughness lines* from [$F_{b2}$, $F_{b3}$] when weighting each optimized parameter from the three experiments equally.**

| | Parameters for | Optimizing with | $\varepsilon_t$ |
|---|---|---|---|
| ***Gaussian Function*** | $[\beta, \sigma]$ | $[\beta, \sigma]$ | 0.0198 |
| | $[F_{b1}, F_{b2}]$ | $[F_{b1}, F_{b2}]$ | 0.0714 |
| | $[F_{b2}, F_{b3}]$ | $[F_{b2}, F_{b3}]$ | 0.1072 |
| | $[\beta, \sigma]$ | $[\beta, \sigma]+[F_{b1}, F_{b2}]+[F_{b2}, F_{b3}]$ | 0.0594 |
| | $[F_{b1}, F_{b2}]$ | $[\beta, \sigma]+[F_{b1}, F_{b2}]+[F_{b2}, F_{b3}]$ | 0.861 |
| | $[F_{b2}, F_{b3}]$ | $[\beta, \sigma]+[F_{b1}, F_{b2}]+[F_{b2}, F_{b3}]$ | 0.1627 |
| | $[\beta, \sigma]+[F_{b1}, F_{b2}]+[F_{b2}, F_{b3}]$ | $[\beta, \sigma]+[F_{b1}, F_{b2}]+[F_{b2}, F_{b3}]$ | **0.3081** |
| ***Power Function*** | $[\beta, \sigma]$ | $[\beta, \sigma]$ | 0.0187 |
| | $[F_{b1}, F_{b2}]$ | $[F_{b1}, F_{b2}]$ | 0.0714 |
| | $[F_{b2}, F_{b3}]$ | $[F_{b2}, F_{b3}]$ | 0.0983 |
| | $[\beta, \sigma]$ | $[\beta, \sigma]+[F_{b1}, F_{b2}]+[F_{b2}, F_{b3}]$ | 0.0462 |
| | $[F_{b1}, F_{b2}]$ | $[\beta, \sigma]+[F_{b1}, F_{b2}]+[F_{b2}, F_{b3}]$ | 0.1091 |
| | $[F_{b2}, F_{b3}]$ | $[\beta, \sigma]+[F_{b1}, F_{b2}]+[F_{b2}, F_{b3}]$ | 0.1004 |
| | $[\beta, \sigma]+[F_{b1}, F_{b2}]+[F_{b2}, F_{b3}]$ | $[\beta, \sigma]+[F_{b1}, F_{b2}]+[F_{b2}, F_{b3}]$ | **0.2556** |

**Table 8-1: Parameters for each of the iso-roughness lines using every single experiment and all of them.**

As observed from the optimal fittings of the *gaussian function* and the *power function*, the optimal $F_1$ in the proposed model is a slope with a positive increment towards high

frequencies. However, none of the two functions could actually match well the [$F_{b1}$, $F_{b2}$] or [$F_{b2}$, $F_{b3}$] experiment at the same time (see *Table 8-1*), therefore this implies that the low and high end sections of the functions needs to be improved. Therefore, in the next section a new function will be used to improve on the previous two.

## 8.4 Improving further the model

As previously described, the two preferred functions (*gaussian* and *power*) do not model well the [$F_{b1}$, $F_{b2}$] and [$F_{b2}$, $F_{b3}$] experiments at the same time; these are the ones testing *mid-range* to *high-range frequencies*. Therefore, this implies that the low-end or high-end part of the filter needs improvement. As a result, in this section, a new function is presented which appears as a *gaussian function* but has variable low and high ends that can be fully described by three parameters.

This function will be described from now on as a *variable Gaussian*. Its mathematical formula is presented in *Equation 8-2*, where $f_p$ is the starting frequency that is set to avoid negative values, $F_c$ is the cut-off frequency set at 30 cycles per degree. The $k_c$ variable is used to normalize the function, $b_c$ is set to -$m_c$ to normalize the functions as well, $m_c$ is the variable that crooks or alters the low-end part of the gaussian and $c_c$ is the variable that crooks or alters the high-end part of the gaussian.

$$\xi_{pr} = \int_{f_p}^{f_c} \mathrm{k_c}.\left(\mathrm{m_c}\cdot\left(f_f - f_p\right) + \mathrm{b_c}\right).\mathrm{e}^{-\left(\mathrm{m_c}\left(f_f - f_p\right)\right)^{\mathrm{cc}}} .\ \mathrm{S}\left(f_f\right)\ \mathrm{d}f_f \qquad \textbf{(8.2)}$$

This function is similar in construction to the formula used by Mannos to describe the contrast sensitivity function (Mannos and Sakrison, 1974). The advantages of using this function are the low count of parameters but high variability of the shape of the gaussian. *Figure 8-24* demonstrates how the $m_c$ and $c_c$ parameters influence the shape of the *variable gaussian*.

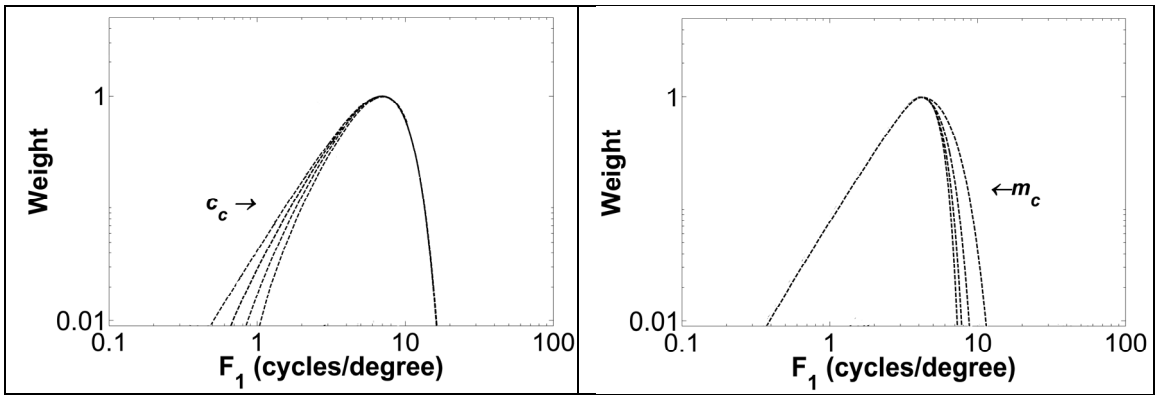


**Figure 8-24: $m_c$ and $c_c$ parameters influencing the *variable gaussian*.**

When optimizing the parameters for the *variable gaussian* for each experiment, it is possible to deduct first the optimal value of $F_p$ from the errors of each experiment, as the other two variables $m_c$ and $c_c$ increase proportionally with $F_p$. As a result, this variable $F_p$ can be optimized separately from the other two. The value $F_p$ was only tested until the start of $F_{b1}$, as higher values would have undermined the experiment using this band. The resulting optimization of this parameter is 0.235 cycles per degree and can clearly be appreciated in *Figure 8-18*.

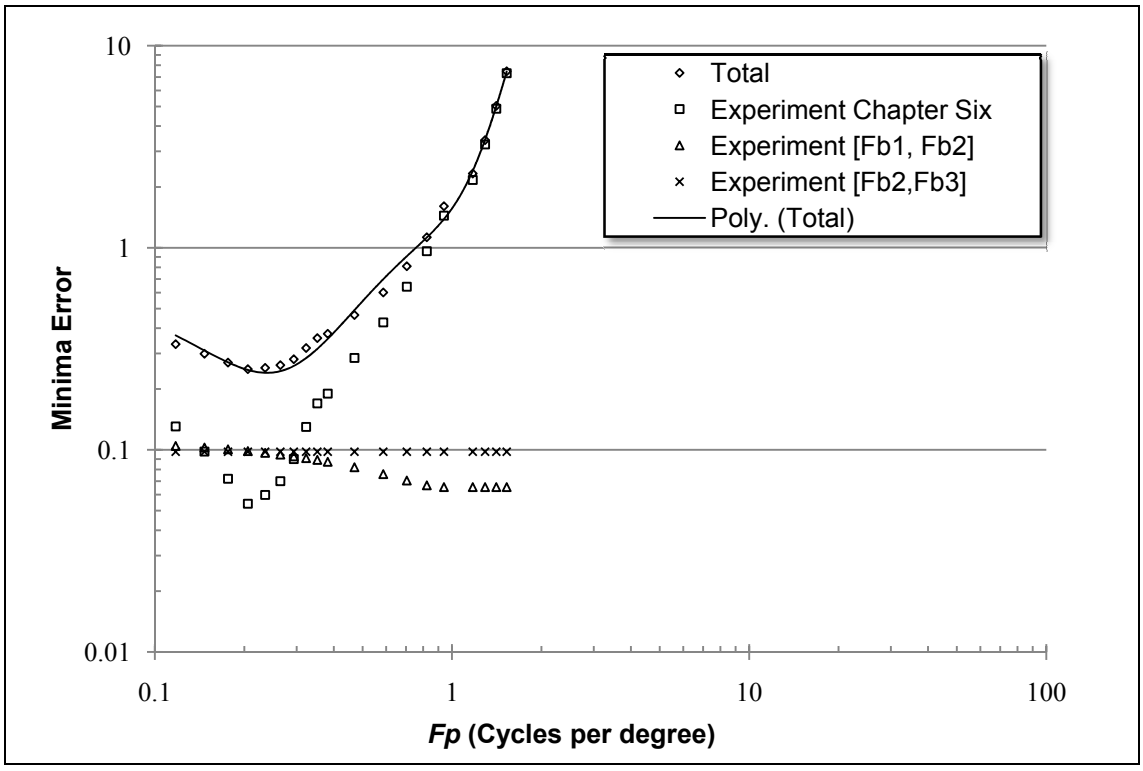


**Figure 8-25: optimizing the $F_p$ value for the *variable gaussian*.**

This optimized $F_p$ value was used to obtain further optimized values of $m_c$ and $c_c$ by minimizing the error for the three experiments, the results show that there are various minima as demonstrated in *Figure 8-26*. These minima are detailed in *Table 8-2*. However, by changing the value of $k_c$, it is possible to tune these minima to a similar shape (as a multiplying a factor does not affect the model) but the high-end part of the *variable gaussian* is still undefined as illustrated in *Figure 8-27* (using multiplied values of $k_c$, defined as $k_{cm}$).

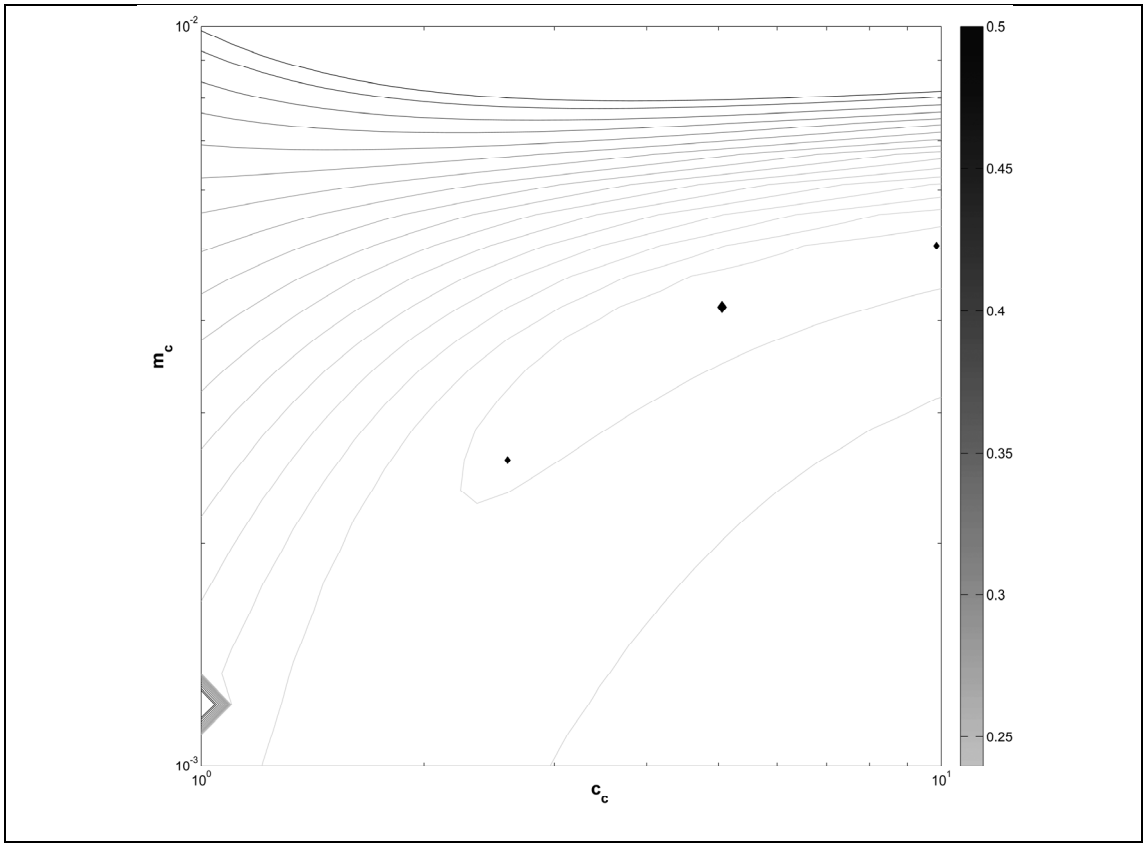


**Figure 8-26: Optimization of the $m_c$ and $c_c$ parameters of the *variable gaussian* using all the three previous experiments. (Minima from left to right $O_{pl}$, $O_p$, $O_{ph}$)**

| *Parameters* | $O_p$ | $O_{pl}$ | $O_{ph}$ |
|---|---|---|---|
| $c_c$ | 5.054 | 2.594 | 9.8497 |
| $m_c$ | 0.0042 | 0.0026 | 0.0051 |
| $k_c$ | 1.6891 | 2.131 | 1.405 |
| $k_{cm}$ | 1.6891 | 2.771 | 1.377 |
| $\varepsilon_t$ | 0.2399 | 0.2408 | 0.2400 |

**Table 8-2: Optimized parameter values for the *variable gaussian* using the three experiments.**

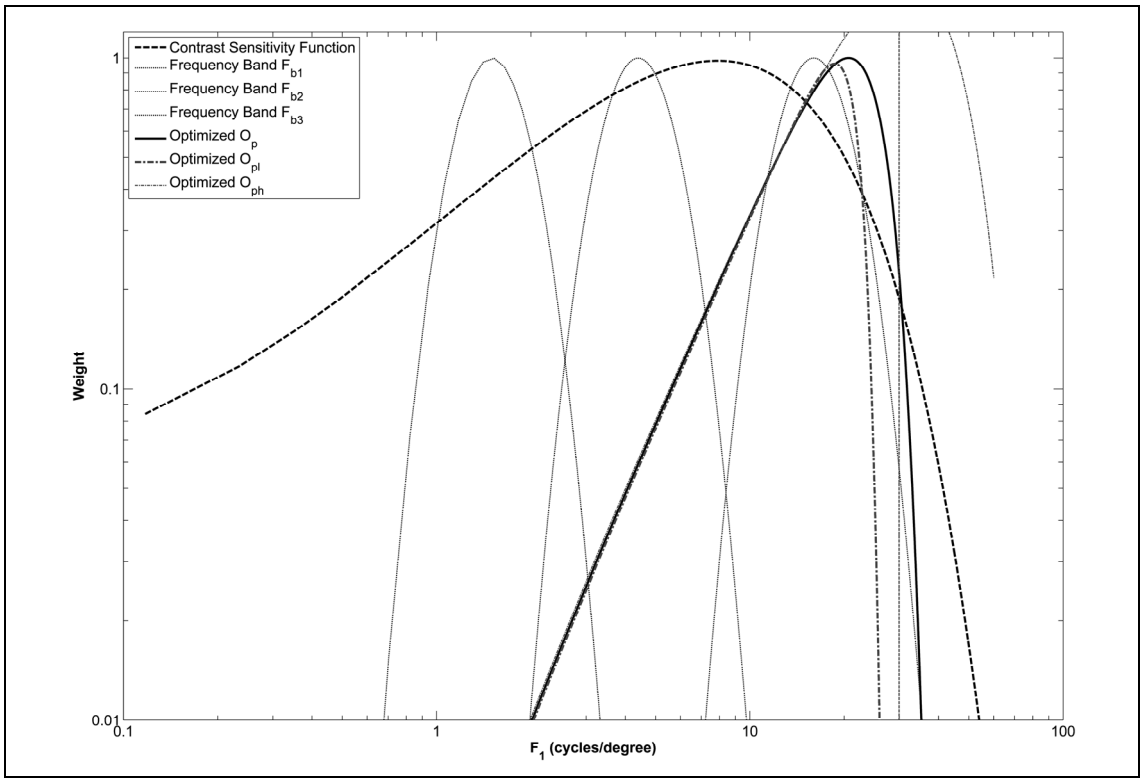


**Figure 8-27: Three optimizations for the *variable gaussians* were they were match by multiplying a factor to them. Please notice that the *variable function* can be multiplied by any factor, as a result the plot for the line can go even further than plotted here.**

When the $O_p$ parameters are compared to the observed data, it is possible to discern that the *variable gaussian* is a much better function for the $F_1$ filter, as shown in *Figure 8-28* to *Figure 8-30.* Although there are some small fitting errors in the lower magnitude bands of the band pass experiments, it is reasonable to assume that these errors are produced because of:

a) the difficulty of matching these bands with small magnitude by the observers and
b) the difficulty of testing even higher frequency bands than $F_{b3}$.

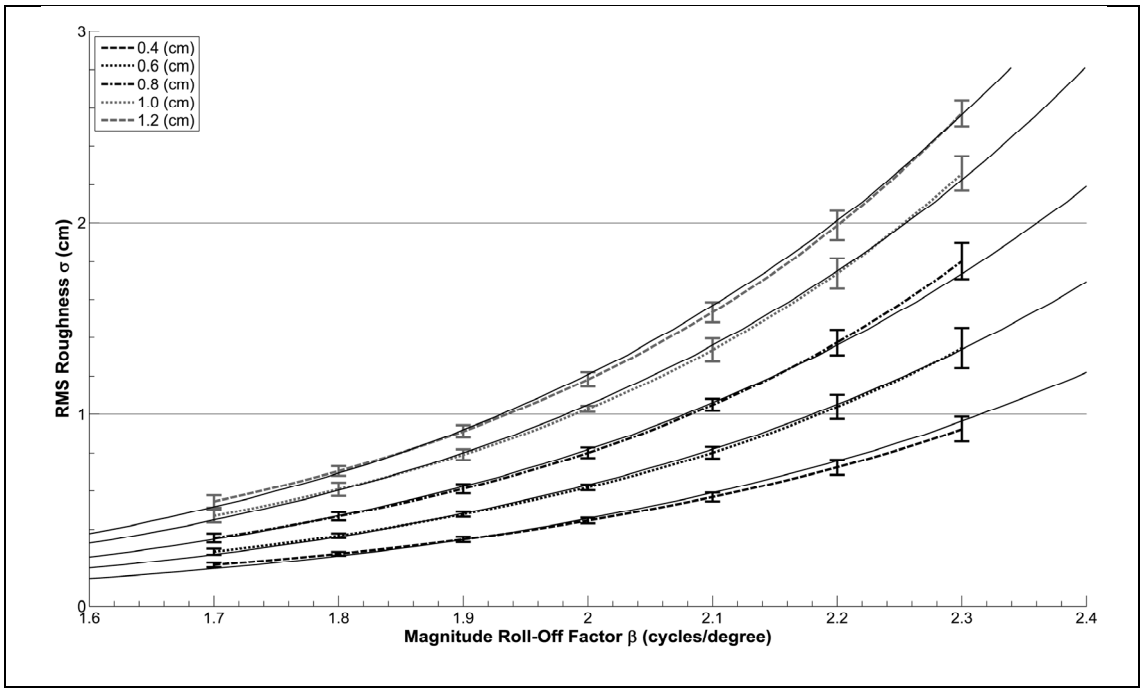


**Figure 8-28*: Iso-roughness lines* from *Chapter 6* compared to the predicted model using a *variable gaussian* with optimized parameters.**

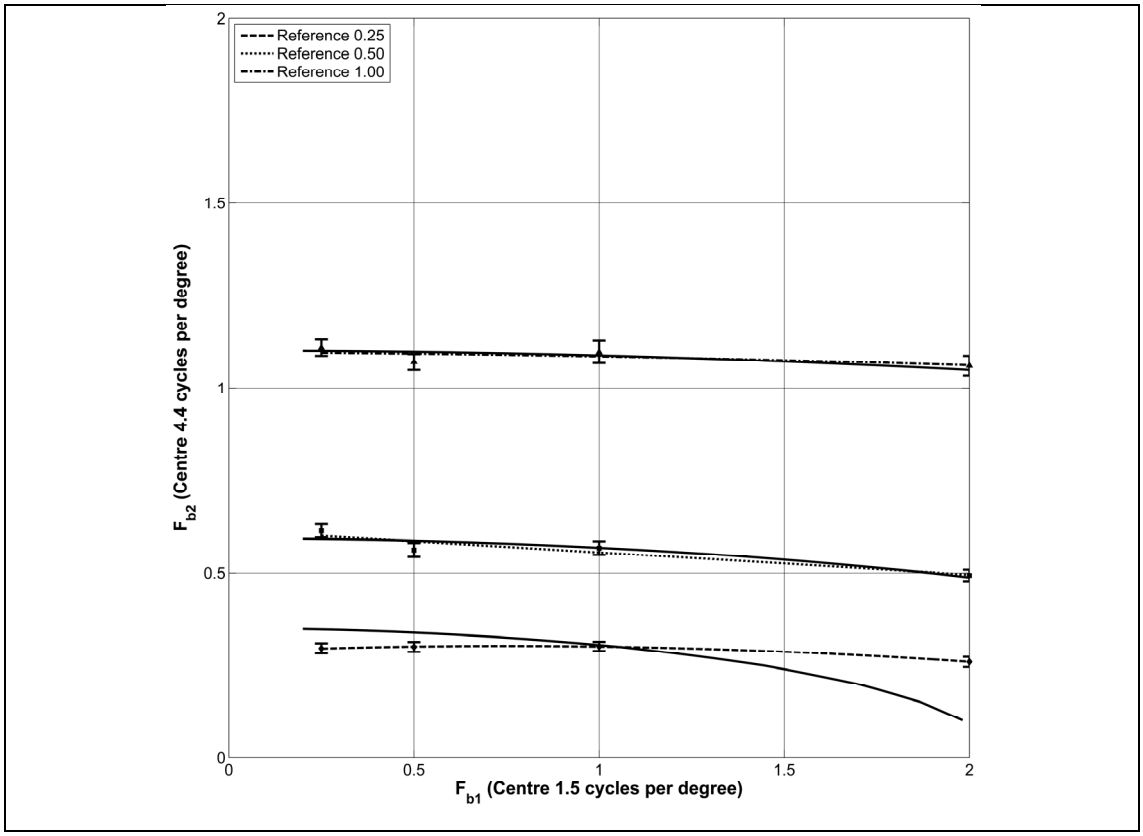


**Figure 8-29: *Iso-roughness lines* from [$F_{b1}$, $F_{b2}$] compared to the predicted model.**

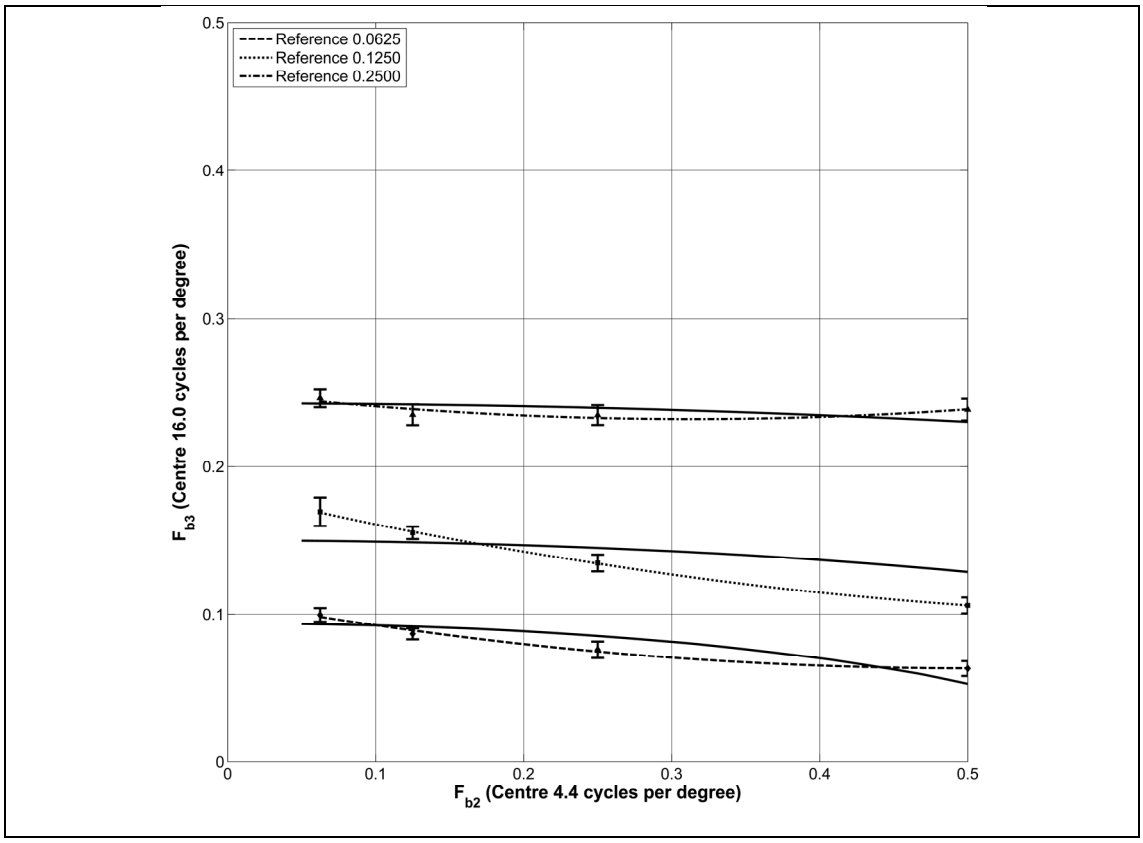


**Figure 8-30: *Iso-roughness lines* from [$F_{b2}$, $F_{b3}$] compared to the predicted model.**

## 8.5 Summary and Discussion

In *Chapter 6* and *Chapter 7*, it was demonstrated that it is possible to construct a model using an *FRF* framework to account for the *iso-roughness lines* from *Chapter 6*. Unfortunately, two functions fitted quite well the first filter of the model; these were a *gaussian function* and a *power function*. The major difficulty in deciding on the most appropriate function was the symmetry in the stimuli and the low magnitude in the high frequencies.

As a result, in this chapter, two new experiments based on spatial frequency channels were constructed, where *frequency bands* are compared to gather two new sets of *iso-roughness lines*. The new experimental data show how frequencies influence perceived roughness. From the results, it was noticed that perceived roughness increments with frequency, until the highest frequency tested by the bands (30 cycles per degree).

Higher frequencies were not tested as it is very difficult to obtain reliable results from the observers, and also because of hardware limitations.

Although the new *iso-roughness lines* from this chapter were not obtained from $1/F^{\beta}$ *noise* surfaces they will serve to justify which model fits best these surfaces. One can argue here that there is no reason to combine these two kinds of surfaces to optimize a model for $1/F^{\beta}$ *noise* surfaces but it would be impossible to discern the correct model from just these surfaces alone. However, it was shown that observers can reliably match perceived roughness from the *frequency band* surfaces and observers also found these to be similar to $1/F^{\beta}$ *noise* surfaces in appearance as they are isotropic surfaces too. As a result, these surfaces were incorporated in the model.

When fittings the *gaussian* and *power functions* to these two new experiments, it was demonstrated that the error of the gaussian model is reduced until the gaussian centre matches the limit of the 20/20 vision (30 cycles per degree), at which point the function loses its characteristic shape. As for the *power function*, it was not possible to match perfectly all the optimized parameters for the three experiments.

As a result, a new function, with variable low and high parts, was constructed. This *variable gaussian* was tested on the experimental data. The results demonstrated that this function is the best fitting one for the $F_1$ filter. Although some *iso-roughness lines* have a slight error, this can be attributed to the unavailable data at high frequency values (>16 cycles per degree).

However, the scale in between the *iso-roughness lines* in each experiment is still unknown, and for that reason in the next chapter, a new experiment testing this scale will be constructed and the proposed model will be scaled accordantly.

# CHAPTER 9

# SCALING THE PROPOSED MODEL

It was demonstrated that an estimator for perceived roughness can be constructed using an *FRF* model were the first $F_1$ filter is unknown in shape and parameters, and the $RF_2$ stages act as a *variance estimator*. The shape of $F_1$ and its parameters were found by optimizing and fitting a model to the data from psychophysical experiments. The final optimized function for $F_1$ was a '*variable gaussian*' with a centre (mean) above 15 cpd as described in the previous chapter. With this optimized estimator, it is possible to output data that matches both the observed *iso-roughness lines* in [$\beta$, $\sigma$] space and the *band pass* experimental data.

A limitation of the estimator developed so far is that it can measure perceived roughness only to an ordinal level. It specifies that a surface lying on one *iso-roughness line* will be perceived as more rough or less rough than one lying on a lower or a higher line, respectively, but the scaling of perceived roughness remains unknown. The aim of this chapter is to extend the estimator, through a further experiment, to achieve this scaling, so that the ratio of the perceived roughnesses of two surfaces can be determined. This scaling will be applied to the estimator to produce a complete measurement for perceived roughness in *$1/F^{\beta}$ noise* surfaces.

This chapter is subdivided into five sections: the first (*9.1*) will explain the new scaling experiment, and *Section 9.2* will show its results. The third Section (*9.3*) will add the scale to the model, followed by a fourth Section (*9.4*) which will summarize the final model for perceived roughness, finishing with a discussion of the results of the chapter as a whole and the implications of the final model (*Section 9.5*).

## 9.1 Perceptual scaling in between iso-roughness lines

From the experiments exploring $\sigma$ and perceived roughness in *chapter six*, it is known that a surface which lies on a higher *iso-roughness line* (with a bigger $\sigma$ reference) will be

perceived as being rougher than a surface lying in a lower *iso-roughness line* (with a smaller σ reference). But there is no way of establishing from the previous experiments the ratio of how much rougher one surface is perceived in comparison with a second one or how much rougher an iso-roughness line is to another. As a result, a new experiment will be designed in this section.

To obtain the ratio or scale in between *iso-roughness lines* it is necessary to obtain somehow a quantitative value from the observers for each *iso-roughness line* in the [$\beta$, $\sigma$] space. Methods like *numerical ratings* or *Likert scaling* were not used because it is not known whether observers can accurately judge roughness numerically. Therefore, a new method had to be devised where observers make a quantitative judgement about the relative roughnesses of surfaces but without expressing the relationship in number form.

The new method was a 'variation' of the *method of adjustment* because the original method was proven to produce reliable observations as previously described in *chapters six* and *eight*. The new method consisted of displaying two *reference surfaces* with different perceived roughness and a third *adjustable surface.* Observers were able to adjust this surface's $\sigma$ until it was equidistant in perceived roughness between the two *reference surfaces*. By using this method, it was possible to obtain a quantitative measurement of roughness indirectly from the observers.

*$1/F^{\beta}$ noise* surfaces were used again for this experiment, a sample of the stimuli is demonstrated in *Figure 9-1* where the $\sigma$ value for each surface equals 0.4cm, 0.8cm and 1.2cm respectively, whilst the $\beta$ value equals 2.0, 2.2 and 2.2 in the same order. The parameters of the *reference* and *adjustable surfaces* used in the experiment were chosen so that the results identified midpoints between iso-roughness lines ($\sigma$ references). The estimator was then scaled using these roughness mid-points. The complete stimuli and process are explained in the following section.

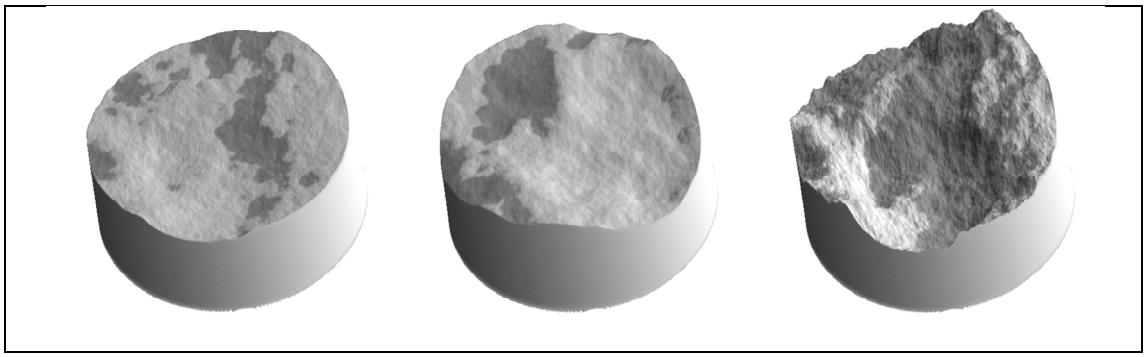

**Figure 9-1: Demonstration of the stimuli for the mid-point experiment, where the surfaces in the sides are the *samples*, whilst the middle surface is the *adjustable* one.**

## 9.2 The mid-point experiment

Pilot experiments were carried out to identify pairs of *reference surfaces* that were far enough apart in perceived roughness to enable observers to judge the midpoint between them. Based on the pilot results, sample surfaces were taken only from three of the *iso-roughness lines* identified in *Chapter 6*; the top, middle, and bottom lines from the [$\beta$, $\sigma$] space (see Figure 6-11).

In each trial of the mid-point experiments, observers were presented with three surfaces:

- two *reference surfaces,* presented in a single column on a display in portrait position, and
- an *adjustable surface*, presented on a second display also in portrait position.

All surfaces were at an equal distance from each other, and standard experimental conditions were used as previously described in *Chapter 5*.

In the experiment, the pair of *reference surfaces'* $\beta$ was always fixed at 2.0 and the $\sigma$ varied between 0.4cm, 0.8cm and 1.2cm (bottom, middle and top *iso-roughness line's* references). On each trial, the two *reference samples* had different $\sigma$ values, but the three possible combinations occurred equally often:

- Bottom and middle iso-roughness reference: $\sigma_{ref1} = 0.4$cm and $\sigma_{ref2} = 0.8$cm;
- Middle and top iso-roughness references: $\sigma_{ref1} = 0.8$cm and $\sigma_{ref2} = 1.2$cm;
- Bottom and top iso-roughness references: $\sigma_{ref1} = 0.4$cm and $\sigma_{ref2} = 1.2$cm.

The *adjustable surface*'s $\beta$ value varied from 1.8 to 2.2 in 0.1 steps [1.8, 1.9, 2.0, 2.1 or 2.2], and the $\sigma$ value could be adjusted by the observer in the same way as in the previous experiments. Each of the five $\beta$ values was tested for each of the three combinations of *reference surfaces* (5 $\beta$ x 3 combinations = 15 stimuli).

The fifteen stimuli combinations were repeated three times (with different θ) to add robustness, giving a sum of 45 trials for each observer (plus 5 learning trials), the complete description of the experiment, including information of the stimuli for each trial, is detailed in *Appendix 9-1*. Ten volunteers took part in the experiment, and they were instructed to set the *adjustable surface* so that it appeared to be midway in roughness between the two *reference surfaces*, again imagining how the surfaces would feel if touched.

The results from individual observers are shown in *Figure 9-2*, *9-3* and *9-4* for each of the reference combinations (the statistical significance of each reference sample is $p < 0.00001$). Shown is the value of $\sigma$ for the *adjustable surface* set on each trial (three trials for each of 10 observers, for the 15 different combinations of parameter $\sigma$; tabulated values are described in *Appendix 9-2*).

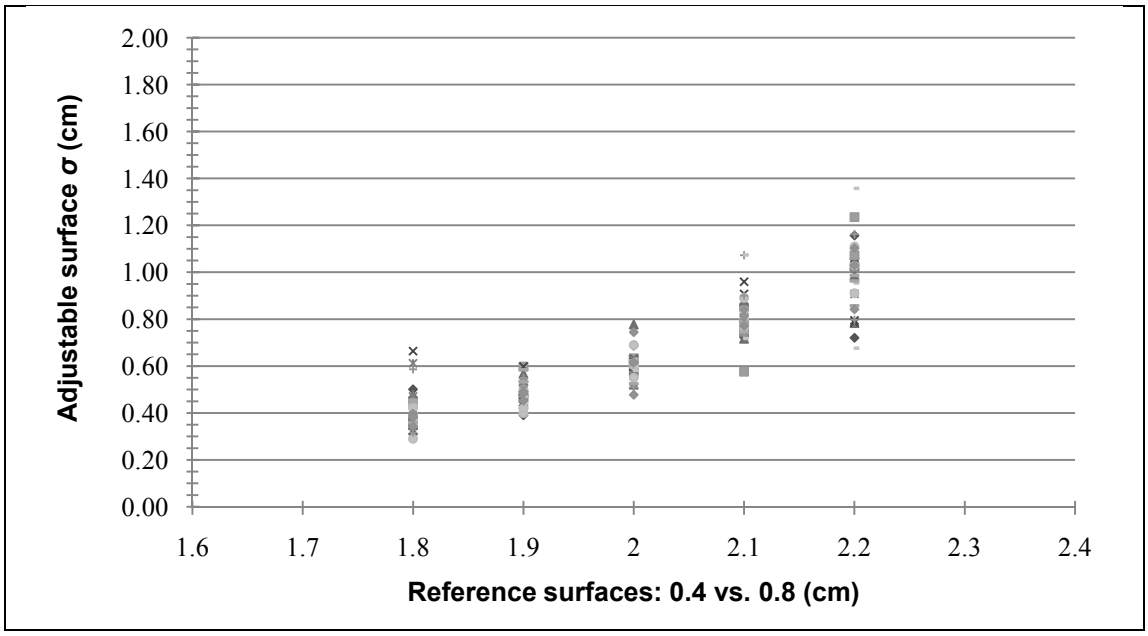


**Figure 9-2: Observation for each trial of the ten observers of the lower and middle iso-roughness reference.**

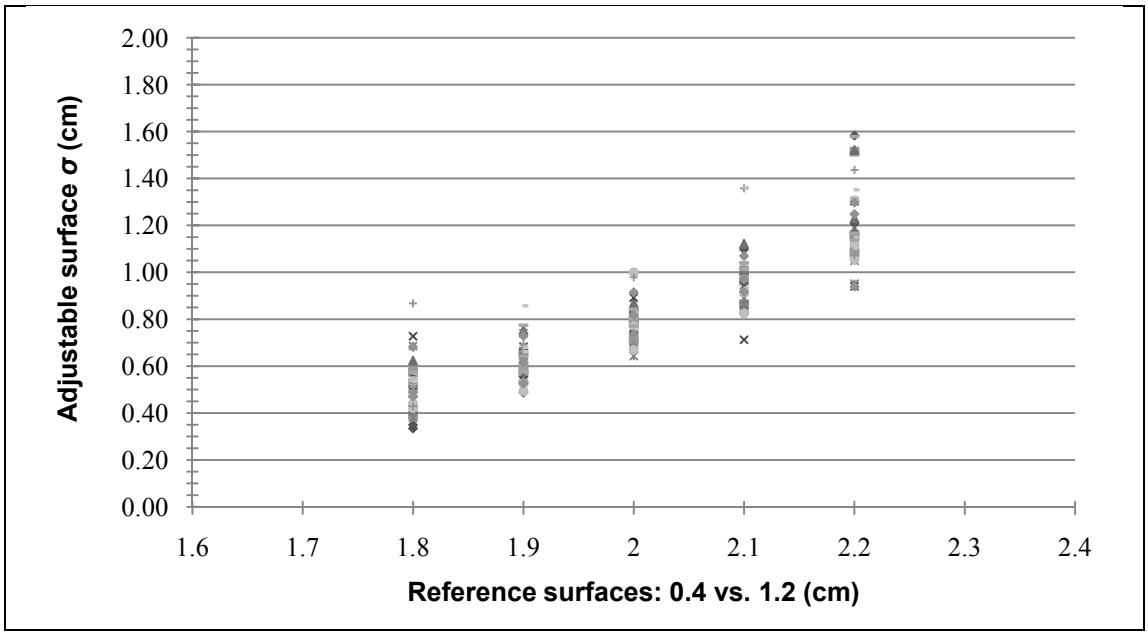


**Figure 9-3: Observation for each trial of the ten observers of the lower and top iso-roughness reference.**

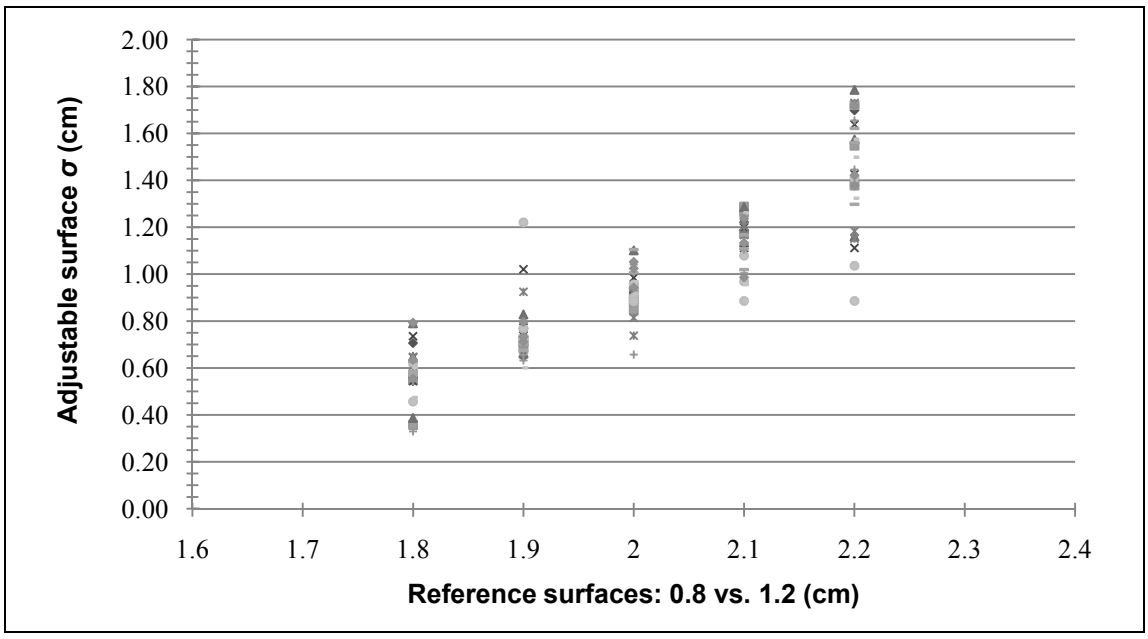


**Figure 9-4: Observation for each trial of the ten observers of the middle and top iso-roughness reference.**

The consistency of the data from the mid-point experiment shows that the observers had no problem adjusting a surface so it would be equidistant in perceived roughness between the two *reference surfaces*. Therefore, in the next section, the median values of σ from each of

the three midpoints and for every $\beta$ value (15 values, demonstrated in *Figure 9-5 and Appendix 9-3*) will be used to obtain the scaled perceived roughness model.

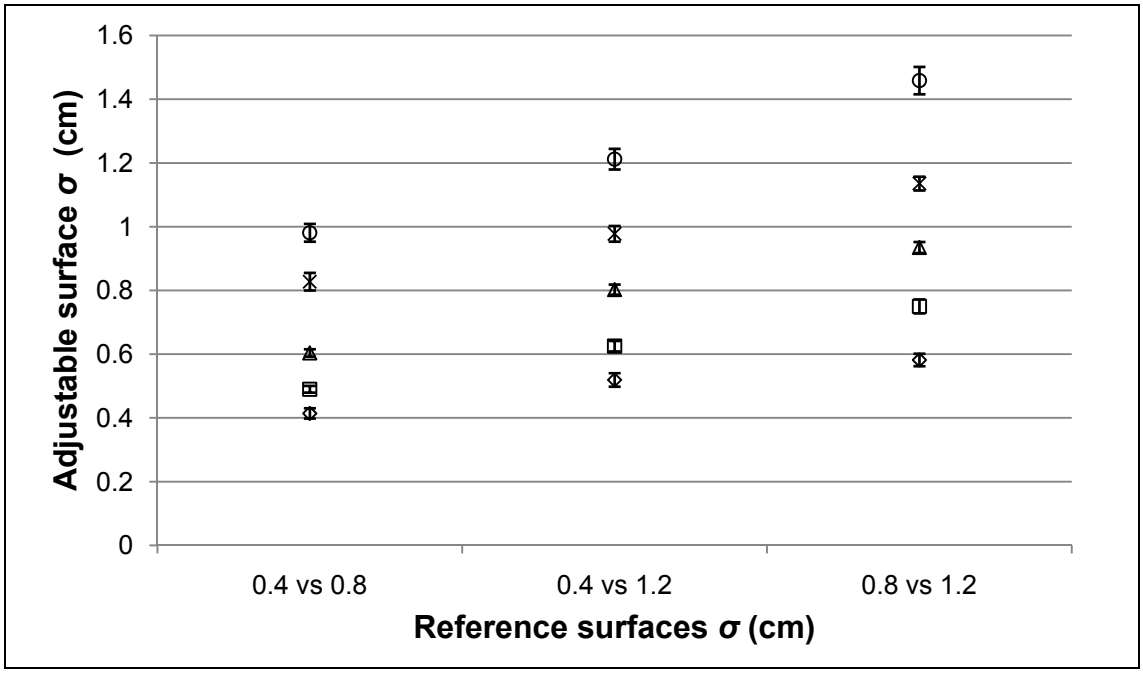


**Figure 9-5: Medians from the results in the mid-point experiment.**

## 9.3 Adding units to the model

It is possible to scale the previous *un-scaled estimator* by injecting the mid-point experiment median values into it. The final resulting *scaled model* will wrap the *un-scaled estimator*. As a result, the *scaled estimator* will be a function of the *un-scaled one*.

To discover the *scaled model* ($\xi_{spr}$), first the un-scaled $\xi_{pr}$ values were calculated using the best the *variable gaussian* from *chapter eight* with the $O_p$, for all the fifteen median points from the mid-point experiment, these are given in *Appendix 9-4*. By knowing that each of these $\xi_{pr}$ values is the perceptual average of the two *reference surfaces* and that in each pair of references all different values of $\beta$ (five) have the same scale perceived value ($\xi_{spr}$), it is possible to construct a relationship between the *scaled* and *un-scaled* values.

When mapping the *un-scaled estimator* to the *scaled one* using just one reference pair combination it is possible to appreciate that the five mid-points $P_1$, $P_2$, $P_3$, $P_4$, and $P_5$ (see *Figure 9-4)* have the same value of scaled perceived roughness, which is the mean

of the values of the two sample surfaces (H+L)/2. Their un-scaled values will differ slightly, as each is the output of the *un-scaled estimator* for the particular combination of parameters chosen by the observers as the midpoint between the samples, at different values of $\beta$ for the *adjustable surface*.

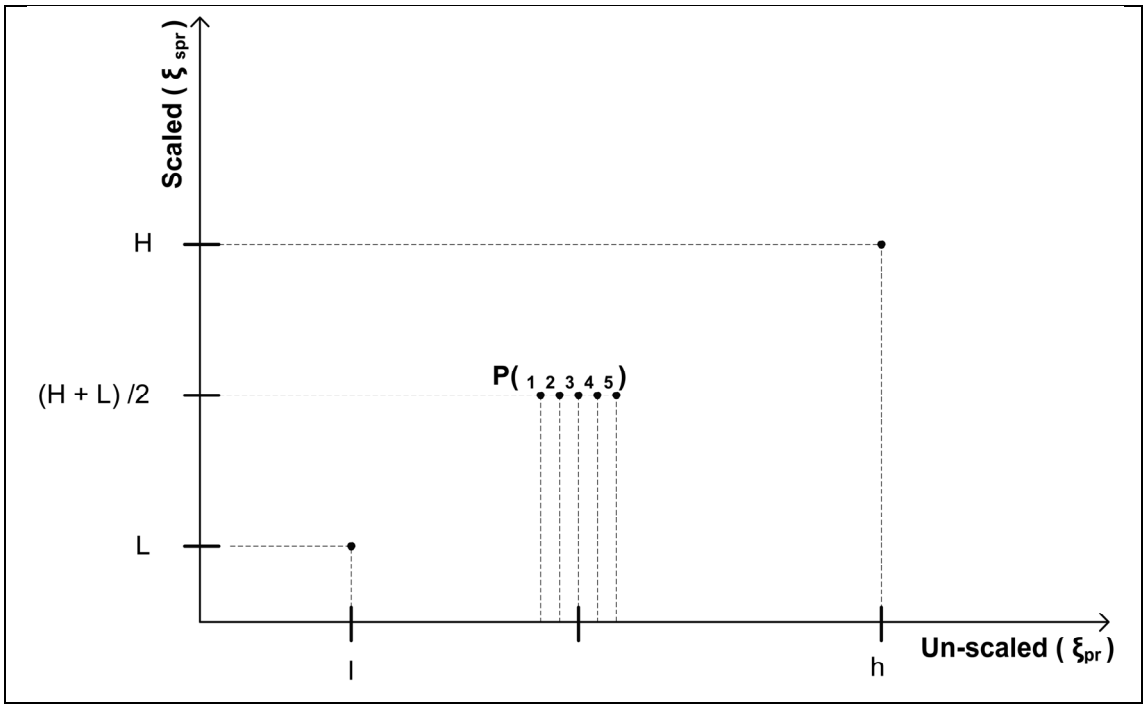


**Figure 9-6: Mapping the *un-scaled estimator* to the *scaled one* for just one pair of reference surfaces**

By knowing the relationship between the *scaled* and *un-scaled estimators*, then it is possible to construct five equations for each of the three combinations of pairs of references (0.4cm vs. 0.8cm, 0.4cm vs. 1.2cm and 0.4cm vs. 1.2cm). As shown in *Equation 9-1* to *9-5* for just one combination when assuming the *scaled estimator* is a polynomial function of the *un-scaled one* (where $u$ are the $\xi_{pr}$ mid-points).

$$\frac{H + L}{2} = a \cdot u_1{}^2 + b \cdot u_1 + c \quad \textbf{(9.1)}$$

$$\frac{H + L}{2} = a \cdot u_2{}^2 + b \cdot u_2 + c \quad \textbf{(9.2)}$$

$$\frac{H + L}{2} = a \cdot {u_3}^2 + b \cdot u_3 + c \quad \textbf{(9.3)}$$

$$\frac{H + L}{2} = a \cdot {u_4}^2 + b \cdot u_4 + c \quad \textbf{(9.4)}$$

$$\frac{H + L}{2} = a \cdot {u_5}^2 + b \cdot u_5 + c \quad \textbf{(9.5)}$$

By having five equations per combination and adding the three formulas for the reference points (*Equations 9-6* to *9-8*), it is possible to describe the relationship in a set of eighteen equations. This set must be resolved to get the final *scaled estimator* but because all the equations' left side are unknowns and this is a homogenous set of equations then two assumptions are needed to find a solution to the system:

1. The value of *c* will equal zero because if the value of the estimator is zero then the perceived roughness of the surface will also be zero, and
2. The perceived roughness of the roughest reference (*H*) will be a predefined value (100).

$$H = a \cdot h^2 + b \cdot h + c \quad \textbf{(9.6)}$$

$$M = a \cdot m^2 + b \cdot m + c \quad \textbf{(9.7)}$$

$$L = a \cdot l^2 + b \cdot l + c \quad \textbf{(9.8)}$$

The final set of equations with their corresponding $\xi_{pr}$ values (*Appendix 9-4*) are fully shown in *Appendix 9-5*. A less square fitting was used to resolve the set (residue was 0.971). The final *scaled model* is described in *Formula 8.9*, were $k_s$ is a multiplier equal to the predefined value of 100 as previously explained.

$$\xi_{spr} = k_s \cdot (-(1.6986 \cdot 10^{-6}) \cdot {\xi_{pr}}^2 + 0.2543 \cdot \xi_{pr}) \quad \textbf{(9.9)}$$

Apart from the polynomial function others were also fitted to the data, these include:

- A *linear function* that had the next fitting parameters: ($k_s \cdot (\ 0.1537 \cdot \ \xi_{pr}$), this linear function had an $r^2$ equal to 0.944. In addition,
- A *quadratic function* was impossible to fit because the solution to the least squares is not unique.

The polynomial therefore was used as this function because it produces the least error of them all. The final function is demonstrated in *Figure 9-7*.

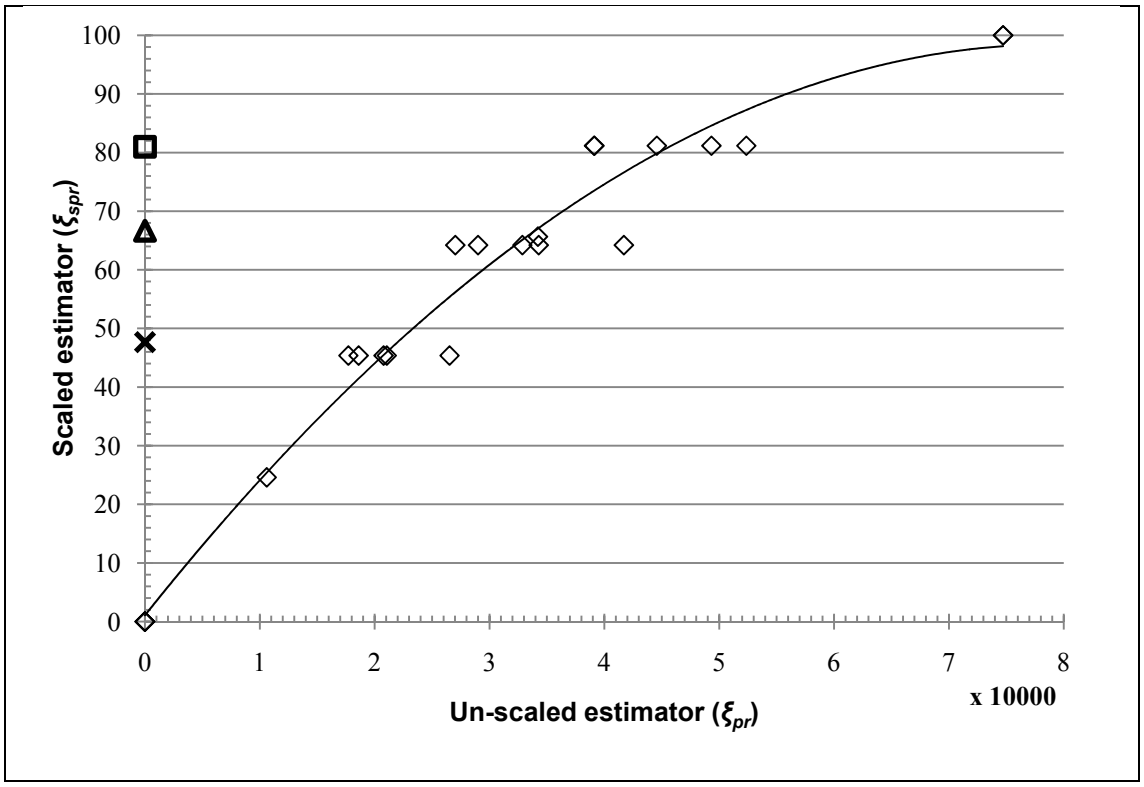


**Figure 9-7: Scaling the estimator with a polynomial function.**

## 9.4 The optimal model for perceived roughness of *1/F$^{\beta}$* surfaces

The final model therefore is the best fitting *variable gaussian* ($O_p$) for the $F_1$ filter wrapped into a polynomial function to scale it. The actual mapping of the scaled perceived roughness and the [$\beta$, $\sigma$] space is show in *Figure 9-8*, where the different colours represent the perceived roughness units. Only values topping 100 units were plotted, as it is still know if bigger values will be perceived in this same continuous

scale. The final parameters for the complete measurement are described in *Equation 9-10* and *Equation 9-11* for the scaling.

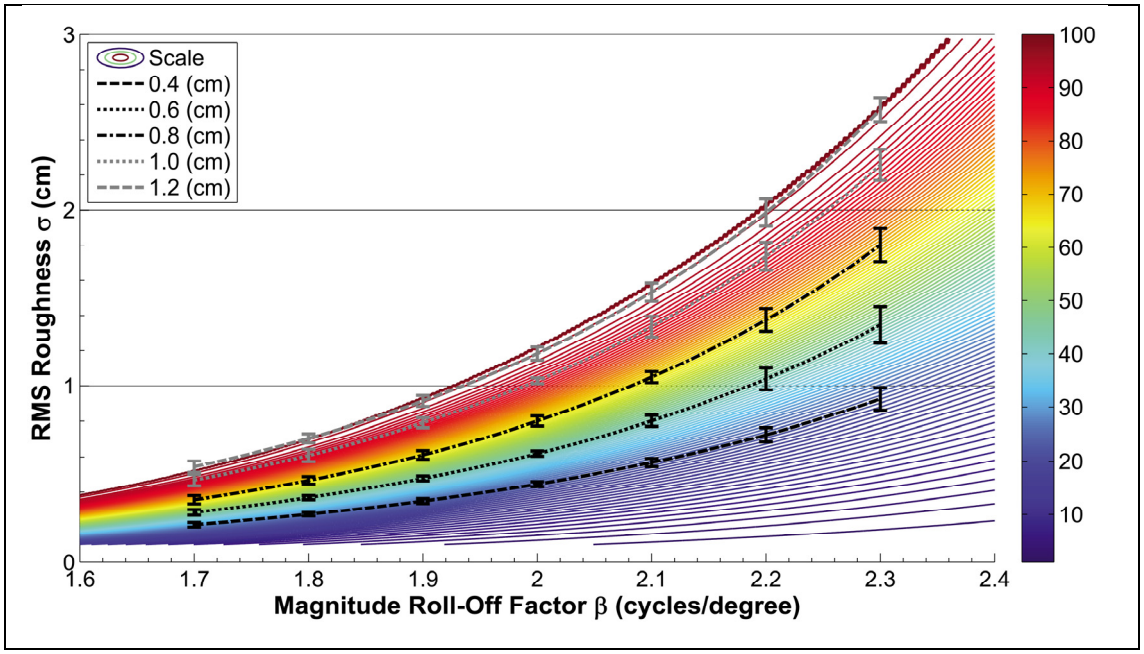


**Figure 9-8: Mapping perceived roughness in the [*β*, *σ*] space.**

$$\xi_{pr} = \int_{0.29}^{30} \left( 1.69.\left(0.0041 \cdot \left(f_f - 0.29\right) - 0.0041\right).e^{-\left(0.0041\left(f_f - 0.29\right)\right)^{5.05}} \right)^2 . \; S_{(f_f)}{}^2 \; df_f \qquad (9.10)$$

$$\xi_{spr} = k_s \cdot \left(-\left(1.6986 \cdot 10^{-6}\right) \cdot \xi_{pr}{}^2 + 0.2543 \cdot \xi_{pr}\right) \qquad (9.11)$$

## 9.5 Summary and Discussion

In previous chapters, an estimator was discovered which simulated the observers' perception of roughness in *1/F$^{\beta}$ noise* surfaces. Although the estimator produces *iso-roughness lines* that match the observers perception, it was still unknown the scale in between *iso-roughness lines*. As a result, a new experiment was constructed to get quantitative values for these *iso-roughness lines*.

Ten observers took part in the experiment, they were asked to adjust a surface until it was equidistant in roughness to two other *reference surfaces*. The results from this experiment were later incorporated into the previous *un-scaled model* to scale it correctly.

The scaling of the model was done by constructing a set of 18 equations that encapsulated the relationship between the un-scaled and the *scaled model*. By solving this set of equations, it was possible to wrap the un-scaled estimator into a polynomial function giving the final scaled model that can fully describe perceived roughness for *1/F$^{\beta}$ noise* surfaces.

# CHAPTER 10

# SUMMARY AND CONCLUSIONS

This final chapter will summarize the thesis as whole in *Section 10.1* including a discussion about how the goals of the thesis were achieved. *Section 10.2* will discuss some implications about the results and future work, finally *Section 10.3* will analyse the thesis and conclude it.

## 10.1 Summary

The first goal of this thesis was to find a common or starting surface characteristic to research, as it would be impossible for the author to research the hundreds of characteristics that exist for textured surfaces. The most common characteristic was researched from previous studies, it was found that roughness, or similar associated terms, reoccur in visual studies of surfaces dimensions. This term was also been found to be the most reoccurring term for tactile dimensions, and it is possible to relate the visual and tactile dimensions because studies have proven that there are relationships between how human see and touch objects, finally in linguistics, roughness is the most used term used to describe surfaces after qualitative terms (soft, warm, harsh). Therefore, it was concluded that this term is the most appropriate one to research in this thesis as fully described in the first part of *Chapter 2*.

After targeting roughness as the research quality, physical and perceptual related measurements were researched in the second part of *Chapter 2*. The international standards organization defines sixteen parameters to describe roughness; from these it was found that the three most suitable parameters are root mean square deviation $R_q$, skewness $R_{sk}$ and kurtosis $R_{ku}$, from these only Rq was used at it encompass the same statistical information as the other two suitable parameters. When researching perceptual measurements for roughness there were only three studies investigating perceived roughness and either fractal dimension, light position or viewpoint.

The lack of more studies for perceived roughness motivated the development of a general methodology to discover perceptual characteristic. This was fully described and discussed in *Chapter 3*, starting with the importance of controlling the illuminant position and the surface viewpoint, to solve ambiguities a motion was added to the surfaces. For the stimuli, it was decided that synthetic surfaces would be used; this offered great advantages over real samples as observers can adjust parameters of this. Finally, *$1/F^{\beta}$ noise surfaces* were chosen to be use in this thesis as these are parsimonious and have a natural appearance, therefore avoiding boxing the observations of the subjects to some unrealistic propose-build surface.

To conclude the general methodology, a summary of psychophysical methods was described in the last section of *Chapter 3*. The method of adjustment was chosen to be use for most of the experiments in this thesis, as this is the most flexible and fastest method to discover how the parameters of the surface interact with perceived roughness. Other methods as category scaling or pairwise comparisons are also use sparely throughout this thesis.

Once the general methodology was defined were natural synthetic stimuli, movement and psychophysical methods was defined, the next goal is to render this stimuli correctly. The mathematical formulation of the surfaces was described in the first section of *Chapter 4*, followed by how these surfaces were constructed and rendered.

To display correctly the surfaces, a per-pixel Lambertian illumination was used for rendering the reflectance, whilst per-vertex displacement was used to displace correctly the geometry of the surface to add correct occlusion and edges. Finally, to give the surface cast-shadows a shadow mapping was applied. Using all these techniques, surfaces compose of a quarter of a million polygons were rendered realistically at 15 frames per second (including the ability to morph their height in real-time).

As previously discussed in the methodology, the surfaces were rotated to avoid ambiguities. The animation was developed from a short experiment capturing the observers natural movements of the surface, it was discover from this experiment that observers like an angle between the light position and the surface normal of around 60

degrees. By exploiting this new data, a movement path was developed as described in the last section of *Chapter 4*.

Before any experiment took place all the equipment was setup correctly, including brightness levels (100 cd/m$^2$), monitor calibration, controlling the distance between stimuli and observer, etc. This setup and calibrations procedures are fully described in *Chapter 5*.

The next goal of this thesis was to define the *1/F$^\beta$ noise surface* parameters ($\sigma$, $\beta$ and seed of $\theta$) in terms of perceived roughness. By using the proposed methodology in three experiments, it was proven that perceived roughness increases when increasing $\sigma$, in addition perceived roughness decreases when increasing $\beta$ and the random seed $\theta$ of the surfaces did not affect perceived roughness as described fully in *Chapter 6*.

Because the random $\theta$ value does not change perceived roughness in the surfaces, these can be described only using $\beta$ and $\sigma$; as a result in the last section of *Chapter 6* a new experiment was developed to map the relationship between the [$\beta$, $\sigma$] space and perceived roughness. From the observations of this experiment, it is demonstrated that there is a clear linear relationship between log σ and β for the lines of constant perceived roughness in the *1/F$^\beta$ noise surfaces*.

With the help of the [$\beta$, $\sigma$] space it was possible to construct an estimator for perceived roughness for this kind of surface. The estimator was inspired by common FRF models were the first F is a filter whilst the RF section forms a variance estimator. The filter shape and parameters were optimized and it was discovered that two shapes fitted the best the observed data, a power shape and a gaussian shape. Unfortunately, from the experimental observations it was impossible to distinguish the best fitting model as described in *Chapter 7*. Therefore, a new textured surface, but similar in kind was used to obtain more observations.

This new stimuli consisted of gaussian band pass surfaces, where the magnitude and position of the gaussian were chosen in anticipation for new experiment, the objective of this was to further study how high and mid frequencies affected perceived roughness. *Chapter 8* describes the construction of these new surfaces. Also in this chapter, a new

set of experiments was developer and it was found that the higher the frequency is the more important this is to perceived roughness.

With the new observations, it was finally discovered that the best fitting gaussian function for the F filter has a centre pass 30 cycles per degree and therefore it becomes a power function. However, the filter optimization was further improved by introducing a gaussian function with a variable low and high ends, this produce better fittings to the data and it is fully described in the last section of *Chapter 8*. Finally, the estimator was modified to account for the scaling between iso-roughness lines in the [$\beta$, $\sigma$] space.

The method consisted of wrapping the un-scaled optimized model into a function that would scale it correctly. A final experiment was developed that measured the mid points between iso-roughness lines; with these new observations it was found that a polynomial best wraps the un-scaled model. As described in *Chapter 9* with this final modification to the model, it is possible to estimate perceived roughness in *$1/F^{\beta}$ noise surface*.

## 10.2 Discussion and future work

I would like to discuss in this section a few open questions about the model. First, the model works well estimating perceived roughness for surfaces but all the calculations in the model are distance dependant (cycles per degree). Observers seem to judge roughness independently of the distance, therefore they must somehow compensate for the differences in distance whilst judging roughness, this is unknown and out of the scope of this thesis. Note that to reduce the variations of this compensation each observer was asked in every experiment to think about how the texture would feel if touched. Therefore, they would mentally compensate for the distance.

Another open question about the model is how this is going to react with external changes in the surface like colour, gloss, etc. This is still unknown but Ho, Landy and Maloney (2008) have started studying the effects of these external changes in the surface appearance and perceived roughness. Studying the effect of these external changes and perceived roughness is very extensive and out of reach for this thesis but it is worth as future work.

## 10.3 Final conclusions

In this thesis, a new methodology was developed to study perception of surface characteristics. From previous studies and theory, it was decided that roughness is the most suitable characteristic to start the research. A new methodology was also developed which can be used in future studies related to the appearance of material.

With the help of the new methodology and various experiments an estimator for perceived roughness was discover, this is based on common FRF models for perception. This model can fully describe perceived roughness for *$1/F^{\beta}$ noise surfaces*. The mayor achievement of this thesis is that it will serve as a first step to discover more systematically how textured surfaces are perceived by humans.

# THE APPENDICES

**Appendix 3-A:** The performance of the method of adjustment was calculated from the experiment in *Section 6-4* where by accumulating all the comparisons from the observers, were they used the method of adjustment to match surfaces with similar $\beta$ values. It is possible to show, as detailed in the table below that the method of adjustment is a very accurate method when matching perceived roughness.

| **Matching $\sigma$(cm) with similar pair of surfaces** | | | | | |
|---|---|---|---|---|---|
| **σ reference** | 0.4 | 0.6 | 0.8 | 1.0 | 1.2 |
| **Number of samples** | **40** | **40** | **40** | **40** | **40** |
| **Mean** | 0.449 | 0.626 | 0.789 | 1.080 | 1.256 |
| **Median** | **0.458** | **0.616** | **0.792** | **1.086** | **1.288** |
| **Standard Error** | 0.013 | 0.015 | 0.022 | 0.016 | 0.034 |
| **Standard Deviation** | 0.084 | 0.098 | 0.141 | 0.100 | 0.216 |
| **Minimum** | 0.251 | 0.354 | 0.462 | 0.828 | 0.779 |
| **Maximum** | 0.613 | 0.814 | 1.173 | 1.217 | 1.914 |
| **Confidence Level (95.0%)** | **0.027** | **0.031** | **0.045** | **0.032** | **0.069** |
| **Confidence Interval Min** | 0.422 | 0.594 | 0.744 | 1.048 | 1.187 |
| **Confidence Interval Max** | 0.476 | 0.657 | 0.834 | 1.112 | 1.325 |

**Appendix 4-A:** Source code used to generate the random phase in Matlab:

```
01 function phase = generateRandomPhase(varargin)
02 %GENERATERANDOMPHASE(theSize)
03 %GENERATERANDOMPHASE(theSize, state)
04 %
05 % Random Phase Generator
06 % Version 1.0 >> UnOptimized Version
07 %
08 %INPUTS...
09 % theSize = image size
10 % state   = if given, will force state of rand
11 %
12 %OUTPUTS...
13 % phase  = random phase, output can be repeated with state value [0
14 to ...]
15 %
16 % Stefano Padilla
17 % Texture Lab 2005.
18 %
19 % See also: GENERATERANDOMPHASE, GENERATEFRACTALMAGNITUDE
20
21 [cax,args,nargs] = axescheck(varargin{:});
22 error(nargchk(1,3,nargs));
23
24 if nargs > 2
25     error('Too Many Arguments')
26 elseif nargs == 2
27     % Generate random phase with a repeated state
28     n = args{1};
29     state = args{2};
30     rand('state',state);
31     phase = rand(n,n)*2*pi;
32 else
33     % Generate random phase
34     n = args{1};
35     phase = rand(n,n)*2*pi;
36 end
```

**Appendix 4-B:** Source code used to generate the magnitude of the *1/F$^{\beta}$ noise surfaces* in Matlab:

```
01 function magnitude = GenerateFractalMagnitude(theSize, beta)
02 %GENERATEFRACTALMAGNITUDE(theSize, beta)
03 %
04 % Fractal Magnitude Generator
05 % Version 1.0 >> UnOptimized Version
06 %
07 %INPUTS...
08 % theSize = image size
09 % beta    = roll-off factor
10 %
11 %OUTPUTS...
12 % magnitude = array of frequencies
13 %
14 % Stefano Padilla
15 % Texture Lab 2005.
16 %
17 % See also: GENERATERANDOMPHASE, GENERATEFRACTALMAGNITUDE
18
19 % Generate magnitude
20 for col=1:theSize
21     for row=1:theSize
22         u=col-(theSize/2+1);
23         v=(theSize/2+1)-row;
24         if ((u==0) & (v==0))
25             magnitude(row,col)=0;
26         else
27             f=sqrt(u*u + v*v);
28             magnitude(row,col)=power(f,-beta);
29         end
30     end
31 end
```

**Appendix 4-C:** Table detailing the values for the normalizing parameter N($\beta$) as detailed in *Equation 4-1*.

| $\beta$ | N($\beta$) |
|---|---|
| 1.7 | 7434.4 |
| 1.8 | 7721.9 |
| 1.9 | 7967.3 |
| 2.0 | 8178.8 |
| 2.1 | 8362.3 |
| 2.2 | 8522.8 |
| 2.3 | 8663.9 |

**Appendix 4-D:** Source code used to generate the height maps of the *1/F$^{\beta}$ noise surfaces* in Matlab:

```
% Variables:
% sizen = size;
% phaseState = randomSeed;
% beta = roll-off factor
% newRMS = new rms value

phase = GenerateRandomPhase(sizen,phaseState);       % Phase

mag = GenerateFractalMagnitude(sizen,beta);          % Magnitude

[xc,yc]=pol2cart(phase,mag);                         % To Cartesian
f = xc+i*yc;

n = size(f,2);                 % Enforce complex conjugate symmetry
for col=(n/2+1):n
    for row=2:n
        u=col-(n/2+1);
        v=(n/2+1)-row;
        if (~((u==0) & (v==0)))
            f(row,col)=conj(f(n+2-row,n+2-col));
        end
    end
end

                                                % Inverse FFT
unswapF    = ifftshift(f);                      % Unswap

unswapReal = real(ifft2(unswapF));         % Real part from the IFFT
unswapImaginary  = imag(ifft2(unswapF));   % Imaginary part IFFT

realF       = fftshift(unswapReal);           % shift again
imagF       = fftshift(unswapImaginary);      % shift again

mean = double((sum(sum(realF)))/n);
variance = double((sum(sum(((abs(realF - mean)).^2))))/n);
rms = double(sqrt(variance));                  % Rq

s = (realF./rms) * (newRMS);                   % Change to any RMS
```

**Appendix 4-E:** Observers percentage time vs. the angle between the surface normal and the light position.

| Angle | s1 | s2 | s3 | s4 | s5 | s6 | s7 |
|---|---|---|---|---|---|---|---|
| **1.1** | 0.001321 | 0.017455 | 0.029469 | 0.00124 | 0.043869 | 0.005106 | 0.031051 |
| **2.3** | 0.002643 | 0.03491 | 0.058938 | 0.00248 | 0.087738 | 0.010212 | 0.062103 |
| **3.4** | 0.003964 | 0.052365 | 0.088406 | 0.00372 | 0.131606 | 0.015319 | 0.093154 |
| **4.5** | 0.007047 | 0.067493 | 0.168698 | 0.011161 | 0.194398 | 0.022127 | 0.159396 |
| **6.8** | 0.011892 | 0.080293 | 0.299813 | 0.024801 | 0.276113 | 0.030637 | 0.260829 |
| **9.0** | 0.018499 | 0.090765 | 0.48175 | 0.044643 | 0.37675 | 0.04085 | 0.397453 |
| **11.3** | 0.025106 | 0.101238 | 0.663688 | 0.064484 | 0.477388 | 0.051062 | 0.534076 |
| **13.5** | 0.032593 | 0.127614 | 0.822565 | 0.091352 | 0.634369 | 0.060849 | 0.611496 |
| **15.8** | 0.040962 | 0.169895 | 0.958381 | 0.125248 | 0.847694 | 0.070211 | 0.629713 |
| **18.0** | 0.050211 | 0.22808 | 1.071138 | 0.16617 | 1.117363 | 0.079146 | 0.588725 |
| **20.3** | 0.059461 | 0.286265 | 1.183894 | 0.207093 | 1.387031 | 0.088082 | 0.547738 |
| **22.5** | 0.08853 | 0.387503 | 1.347044 | 0.233548 | 1.636913 | 0.120421 | 0.55105 |
| **24.8** | 0.13742 | 0.531794 | 1.560588 | 0.245535 | 1.867006 | 0.176163 | 0.598663 |
| **27.0** | 0.20613 | 0.719138 | 1.824525 | 0.243055 | 2.077313 | 0.255309 | 0.690575 |
| **29.3** | 0.27484 | 0.906481 | 2.088463 | 0.240575 | 2.287619 | 0.334454 | 0.782488 |
| **31.5** | 0.356763 | 1.32385 | 2.31695 | 0.322008 | 2.424813 | 0.501683 | 0.882681 |
| **33.8** | 0.4519 | 1.971244 | 2.509988 | 0.487353 | 2.488894 | 0.756994 | 0.991156 |
| **36.0** | 0.56025 | 2.848663 | 2.667575 | 0.73661 | 2.479863 | 1.100388 | 1.107913 |
| **38.3** | 0.6686 | 3.726081 | 2.825163 | 0.985868 | 2.470831 | 1.443781 | 1.224669 |
| **40.5** | 0.924067 | 4.455694 | 2.861035 | 1.344675 | 2.757265 | 1.908029 | 1.525242 |
| **42.8** | 1.32665 | 5.0375 | 2.775194 | 1.813031 | 3.339163 | 2.493131 | 2.009631 |
| **45.0** | 1.87635 | 5.4715 | 2.567638 | 2.390938 | 4.216525 | 3.199088 | 2.677838 |
| **47.3** | 2.42605 | 5.9055 | 2.360081 | 2.968844 | 5.093888 | 3.905044 | 3.346044 |
| **49.5** | 3.176579 | 6.178167 | 2.539896 | 3.930323 | 5.598379 | 4.703744 | 4.01841 |
| **51.8** | 4.127938 | 6.2895 | 3.107081 | 5.275375 | 5.73 | 5.595188 | 4.694938 |
| **54.0** | 5.280125 | 6.2395 | 4.061638 | 7.004 | 5.48875 | 6.579375 | 5.375625 |
| **56.3** | 6.432313 | 6.1895 | 5.016194 | 8.732625 | 5.2475 | 7.563563 | 6.056313 |
| **58.5** | 7.358125 | 6.03475 | 5.521023 | 9.582875 | 5.01225 | 8.10225 | 6.386708 |
| **60.8** | 8.057563 | 5.77525 | 5.576125 | 9.55475 | 4.783 | 8.195438 | 6.366813 |
| **63.0** | 8.530625 | 5.411 | 5.1815 | 8.64825 | 4.55975 | 7.843125 | 5.996625 |
| **65.3** | 9.003688 | 5.04675 | 4.786875 | 7.74175 | 4.3365 | 7.490813 | 5.626438 |
| **67.5** | 8.787438 | 4.528523 | 4.486208 | 6.719929 | 4.002738 | 6.810419 | 5.211146 |
| **69.8** | 7.881875 | 3.856319 | 4.2795 | 5.582788 | 3.558463 | 5.801944 | 4.75075 |
| **72.0** | 6.287 | 3.030138 | 4.16675 | 4.330325 | 3.003675 | 4.465388 | 4.24525 |
| **74.3** | 4.692125 | 2.203956 | 4.054 | 3.077863 | 2.448888 | 3.128831 | 3.73975 |
| **76.5** | 3.411733 | 1.555809 | 3.681146 | 2.116813 | 1.956454 | 2.128435 | 3.258677 |
| **78.8** | 2.445825 | 1.085696 | 3.048188 | 1.447175 | 1.526375 | 1.4642 | 2.802031 |
| **81.0** | 1.7944 | 0.793616 | 2.155125 | 1.06895 | 1.15865 | 1.136125 | 2.369813 |
| **83.3** | 1.142975 | 0.501537 | 1.262063 | 0.690725 | 0.790925 | 0.80805 | 1.937594 |
| **85.5** | 0.673895 | 0.290138 | 0.642771 | 0.41956 | 0.5204 | 0.551463 | 1.563746 |
| **87.8** | 0.387161 | 0.15942 | 0.29725 | 0.255456 | 0.347076 | 0.366364 | 1.248269 |
| **90.0** | 0.282773 | 0.109383 | 0.2255 | 0.198413 | 0.270951 | 0.252753 | 0.991163 |
| **92.3** | 0.178384 | 0.059346 | 0.15375 | 0.141369 | 0.194827 | 0.139141 | 0.734056 |
| **94.5** | 0.104827 | 0.026376 | 0.100792 | 0.101273 | 0.142357 | 0.062975 | 0.533671 |
| **96.8** | 0.062103 | 0.010473 | 0.066625 | 0.078125 | 0.113542 | 0.024254 | 0.390006 |
| **99.0** | 0.050211 | 0.011637 | 0.05125 | 0.071925 | 0.108381 | 0.022977 | 0.303061 |
| **101.3** | 0.038319 | 0.0128 | 0.035875 | 0.065725 | 0.103221 | 0.021701 | 0.216117 |
| **103.5** | 0.02863 | 0.012412 | 0.044844 | 0.058698 | 0.091609 | 0.019148 | 0.15567 |
| **107.6** | 0.021142 | 0.010473 | 0.078156 | 0.050844 | 0.073545 | 0.015319 | 0.121721 |
| **111.8** | 0.015857 | 0.006982 | 0.135813 | 0.042163 | 0.04903 | 0.010212 | 0.114269 |
| **115.9** | 0.010571 | 0.003491 | 0.193469 | 0.033482 | 0.024515 | 0.005106 | 0.106817 |
| **120.0** | 0.007928 | 0.001746 | 0.222297 | 0.029142 | 0.012258 | 0.002553 | 0.103091 |

**Appendix 6-A:** Table detailing the variables from the *category scaling* experiments described in *Section 6.1*. The first column shows the actual number of observations, including the training stimuli triplets; the next nine rows represent the parameters ($\sigma$, $\beta$ and $\theta$) from surface. The last two rows symbolize the order in which the stimuli were shown to the observers.

| *No* | *Trial* | $\sigma_1$ | $\beta_1$ | $\theta_1$ | $\sigma_2$ | $\beta_2$ | $\theta_2$ | $\sigma_3$ | $\beta_3$ | $\theta_3$ | *Order No* | *Row Order* |
|---|---|---|---|---|---|---|---|---|---|---|---|---|
| **1** | 1 | 0.6 | 1.8 | 25 | 0.8 | 1.8 | 25 | 1.0 | 1.8 | 25 | 07 | 1-3-2 |
| **2** | 1 | 0.6 | 1.8 | 25 | 0.8 | 1.8 | 25 | 1.2 | 1.8 | 25 | 01 | 1-2-3 |
| **3** | 1 | 0.6 | 1.8 | 25 | 0.8 | 1.8 | 25 | 1.4 | 18 | 25 | 09 | 3-2-1 |
| **4** | 1 | 0.6 | 1.8 | 25 | 1.0 | 1.8 | 25 | 1.2 | 1.8 | 25 | 06 | 2-1-3 |
| **5** | 1 | 0.6 | 1.8 | 25 | 1.0 | 1.8 | 25 | 1.4 | 1.8 | 25 | 19 | 3-2-1 |
| **6** | 1 | 0.6 | 1.8 | 25 | 1.2 | 1.8 | 25 | 1.4 | 1.8 | 25 | 20 | 3-1-2 |
| **7** | 1 | 0.8 | 1.8 | 25 | 1.0 | 1.8 | 25 | 1.2 | 1.8 | 25 | 08 | 3-2-1 |
| **8** | 1 | 0.8 | 1.8 | 25 | 1.0 | 1.8 | 25 | 1.4 | 1.8 | 25 | 11 | 1-2-3 |
| **9** | 1 | 0.8 | 1.8 | 25 | 1.2 | 1.8 | 25 | 1.4 | 1.8 | 25 | 17 | 1-3-2 |
| **10** | 1 | 1.0 | 1.8 | 25 | 1.2 | 1.8 | 25 | 1.4 | 1.8 | 25 | 05 | 3-2-1 |
| **11** | 2 | 0.6 | 2.2 | 30 | 0.8 | 2.2 | 30 | 1.0 | 2.2 | 30 | 12 | 3-1-2 |
| **12** | 2 | 0.6 | 2.2 | 30 | 0.8 | 2.2 | 30 | 1.2 | 2.2 | 30 | 04 | 3-2-1 |
| **13** | 2 | 0.6 | 2.2 | 30 | 0.8 | 2.2 | 30 | 1.4 | 2.2 | 30 | 15 | 1-2-3 |
| **14** | 2 | 0.6 | 2.2 | 30 | 1.0 | 2.2 | 30 | 1.2 | 2.2 | 30 | 02 | 2-3-1 |
| **15** | 2 | 0.6 | 2.2 | 30 | 1.0 | 2.2 | 30 | 1.4 | 2.2 | 30 | 16 | 3-2-1 |
| **16** | 2 | 0.6 | 2.2 | 30 | 1.2 | 2.2 | 30 | 1.4 | 2.2 | 30 | 03 | 1-2-3 |
| **17** | 2 | 0.8 | 2.2 | 30 | 1.0 | 2.2 | 30 | 1.2 | 2.2 | 30 | 13 | 3-2-1 |
| **18** | 2 | 0.8 | 2.2 | 30 | 1.0 | 2.2 | 30 | 1.4 | 2.2 | 30 | 10 | 1-2-3 |
| **19** | 2 | 0.8 | 2.2 | 30 | 1.2 | 2.2 | 30 | 1.4 | 2.2 | 30 | 18 | 1-2-3 |
| **20** | 2 | 1.0 | 2.2 | 30 | 1.2 | 2.2 | 30 | 1.4 | 2.2 | 30 | 14 | 3-2-1 |
| **21** | *Practice* | 0.8 | 2.2 | 30 | 1.0 | 2.2 | 30 | 1.2 | 2.2 | 30 | 01 | 1-2-3 |
| **22** | *Practice* | 0.6 | 1.8 | 25 | 1.0 | 1.8 | 25 | 1.4 | 1.8 | 25 | 02 | 3-2-1 |
| **23** | *Practice* | 1.0 | 2.2 | 30 | 1.2 | 2.2 | 30 | 1.4 | 2.2 | 30 | 03 | 1-2-3 |
| **24** | *Practice* | 0.6 | 1.8 | 25 | 0.8 | 1.8 | 25 | 1.0 | 1.8 | 25 | 04 | 1-2-3 |
| **25** | *Practice* | 0.8 | 2.2 | 30 | 1.2 | 2.2 | 30 | 1.4 | 2.2 | 30 | 05 | 3-2-1 |

**Appendix 6-B:** Table detailing the results from the experiment in *Section 6.1* where *Obs1*, *Obs2* and *Obs3* are the rank in which each observer ordered the surfaces, one being the roughest, two the surface with the middle perceived roughness and three the smoothest surface.

| *No* | *Trial* | $\sigma_1$ | $\beta_1$ | $\theta_1$ | $\sigma_2$ | $\beta_2$ | $\theta_2$ | $\sigma_3$ | $\beta_3$ | $\theta_3$ | *Obs1* | *Obs2* | *Obs3* |
|---|---|---|---|---|---|---|---|---|---|---|---|---|---|
| **1** | 1 | 0.6 | 1.8 | 25 | 0.8 | 1.8 | 25 | 1.0 | 1.8 | 25 | 3-2-1 | 3-2-1 | 3-2-1 |
| **2** | 1 | 0.6 | 1.8 | 25 | 0.8 | 1.8 | 25 | 1.2 | 1.8 | 25 | 3-2-1 | 3-2-1 | 3-2-1 |
| **3** | 1 | 0.6 | 1.8 | 25 | 0.8 | 1.8 | 25 | 1.4 | 18 | 25 | 3-2-1 | 3-2-1 | 3-2-1 |
| **4** | 1 | 0.6 | 1.8 | 25 | 1.0 | 1.8 | 25 | 1.2 | 1.8 | 25 | 3-2-1 | 3-2-1 | 3-2-1 |
| **5** | 1 | 0.6 | 1.8 | 25 | 1.0 | 1.8 | 25 | 1.4 | 1.8 | 25 | 3-2-1 | 3-2-1 | 3-2-1 |
| **6** | 1 | 0.6 | 1.8 | 25 | 1.2 | 1.8 | 25 | 1.4 | 1.8 | 25 | 3-2-1 | 3-2-1 | 3-2-1 |
| **7** | 1 | 0.8 | 1.8 | 25 | 1.0 | 1.8 | 25 | 1.2 | 1.8 | 25 | 3-2-1 | 3-2-1 | 3-2-1 |
| **8** | 1 | 0.8 | 1.8 | 25 | 1.0 | 1.8 | 25 | 1.4 | 1.8 | 25 | 3-2-1 | 3-2-1 | 3-2-1 |
| **9** | 1 | 0.8 | 1.8 | 25 | 1.2 | 1.8 | 25 | 1.4 | 1.8 | 25 | 3-2-1 | 3-2-1 | 3-2-1 |
| **10** | 1 | 1.0 | 1.8 | 25 | 1.2 | 1.8 | 25 | 1.4 | 1.8 | 25 | 3-2-1 | 3-2-1 | 3-2-1 |
| **11** | 2 | 0.6 | 2.2 | 30 | 0.8 | 2.2 | 30 | 1.0 | 2.2 | 30 | 3-2-1 | 3-2-1 | 3-2-1 |
| **12** | 2 | 0.6 | 2.2 | 30 | 0.8 | 2.2 | 30 | 1.2 | 2.2 | 30 | 3-2-1 | 3-2-1 | 3-2-1 |
| **13** | 2 | 0.6 | 2.2 | 30 | 0.8 | 2.2 | 30 | 1.4 | 2.2 | 30 | 3-2-1 | 3-2-1 | 3-2-1 |
| **14** | 2 | 0.6 | 2.2 | 30 | 1.0 | 2.2 | 30 | 1.2 | 2.2 | 30 | 3-2-1 | 3-2-1 | 3-2-1 |
| **15** | 2 | 0.6 | 2.2 | 30 | 1.0 | 2.2 | 30 | 1.4 | 2.2 | 30 | 3-2-1 | 3-2-1 | 3-2-1 |
| **16** | 2 | 0.6 | 2.2 | 30 | 1.2 | 2.2 | 30 | 1.4 | 2.2 | 30 | 3-2-1 | 3-2-1 | 3-2-1 |
| **17** | 2 | 0.8 | 2.2 | 30 | 1.0 | 2.2 | 30 | 1.2 | 2.2 | 30 | 3-2-1 | 3-2-1 | 3-2-1 |
| **18** | 2 | 0.8 | 2.2 | 30 | 1.0 | 2.2 | 30 | 1.4 | 2.2 | 30 | 3-2-1 | 3-2-1 | 3-2-1 |
| **19** | 2 | 0.8 | 2.2 | 30 | 1.2 | 2.2 | 30 | 1.4 | 2.2 | 30 | 3-2-1 | 3-2-1 | 3-2-1 |
| **20** | 2 | 1.0 | 2.2 | 30 | 1.2 | 2.2 | 30 | 1.4 | 2.2 | 30 | 3-2-1 | 3-2-1 | 3-2-1 |

**Appendix 6-C:** Table detailing the variables from the *category scaling* experiments described in *Section 6.2*, the column description is as *Appendix 6-A*.

| *No* | *Trial* | $\sigma_1$ | $\beta_1$ | $\theta_1$ | $\sigma_2$ | $\beta_2$ | $\theta_2$ | $\sigma_3$ | $\beta_3$ | $\theta_3$ | *Order No* | *Row Order* |
|---|---|---|---|---|---|---|---|---|---|---|---|---|
| **01** | 1 | 0.8 | 1.7 | 20 | 0.8 | 1.8 | 20 | 0.8 | 1.9 | 20 | 33 | 1-3-2 |
| **02** | 1 | 0.8 | 1.7 | 20 | 0.8 | 1.8 | 20 | 0.8 | 2.0 | 20 | 08 | 1-2-3 |
| **03** | 1 | 0.8 | 1.7 | 20 | 0.8 | 1.8 | 20 | 0.8 | 2.1 | 20 | 28 | 3-2-1 |
| **04** | 1 | 0.8 | 1.7 | 20 | 0.8 | 1.8 | 20 | 0.8 | 2.2 | 20 | 43 | 2-1-3 |
| **05** | 1 | 0.8 | 1.7 | 20 | 0.8 | 1.9 | 20 | 0.8 | 2.0 | 20 | 25 | 3-2-1 |
| **06** | 1 | 0.8 | 1.7 | 20 | 0.8 | 1.9 | 20 | 0.8 | 2.1 | 20 | 15 | 3-1-2 |
| **07** | 1 | 0.8 | 1.7 | 20 | 0.8 | 1.9 | 20 | 0.8 | 2.2 | 20 | 19 | 3-2-1 |
| **08** | 1 | 0.8 | 1.7 | 20 | 0.8 | 2.0 | 20 | 0.8 | 2.1 | 20 | 12 | 1-2-3 |
| **09** | 1 | 0.8 | 1.7 | 20 | 0.8 | 2.0 | 20 | 0.8 | 2.2 | 20 | 26 | 1-2-3 |
| **10** | 1 | 0.8 | 1.7 | 20 | 0.8 | 2.1 | 20 | 0.8 | 2.2 | 20 | 38 | 1-3-2 |
| **11** | 1 | 0.8 | 1.8 | 20 | 0.8 | 1.9 | 20 | 0.8 | 2.0 | 20 | 16 | 3-2-1 |
| **12** | 1 | 0.8 | 1.8 | 20 | 0.8 | 1.9 | 20 | 0.8 | 2.1 | 20 | 34 | 3-1-2 |
| **13** | 1 | 0.8 | 1.8 | 20 | 0.8 | 1.9 | 20 | 0.8 | 2.2 | 20 | 11 | 3-2-1 |
| **14** | 1 | 0.8 | 1.8 | 20 | 0.8 | 2.0 | 20 | 0.8 | 2.1 | 20 | 35 | 1-2-3 |
| **15** | 1 | 0.8 | 1.8 | 20 | 0.8 | 2.0 | 20 | 0.8 | 2.2 | 20 | 14 | 2-3-1 |
| **16** | 1 | 0.8 | 1.8 | 20 | 0.8 | 2.1 | 20 | 0.8 | 2.2 | 20 | 45 | 3-2-1 |
| **17** | 1 | 0.8 | 1.9 | 20 | 0.8 | 2.0 | 20 | 0.8 | 2.1 | 20 | 24 | 1-2-3 |
| **18** | 1 | 0.8 | 1.9 | 20 | 0.8 | 2.0 | 20 | 0.8 | 2.2 | 20 | 36 | 1-2-3 |
| **19** | 1 | 0.8 | 1.9 | 20 | 0.8 | 2.1 | 20 | 0.8 | 2.2 | 20 | 18 | 3-2-1 |
| **20** | 1 | 0.8 | 2.0 | 20 | 0.8 | 2.1 | 20 | 0.8 | 2.2 | 20 | 37 | 1-2-3 |
| **21** | 2 | 1.2 | 1.7 | 35 | 1.2 | 1.8 | 35 | 1.2 | 1.9 | 35 | 10 | 1-3-2 |
| **22** | 2 | 1.2 | 1.7 | 35 | 1.2 | 1.8 | 35 | 1.2 | 2.0 | 35 | 21 | 1-2-3 |
| **23** | 2 | 1.2 | 1.7 | 35 | 1.2 | 1.8 | 35 | 1.2 | 2.1 | 35 | 40 | 3-2-1 |
| **24** | 2 | 1.2 | 1.7 | 35 | 1.2 | 1.8 | 35 | 1.2 | 2.2 | 35 | 23 | 2-1-3 |
| **25** | 2 | 1.2 | 1.7 | 35 | 1.2 | 1.9 | 35 | 1.2 | 2.0 | 35 | 32 | 3-2-1 |
| **26** | 2 | 1.2 | 1.7 | 35 | 1.2 | 1.9 | 35 | 1.2 | 2.1 | 35 | 42 | 3-1-2 |
| **27** | 2 | 1.2 | 1.7 | 35 | 1.2 | 1.9 | 35 | 1.2 | 2.2 | 35 | 22 | 3-2-1 |
| **28** | 2 | 1.2 | 1.7 | 35 | 1.2 | 2.0 | 35 | 1.2 | 2.1 | 35 | 27 | 1-2-3 |
| **29** | 2 | 1.2 | 1.7 | 35 | 1.2 | 2.0 | 35 | 1.2 | 2.2 | 35 | 17 | 1-3-2 |
| **30** | 2 | 1.2 | 1.7 | 35 | 1.2 | 2.1 | 35 | 1.2 | 2.2 | 35 | 13 | 1-3-2 |
| **31** | 2 | 1.2 | 1.8 | 35 | 1.2 | 1.9 | 35 | 1.2 | 2.0 | 35 | 39 | 3-2-1 |
| **32** | 2 | 1.2 | 1.8 | 35 | 1.2 | 1.9 | 35 | 1.2 | 2.1 | 35 | 41 | 3-1-2 |
| **33** | 2 | 1.2 | 1.8 | 35 | 1.2 | 1.9 | 35 | 1.2 | 2.2 | 35 | 07 | 3-2-1 |
| **34** | 2 | 1.2 | 1.8 | 35 | 1.2 | 2.0 | 35 | 1.2 | 2.1 | 35 | 6 | 1-2-3 |
| **35** | 2 | 1.2 | 1.8 | 35 | 1.2 | 2.0 | 35 | 1.2 | 2.2 | 35 | 20 | 2-3-1 |
| **36** | 2 | 1.2 | 1.8 | 35 | 1.2 | 2.1 | 35 | 1.2 | 2.2 | 35 | 09 | 3-2-1 |
| **37** | 2 | 1.2 | 1.9 | 35 | 1.2 | 2.0 | 35 | 1.2 | 2.1 | 35 | 44 | 1-2-3 |
| **38** | 2 | 1.2 | 1.9 | 35 | 1.2 | 2.0 | 35 | 1.2 | 2.2 | 35 | 30 | 1-3-2 |
| **39** | 2 | 1.2 | 1.9 | 35 | 1.2 | 2.1 | 35 | 1.2 | 2.2 | 35 | 29 | 3-2-1 |
| **40** | 2 | 1.2 | 2.0 | 35 | 1.2 | 2.1 | 35 | 1.2 | 2.2 | 35 | 31 | 1-2-3 |
| **41** | *Practice* | 0.8 | 1.9 | 20 | 0.8 | 2.0 | 20 | 0.8 | 2.2 | 20 | 01 | 1-2-3 |
| **42** | *Practice* | 0.8 | 1.9 | 20 | 0.8 | 2.1 | 20 | 0.8 | 2.2 | 20 | 02 | 3-2-1 |
| **43** | *Practice* | 0.8 | 2.0 | 20 | 0.8 | 2.1 | 20 | 0.8 | 2.2 | 20 | 03 | 1-2-3 |
| **44** | *Practice* | 1.2 | 1.7 | 35 | 1.2 | 1.8 | 35 | 1.2 | 1.9 | 35 | 04 | 1-2-3 |
| **45** | *Practice* | 1.2 | 1.7 | 35 | 1.2 | 1.8 | 35 | 1.2 | 2.0 | 35 | 05 | 3-2-1 |

**Appendix 6-D:** Table detailing the results from the *category scaling* experiments described in *Section 6.2*, where *Obs1*, *Obs2* and *Obs3* are the rank in which each observer ordered the surfaces, one being the roughest, two the surface with the middle perceived roughness and three the smoothest surface.

| *No* | *Trial* | $\sigma_1$ | $\beta_1$ | $\theta_1$ | $\sigma_2$ | $\beta_2$ | $\theta_2$ | $\sigma_3$ | $\beta_3$ | $\theta_3$ | *Obs1* | *Obs2* | *Obs3* |
|---|---|---|---|---|---|---|---|---|---|---|---|---|---|
| **01** | 1 | 0.8 | 1.7 | 20 | 0.8 | 1.8 | 20 | 0.8 | 1.9 | 20 | 2-1-3 | 1-2-3 | 2-1-3 |
| **02** | 1 | 0.8 | 1.7 | 20 | 0.8 | 1.8 | 20 | 0.8 | 2.0 | 20 | 1-2-3 | 1-2-3 | 1-2-3 |
| **03** | 1 | 0.8 | 1.7 | 20 | 0.8 | 1.8 | 20 | 0.8 | 2.1 | 20 | 1-2-3 | 1-2-3 | 1-2-3 |
| **04** | 1 | 0.8 | 1.7 | 20 | 0.8 | 1.8 | 20 | 0.8 | 2.2 | 20 | 1-2-3 | 1-2-3 | 1-2-3 |
| **05** | 1 | 0.8 | 1.7 | 20 | 0.8 | 1.9 | 20 | 0.8 | 2.0 | 20 | 1-2-3 | 1-2-3 | 1-2-3 |
| **06** | 1 | 0.8 | 1.7 | 20 | 0.8 | 1.9 | 20 | 0.8 | 2.1 | 20 | 1-2-3 | 1-2-3 | 1-2-3 |
| **07** | 1 | 0.8 | 1.7 | 20 | 0.8 | 1.9 | 20 | 0.8 | 2.2 | 20 | 1-2-3 | 1-2-3 | 1-2-3 |
| **08** | 1 | 0.8 | 1.7 | 20 | 0.8 | 2.0 | 20 | 0.8 | 2.1 | 20 | 1-2-3 | 1-2-3 | 1-2-3 |
| **09** | 1 | 0.8 | 1.7 | 20 | 0.8 | 2.0 | 20 | 0.8 | 2.2 | 20 | 1-2-3 | 2-3-1 | 1-2-3 |
| **10** | 1 | 0.8 | 1.7 | 20 | 0.8 | 2.1 | 20 | 0.8 | 2.2 | 20 | 1-2-3 | 1-2-3 | 1-2-3 |
| **11** | 1 | 0.8 | 1.8 | 20 | 0.8 | 1.9 | 20 | 0.8 | 2.0 | 20 | 1-2-3 | 1-2-3 | 1-2-3 |
| **12** | 1 | 0.8 | 1.8 | 20 | 0.8 | 1.9 | 20 | 0.8 | 2.1 | 20 | 1-2-3 | 1-2-3 | 1-2-3 |
| **13** | 1 | 0.8 | 1.8 | 20 | 0.8 | 1.9 | 20 | 0.8 | 2.2 | 20 | 1-2-3 | 1-2-3 | 1-2-3 |
| **14** | 1 | 0.8 | 1.8 | 20 | 0.8 | 2.0 | 20 | 0.8 | 2.1 | 20 | 1-2-3 | 1-2-3 | 1-2-3 |
| **15** | 1 | 0.8 | 1.8 | 20 | 0.8 | 2.0 | 20 | 0.8 | 2.2 | 20 | 1-2-3 | 1-2-3 | 1-2-3 |
| **16** | 1 | 0.8 | 1.8 | 20 | 0.8 | 2.1 | 20 | 0.8 | 2.2 | 20 | 1-2-3 | 2-1-3 | 1-2-3 |
| **17** | 1 | 0.8 | 1.9 | 20 | 0.8 | 2.0 | 20 | 0.8 | 2.1 | 20 | 1-2-3 | 1-2-3 | 1-2-3 |
| **18** | 1 | 0.8 | 1.9 | 20 | 0.8 | 2.0 | 20 | 0.8 | 2.2 | 20 | 1-2-3 | 1-2-3 | 1-2-3 |
| **19** | 1 | 0.8 | 1.9 | 20 | 0.8 | 2.1 | 20 | 0.8 | 2.2 | 20 | 1-2-3 | 1-2-3 | 1-2-3 |
| **20** | 1 | 0.8 | 2.0 | 20 | 0.8 | 2.1 | 20 | 0.8 | 2.2 | 20 | 1-2-3 | 1-2-3 | 1-2-3 |
| **21** | 2 | 1.2 | 1.7 | 35 | 1.2 | 1.8 | 35 | 1.2 | 1.9 | 35 | 1-2-3 | 1-2-3 | 1-2-3 |
| **22** | 2 | 1.2 | 1.7 | 35 | 1.2 | 1.8 | 35 | 1.2 | 2.0 | 35 | 1-2-3 | 1-2-3 | 1-2-3 |
| **23** | 2 | 1.2 | 1.7 | 35 | 1.2 | 1.8 | 35 | 1.2 | 2.1 | 35 | 1-2-3 | 1-2-3 | 2-1-3 |
| **24** | 2 | 1.2 | 1.7 | 35 | 1.2 | 1.8 | 35 | 1.2 | 2.2 | 35 | 1-2-3 | 1-2-3 | 1-2-3 |
| **25** | 2 | 1.2 | 1.7 | 35 | 1.2 | 1.9 | 35 | 1.2 | 2.0 | 35 | 1-2-3 | 1-2-3 | 1-2-3 |
| **26** | 2 | 1.2 | 1.7 | 35 | 1.2 | 1.9 | 35 | 1.2 | 2.1 | 35 | 1-2-3 | 1-2-3 | 1-2-3 |
| **27** | 2 | 1.2 | 1.7 | 35 | 1.2 | 1.9 | 35 | 1.2 | 2.2 | 35 | 1-2-3 | 1-2-3 | 1-2-3 |
| **28** | 2 | 1.2 | 1.7 | 35 | 1.2 | 2.0 | 35 | 1.2 | 2.1 | 35 | 1-2-3 | 1-2-3 | 1-2-3 |
| **29** | 2 | 1.2 | 1.7 | 35 | 1.2 | 2.0 | 35 | 1.2 | 2.2 | 35 | 1-2-3 | 1-2-3 | 1-2-3 |
| **30** | 2 | 1.2 | 1.7 | 35 | 1.2 | 2.1 | 35 | 1.2 | 2.2 | 35 | 1-2-3 | 1-2-3 | 1-2-3 |
| **31** | 2 | 1.2 | 1.8 | 35 | 1.2 | 1.9 | 35 | 1.2 | 2.0 | 35 | 1-2-3 | 1-2-3 | 1-2-3 |
| **32** | 2 | 1.2 | 1.8 | 35 | 1.2 | 1.9 | 35 | 1.2 | 2.1 | 35 | 1-2-3 | 1-2-3 | 1-2-3 |
| **33** | 2 | 1.2 | 1.8 | 35 | 1.2 | 1.9 | 35 | 1.2 | 2.2 | 35 | 1-2-3 | 1-2-3 | 1-2-3 |
| **34** | 2 | 1.2 | 1.8 | 35 | 1.2 | 2.0 | 35 | 1.2 | 2.1 | 35 | 1-2-3 | 1-2-3 | 1-2-3 |
| **35** | 2 | 1.2 | 1.8 | 35 | 1.2 | 2.0 | 35 | 1.2 | 2.2 | 35 | 1-2-3 | 1-2-3 | 1-2-3 |
| **36** | 2 | 1.2 | 1.8 | 35 | 1.2 | 2.1 | 35 | 1.2 | 2.2 | 35 | 1-2-3 | 1-2-3 | 1-2-3 |
| **37** | 2 | 1.2 | 1.9 | 35 | 1.2 | 2.0 | 35 | 1.2 | 2.1 | 35 | 1-2-3 | 1-2-3 | 1-2-3 |
| **38** | 2 | 1.2 | 1.9 | 35 | 1.2 | 2.0 | 35 | 1.2 | 2.2 | 35 | 1-2-3 | 1-2-3 | 1-2-3 |
| **39** | 2 | 1.2 | 1.9 | 35 | 1.2 | 2.1 | 35 | 1.2 | 2.2 | 35 | 1-2-3 | 1-2-3 | 1-2-3 |
| **40** | 2 | 1.2 | 2.0 | 35 | 1.2 | 2.1 | 35 | 1.2 | 2.2 | 35 | 1-2-3 | 1-2-3 | 1-2-3 |

**Appendix 6-E:** Table detailing the order and parameters from the values of the experiment described in *Section 6.3*.

| *No* | *Trial* | $\beta_{ref}$ | $\theta_{ref}$ | $\sigma_{ref}$ | $\beta_{adj}$ | $\theta_{adj}$ | $\sigma_{adj}$ | *Order* |
|---|---|---|---|---|---|---|---|---|
| **01** | 1 | 2.0 | 05 | 0.4 | 2.0 | 25 | | 16 |
| **02** | 1 | 2.0 | 12 | 0.6 | 2.0 | 32 | | 23 |
| **03** | 1 | 2.0 | 45 | 0.8 | 2.0 | 65 | | 26 |
| **04** | 1 | 2.0 | 41 | 1.0 | 2.0 | 61 | | 29 |
| **05** | 1 | 2.0 | 14 | 1.2 | 2.0 | 34 | | 30 |
| **06** | 2 | 2.0 | 05 | 0.4 | 2.0 | 25 | | 11 |
| **07** | 2 | 2.0 | 12 | 0.6 | 2.0 | 32 | | 20 |
| **08** | 2 | 2.0 | 45 | 0.8 | 2.0 | 65 | | 06 |
| **09** | 2 | 2.0 | 41 | 1.0 | 2.0 | 61 | | 08 |
| **10** | 2 | 2.0 | 14 | 1.2 | 2.0 | 34 | | 21 |
| **11** | 3 | 2.0 | 05 | 0.4 | 2.0 | 25 | | 22 |
| **12** | 3 | 2.0 | 12 | 0.6 | 2.0 | 32 | | 28 |
| **13** | 3 | 2.0 | 45 | 0.8 | 2.0 | 65 | | 27 |
| **14** | 3 | 2.0 | 41 | 1.0 | 2.0 | 61 | | 14 |
| **15** | 3 | 2.0 | 14 | 1.2 | 2.0 | 34 | | 09 |
| **16** | 4 | 2.0 | 05 | 0.4 | 2.0 | 25 | | 17 |
| **17** | 4 | 2.0 | 12 | 0.6 | 2.0 | 32 | | 07 |
| **18** | 4 | 2.0 | 45 | 0.8 | 2.0 | 65 | | 25 |
| **19** | 4 | 2.0 | 41 | 1.0 | 2.0 | 61 | | 12 |
| **20** | 4 | 2.0 | 14 | 1.2 | 2.0 | 34 | | 19 |
| **21** | 5 | 2.0 | 05 | 0.4 | 2.0 | 25 | | 24 |
| **22** | 5 | 2.0 | 12 | 0.6 | 2.0 | 32 | | 15 |
| **23** | 5 | 2.0 | 45 | 0.8 | 2.0 | 65 | | 18 |
| **24** | 5 | 2.0 | 41 | 1.0 | 2.0 | 61 | | 13 |
| **25** | 5 | 2.0 | 14 | 1.2 | 2.0 | 34 | | 10 |
| **26** | *Practice* | 2.0 | 41 | 1.0 | 2.0 | 61 | | 01 |
| **27** | *Practice* | 2.0 | 14 | 1.2 | 2.0 | 34 | | 02 |
| **28** | *Practice* | 2.0 | 05 | 0.4 | 2.0 | 25 | | 03 |
| **29** | *Practice* | 2.0 | 14 | 1.2 | 2.0 | 34 | | 04 |
| **30** | *Practice* | 2.0 | 05 | 0.4 | 2.0 | 25 | | 05 |

**Appendix 6-F:** Table detailing the order and parameters from the values of the experiment described in *Section 6.3*.

| *No* | $\theta_{ref}$ | $\sigma_{ref}$ | $\theta_{adj}$ | $\sigma 1_{adj}$ | $\sigma 2_{adj}$ | $\sigma 3_{adj}$ | $\sigma 4_{adj}$ | $\sigma 5_{adj}$ | $\sigma 6_{adj}$ | $\sigma 7_{adj}$ | $\sigma 8_{adj}$ | $\sigma 9_{adj}$ | $\sigma 10_{adj}$ |
|---|---|---|---|---|---|---|---|---|---|---|---|---|---|
| **01** | 5 | 0.4 | 25 | 0.45 | 0.32 | 0.43 | 0.43 | 0.43 | 0.50 | 0.45 | 0.44 | 0.32 | 0.43 |
| **02** | 12 | 0.6 | 32 | 0.79 | 0.53 | 0.62 | 0.57 | 0.57 | 0.60 | 0.61 | 0.59 | 0.53 | 0.61 |
| **03** | 45 | 0.8 | 65 | 0.89 | 0.80 | 0.71 | 0.76 | 0.76 | 0.76 | 0.99 | 0.79 | 0.95 | 0.73 |
| **04** | 41 | 1 | 61 | 1.14 | 1.01 | 1.09 | 1.10 | 1.21 | 1.20 | 1.08 | 1.07 | 1.14 | 1.08 |
| **05** | 14 | 1.2 | 34 | 1.10 | 1.12 | 1.18 | 1.27 | 0.78 | 1.10 | 1.28 | 1.29 | 1.30 | 1.21 |
| **06** | 5 | 0.4 | 25 | 0.48 | 0.38 | 0.55 | 0.49 | 0.49 | 0.33 | 0.27 | 0.49 | 0.50 | 0.53 |
| **07** | 12 | 0.6 | 32 | 0.67 | 0.81 | 0.62 | 0.71 | 0.54 | 0.74 | 0.49 | 0.71 | 0.69 | 0.64 |
| **08** | 45 | 0.8 | 65 | 0.91 | 0.92 | 0.82 | 0.79 | 1.17 | 0.85 | 0.55 | 0.70 | 0.78 | 0.78 |
| **09** | 41 | 1 | 61 | 1.16 | 1.01 | 1.09 | 0.90 | 0.85 | 1.20 | 1.06 | 1.07 | 1.22 | 1.08 |
| **10** | 14 | 1.2 | 34 | 1.48 | 1.36 | 1.46 | 1.56 | 1.00 | 1.28 | 1.09 | 1.39 | 1.58 | 1.44 |
| **11** | 5 | 0.4 | 25 | 0.49 | 0.37 | 0.55 | 0.43 | 0.43 | 0.47 | 0.61 | 0.34 | 0.50 | 0.49 |
| **12** | 12 | 0.6 | 32 | 0.64 | 0.59 | 0.62 | 0.58 | 0.58 | 0.80 | 0.54 | 0.61 | 0.65 | 0.62 |
| **13** | 45 | 0.8 | 65 | 0.69 | 0.87 | 0.48 | 0.92 | 0.92 | 0.46 | 0.70 | 0.65 | 0.81 | 0.53 |
| **14** | 41 | 1 | 61 | 1.14 | 1.17 | 1.20 | 1.17 | 1.04 | 1.19 | 1.17 | 1.05 | 1.16 | 1.16 |
| **15** | 14 | 1.2 | 34 | 1.37 | 1.43 | 1.12 | 0.97 | 0.97 | 0.98 | 0.97 | 0.91 | 1.29 | 1.06 |
| **16** | 5 | 0.4 | 25 | 0.51 | 0.59 | 0.59 | 0.41 | 0.73 | 0.71 | 0.42 | 0.57 | 0.75 | 0.58 |
| **17** | 12 | 0.6 | 32 | 0.97 | 0.78 | 0.80 | 0.88 | 0.88 | 0.42 | 0.63 | 0.74 | 0.69 | 0.78 |
| **18** | 45 | 0.8 | 65 | 1.03 | 0.98 | 0.72 | 0.73 | 0.73 | 1.02 | 0.87 | 1.19 | 0.85 | 0.86 |
| **19** | 41 | 1 | 61 | 1.17 | 1.33 | 1.19 | 1.00 | 1.00 | 1.17 | 1.10 | 1.12 | 1.22 | 1.17 |
| **20** | 14 | 1.2 | 34 | 1.31 | 1.37 | 1.36 | 1.58 | 1.29 | 1.23 | 1.32 | 1.12 | 1.31 | 1.29 |
| **21** | 5 | 0.4 | 25 | 0.40 | 0.50 | 0.53 | 0.48 | 0.40 | 0.61 | 0.25 | 0.50 | 0.36 | 0.52 |
| **22** | 12 | 0.6 | 32 | 0.80 | 0.45 | 0.77 | 0.57 | 0.70 | 0.65 | 0.35 | 0.54 | 0.66 | 0.70 |
| **23** | 45 | 0.8 | 65 | 0.78 | 0.79 | 0.80 | 0.82 | 0.82 | 0.79 | 0.62 | 0.83 | 1.04 | 0.81 |
| **24** | 41 | 1 | 61 | 0.95 | 1.06 | 0.92 | 1.02 | 1.14 | 0.98 | 0.83 | 1.05 | 1.10 | 0.96 |
| **25** | 14 | 1.2 | 34 | 1.32 | 1.32 | 1.37 | 1.31 | 1.31 | 1.39 | 1.16 | 1.40 | 1.91 | 1.38 |

**Appendix 6-G:** Table detailing the order and parameters from the values of the experiment described in *Section 6.4*, where *ref* is the parameters from the *reference surfaces* and *adj* are the parameters from the *adjustable surface*.

| *No* | *Trial* | $\beta_{ref}$ | $\theta_{ref}$ | $\sigma_{ref}$ | $\beta_{adj}$ | $\theta_{adj}$ | $\sigma_{adj}$ | *Order* |
|---|---|---|---|---|---|---|---|---|
| **01** | 1 | 2.0 | 01 | 0.40 | 1.7 | 21 | | 078 |
| **02** | 1 | 2.0 | 01 | 0.40 | 1.8 | 21 | | 088 |
| **03** | 1 | 2.0 | 01 | 0.40 | 1.9 | 21 | | 094 |
| **04** | 1 | 2.0 | 01 | 0.40 | 2.0 | 21 | | 100 |
| **05** | 1 | 2.0 | 01 | 0.40 | 2.1 | 21 | | 015 |
| **06** | 1 | 2.0 | 01 | 0.40 | 2.2 | 21 | | 062 |
| **07** | 1 | 2.0 | 01 | 0.40 | 2.3 | 21 | | 105 |
| **08** | 1 | 2.0 | 02 | 0.60 | 1.7 | 22 | | 089 |
| **09** | 1 | 2.0 | 02 | 0.60 | 1.8 | 22 | | 042 |
| **10** | 1 | 2.0 | 02 | 0.60 | 1.9 | 22 | | 016 |
| **11** | 1 | 2.0 | 02 | 0.60 | 2.0 | 22 | | 044 |
| **12** | 1 | 2.0 | 02 | 0.60 | 2.1 | 22 | | 007 |
| **13** | 1 | 2.0 | 02 | 0.60 | 2.2 | 22 | | 093 |
| **14** | 1 | 2.0 | 02 | 0.60 | 2.3 | 22 | | 049 |
| **15** | 1 | 2.0 | 03 | 0.80 | 1.7 | 23 | | 034 |
| **16** | 1 | 2.0 | 03 | 0.80 | 1.8 | 23 | | 060 |
| **17** | 1 | 2.0 | 03 | 0.80 | 1.9 | 23 | | 014 |
| **18** | 1 | 2.0 | 03 | 0.80 | 2.0 | 23 | | 074 |
| **19** | 1 | 2.0 | 03 | 0.80 | 2.1 | 23 | | 059 |
| **20** | 1 | 2.0 | 03 | 0.80 | 2.2 | 23 | | 085 |
| **21** | 1 | 2.0 | 03 | 0.80 | 2.3 | 23 | | 092 |
| **22** | 1 | 2.0 | 04 | 1.00 | 1.7 | 24 | | 110 |
| **23** | 1 | 2.0 | 04 | 1.00 | 1.8 | 24 | | 076 |
| **24** | 1 | 2.0 | 04 | 1.00 | 1.9 | 24 | | 083 |
| **25** | 1 | 2.0 | 04 | 1.00 | 2.0 | 24 | | 069 |
| **26** | 1 | 2.0 | 04 | 1.00 | 2.1 | 24 | | 053 |
| **27** | 1 | 2.0 | 04 | 1.00 | 2.2 | 24 | | 101 |
| **28** | 1 | 2.0 | 04 | 1.00 | 2.3 | 24 | | 065 |
| **29** | 1 | 2.0 | 05 | 1.20 | 1.7 | 25 | | 075 |
| **30** | 1 | 2.0 | 05 | 1.20 | 1.8 | 25 | | 019 |
| **31** | 1 | 2.0 | 05 | 1.20 | 1.9 | 25 | | 024 |
| **32** | 1 | 2.0 | 05 | 1.20 | 2.0 | 25 | | 051 |
| **33** | 1 | 2.0 | 05 | 1.20 | 2.1 | 25 | | 061 |
| **34** | 1 | 2.0 | 05 | 1.20 | 2.2 | 25 | | 073 |
| **35** | 1 | 2.0 | 05 | 1.20 | 2.3 | 25 | | 057 |
| **36** | 2 | 2.0 | 06 | 0.40 | 1.7 | 26 | | 023 |
| **37** | 2 | 2.0 | 06 | 0.40 | 1.8 | 26 | | 082 |
| **38** | 2 | 2.0 | 06 | 0.40 | 1.9 | 26 | | 035 |
| **39** | 2 | 2.0 | 06 | 0.40 | 2.0 | 26 | | 008 |
| **40** | 2 | 2.0 | 06 | 0.40 | 2.1 | 26 | | 010 |
| **41** | 2 | 2.0 | 06 | 0.40 | 2.2 | 26 | | 040 |
| **42** | 2 | 2.0 | 06 | 0.40 | 2.3 | 26 | | 108 |
| **43** | 2 | 2.0 | 07 | 0.60 | 1.7 | 27 | | 072 |
| **44** | 2 | 2.0 | 07 | 0.60 | 1.8 | 27 | | 029 |
| **45** | 2 | 2.0 | 07 | 0.60 | 1.9 | 27 | | 041 |
| **46** | 2 | 2.0 | 07 | 0.60 | 2.0 | 27 | | 037 |
| **47** | 2 | 2.0 | 07 | 0.60 | 2.1 | 27 | | 052 |
| **48** | 2 | 2.0 | 07 | 0.60 | 2.2 | 27 | | 018 |

| | | | | | | | |
|---|---|---|---|---|---|---|---|
| **49** | 2 | 2.0 | 07 | 0.60 | 2.3 | 27 | 071 |
| **50** | 2 | 2.0 | 08 | 0.80 | 1.7 | 28 | 080 |
| **51** | 2 | 2.0 | 08 | 0.80 | 1.8 | 28 | 109 |
| **52** | 2 | 2.0 | 08 | 0.80 | 1.9 | 28 | 097 |
| **53** | 2 | 2.0 | 08 | 0.80 | 2.0 | 28 | 086 |
| **54** | 2 | 2.0 | 08 | 0.80 | 2.1 | 28 | 087 |
| **55** | 2 | 2.0 | 08 | 0.80 | 2.2 | 28 | 058 |
| **56** | 2 | 2.0 | 08 | 0.80 | 2.3 | 28 | 055 |
| **57** | 2 | 2.0 | 09 | 1.00 | 1.7 | 29 | 046 |
| **58** | 2 | 2.0 | 09 | 1.00 | 1.8 | 29 | 098 |
| **59** | 2 | 2.0 | 09 | 1.00 | 1.9 | 29 | 022 |
| **60** | 2 | 2.0 | 09 | 1.00 | 2.0 | 29 | 021 |
| **61** | 2 | 2.0 | 09 | 1.00 | 2.1 | 29 | 067 |
| **62** | 2 | 2.0 | 09 | 1.00 | 2.2 | 29 | 096 |
| **63** | 2 | 2.0 | 09 | 1.00 | 2.3 | 29 | 047 |
| **64** | 2 | 2.0 | 10 | 1.20 | 1.7 | 30 | 091 |
| **65** | 2 | 2.0 | 10 | 1.20 | 1.8 | 30 | 009 |
| **66** | 2 | 2.0 | 10 | 1.20 | 1.9 | 30 | 102 |
| **67** | 2 | 2.0 | 10 | 1.20 | 2.0 | 30 | 106 |
| **68** | 2 | 2.0 | 10 | 1.20 | 2.1 | 30 | 032 |
| **69** | 2 | 2.0 | 10 | 1.20 | 2.2 | 30 | 027 |
| **70** | 2 | 2.0 | 10 | 1.20 | 2.3 | 30 | 063 |
| **71** | 3 | 2.0 | 11 | 0.40 | 1.7 | 31 | 033 |
| **72** | 3 | 2.0 | 11 | 0.40 | 1.8 | 31 | 012 |
| **73** | 3 | 2.0 | 11 | 0.40 | 1.9 | 31 | 036 |
| **74** | 3 | 2.0 | 11 | 0.40 | 2.0 | 31 | 028 |
| **75** | 3 | 2.0 | 11 | 0.40 | 2.1 | 31 | 038 |
| **76** | 3 | 2.0 | 11 | 0.40 | 2.2 | 31 | 103 |
| **77** | 3 | 2.0 | 11 | 0.40 | 2.3 | 31 | 020 |
| **78** | 3 | 2.0 | 12 | 0.60 | 1.7 | 32 | 077 |
| **79** | 3 | 2.0 | 12 | 0.60 | 1.8 | 32 | 031 |
| **80** | 3 | 2.0 | 12 | 0.60 | 1.9 | 32 | 068 |
| **81** | 3 | 2.0 | 12 | 0.60 | 2.0 | 32 | 048 |
| **82** | 3 | 2.0 | 12 | 0.60 | 2.1 | 32 | 039 |
| **83** | 3 | 2.0 | 12 | 0.60 | 2.2 | 32 | 084 |
| **84** | 3 | 2.0 | 12 | 0.60 | 2.3 | 32 | 070 |
| **85** | 3 | 2.0 | 13 | 0.80 | 1.7 | 33 | 099 |
| **86** | 3 | 2.0 | 13 | 0.80 | 1.8 | 33 | 043 |
| **87** | 3 | 2.0 | 13 | 0.80 | 1.9 | 33 | 064 |
| **88** | 3 | 2.0 | 13 | 0.80 | 2.0 | 33 | 045 |
| **89** | 3 | 2.0 | 13 | 0.80 | 2.1 | 33 | 079 |
| **90** | 3 | 2.0 | 13 | 0.80 | 2.2 | 33 | 095 |
| **91** | 3 | 2.0 | 13 | 0.80 | 2.3 | 33 | 026 |
| **92** | 3 | 2.0 | 14 | 1.00 | 1.7 | 34 | 050 |
| **93** | 3 | 2.0 | 14 | 1.00 | 1.8 | 34 | 090 |
| **94** | 3 | 2.0 | 14 | 1.00 | 1.9 | 34 | 054 |
| **95** | 3 | 2.0 | 14 | 1.00 | 2.0 | 34 | 025 |
| **96** | 3 | 2.0 | 14 | 1.00 | 2.1 | 34 | 104 |
| **97** | 3 | 2.0 | 14 | 1.00 | 2.2 | 34 | 017 |
| **98** | 3 | 2.0 | 14 | 1.00 | 2.3 | 34 | 056 |
| **99** | 3 | 2.0 | 15 | 1.20 | 1.7 | 35 | 107 |
| **100** | 3 | 2.0 | 15 | 1.20 | 1.8 | 35 | 030 |
| **101** | 3 | 2.0 | 15 | 1.20 | 1.9 | 35 | 066 |
| **102** | 3 | 2.0 | 15 | 1.20 | 2.0 | 35 | 006 |
| **103** | 3 | 2.0 | 15 | 1.20 | 2.1 | 35 | 081 |

| | | | | | | | |
|---|---|---|---|---|---|---|---|
| **104** | 3 | 2.0 | 15 | 1.20 | 2.2 | 35 | 013 |
| **105** | 3 | 2.0 | 15 | 1.20 | 2.3 | 35 | 011 |
| **106** | Practice | 2.0 | 12 | 0.60 | 1.9 | 32 | 001 |
| **107** | Practice | 2.0 | 06 | 0.40 | 2.0 | 26 | 002 |
| **108** | Practice | 2.0 | 09 | 1.00 | 2.3 | 29 | 003 |
| **109** | Practice | 2.0 | 13 | 0.80 | 1.7 | 33 | 004 |
| **110** | Practice | 2.0 | 15 | 1.20 | 2.3 | 35 | 005 |

**Appendix 6-H:** Table detailing each of the observations from the ten observers in the experiment of Section 6-4.

| *No* | $\sigma_{ref}$ | $\sigma 1_{adj}$ | $\sigma 2_{adj}$ | $\sigma 3_{adj}$ | $\sigma 4_{adj}$ | $\sigma 5_{adj}$ | $\sigma 6_{adj}$ | $\sigma 7_{adj}$ | $\sigma 8_{adj}$ | $\sigma 9_{adj}$ | $\sigma 10_{adj}$ |
|---|---|---|---|---|---|---|---|---|---|---|---|
| **01** | 0.40 | 0.178 | 0.225 | 0.090 | 0.152 | 0.258 | 0.211 | 0.263 | 0.200 | 0.229 | 0.123 |
| **02** | 0.40 | 0.255 | 0.304 | 0.274 | 0.252 | 0.290 | 0.227 | 0.258 | 0.260 | 0.244 | 0.270 |
| **03** | 0.40 | 0.359 | 0.303 | 0.343 | 0.328 | 0.462 | 0.562 | 0.274 | 0.326 | 0.419 | 0.338 |
| **04** | 0.40 | 0.446 | 0.319 | 0.428 | 0.427 | 0.427 | 0.496 | 0.449 | 0.441 | 0.316 | 0.432 |
| **05** | 0.40 | 0.696 | 0.559 | 0.430 | 0.506 | 0.547 | 0.757 | 0.326 | 0.505 | 0.608 | 0.452 |
| **06** | 0.40 | 0.907 | 0.478 | 0.462 | 0.965 | 0.965 | 0.662 | 0.422 | 0.765 | 0.343 | 0.553 |
| **07** | 0.40 | 1.468 | 0.533 | 0.798 | 0.884 | 0.440 | 1.535 | 0.828 | 1.212 | 0.703 | 0.922 |
| **08** | 0.60 | 0.211 | 0.272 | 0.191 | 0.175 | 0.413 | 0.344 | 0.307 | 0.269 | 0.286 | 0.214 |
| **09** | 0.60 | 0.334 | 0.379 | 0.300 | 0.299 | 0.498 | 0.371 | 0.350 | 0.299 | 0.405 | 0.300 |
| **10** | 0.60 | 0.438 | 0.510 | 0.547 | 0.444 | 0.444 | 0.373 | 0.532 | 0.626 | 0.470 | 0.571 |
| **11** | 0.60 | 0.788 | 0.530 | 0.617 | 0.566 | 0.566 | 0.597 | 0.612 | 0.587 | 0.527 | 0.608 |
| **12** | 0.60 | 0.976 | 0.874 | 0.668 | 0.828 | 0.685 | 0.698 | 0.544 | 0.810 | 0.905 | 0.711 |
| **13** | 0.60 | 1.359 | 1.065 | 0.857 | 1.254 | 0.597 | 1.449 | 0.724 | 1.351 | 0.828 | 1.005 |
| **14** | 0.60 | 1.993 | 0.732 | 0.617 | 1.767 | 1.767 | 1.320 | 0.783 | 1.185 | 0.845 | 0.788 |
| **15** | 0.80 | 0.303 | 0.396 | 0.286 | 0.365 | 0.624 | 0.335 | 0.313 | 0.247 | 0.291 | 0.274 |
| **16** | 0.80 | 0.510 | 0.575 | 0.370 | 0.347 | 0.347 | 0.391 | 0.599 | 0.569 | 0.605 | 0.429 |
| **17** | 0.80 | 0.610 | 0.715 | 0.533 | 0.728 | 0.773 | 0.635 | 0.728 | 0.775 | 0.483 | 0.606 |
| **18** | 0.80 | 0.886 | 0.800 | 0.711 | 0.765 | 0.765 | 0.759 | 0.989 | 0.790 | 0.948 | 0.735 |
| **19** | 0.80 | 1.135 | 1.000 | 0.922 | 1.063 | 1.063 | 0.939 | 0.646 | 0.943 | 1.188 | 0.928 |
| **20** | 0.80 | 1.603 | 1.086 | 1.546 | 1.482 | 1.038 | 1.606 | 0.941 | 1.422 | 0.857 | 1.509 |
| **21** | 0.80 | 2.661 | 1.767 | 2.669 | 2.020 | 1.302 | 2.381 | 1.234 | 2.569 | 1.433 | 2.639 |
| **22** | 1.00 | 0.319 | 0.675 | 0.430 | 0.592 | 0.592 | 0.329 | 0.585 | 0.306 | 0.350 | 0.393 |
| **23** | 1.00 | 0.585 | 0.559 | 0.615 | 0.802 | 0.784 | 0.335 | 0.662 | 0.550 | 0.635 | 0.596 |
| **24** | 1.00 | 0.812 | 0.767 | 0.700 | 0.763 | 0.948 | 0.779 | 0.798 | 0.666 | 1.075 | 0.690 |
| **25** | 1.00 | 1.142 | 1.007 | 1.088 | 1.095 | 1.210 | 1.202 | 1.084 | 1.070 | 1.137 | 1.083 |
| **26** | 1.00 | 1.572 | 0.818 | 1.229 | 1.200 | 1.200 | 1.406 | 1.173 | 1.317 | 1.084 | 1.256 |
| **27** | 1.00 | 2.160 | 1.119 | 1.279 | 1.782 | 1.782 | 1.612 | 1.244 | 1.455 | 1.706 | 1.332 |
| **28** | 1.00 | 2.645 | 1.485 | 1.721 | 2.174 | 1.154 | 2.441 | 1.292 | 2.569 | 1.973 | 1.975 |
| **29** | 1.20 | 0.470 | 0.835 | 0.435 | 0.612 | 0.612 | 0.402 | 0.711 | 0.386 | 0.465 | 0.420 |
| **30** | 1.20 | 0.578 | 0.790 | 0.500 | 0.843 | 0.749 | 0.672 | 0.520 | 0.550 | 0.508 | 0.515 |
| **31** | 1.20 | 0.937 | 0.771 | 0.987 | 1.031 | 1.031 | 0.806 | 0.952 | 0.775 | 0.920 | 0.923 |
| **32** | 1.20 | 1.105 | 1.116 | 1.183 | 1.267 | 0.779 | 1.105 | 1.284 | 1.287 | 1.300 | 1.214 |
| **33** | 1.20 | 1.870 | 1.325 | 1.468 | 1.794 | 1.794 | 1.908 | 1.404 | 1.535 | 1.493 | 1.488 |
| **34** | 1.20 | 2.518 | 1.886 | 2.010 | 1.764 | 0.918 | 2.156 | 2.665 | 2.118 | 1.650 | 2.042 |
| **35** | 1.20 | 2.641 | 1.289 | 2.199 | 1.895 | 2.267 | 2.645 | 2.625 | 2.514 | 1.876 | 2.293 |
| **36** | 0.40 | 0.258 | 0.280 | 0.245 | 0.126 | 0.386 | 0.227 | 0.191 | 0.157 | 0.202 | 0.219 |

| | | | | | | | | | | | |
|---|---|---|---|---|---|---|---|---|---|---|---|
| **37** | 0.40 | 0.313 | 0.316 | 0.376 | 0.206 | 0.206 | 0.353 | 0.413 | 0.306 | 0.289 | 0.355 |
| **38** | 0.40 | 0.297 | 0.459 | 0.353 | 0.273 | 0.273 | 0.433 | 0.296 | 0.411 | 0.302 | 0.370 |
| **39** | 0.40 | 0.482 | 0.377 | 0.554 | 0.490 | 0.490 | 0.328 | 0.272 | 0.490 | 0.498 | 0.535 |
| **40** | 0.40 | 0.633 | 0.587 | 0.642 | 0.552 | 0.596 | 0.922 | 0.617 | 0.702 | 0.589 | 0.660 |
| **41** | 0.40 | 0.930 | 0.525 | 1.020 | 0.755 | 0.406 | 0.865 | 0.520 | 0.892 | 0.542 | 0.982 |
| **42** | 0.40 | 1.736 | 0.928 | 1.135 | 1.257 | 0.661 | 1.294 | 0.814 | 1.135 | 0.688 | 1.135 |
| **43** | 0.60 | 0.273 | 0.256 | 0.182 | 0.202 | 0.202 | 0.290 | 0.340 | 0.249 | 0.380 | 0.202 |
| **44** | 0.60 | 0.343 | 0.376 | 0.329 | 0.376 | 0.376 | 0.363 | 0.475 | 0.425 | 0.495 | 0.358 |
| **45** | 0.60 | 0.511 | 0.452 | 0.462 | 0.440 | 0.440 | 0.496 | 0.451 | 0.537 | 0.719 | 0.484 |
| **46** | 0.60 | 0.670 | 0.814 | 0.615 | 0.711 | 0.538 | 0.736 | 0.495 | 0.705 | 0.688 | 0.642 |
| **47** | 0.60 | 1.173 | 0.677 | 0.892 | 0.824 | 0.692 | 1.018 | 0.646 | 0.933 | 0.899 | 0.904 |
| **48** | 0.60 | 1.623 | 0.863 | 0.720 | 1.482 | 0.661 | 1.618 | 1.011 | 1.183 | 0.833 | 0.859 |
| **49** | 0.60 | 2.601 | 0.911 | 0.622 | 1.526 | 1.526 | 1.791 | 0.851 | 1.886 | 1.535 | 1.001 |
| **50** | 0.80 | 0.206 | 0.443 | 0.272 | 0.389 | 0.786 | 0.258 | 0.354 | 0.312 | 0.319 | 0.284 |
| **51** | 0.80 | 0.451 | 0.711 | 0.477 | 0.470 | 0.470 | 0.334 | 0.473 | 0.571 | 0.759 | 0.505 |
| **52** | 0.80 | 0.613 | 0.740 | 0.646 | 0.810 | 0.788 | 0.728 | 0.601 | 0.428 | 0.648 | 0.581 |
| **53** | 0.80 | 0.911 | 0.918 | 0.822 | 0.792 | 1.173 | 0.853 | 0.550 | 0.696 | 0.783 | 0.784 |
| **54** | 0.80 | 1.098 | 1.029 | 1.164 | 1.312 | 1.130 | 1.232 | 0.913 | 1.040 | 1.200 | 1.127 |
| **55** | 0.80 | 1.963 | 1.025 | 1.007 | 2.033 | 2.033 | 1.927 | 0.892 | 1.560 | 1.168 | 1.173 |
| **56** | 0.80 | 2.553 | 1.398 | 1.679 | 1.538 | 1.049 | 2.303 | 1.422 | 2.625 | 1.873 | 1.963 |
| **57** | 1.00 | 0.320 | 0.610 | 0.424 | 0.312 | 0.312 | 0.452 | 0.587 | 0.379 | 0.440 | 0.410 |
| **58** | 1.00 | 0.556 | 0.661 | 0.624 | 0.501 | 0.501 | 0.685 | 0.761 | 0.626 | 0.587 | 0.625 |
| **59** | 1.00 | 0.869 | 1.065 | 0.757 | 0.631 | 0.631 | 0.786 | 0.903 | 1.061 | 0.939 | 0.848 |
| **60** | 1.00 | 1.159 | 1.007 | 1.088 | 0.901 | 0.847 | 1.202 | 1.058 | 1.070 | 1.217 | 1.083 |
| **61** | 1.00 | 2.167 | 1.200 | 1.077 | 1.770 | 1.770 | 1.595 | 0.989 | 1.166 | 1.219 | 1.104 |
| **62** | 1.00 | 2.569 | 1.586 | 2.000 | 1.460 | 1.346 | 1.706 | 1.367 | 2.016 | 2.040 | 2.005 |
| **63** | 1.00 | 2.629 | 1.338 | 2.023 | 2.355 | 2.355 | 2.645 | 1.569 | 2.593 | 1.396 | 2.194 |
| **64** | 1.20 | 0.410 | 0.703 | 0.389 | 0.812 | 0.740 | 0.408 | 0.633 | 0.402 | 0.403 | 0.393 |
| **65** | 1.20 | 0.619 | 0.677 | 0.610 | 0.719 | 0.747 | 0.559 | 0.755 | 0.571 | 0.769 | 0.598 |
| **66** | 1.20 | 1.133 | 1.210 | 0.935 | 1.105 | 1.105 | 1.043 | 0.855 | 1.181 | 1.380 | 1.008 |
| **67** | 1.20 | 1.485 | 1.356 | 1.458 | 1.557 | 1.000 | 1.279 | 1.093 | 1.393 | 1.580 | 1.438 |
| **68** | 1.20 | 2.026 | 1.529 | 1.661 | 2.388 | 2.388 | 1.618 | 1.609 | 1.944 | 1.761 | 1.746 |
| **69** | 1.20 | 2.318 | 1.600 | 2.053 | 2.366 | 2.366 | 2.514 | 2.565 | 2.653 | 2.263 | 2.233 |
| **70** | 1.20 | 2.585 | 2.321 | 1.905 | 2.046 | 1.333 | 2.538 | 2.216 | 2.526 | 2.581 | 2.091 |
| **71** | 0.40 | 0.221 | 0.270 | 0.238 | 0.117 | 0.117 | 0.316 | 0.363 | 0.125 | 0.190 | 0.204 |
| **72** | 0.40 | 0.177 | 0.238 | 0.258 | 0.215 | 0.215 | 0.304 | 0.267 | 0.344 | 0.262 | 0.284 |
| **73** | 0.40 | 0.408 | 0.344 | 0.477 | 0.263 | 0.427 | 0.416 | 0.516 | 0.389 | 0.457 | 0.450 |
| **74** | 0.40 | 0.493 | 0.370 | 0.552 | 0.433 | 0.433 | 0.469 | 0.613 | 0.341 | 0.498 | 0.489 |
| **75** | 0.40 | 0.810 | 0.300 | 0.631 | 0.527 | 0.527 | 0.603 | 0.554 | 0.612 | 0.438 | 0.625 |
| **76** | 0.40 | 1.061 | 0.496 | 0.749 | 0.673 | 0.562 | 0.926 | 0.417 | 0.872 | 0.657 | 0.786 |
| **77** | 0.40 | 1.244 | 0.783 | 1.038 | 1.036 | 0.569 | 1.623 | 0.403 | 1.217 | 0.617 | 1.092 |
| **78** | 0.60 | 0.245 | 0.283 | 0.258 | 0.210 | 0.210 | 0.371 | 0.568 | 0.419 | 0.380 | 0.306 |
| **79** | 0.60 | 0.334 | 0.391 | 0.289 | 0.341 | 0.462 | 0.315 | 0.485 | 0.289 | 0.459 | 0.289 |
| **80** | 0.60 | 0.400 | 0.542 | 0.379 | 0.513 | 0.513 | 0.462 | 0.550 | 0.516 | 0.582 | 0.420 |
| **81** | 0.60 | 0.637 | 0.589 | 0.619 | 0.580 | 0.580 | 0.802 | 0.535 | 0.613 | 0.653 | 0.617 |
| **82** | 0.60 | 1.020 | 0.786 | 0.664 | 0.958 | 0.659 | 1.264 | 0.826 | 0.974 | 0.608 | 0.757 |
| **83** | 0.60 | 2.057 | 0.800 | 1.107 | 1.190 | 0.828 | 1.284 | 0.626 | 1.121 | 1.193 | 1.111 |
| **84** | 0.60 | 1.751 | 0.781 | 0.679 | 1.937 | 1.937 | 1.825 | 1.526 | 2.657 | 1.615 | 1.272 |
| **85** | 0.80 | 0.258 | 0.388 | 0.263 | 0.302 | 0.657 | 0.338 | 0.280 | 0.284 | 0.316 | 0.270 |
| **86** | 0.80 | 0.485 | 0.792 | 0.402 | 0.435 | 0.435 | 0.475 | 0.590 | 0.430 | 0.571 | 0.410 |
| **87** | 0.80 | 0.508 | 1.107 | 0.631 | 0.515 | 0.515 | 0.603 | 0.757 | 0.657 | 0.828 | 0.639 |
| **88** | 0.80 | 0.692 | 0.865 | 0.483 | 0.918 | 0.918 | 0.462 | 0.700 | 0.651 | 0.808 | 0.534 |
| **89** | 0.80 | 1.123 | 0.996 | 0.631 | 1.112 | 1.112 | 1.404 | 1.065 | 1.317 | 1.040 | 0.837 |
| **90** | 0.80 | 1.970 | 1.284 | 1.606 | 1.351 | 1.351 | 1.546 | 0.890 | 1.650 | 1.385 | 1.619 |
| **91** | 0.80 | 2.314 | 1.114 | 1.552 | 1.471 | 1.471 | 1.566 | 1.595 | 1.422 | 1.927 | 1.513 |

| | | | | | | | | | | | |
|---|---|---|---|---|---|---|---|---|---|---|---|
| **92** | 1.00 | 0.255 | 0.728 | 0.383 | 0.521 | 1.154 | 0.405 | 0.467 | 0.368 | 0.316 | 0.379 |
| **93** | 1.00 | 0.388 | 0.749 | 0.362 | 0.478 | 1.388 | 0.545 | 0.800 | 0.505 | 0.490 | 0.405 |
| **94** | 1.00 | 1.018 | 0.928 | 0.722 | 0.899 | 1.058 | 0.920 | 1.269 | 0.761 | 0.872 | 0.734 |
| **95** | 1.00 | 1.145 | 1.166 | 1.202 | 1.173 | 1.038 | 1.185 | 1.171 | 1.052 | 1.164 | 1.157 |
| **96** | 1.00 | 1.976 | 1.323 | 1.455 | 1.526 | 1.436 | 1.986 | 1.205 | 1.767 | 1.721 | 1.548 |
| **97** | 1.00 | 2.613 | 1.892 | 2.609 | 1.822 | 1.224 | 1.860 | 1.953 | 2.355 | 2.163 | 2.533 |
| **98** | 1.00 | 2.581 | 1.876 | 2.593 | 1.471 | 1.905 | 2.609 | 2.347 | 2.625 | 2.177 | 2.602 |
| **99** | 1.20 | 0.422 | 0.897 | 0.470 | 0.382 | 0.963 | 0.475 | 0.711 | 0.359 | 0.424 | 0.437 |
| **100** | 1.20 | 0.477 | 0.812 | 0.633 | 0.585 | 0.916 | 0.608 | 1.070 | 0.596 | 0.464 | 0.622 |
| **101** | 1.20 | 0.950 | 1.436 | 1.137 | 0.890 | 0.890 | 1.145 | 0.713 | 0.831 | 0.816 | 1.045 |
| **102** | 1.20 | 1.367 | 1.433 | 1.121 | 0.971 | 0.971 | 0.985 | 0.974 | 0.907 | 1.289 | 1.057 |
| **103** | 1.20 | 2.139 | 1.335 | 1.580 | 1.529 | 1.529 | 1.430 | 1.788 | 2.010 | 1.289 | 1.709 |
| **104** | 1.20 | 2.437 | 1.333 | 2.318 | 1.879 | 1.879 | 2.329 | 1.287 | 2.128 | 2.483 | 2.261 |
| **105** | 1.20 | 2.422 | 1.700 | 2.238 | 2.111 | 2.111 | 2.629 | 2.605 | 2.665 | 2.633 | 2.366 |

**Appendix 6-I:** Fitting values from the *exponential* and *power regressions* in experiment described in *Section 6.4*.

| *Reference* | *a* | *b* | *Formula* | $r^2$ |
|---|---|---|---|---|
| 0.4 cm | 0.003392 | 2.437990 | $y(x) = 0.0034 \cdot e^{2.438}$ | 0.737 |
| 0.6 cm | 0.003455 | 2.593581 | $y(x) = 0.0035 \cdot e^{2.594}$ | 0.787 |
| 0.8 cm | 0.003597 | 2.702676 | $y(x) = 0.0036 \cdot e^{2.703}$ | 0.831 |
| 1.0 cm | 0.005418 | 2.622859 | $y(x) = 0.0054 \cdot e^{2.623}$ | 0.821 |
| 1.2 cm | 0.006657 | 2.590088 | $y(x) = 0.0067 \cdot e^{2.590}$ | 0.837 |
| | | | | |
| 0.4 cm | 0.015755 | 4.851408 | $y(x) = 0.0156 \cdot 10^{4.851}$ | 0.740 |
| 0.6 cm | 0.01771 | 5.160099 | $y(x) = 0.0177 \cdot 10^{5.160}$ | 0.790 |
| 0.8 cm | 0.019793 | 5.373799 | $y(x) = 0.0198 \cdot 10^{5.374}$ | 0.834 |
| 1.0 cm | 0.028046 | 5.230737 | $y(x) = 0.0280 \cdot 10^{6.230}$ | 0.828 |
| 1.2 cm | 0.012138 | 4.476331 | $y(x) = 0.0121 \cdot 10^{4.476}$ | 0.846 |

**Appendix 6-J:** *Slopes of the iso-roughness lines* from the experiment described in *Section 6.4*.

| *Observer* | *Reference 0.4* | *Reference 0.6* | *Reference 0.8* | *Reference 1.0* | *Reference 1.2* | *Mean* |
|---|---|---|---|---|---|---|
| 1 | 1.4295 | 1.6297 | 1.5869 | 1.6200 | 1.3897 | 1.5311 |
| 2 | 0.6973 | 0.8430 | 0.7567 | 0.6768 | 0.6183 | 0.7184 |
| 3 | 1.1290 | 0.9247 | 1.3316 | 1.2380 | 1.2105 | 1.1668 |
| 4 | 1.4539 | 1.5334 | 1.2273 | 1.1117 | 1.0007 | 1.2654 |
| 5 | 0.7653 | 1.0805 | 0.7407 | 0.7501 | 0.7272 | 0.8128 |
| 6 | 1.2233 | 1.3004 | 1.4223 | 1.3643 | 1.3349 | 1.3290 |
| 7 | 0.5903 | 0.6614 | 0.8859 | 0.7658 | 1.0132 | 0.7833 |
| 8 | 1.3309 | 1.3074 | 1.3734 | 1.3976 | 1.4233 | 1.3665 |
| 9 | 0.7944 | 0.8832 | 1.0645 | 1.1806 | 1.2558 | 1.0357 |
| 10 | 1.1743 | 1.1001 | 1.3483 | 1.2862 | 1.2751 | 1.2368 |
| All | 1.0588 | 1.1264 | 1.1738 | 1.1391 | 1.1249 | **1.1246** |

**Appendix 6-K:** Fittings from observer number one where the change in the slope of the fittings is more than 1.0.

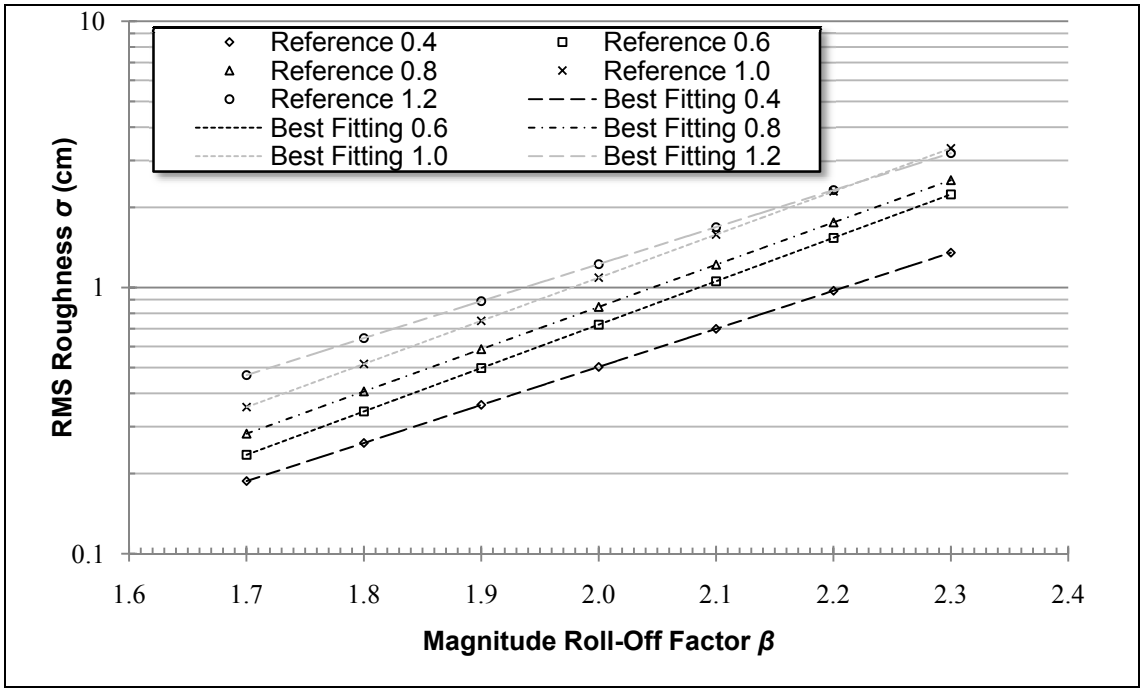


**Appendix 6-L:** Fittings from observer number two where the change in the slope of the fittings is less than 1.0.

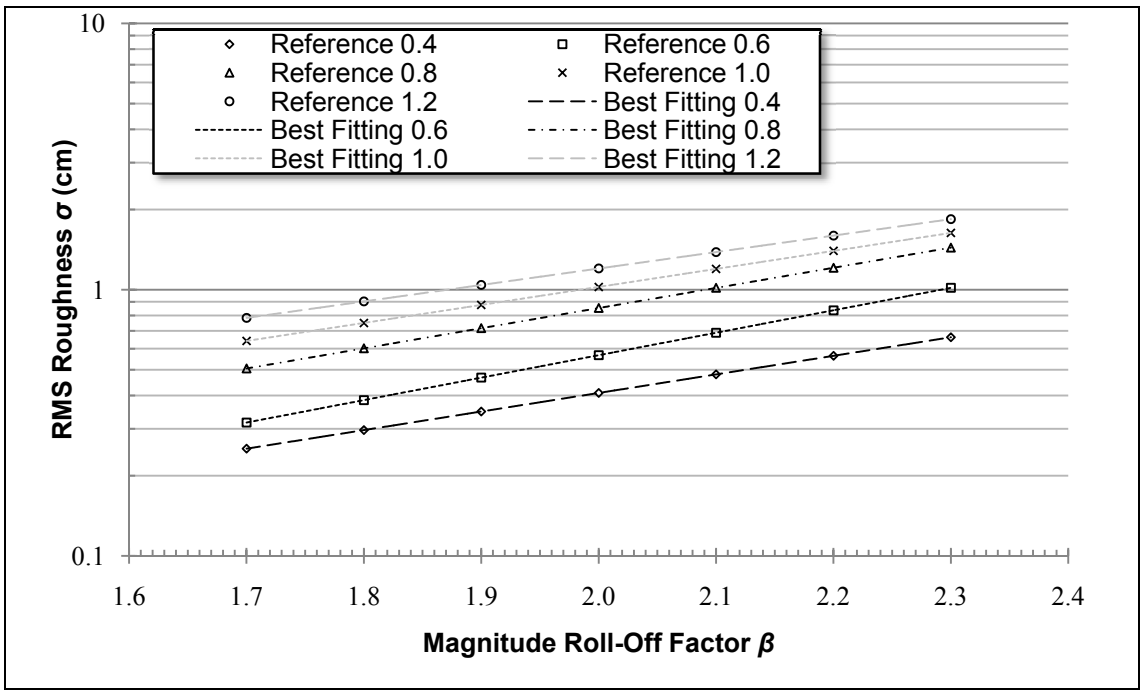

**Appendix 7-A:** Parseval's theorem states that the sum or integral of the square of a function equates to the sum or integral of the square of its Fourier transform as described in the formulas below, where x(t) a function and X(f) is the continuous Fourier transform of x(t).

$$\int_{-\infty}^{+\infty} |x(t)|^2 \, dt \; = \; \int_{-\infty}^{+\infty} |X(f)|^2 \, df$$

One can also think that by Parseval's theorem the variance of an image is equal to the integral of the power spectrum, which in the discrete case looks like the formula:

$$\frac{1}{n} \cdot \sum_{x=0}^{n-1} |g(x)|^2 = \sum_{f=0}^{n-1} |G(f)|^2$$

**Appendix 8-A:** Parameters and order of the experiment described in *Section 8.2.1* where the parameters followed by *ref* are from the *reference surfaces* whilst the one followed by *adj* are from the *adjustable surface*.

| *No* | *Base θ* | $F_{b1ref}$ | $F_{b2ref}$ | $F_{b1adj}$ | $F_{b2adj}$ | *Order* |
|---|---|---|---|---|---|---|
| 01 | 1 | 1 | 0.25 | 0.25 | | 12 |
| 02 | 1 | 1 | 0.25 | 0.50 | | 31 |
| 03 | 1 | 1 | 0.25 | 1.00 | | 23 |
| 04 | 1 | 1 | 0.25 | 2.00 | | 26 |
| 05 | 1 | 1 | 0.50 | 0.25 | | 27 |
| 06 | 1 | 1 | 0.50 | 0.50 | | 21 |
| 07 | 1 | 1 | 0.50 | 1.00 | | 11 |
| 08 | 1 | 1 | 0.50 | 2.00 | | 13 |
| 09 | 1 | 1 | 1.00 | 0.25 | | 08 |
| 10 | 1 | 1 | 1.00 | 0.50 | | 28 |
| 11 | 1 | 1 | 1.00 | 1.00 | | 40 |
| 12 | 1 | 1 | 1.00 | 2.00 | | 30 |
| 13 | 2 | 1 | 0.25 | 0.25 | | 37 |
| 14 | 2 | 1 | 0.25 | 0.50 | | 16 |
| 15 | 2 | 1 | 0.25 | 1.00 | | 14 |
| 16 | 2 | 1 | 0.25 | 2.00 | | 24 |
| 17 | 2 | 1 | 0.50 | 0.25 | | 29 |
| 18 | 2 | 1 | 0.50 | 0.50 | | 25 |
| 19 | 2 | 1 | 0.50 | 1.00 | | 15 |
| 20 | 2 | 1 | 0.50 | 2.00 | | 05 |
| 21 | 2 | 1 | 1.00 | 0.25 | | 36 |
| 22 | 2 | 1 | 1.00 | 0.50 | | 17 |
| 23 | 2 | 1 | 1.00 | 1.00 | | 18 |
| 24 | 2 | 1 | 1.00 | 2.00 | | 06 |
| 25 | 3 | 1 | 0.25 | 0.25 | | 09 |
| 26 | 3 | 1 | 0.25 | 0.50 | | 39 |
| 27 | 3 | 1 | 0.25 | 1.00 | | 33 |
| 28 | 3 | 1 | 0.25 | 2.00 | | 38 |
| 29 | 3 | 1 | 0.50 | 0.25 | | 34 |
| 30 | 3 | 1 | 0.50 | 0.50 | | 07 |
| 31 | 3 | 1 | 0.50 | 1.00 | | 20 |
| 32 | 3 | 1 | 0.50 | 2.00 | | 32 |
| 33 | 3 | 1 | 1.00 | 0.25 | | 19 |
| 34 | 3 | 1 | 1.00 | 0.50 | | 22 |
| 35 | 3 | 1 | 1.00 | 1.00 | | 10 |
| 36 | 3 | 1 | 1.00 | 2.00 | | 35 |
| 37 | 1 | 1 | 0.25 | 2.00 | | 01 |
| 38 | 1 | 1 | 0.50 | 0.25 | | 02 |
| 39 | 3 | 1 | 1.00 | 0.50 | | 03 |
| 40 | 3 | 1 | 0.50 | 0.25 | | 04 |

**Appendix 8-B:** Results from each of the ten observers from the experiment detailed in *Section 8.2.1*.

| *No* | $Obs_1$ | $Obs_2$ | $Obs_3$ | $Obs_4$ | $Obs_5$ | $Obs_6$ | $Obs_7$ | $Obs_8$ | $Obs_9$ | $Obs_{10}$ |
|---|---|---|---|---|---|---|---|---|---|---|
| 01 | 0.312 | 0.334 | 0.295 | 0.310 | 0.293 | 0.261 | 0.470 | 0.266 | 0.254 | 0.286 |
| 02 | 0.356 | 0.227 | 0.237 | 0.264 | 0.383 | 0.445 | 0.370 | 0.266 | 0.266 | 0.254 |
| 03 | 0.274 | 0.339 | 0.392 | 0.227 | 0.337 | 0.223 | 0.286 | 0.308 | 0.366 | 0.318 |
| 04 | 0.199 | 0.312 | 0.237 | 0.271 | 0.267 | 0.528 | 0.249 | 0.298 | 0.187 | 0.302 |
| 05 | 0.644 | 0.588 | 0.569 | 0.455 | 0.629 | 0.528 | 0.852 | 0.480 | 0.627 | 0.513 |
| 06 | 0.511 | 0.692 | 0.497 | 0.506 | 0.560 | 0.564 | 0.853 | 0.523 | 0.731 | 0.574 |
| 07 | 0.663 | 0.649 | 0.535 | 0.559 | 0.492 | 0.434 | 0.537 | 0.642 | 0.767 | 0.644 |
| 08 | 0.514 | 0.366 | 0.428 | 0.499 | 0.434 | 0.487 | 0.414 | 0.457 | 0.342 | 0.429 |
| 09 | 1.136 | 1.109 | 0.814 | 1.072 | 1.066 | 0.922 | 1.233 | 1.116 | 0.802 | 1.114 |
| 10 | 1.090 | 1.153 | 0.944 | 1.089 | 0.985 | 1.068 | 0.896 | 1.010 | 1.170 | 1.053 |
| 11 | 1.376 | 1.072 | 1.124 | 0.828 | 0.957 | 1.070 | 1.150 | 1.102 | 0.990 | 1.093 |
| 12 | 1.332 | 0.956 | 1.438 | 1.228 | 1.090 | 1.302 | 1.145 | 1.010 | 0.981 | 0.994 |
| 13 | 0.303 | 0.411 | 0.218 | 0.300 | 0.216 | 0.526 | 0.273 | 0.305 | 0.300 | 0.337 |
| 14 | 0.293 | 0.380 | 0.433 | 0.256 | 0.273 | 0.339 | 0.213 | 0.276 | 0.320 | 0.307 |
| 15 | 0.138 | 0.334 | 0.308 | 0.266 | 0.337 | 0.445 | 0.262 | 0.242 | 0.266 | 0.270 |
| 16 | 0.261 | 0.273 | 0.164 | 0.240 | 0.300 | 0.215 | 0.157 | 0.378 | 0.259 | 0.347 |
| 17 | 0.509 | 0.632 | 0.601 | 0.550 | 0.620 | 0.477 | 0.675 | 0.620 | 0.385 | 0.624 |
| 18 | 0.596 | 0.716 | 0.486 | 0.441 | 0.613 | 0.608 | 0.663 | 0.479 | 0.474 | 0.550 |
| 19 | 0.571 | 0.692 | 0.497 | 0.540 | 0.687 | 0.564 | 0.853 | 0.523 | 0.618 | 0.574 |
| 20 | 0.543 | 0.596 | 0.392 | 0.492 | 0.603 | 0.445 | 0.400 | 0.523 | 0.366 | 0.545 |
| 21 | 0.952 | 1.181 | 1.119 | 1.109 | 1.189 | 1.077 | 1.244 | 1.109 | 0.860 | 1.130 |
| 22 | 1.090 | 1.143 | 0.944 | 0.974 | 1.094 | 1.068 | 0.918 | 1.145 | 1.145 | 1.144 |
| 23 | 1.250 | 0.840 | 0.997 | 1.104 | 1.257 | 1.162 | 1.053 | 0.922 | 0.862 | 0.897 |
| 24 | 1.066 | 1.153 | 0.944 | 1.055 | 0.874 | 1.245 | 0.896 | 1.203 | 0.760 | 1.188 |
| 25 | 0.288 | 0.235 | 0.295 | 0.203 | 0.298 | 0.434 | 0.387 | 0.317 | 0.256 | 0.292 |
| 26 | 0.291 | 0.310 | 0.266 | 0.324 | 0.344 | 0.497 | 0.472 | 0.276 | 0.329 | 0.286 |
| 27 | 0.342 | 0.376 | 0.203 | 0.237 | 0.329 | 0.446 | 0.293 | 0.295 | 0.288 | 0.319 |
| 28 | 0.302 | 0.259 | 0.228 | 0.302 | 0.235 | 0.250 | 0.094 | 0.261 | 0.225 | 0.260 |
| 29 | 0.727 | 0.540 | 0.468 | 0.647 | 0.683 | 0.608 | 0.663 | 0.651 | 0.474 | 0.618 |
| 30 | 0.554 | 0.532 | 0.593 | 0.494 | 0.704 | 0.698 | 0.705 | 0.516 | 0.761 | 0.521 |
| 31 | 0.617 | 0.545 | 0.463 | 0.451 | 0.523 | 0.532 | 0.688 | 0.620 | 0.405 | 0.598 |
| 32 | 0.468 | 0.692 | 0.526 | 0.564 | 0.330 | 0.494 | 0.537 | 0.523 | 0.514 | 0.574 |
| 33 | 1.174 | 1.147 | 1.041 | 0.998 | 1.223 | 0.983 | 0.918 | 1.089 | 1.145 | 1.106 |
| 34 | 1.063 | 1.065 | 1.121 | 1.073 | 0.951 | 0.748 | 1.135 | 1.264 | 0.761 | 1.204 |
| 35 | 0.908 | 1.155 | 1.020 | 0.925 | 1.279 | 1.104 | 1.332 | 1.337 | 1.349 | 1.283 |
| 36 | 1.196 | 0.991 | 0.998 | 0.971 | 0.973 | 0.985 | 1.111 | 1.196 | 1.032 | 1.135 |

**Appendix 8-C:** In the table, the fittings and their parameters are demonstrated from the experiment in *Section 8-2.1*.

| *Reference* | $x^2$ | $x$ | *Intersect* | *Formula* | $R^2$ |
|---|---|---|---|---|---|
| **0.25** | 0.0414 | -0.0276 | 0.2872 | $y = \ 0.0414x^2 - 0.0276x + 0.2872$ | 0.9988 |
| **0.50** | -0.0569 | -0.0014 | 0.6170 | $y = -0.0569x^2 - 0.0014x + 0.6170$ | 0.8851 |
| **1.00** | -0.0052 | -0.0063 | 1.0977 | $y = -0.0052x^2 - 0.0063x + 1.0977$ | 0.4656 |

**Appendix 8-D:** In the table, the fittings and their parameters are demonstrated from the experiment in *Section 8.2.1*.

| *Reference* | $x^2$ | $x$ | *Intersect* | *Formula* | $R^2$ |
|---|---|---|---|---|---|
| **0.0625** | -0.1799 | 0.1795 | 0.1088 | $y = -0.1799x^2 + 0.1795x + 0.1088$ | 0.9880 |
| **0.1250** | -0.2357 | 0.1641 | 0.1829 | $y = -0.2357x^2 - 0.1641x + 0.1829$ | 0.9996 |
| **0.2500** | -0.1195 | 0.1907 | 0.2507 | $y = -0.1195x^2 - 0.1907x + 0.2507$ | 0.7308 |

**Appendix 8-E:** Parameters and order of the experiment described in *Section 8.2.2* where the parameters followed by *ref* are from the *reference surfaces* whilst the ones followed by *adj* are from the *adjustable surface*.

| *No* | *Base θ* | $F_{b2ref}$ | $F_{b3ref}$ | $F_{b2adj}$ | $F_{b3adj}$ | *Order* |
|---|---|---|---|---|---|---|
| 01 | 1 | 0.2500 | 0.0625 | 0.0625 | | 24 |
| 02 | 1 | 0.2500 | 0.0625 | 0.1250 | | 39 |
| 03 | 1 | 0.2500 | 0.0625 | 0.2500 | | 18 |
| 04 | 1 | 0.2500 | 0.0625 | 0.5000 | | 17 |
| 05 | 1 | 0.2500 | 0.1250 | 0.0625 | | 14 |
| 06 | 1 | 0.2500 | 0.1250 | 0.1250 | | 10 |
| 07 | 1 | 0.2500 | 0.1250 | 0.2500 | | 11 |
| 08 | 1 | 0.2500 | 0.1250 | 0.5000 | | 15 |
| 09 | 1 | 0.2500 | 0.2500 | 0.0625 | | 29 |
| 10 | 1 | 0.2500 | 0.2500 | 0.1250 | | 20 |
| 11 | 1 | 0.2500 | 0.2500 | 0.2500 | | 30 |
| 12 | 1 | 0.2500 | 0.2500 | 0.5000 | | 36 |
| 13 | 2 | 0.2500 | 0.0625 | 0.0625 | | 31 |
| 14 | 2 | 0.2500 | 0.0625 | 0.1250 | | 27 |
| 15 | 2 | 0.2500 | 0.0625 | 0.2500 | | 09 |
| 16 | 2 | 0.2500 | 0.0625 | 0.5000 | | 32 |
| 17 | 2 | 0.2500 | 0.1250 | 0.0625 | | 26 |
| 18 | 2 | 0.2500 | 0.1250 | 0.1250 | | 25 |
| 19 | 2 | 0.2500 | 0.1250 | 0.2500 | | 34 |
| 20 | 2 | 0.2500 | 0.1250 | 0.5000 | | 19 |
| 21 | 2 | 0.2500 | 0.2500 | 0.0625 | | 37 |
| 22 | 2 | 0.2500 | 0.2500 | 0.1250 | | 06 |
| 23 | 2 | 0.2500 | 0.2500 | 0.2500 | | 23 |
| 24 | 2 | 0.2500 | 0.2500 | 0.5000 | | 13 |
| 25 | 3 | 0.2500 | 0.0625 | 0.0625 | | 16 |
| 26 | 3 | 0.2500 | 0.0625 | 0.1250 | | 22 |
| 27 | 3 | 0.2500 | 0.0625 | 0.2500 | | 40 |
| 28 | 3 | 0.2500 | 0.0625 | 0.5000 | | 28 |
| 29 | 3 | 0.2500 | 0.1250 | 0.0625 | | 12 |
| 30 | 3 | 0.2500 | 0.1250 | 0.1250 | | 38 |
| 31 | 3 | 0.2500 | 0.1250 | 0.2500 | | 08 |
| 32 | 3 | 0.2500 | 0.1250 | 0.5000 | | 05 |
| 33 | 3 | 0.2500 | 0.2500 | 0.0625 | | 33 |
| 34 | 3 | 0.2500 | 0.2500 | 0.1250 | | 35 |
| 35 | 3 | 0.2500 | 0.2500 | 0.2500 | | 07 |
| 36 | 3 | 0.2500 | 0.2500 | 0.5000 | | 21 |
| 37 | 1 | 0.2500 | 0.2500 | 0.0625 | | 01 |
| 38 | 1 | 0.2500 | 0.2500 | 0.1250 | | 02 |
| 39 | 3 | 0.2500 | 0.1250 | 0.2500 | | 03 |
| 40 | 3 | 0.2500 | 0.1250 | 0.5000 | | 04 |

**Appendix 8-F:** Results from each of the ten observers from the experiment detailed in *Section 8.2.2*.

| *No* | $Obs_1$ | $Obs_2$ | $Obs_3$ | $Obs_4$ | $Obs_5$ | $Obs_6$ | $Obs_7$ | $Obs_8$ | $Obs_9$ | $Obs_{10}$ |
|---|---|---|---|---|---|---|---|---|---|---|
| 01 | 0.1050 | 0.1037 | 0.0746 | 0.0521 | 0.1211 | 0.0846 | 0.0654 | 0.0782 | 0.1096 | 0.0859 |
| 02 | 0.0767 | 0.0976 | 0.0958 | 0.1037 | 0.0945 | 0.1035 | 0.1112 | 0.0838 | 0.0966 | 0.0880 |
| 03 | 0.0685 | 0.0713 | 0.0662 | 0.0925 | 0.0672 | 0.0685 | 0.1952 | 0.0654 | 0.0391 | 0.0672 |
| 04 | 0.1043 | 0.0940 | 0.0682 | 0.0455 | 0.0399 | 0.0381 | 0.0493 | 0.0506 | 0.0664 | 0.0636 |
| 05 | 0.1559 | 0.1487 | 0.1209 | 0.1584 | 0.1352 | 0.1308 | 0.1952 | 0.1595 | 0.1528 | 0.1562 |
| 06 | 0.1620 | 0.1819 | 0.1290 | 0.1469 | 0.1526 | 0.0667 | 0.1592 | 0.1306 | 0.1423 | 0.1460 |
| 07 | 0.1344 | 0.1293 | 0.0800 | 0.1060 | 0.1503 | 0.1423 | 0.1771 | 0.1372 | 0.1541 | 0.1348 |
| 08 | 0.1403 | 0.1257 | 0.1045 | 0.0851 | 0.1050 | 0.1720 | 0.1209 | 0.0961 | 0.0616 | 0.1050 |
| 09 | 0.2918 | 0.2980 | 0.2131 | 0.2596 | 0.2752 | 0.1929 | 0.2208 | 0.2502 | 0.2272 | 0.2645 |
| 10 | 0.2581 | 0.2675 | 0.2003 | 0.2144 | 0.2415 | 0.2177 | 0.2098 | 0.2632 | 0.2203 | 0.2645 |
| 11 | 0.2586 | 0.2443 | 0.1942 | 0.2251 | 0.2198 | 0.1881 | 0.1725 | 0.2612 | 0.1796 | 0.2561 |
| 12 | 0.2474 | 0.2438 | 0.1561 | 0.2251 | 0.1960 | 0.2548 | 0.1377 | 0.1692 | 0.2399 | 0.1916 |
| 13 | 0.1037 | 0.0823 | 0.0639 | 0.0879 | 0.0723 | 0.0703 | 0.1398 | 0.1382 | 0.1293 | 0.1215 |
| 14 | 0.0616 | 0.0981 | 0.0634 | 0.0649 | 0.0767 | 0.0848 | 0.0876 | 0.1055 | 0.0979 | 0.1033 |
| 15 | 0.1009 | 0.0882 | 0.0853 | 0.0342 | 0.1267 | 0.0792 | 0.1278 | 0.0721 | 0.0940 | 0.0769 |
| 16 | 0.0657 | 0.1020 | 0.0463 | 0.0123 | 0.1101 | 0.0667 | 0.0256 | 0.0363 | 0.0399 | 0.0560 |
| 17 | 0.1888 | 0.1592 | 0.1344 | 0.1372 | 0.1520 | 0.1403 | 0.1032 | 0.1876 | 0.1991 | 0.1791 |
| 18 | 0.1710 | 0.1500 | 0.1497 | 0.1656 | 0.1679 | 0.1477 | 0.1666 | 0.1794 | 0.1549 | 0.1706 |
| 19 | 0.1595 | 0.1434 | 0.1681 | 0.0956 | 0.0953 | 0.1122 | 0.1702 | 0.1354 | 0.1142 | 0.1378 |
| 20 | 0.1334 | 0.1063 | 0.1687 | 0.0856 | 0.1096 | 0.1344 | 0.1725 | 0.1014 | 0.1094 | 0.1029 |
| 21 | 0.2440 | 0.2831 | 0.2060 | 0.2101 | 0.2484 | 0.2576 | 0.2205 | 0.2808 | 0.2287 | 0.2815 |
| 22 | 0.3000 | 0.2783 | 0.1929 | 0.2374 | 0.2282 | 0.1743 | 0.1579 | 0.2778 | 0.2295 | 0.2779 |
| 23 | 0.2964 | 0.2190 | 0.2210 | 0.2576 | 0.1947 | 0.2144 | 0.1771 | 0.2847 | 0.2849 | 0.2650 |
| 24 | 0.2369 | 0.2900 | 0.2402 | 0.2512 | 0.2428 | 0.2310 | 0.1998 | 0.2425 | 0.2517 | 0.2568 |
| 25 | 0.0905 | 0.1252 | 0.0746 | 0.0744 | 0.0953 | 0.1122 | 0.1329 | 0.1334 | 0.1096 | 0.1309 |
| 26 | 0.0859 | 0.0659 | 0.0588 | 0.0945 | 0.0851 | 0.0335 | 0.0429 | 0.0764 | 0.1219 | 0.0733 |
| 27 | 0.0774 | 0.0841 | 0.0756 | 0.0652 | 0.0767 | 0.0953 | 0.0427 | 0.0708 | 0.0984 | 0.0748 |
| 28 | 0.0866 | 0.1280 | 0.0634 | 0.0470 | 0.0452 | 0.0848 | 0.0876 | 0.0360 | 0.1025 | 0.0636 |
| 29 | 0.1482 | 0.1664 | 0.1183 | 0.1145 | 0.1436 | 0.1408 | 0.1850 | 0.1674 | 0.1382 | 0.1671 |
| 30 | 0.1411 | 0.1876 | 0.1485 | 0.1758 | 0.1329 | 0.1641 | 0.1224 | 0.1715 | 0.1556 | 0.1763 |
| 31 | 0.1339 | 0.1275 | 0.0649 | 0.0813 | 0.1073 | 0.1899 | 0.1835 | 0.1352 | 0.1296 | 0.1329 |
| 32 | 0.0797 | 0.1058 | 0.1265 | 0.0603 | 0.1520 | 0.0991 | 0.1326 | 0.0823 | 0.1497 | 0.0893 |
| 33 | 0.2972 | 0.2900 | 0.2402 | 0.2369 | 0.2180 | 0.1773 | 0.1906 | 0.2425 | 0.2655 | 0.2568 |
| 34 | 0.2951 | 0.2438 | 0.2302 | 0.2433 | 0.1927 | 0.2548 | 0.1377 | 0.2277 | 0.2425 | 0.2325 |
| 35 | 0.2443 | 0.2438 | 0.2302 | 0.2392 | 0.2499 | 0.2548 | 0.1377 | 0.2101 | 0.2425 | 0.2202 |
| 36 | 0.1597 | 0.2849 | 0.2236 | 0.2098 | 0.1924 | 0.2867 | 0.1771 | 0.2514 | 0.1804 | 0.2615 |

**Appendix 8-G:** Model fit using a *gaussian function* to the *iso-roughness lines* [$\beta$, $\sigma$] when weighing the model more towards the data from the *iso-roughness lines* [$\beta$, $\sigma$].

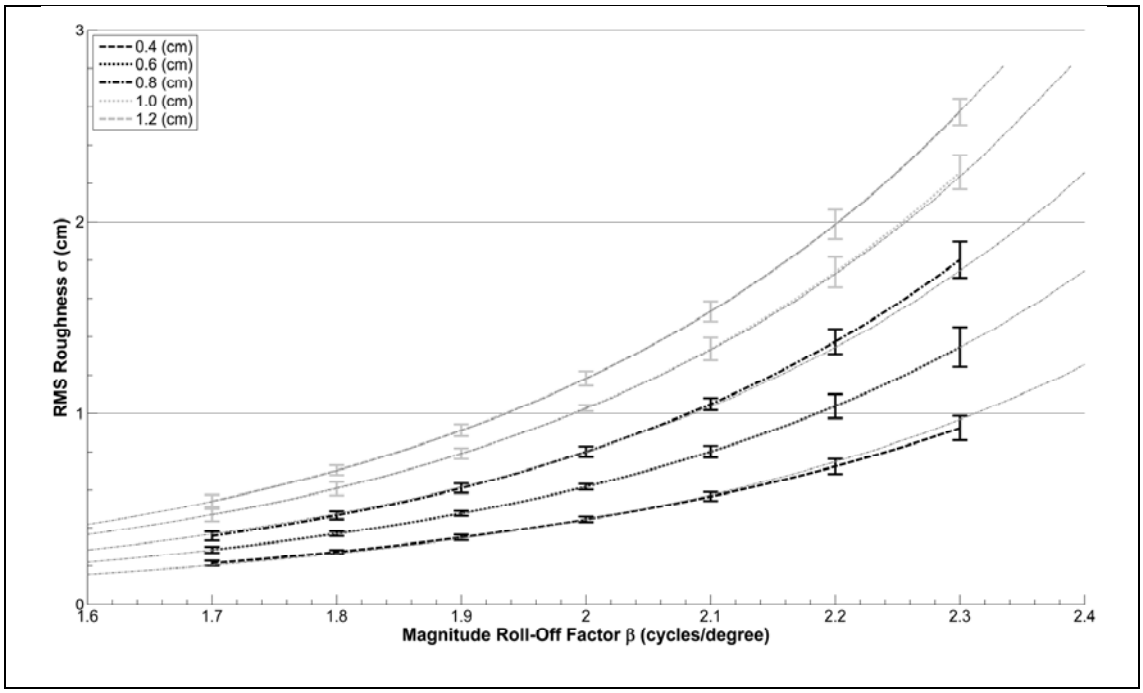


**Appendix 8-H:** Model fit using a *gaussian function* to the *iso-roughness lines* [$\beta$, $\sigma$] when weighing the model more towards the data from the *iso-roughness lines* [$F_{b1}$, $F_{b2}$].

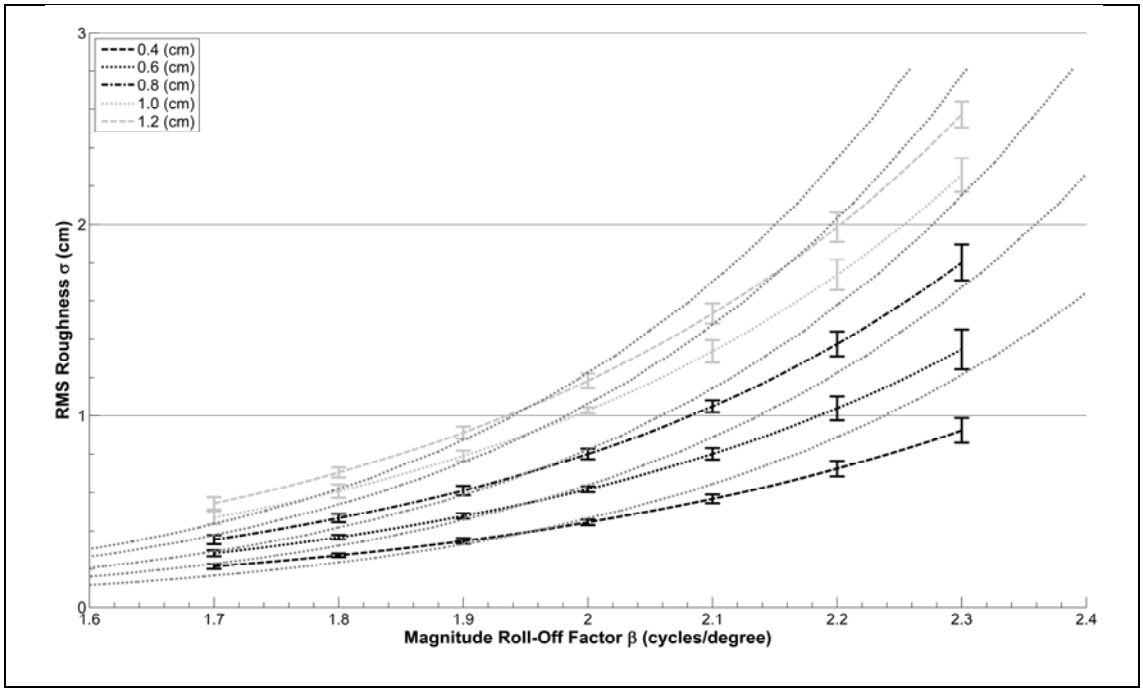

**Appendix 8-I:** Model fit using a *gaussian function* to the *iso-roughness lines* [$\beta$, $\sigma$] when weighing the model more towards the data from the *iso-roughness lines* [$F_{b2}$, $F_{b3}$].

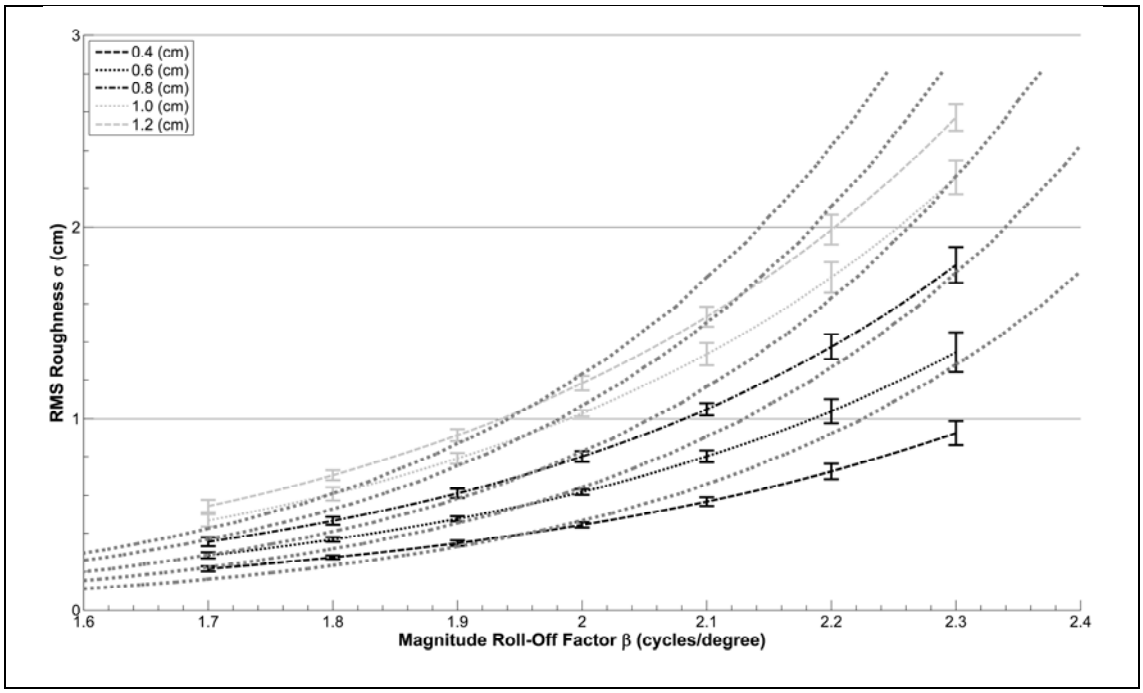


**Appendix 8-J:** Model fit using a *gaussian function* to the *iso-roughness lines* [$F_{b1}$, $F_{b2}$] when weighing the model more towards the data from the *iso-roughness lines* [$\beta$, $\sigma$].

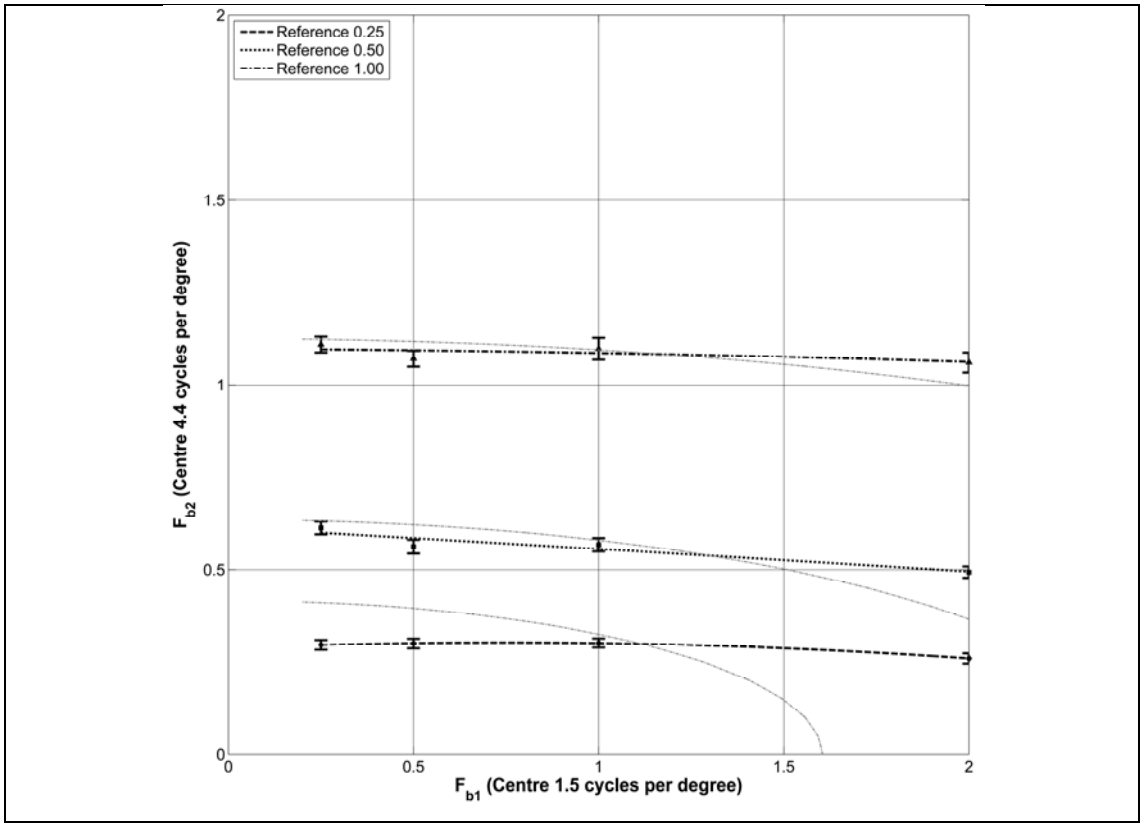

**Appendix 8-K:** Model fit using a *gaussian function* to the *iso-roughness lines* [$F_{b1}$, $F_{b2}$] when weighing the model more towards the data from the *iso-roughness lines* [$F_{b1}$, $F_{b2}$].

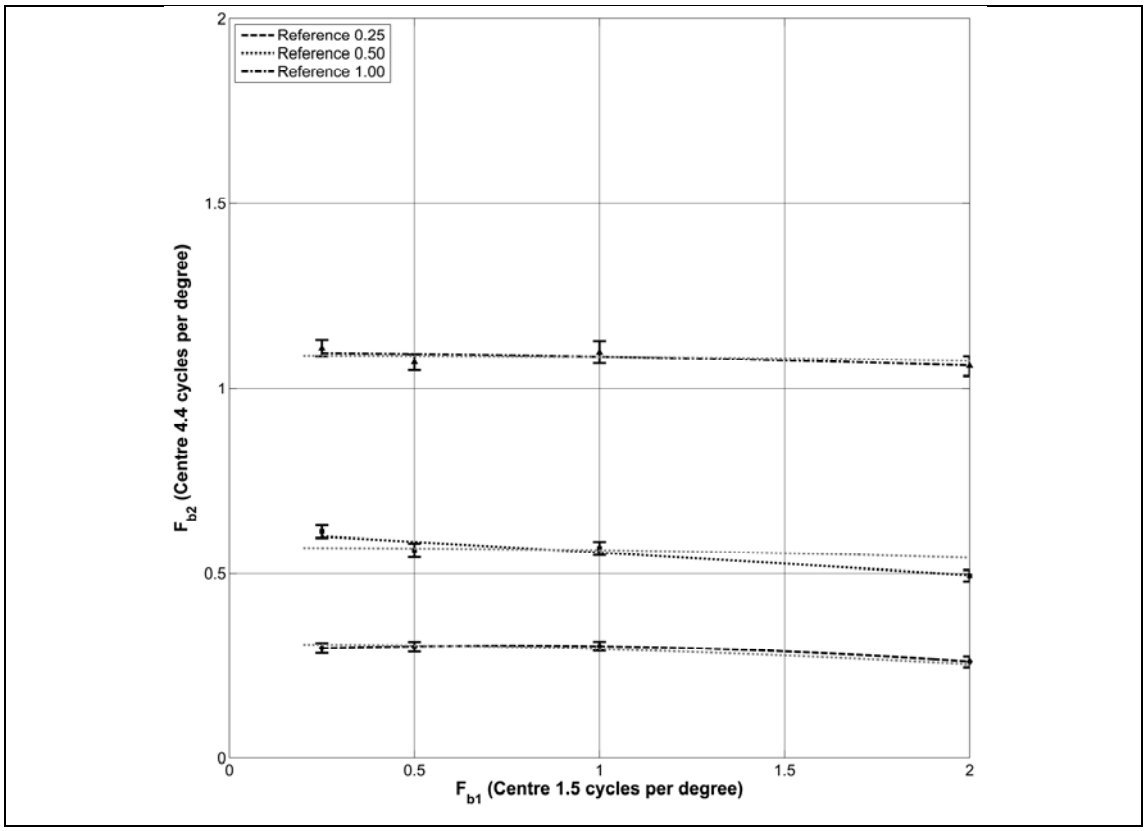


**Appendix 8-L:** Model fit using a *gaussian function* to the *iso-roughness lines* [$F_{b1}$, $F_{b2}$] when weighing the model more towards the data from the *iso-roughness lines* [$F_{b2}$, $F_{b3}$].

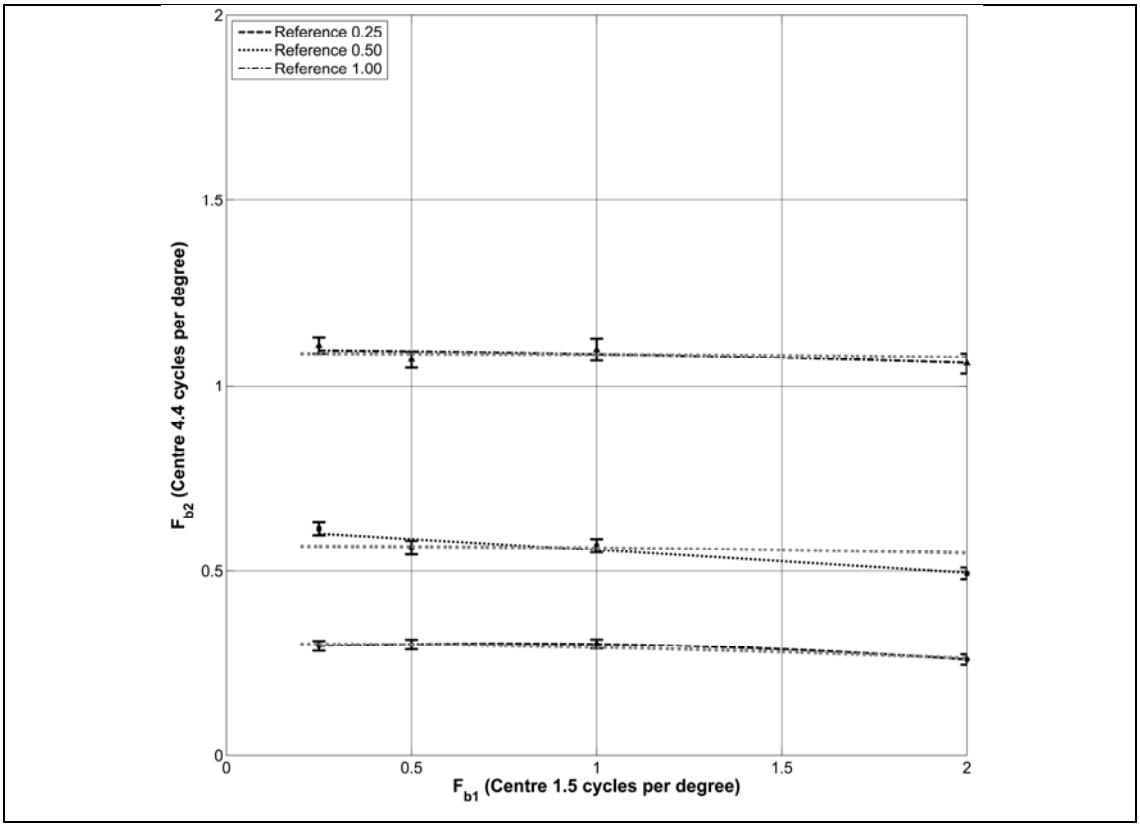

**Appendix 8-M:** Model fit using a *gaussian function* to *iso-roughness lines* [$F_{b2}$, $F_{b3}$] when weighing the model more towards the data from the *iso-roughness lines* [$\beta$, $\sigma$]

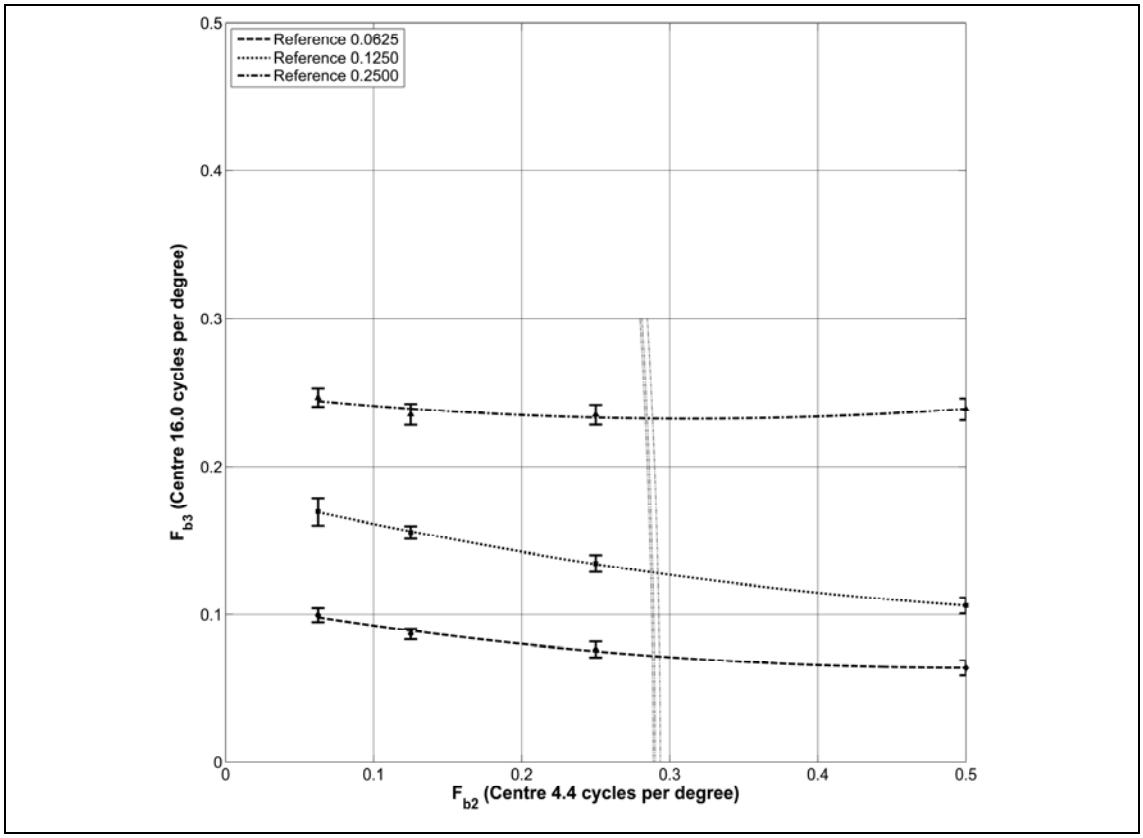


**Appendix 8-N:** Model fit using a *gaussian function* to the *iso-roughness lines* [$F_{b2}$, $F_{b3}$] when weighing the model more towards the data from the *iso-roughness lines* [$F_{b1}$, $F_{b2}$].

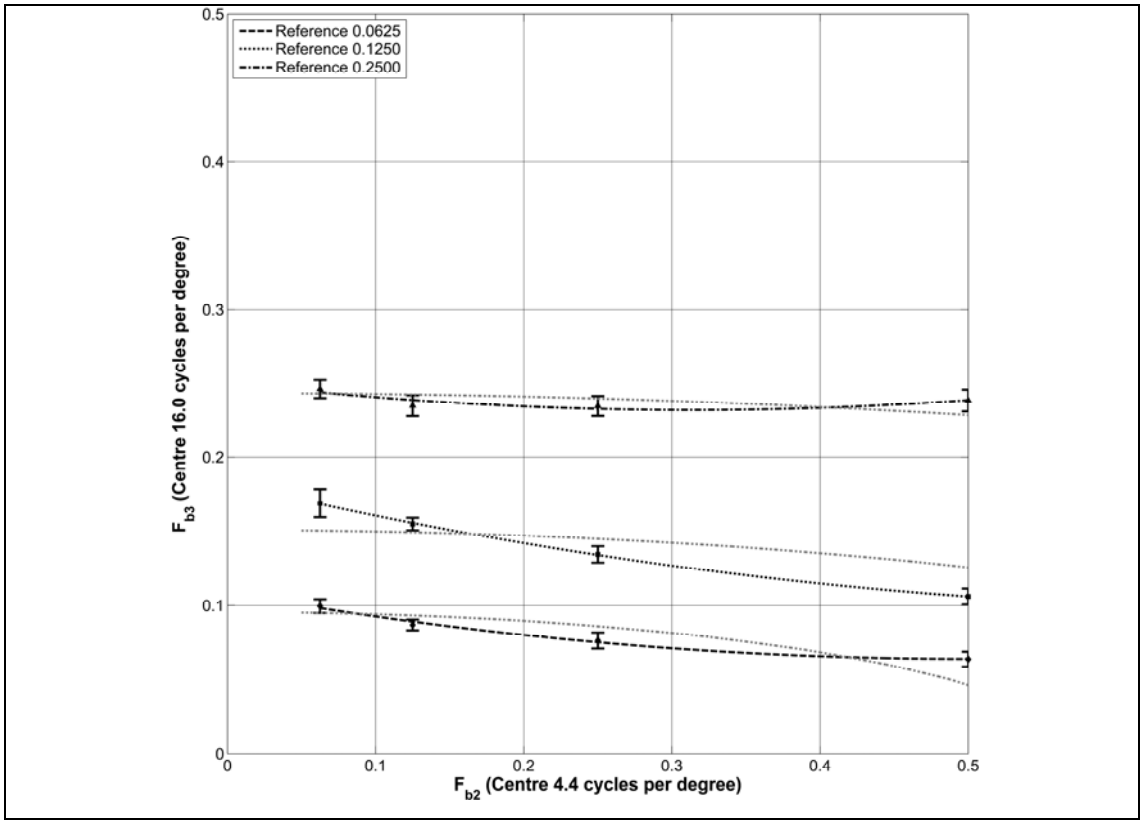

**Appendix 8-O:** Model fit using a *gaussian function* to the *iso-roughness lines* [$F_{b2}$, $F_{b3}$] when weighing the model more towards the data from the *iso-roughness lines* [$F_{b2}$, $F_{b3}$].

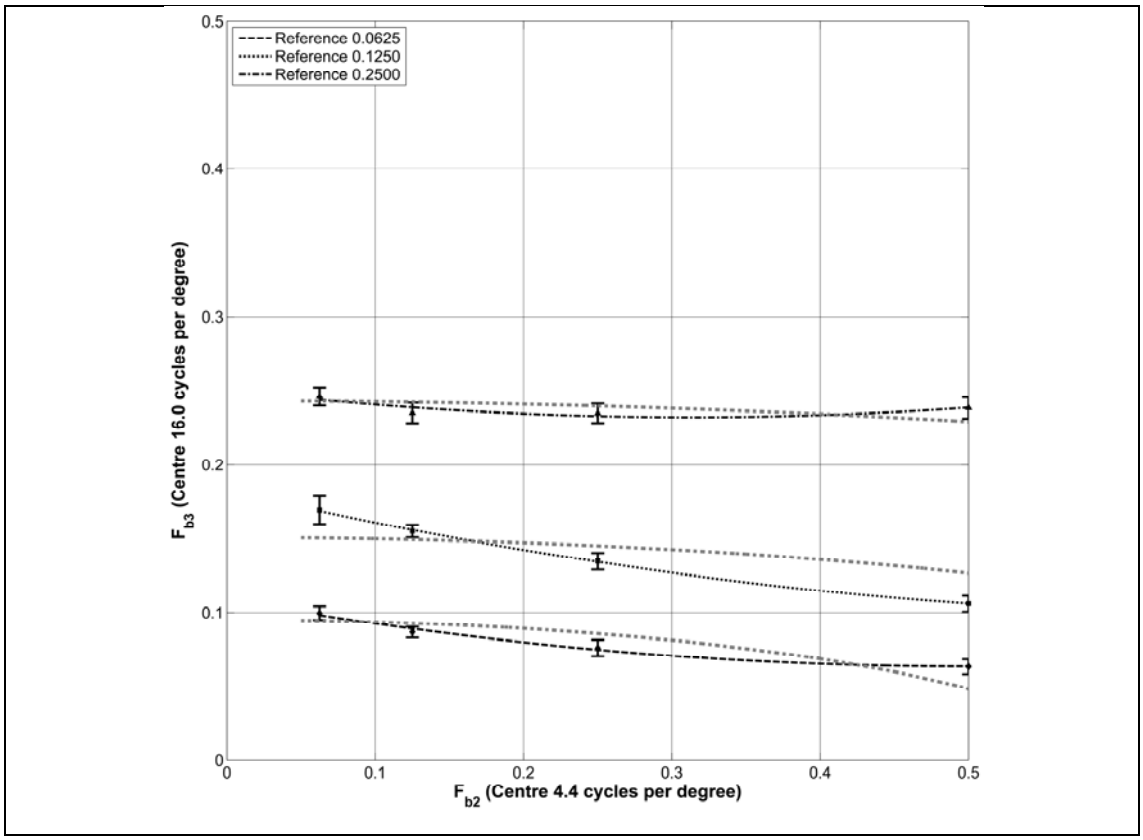


**Appendix 8-P:** Model fit using a *power function* to the *iso-roughness lines* [$\beta$, $\sigma$] when weighing the model more towards the data from the *iso-roughness lines* [$\beta$, $\sigma$].

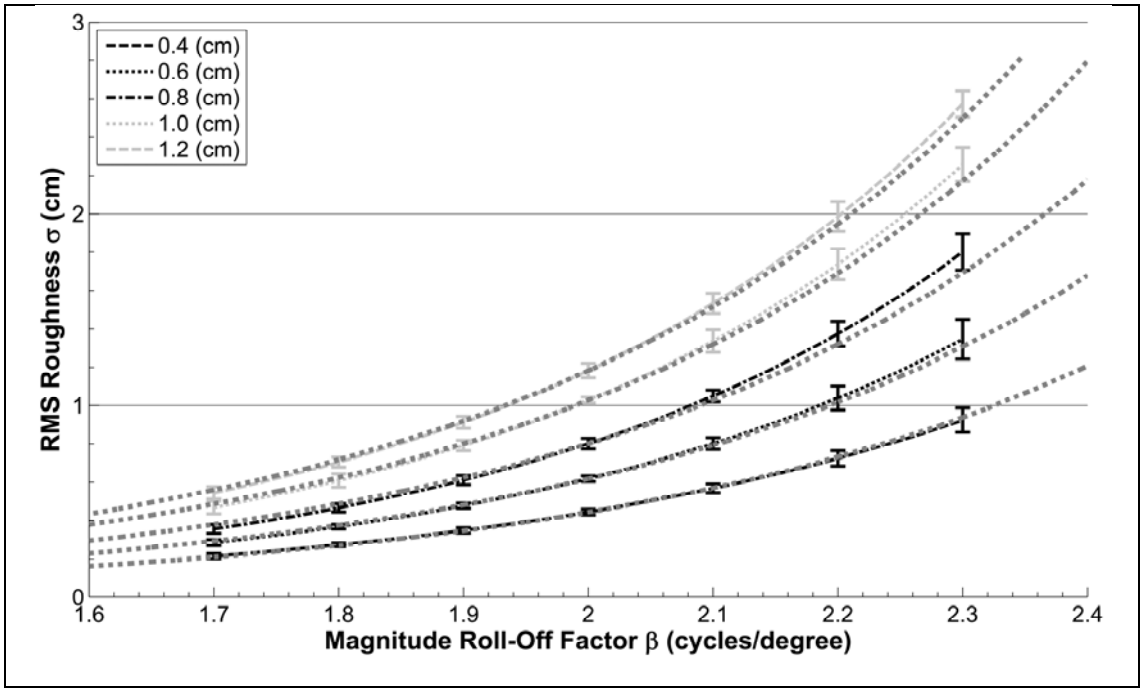

**Appendix 8-Q:** Model fit using *power function* to the *iso-roughness lines* [$\beta$, $\sigma$] when weighing the model more towards the data from the *iso-roughness lines* [$F_{b1}$, $F_{b2}$].

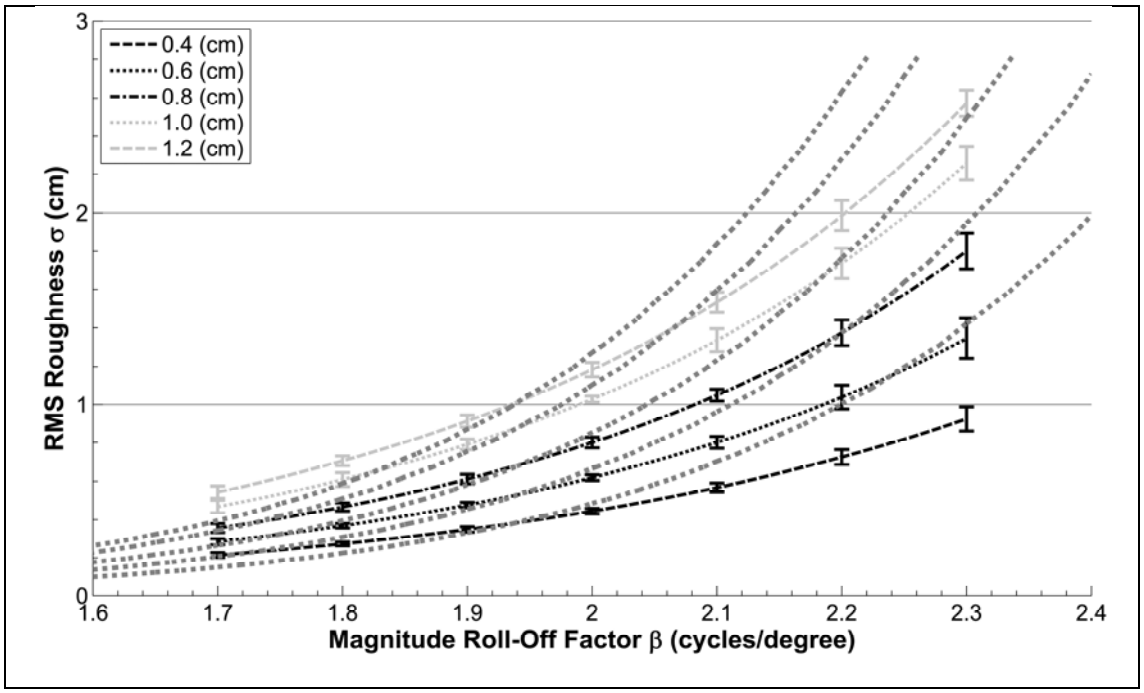


**Appendix 8-R:** Model fit using a *power function* to the *iso-roughness lines* [$\beta$, $\sigma$] when weighing the model more towards the data from the *iso-roughness lines* [$F_{b2}$, $F_{b3}$].

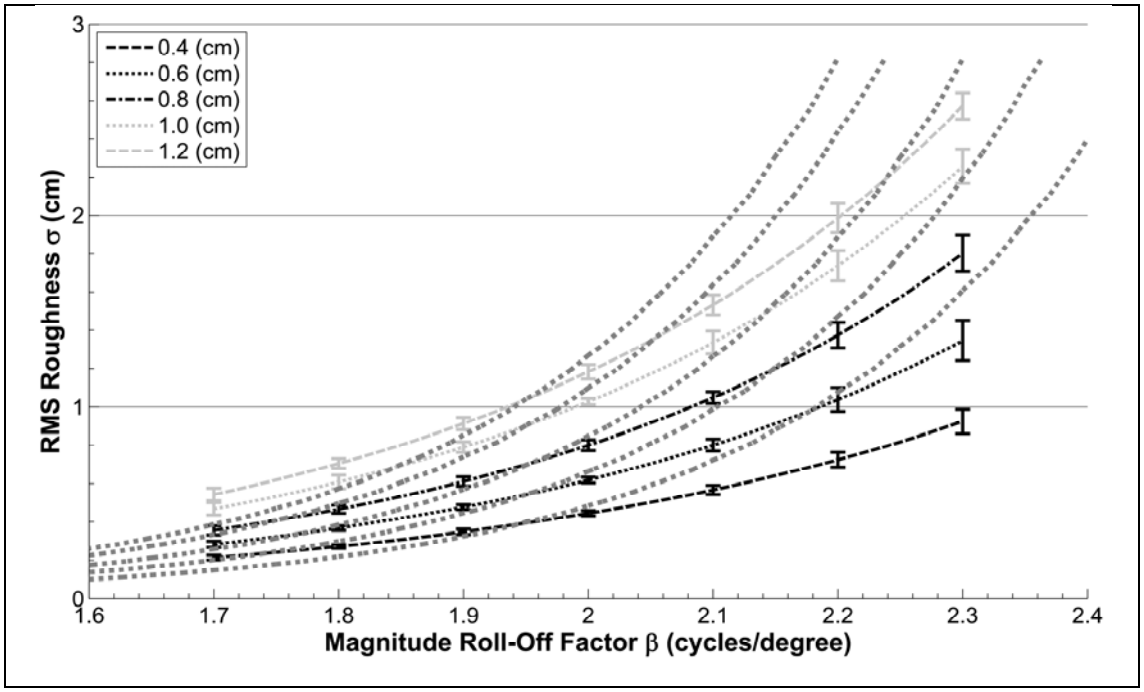

**Appendix 8-S:** Model fit using a *power function* to the *iso-roughness lines* [$F_{b1}$, $F_{b2}$] when weighing the model more towards the data from the *iso-roughness lines* [$\beta$, $\sigma$].

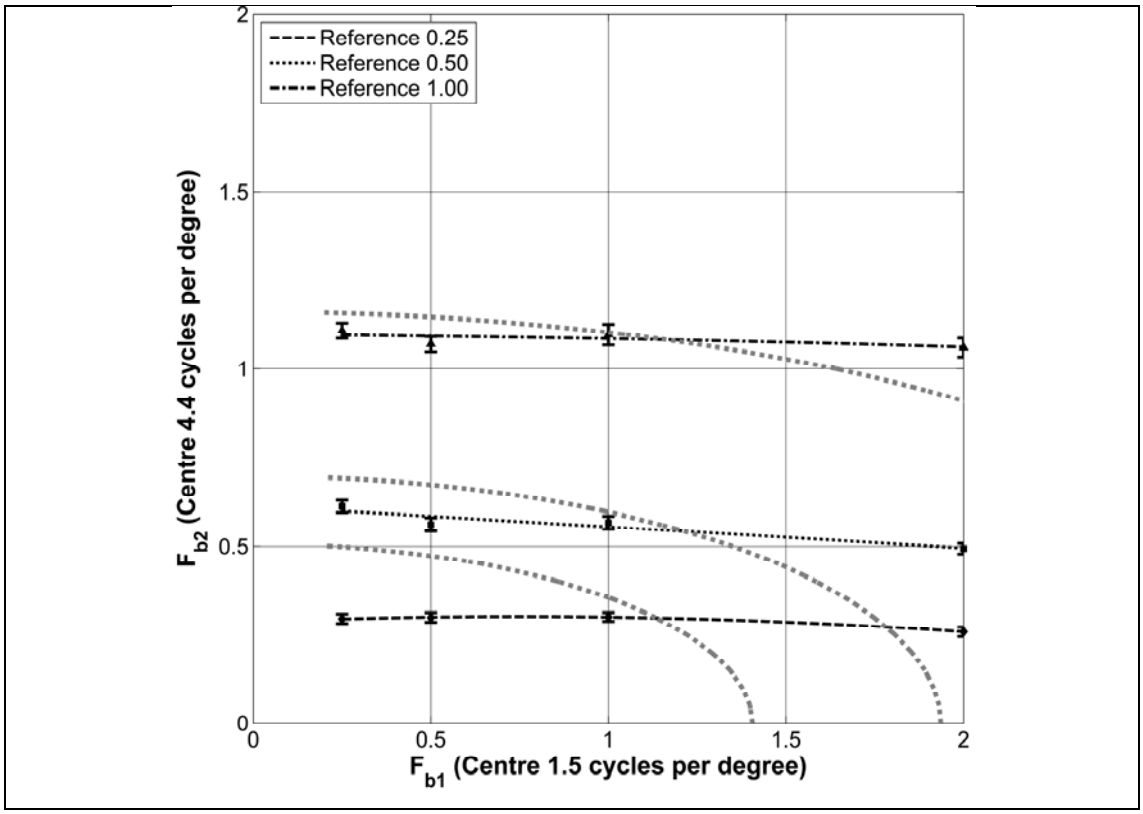


**Appendix 8-T:** Model fit using a *power function* to the *iso-roughness lines* [$F_{b1}$, $F_{b2}$] when weighing the model more towards the data from the *iso-roughness lines* [$F_{b1}$, $F_{b2}$].

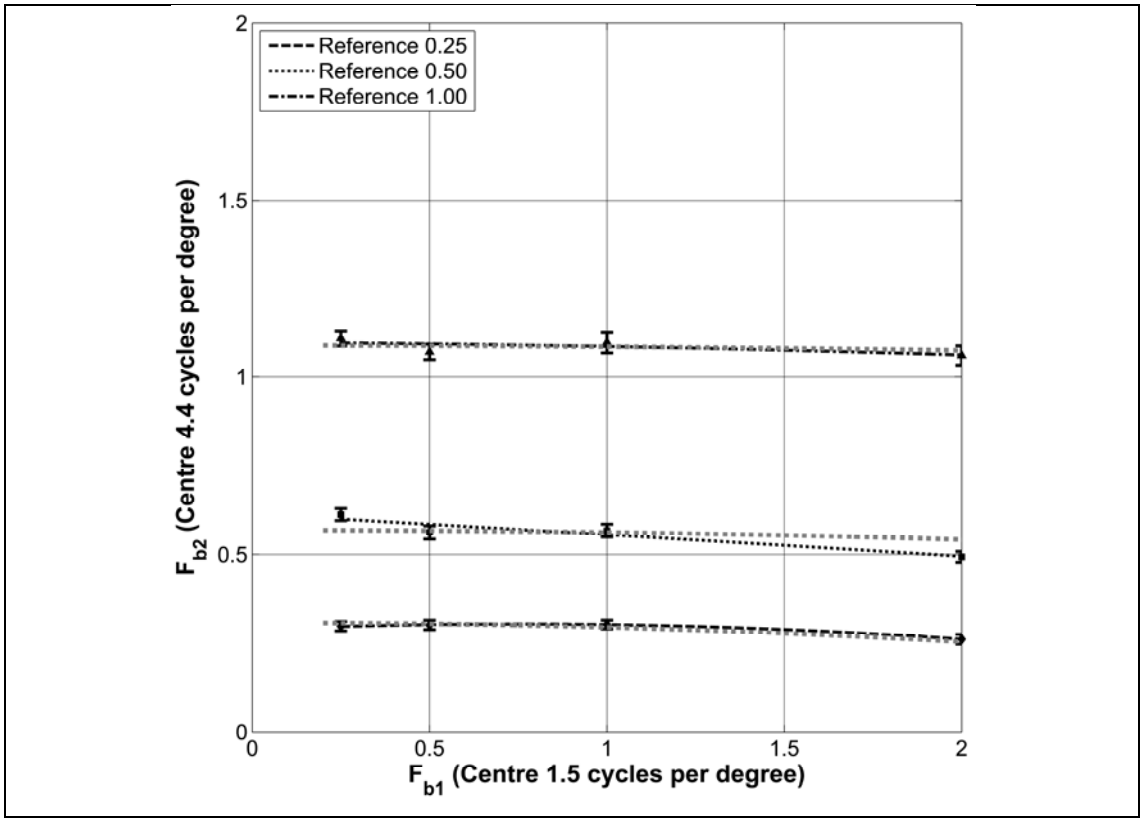

**Appendix 8-U:** Model fit using a power function to the *iso-roughness lines* [$F_{b1}$, $F_{b2}$] when weighing the model more towards the data from the *iso-roughness lines* [$F_{b2}$, $F_{b3}$].

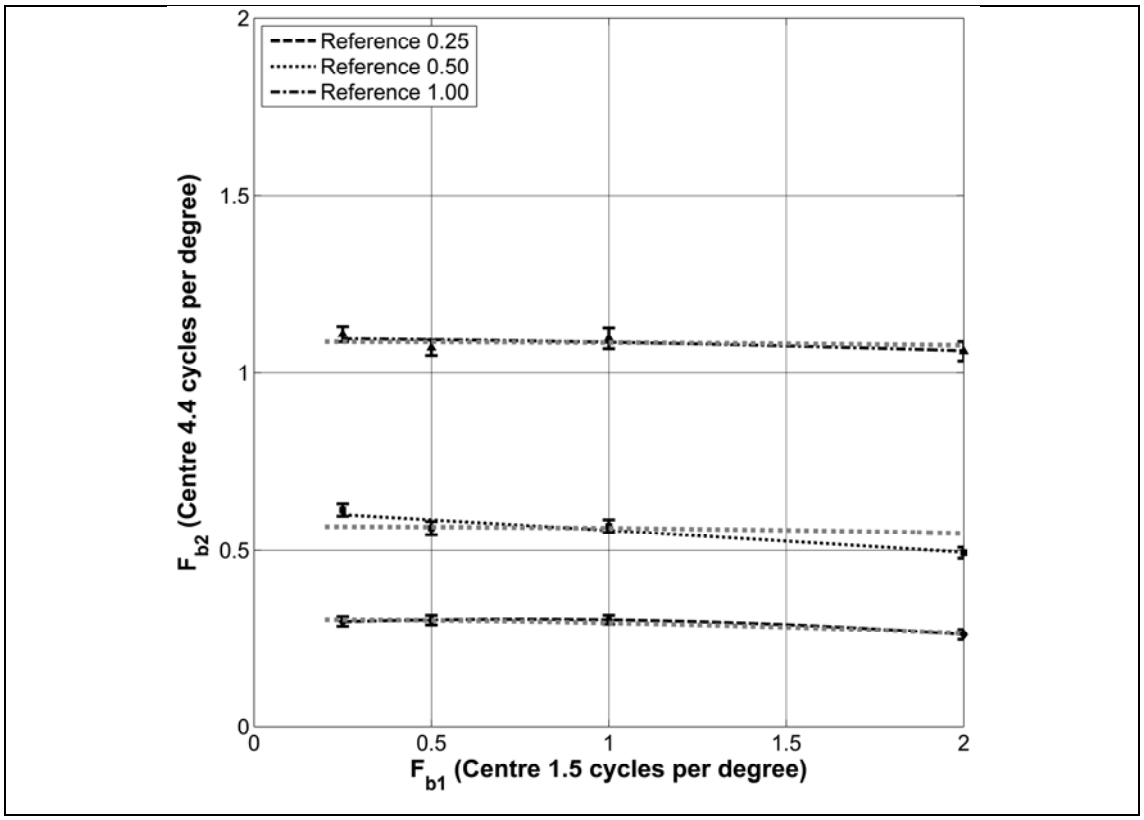


**Appendix 8-V:** Model fit using a *power function* to the *iso-roughness lines* [$F_{b2}$, $F_{b3}$] when weighing the model more towards the data from the *iso-roughness lines* [$\beta$, $\sigma$].

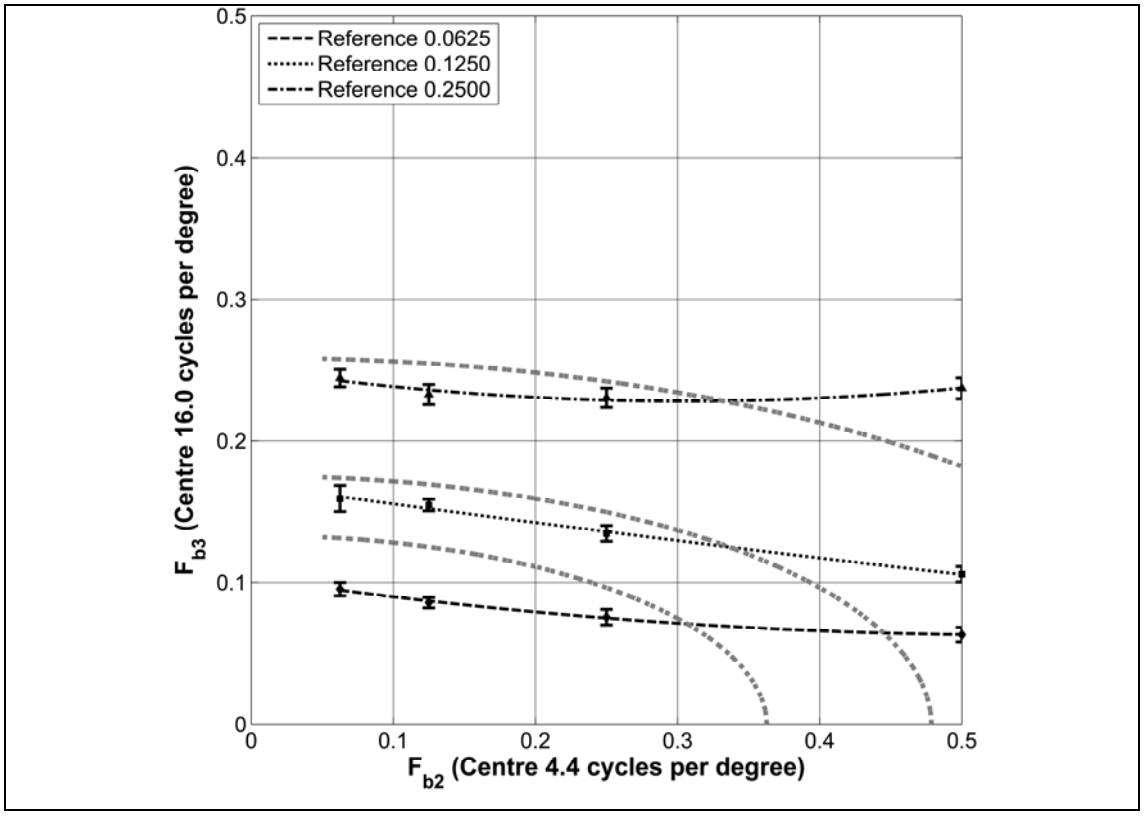

**Appendix 8-W:** Model fit using a *power function* to the *iso-roughness lines* [$F_{b2}$, $F_{b3}$] when weighing the model more towards the data from the *iso-roughness lines* [$F_{b1}$, $F_{b2}$].

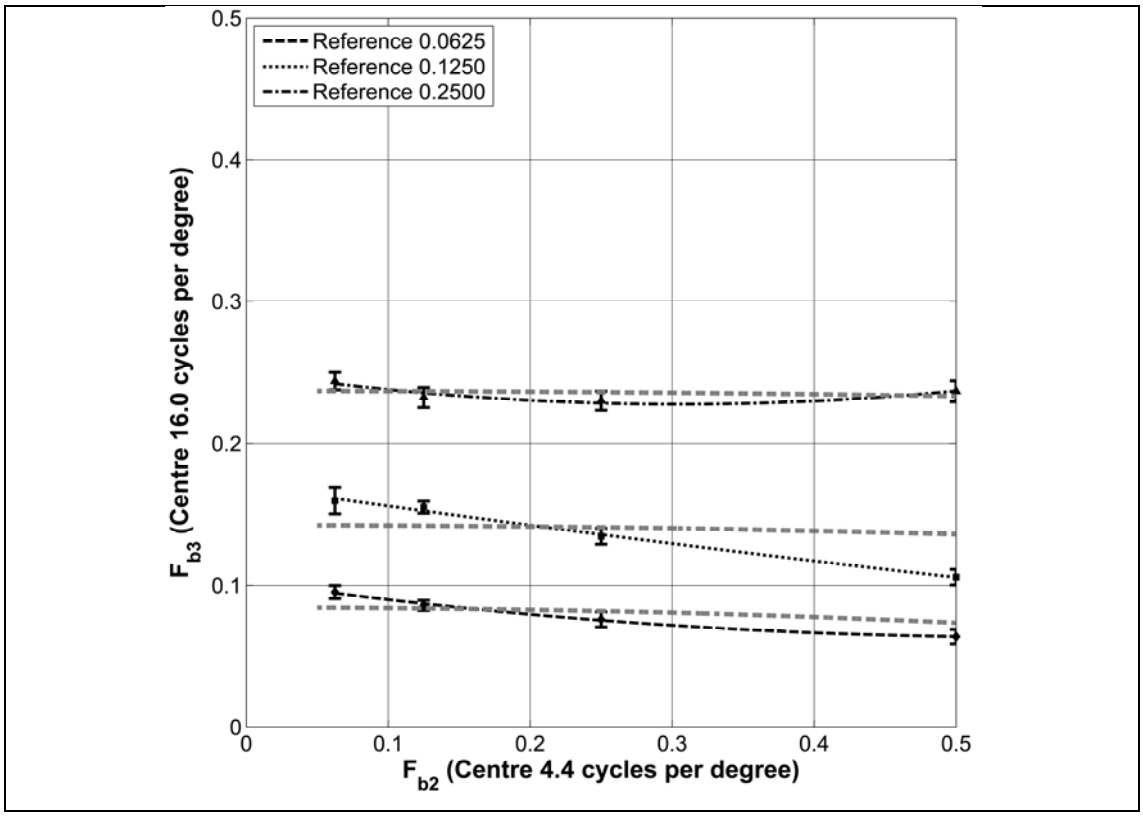


**Appendix 8-X:** Model fit using a *power function* to the *iso-roughness lines* [$F_{b2}$, $F_{b3}$] when weighing the model more towards the data from the *iso-roughness lines* [$F_{b2}$, $F_{b3}$].

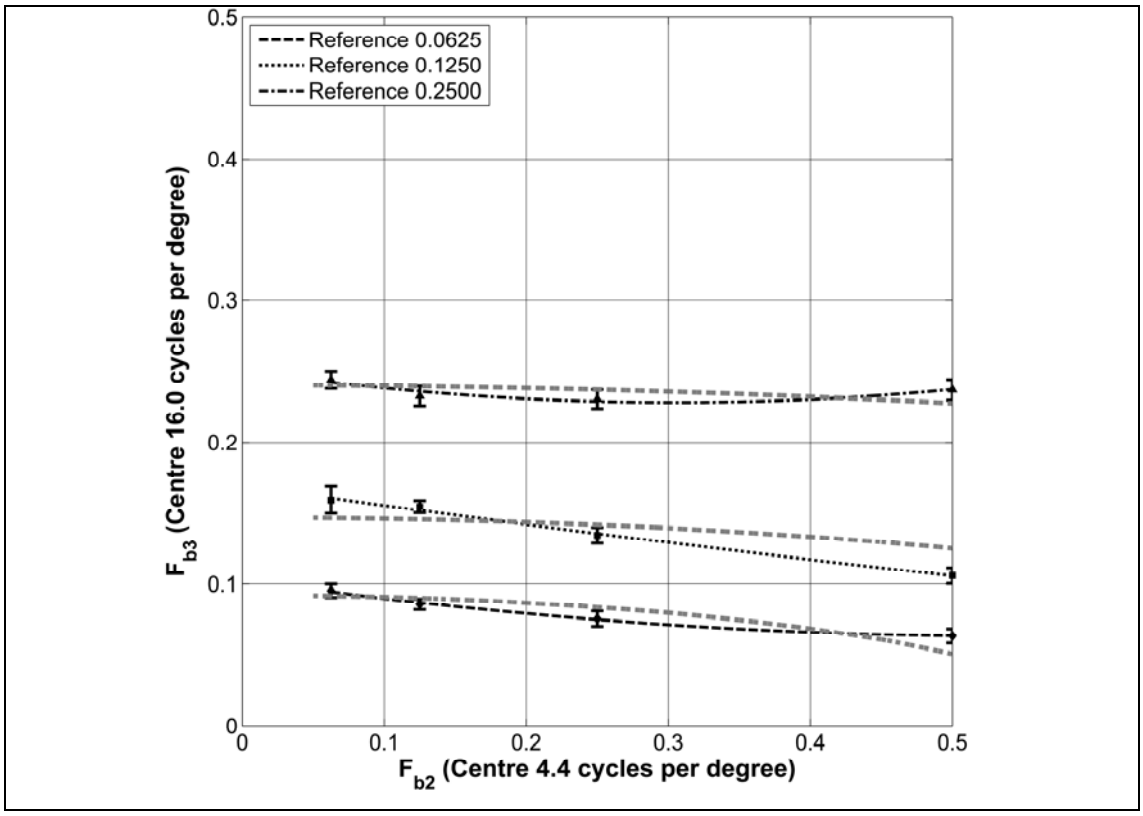

**Appendix 9-1:** The parameter values from the surfaces for the mid-point experiment. The two *reference surfaces* are labelled with subscripts $_{ref1}$ and $_{ref2}$ whilst the *adjustable surface* is labelled $_{adj}$.

| *No* | *Trial* | $\beta_{ref1}$ | $\sigma_{ref1}$ | $\theta_{ref1}$ | $\beta_{adj}$ | $\sigma_{adj}$ | $\theta_{adj}$ | $\beta_{ref2}$ | $\sigma_{ref2}$ | $\theta_{ref2}$ | *Order* |
|---|---|---|---|---|---|---|---|---|---|---|---|
| 01 | 1 | 2.0 | 1.2 | 11 | 1.8 | | 11 | 2.0 | 0.4 | 11 | 07 |
| 02 | 1 | 2.0 | 1.2 | 11 | 1.9 | | 11 | 2.0 | 0.4 | 11 | 43 |
| 03 | 1 | 2.0 | 1.2 | 11 | 2.0 | | 11 | 2.0 | 0.4 | 11 | 46 |
| 04 | 1 | 2.0 | 1.2 | 11 | 2.1 | | 11 | 2.0 | 0.4 | 11 | 11 |
| 05 | 1 | 2.0 | 1.2 | 11 | 2.2 | | 11 | 2.0 | 0.4 | 11 | 32 |
| 06 | 2 | 2.0 | 1.2 | 12 | 1.8 | | 12 | 2.0 | 0.4 | 12 | 10 |
| 07 | 2 | 2.0 | 1.2 | 12 | 1.9 | | 12 | 2.0 | 0.4 | 12 | 15 |
| 08 | 2 | 2.0 | 1.2 | 12 | 2.0 | | 12 | 2.0 | 0.4 | 12 | 12 |
| 09 | 2 | 2.0 | 1.2 | 12 | 2.1 | | 12 | 2.0 | 0.4 | 12 | 22 |
| 10 | 2 | 2.0 | 1.2 | 12 | 2.2 | | 12 | 2.0 | 0.4 | 12 | 28 |
| 11 | 3 | 2.0 | 1.2 | 13 | 1.8 | | 13 | 2.0 | 0.4 | 13 | 21 |
| 12 | 3 | 2.0 | 1.2 | 13 | 1.9 | | 13 | 2.0 | 0.4 | 13 | 50 |
| 13 | 3 | 2.0 | 1.2 | 13 | 2.0 | | 13 | 2.0 | 0.4 | 13 | 20 |
| 14 | 3 | 2.0 | 1.2 | 13 | 2.1 | | 13 | 2.0 | 0.4 | 13 | 29 |
| 15 | 3 | 2.0 | 1.2 | 13 | 2.2 | | 13 | 2.0 | 0.4 | 13 | 42 |
| 16 | 1 | 2.0 | 0.8 | 14 | 1.8 | | 14 | 2.0 | 0.4 | 14 | 26 |
| 17 | 1 | 2.0 | 0.8 | 14 | 1.9 | | 14 | 2.0 | 0.4 | 14 | 39 |
| 18 | 1 | 2.0 | 0.8 | 14 | 2.0 | | 14 | 2.0 | 0.4 | 14 | 47 |
| 19 | 1 | 2.0 | 0.8 | 14 | 2.1 | | 14 | 2.0 | 0.4 | 14 | 49 |
| 20 | 1 | 2.0 | 0.8 | 14 | 2.2 | | 14 | 2.0 | 0.4 | 14 | 09 |
| 21 | 2 | 2.0 | 0.8 | 15 | 1.8 | | 15 | 2.0 | 0.4 | 15 | 34 |
| 22 | 2 | 2.0 | 0.8 | 15 | 1.9 | | 15 | 2.0 | 0.4 | 15 | 30 |
| 23 | 2 | 2.0 | 0.8 | 15 | 2.0 | | 15 | 2.0 | 0.4 | 15 | 16 |
| 24 | 2 | 2.0 | 0.8 | 15 | 2.1 | | 15 | 2.0 | 0.4 | 15 | 25 |
| 25 | 2 | 2.0 | 0.8 | 15 | 2.2 | | 15 | 2.0 | 0.4 | 15 | 23 |
| 26 | 3 | 2.0 | 0.8 | 16 | 1.8 | | 16 | 2.0 | 0.4 | 16 | 24 |
| 27 | 3 | 2.0 | 0.8 | 16 | 1.9 | | 16 | 2.0 | 0.4 | 16 | 40 |
| 28 | 3 | 2.0 | 0.8 | 16 | 2.0 | | 16 | 2.0 | 0.4 | 16 | 44 |
| 29 | 3 | 2.0 | 0.8 | 16 | 2.1 | | 16 | 2.0 | 0.4 | 16 | 27 |
| 30 | 3 | 2.0 | 0.8 | 16 | 2.2 | | 16 | 2.0 | 0.4 | 16 | 19 |
| 31 | 1 | 2.0 | 1.2 | 17 | 1.8 | | 17 | 2.0 | 0.8 | 17 | 08 |
| 32 | 1 | 2.0 | 1.2 | 17 | 1.9 | | 17 | 2.0 | 0.8 | 17 | 35 |
| 33 | 1 | 2.0 | 1.2 | 17 | 2.0 | | 17 | 2.0 | 0.8 | 17 | 37 |
| 34 | 1 | 2.0 | 1.2 | 17 | 2.1 | | 17 | 2.0 | 0.8 | 17 | 36 |
| 35 | 1 | 2.0 | 1.2 | 17 | 2.2 | | 17 | 2.0 | 0.8 | 17 | 38 |
| 36 | 2 | 2.0 | 1.2 | 18 | 1.8 | | 18 | 2.0 | 0.8 | 18 | 13 |
| 37 | 2 | 2.0 | 1.2 | 18 | 1.9 | | 18 | 2.0 | 0.8 | 18 | 33 |
| 38 | 2 | 2.0 | 1.2 | 18 | 2.0 | | 18 | 2.0 | 0.8 | 18 | 14 |
| 39 | 2 | 2.0 | 1.2 | 18 | 2.1 | | 18 | 2.0 | 0.8 | 18 | 18 |
| 40 | 2 | 2.0 | 1.2 | 18 | 2.2 | | 18 | 2.0 | 0.8 | 18 | 41 |
| 41 | 3 | 2.0 | 1.2 | 19 | 1.8 | | 19 | 2.0 | 0.8 | 19 | 17 |
| 42 | 3 | 2.0 | 1.2 | 19 | 1.9 | | 19 | 2.0 | 0.8 | 19 | 48 |
| 43 | 3 | 2.0 | 1.2 | 19 | 2.0 | | 19 | 2.0 | 0.8 | 19 | 31 |
| 44 | 3 | 2.0 | 1.2 | 19 | 2.1 | | 19 | 2.0 | 0.8 | 19 | 06 |
| 45 | 3 | 2.0 | 1.2 | 19 | 2.2 | | 19 | 2.0 | 0.8 | 19 | 45 |
| 46 | trial | 2.0 | 1.2 | 11 | 2.2 | | 11 | 2.0 | 0.4 | 11 | 01 |
| 47 | trial | 2.0 | 1.2 | 12 | 1.8 | | 12 | 2.0 | 0.4 | 12 | 02 |
| 48 | trial | 2.0 | 0.8 | 16 | 2.2 | | 16 | 2.0 | 0.4 | 16 | 03 |
| 49 | trial | 2.0 | 1.2 | 17 | 1.8 | | 17 | 2.0 | 0.8 | 17 | 04 |
| 50 | trial | 2.0 | 1.2 | 11 | 1.8 | | 11 | 2.0 | 0.4 | 11 | 05 |

**Appendix 9-2:** Observations from the ten subjects for the mid-point experiment from Section 9-2.

| No | $\sigma_{adj1}$ | $\sigma_{adj2}$ | $\sigma_{adj3}$ | $\sigma_{adj4}$ | $\sigma_{adj5}$ | $\sigma_{adj6}$ | $\sigma_{adj7}$ | $\sigma_{adj8}$ | $\sigma_{adj9}$ | $\sigma_{adj10}$ |
|---|---|---|---|---|---|---|---|---|---|---|
| 01 | 0.334 | 0.556 | 0.528 | 0.682 | 0.624 | 0.422 | 0.493 | 0.575 | 0.380 | 0.569 |
| 02 | 0.488 | 0.683 | 0.666 | 0.729 | 0.755 | 0.527 | 0.775 | 0.652 | 0.740 | 0.662 |
| 03 | 0.810 | 0.892 | 0.979 | 0.916 | 0.860 | 1.000 | 0.770 | 0.796 | 0.700 | 0.825 |
| 04 | 0.966 | 0.863 | 0.979 | 0.917 | 0.844 | 0.916 | 1.013 | 0.964 | 0.866 | 0.934 |
| 05 | 1.583 | 1.120 | 1.073 | 0.939 | 1.230 | 1.307 | 1.579 | 1.160 | 1.049 | 1.148 |
| 06 | 0.390 | 0.528 | 0.536 | 0.350 | 0.728 | 0.868 | 0.488 | 0.446 | 0.537 | 0.471 |
| 07 | 0.571 | 0.644 | 0.681 | 0.574 | 0.663 | 0.533 | 0.619 | 0.548 | 0.526 | 0.577 |
| 08 | 0.712 | 0.785 | 0.757 | 0.835 | 0.674 | 0.914 | 0.818 | 0.868 | 0.772 | 0.843 |
| 09 | 0.862 | 0.854 | 0.968 | 0.958 | 0.712 | 1.358 | 1.069 | 1.122 | 0.824 | 1.042 |
| 10 | 1.083 | 1.132 | 1.353 | 1.208 | 0.941 | 1.248 | 1.298 | 1.180 | 1.056 | 1.166 |
| 11 | 0.416 | 0.441 | 0.572 | 0.528 | 0.686 | 0.538 | 0.509 | 0.484 | 0.430 | 0.471 |
| 12 | 0.552 | 0.494 | 0.642 | 0.601 | 0.666 | 0.857 | 0.571 | 0.541 | 0.693 | 0.527 |
| 13 | 0.844 | 0.670 | 0.802 | 0.796 | 0.643 | 0.839 | 0.743 | 0.766 | 0.711 | 0.737 |
| 14 | 1.010 | 1.026 | 0.979 | 1.006 | 0.889 | 1.360 | 1.098 | 0.944 | 1.023 | 0.968 |
| 15 | 1.521 | 1.119 | 1.138 | 1.515 | 0.952 | 1.105 | 1.169 | 1.304 | 1.436 | 1.248 |
| 16 | 0.311 | 0.433 | 0.396 | 0.398 | 0.479 | 0.291 | 0.456 | 0.383 | 0.471 | 0.398 |
| 17 | 0.431 | 0.447 | 0.550 | 0.491 | 0.567 | 0.400 | 0.585 | 0.478 | 0.436 | 0.469 |
| 18 | 0.561 | 0.631 | 0.611 | 0.745 | 0.778 | 0.690 | 0.618 | 0.628 | 0.585 | 0.629 |
| 19 | 0.748 | 0.908 | 0.731 | 0.842 | 0.875 | 0.839 | 0.792 | 0.753 | 0.780 | 0.800 |
| 20 | 1.056 | 0.795 | 0.798 | 0.842 | 0.783 | 1.110 | 0.857 | 1.023 | 1.024 | 0.954 |
| 21 | 0.351 | 0.390 | 0.371 | 0.501 | 0.664 | 0.586 | 0.343 | 0.347 | 0.423 | 0.360 |
| 22 | 0.463 | 0.533 | 0.493 | 0.391 | 0.598 | 0.511 | 0.484 | 0.534 | 0.420 | 0.534 |
| 23 | 0.634 | 0.536 | 0.598 | 0.569 | 0.570 | 0.510 | 0.478 | 0.521 | 0.551 | 0.525 |
| 24 | 0.850 | 0.805 | 0.718 | 0.724 | 0.960 | 1.073 | 0.772 | 0.717 | 0.891 | 0.743 |
| 25 | 1.235 | 0.908 | 0.677 | 1.157 | 0.786 | 1.023 | 1.103 | 0.987 | 0.911 | 0.963 |
| 26 | 0.382 | 0.429 | 0.448 | 0.451 | 0.612 | 0.353 | 0.339 | 0.361 | 0.316 | 0.381 |
| 27 | 0.494 | 0.499 | 0.534 | 0.598 | 0.534 | 0.441 | 0.422 | 0.433 | 0.473 | 0.453 |
| 28 | 0.599 | 0.603 | 0.623 | 0.593 | 0.627 | 0.583 | 0.688 | 0.620 | 0.603 | 0.615 |
| 29 | 0.746 | 0.766 | 0.778 | 0.576 | 0.839 | 1.474 | 0.786 | 0.832 | 0.900 | 0.812 |
| 30 | 1.029 | 1.028 | 0.987 | 1.073 | 1.019 | 1.358 | 0.721 | 1.031 | 1.162 | 1.030 |
| 31 | 0.544 | 0.646 | 0.585 | 0.635 | 0.791 | 0.457 | 0.584 | 0.550 | 0.597 | 0.578 |
| 32 | 0.650 | 0.772 | 0.692 | 0.712 | 0.829 | 1.221 | 0.736 | 0.708 | 0.752 | 0.727 |
| 33 | 0.875 | 0.936 | 1.008 | 1.053 | 1.101 | 0.900 | 1.105 | 0.912 | 0.814 | 0.919 |
| 34 | 1.283 | 1.199 | 1.005 | 1.237 | 1.239 | 0.886 | 1.108 | 1.289 | 1.205 | 1.262 |
| 35 | 1.699 | 1.638 | 1.383 | 1.378 | 1.160 | 0.886 | 1.298 | 1.548 | 1.152 | 1.575 |
| 36 | 0.357 | 0.580 | 0.603 | 0.707 | 0.736 | 0.330 | 0.794 | 0.648 | 0.623 | 0.628 |
| 37 | 0.715 | 0.707 | 0.714 | 0.733 | 1.021 | 0.656 | 0.796 | 0.662 | 0.767 | 0.675 |
| 38 | 0.882 | 0.914 | 0.939 | 0.939 | 0.985 | 0.658 | 1.024 | 0.955 | 0.885 | 0.943 |
| 39 | 1.265 | 1.119 | 0.956 | 1.120 | 1.112 | 1.105 | 0.987 | 1.189 | 1.079 | 1.168 |
| 40 | 1.721 | 1.730 | 1.498 | 1.725 | 1.112 | 1.655 | 1.719 | 1.575 | 1.036 | 1.621 |
| 41 | 0.387 | 0.577 | 0.572 | 0.557 | 0.647 | 0.475 | 0.586 | 0.544 | 0.584 | 0.554 |
| 42 | 0.786 | 0.718 | 0.701 | 0.682 | 0.925 | 0.601 | 0.736 | 0.738 | 0.632 | 0.732 |
| 43 | 0.902 | 0.956 | 1.006 | 0.845 | 0.738 | 0.968 | 0.960 | 0.937 | 1.041 | 0.943 |
| 44 | 1.287 | 0.969 | 1.019 | 1.173 | 1.167 | 0.886 | 1.287 | 1.205 | 1.125 | 1.134 |
| 45 | 1.786 | 1.411 | 1.560 | 1.378 | 1.183 | 1.324 | 1.710 | 1.426 | 1.446 | 1.422 |

**Appendix 9-3:** The fifteen median values of $\sigma_{adj}$ compiled from the results of the mid-point experiment described in *Section 9.2*.

| ***Median*** | ***β = 1.8*** | ***β = 1.9*** | ***β = 2.0*** | ***β = 2.1*** | ***β = 2.2*** |
|---|---|---|---|---|---|
| $\sigma_{ref1} = 0.4$ ***vs.*** $\sigma_{ref2} = 0.8$ | 0.3931 | 0.4878 | 0.6033 | 0.7958 | 1.0211 |
| $\sigma_{ref1} = 0.4$ ***vs.*** $\sigma_{ref2} = 1.2$ | 0.5184 | 0.6303 | 0.7994 | 0.9668 | 1.1673 |
| $\sigma_{ref1} = 0.8$ ***vs.*** $\sigma_{ref2} = 1.2$ | 0.5839 | 0.7226 | 0.9390 | 1.1507 | 1.4724 |

**Appendix 9-4:** $\xi_{pr}$ values for the fifteen medians as described in *Section 9.2*.

| $\xi_{pr}$ | ***β = 1.8*** | ***β = 1.9*** | ***β = 2.0*** | ***β = 2.1*** | ***β = 2.2*** |
|---|---|---|---|---|---|
| $\sigma_{ref1} = 0.4$ ***vs.*** $\sigma_{ref2} = 0.8$ | 26518.27 | 21056.77 | 18610.17 | 20778.93 | 17707.93 |
| $\sigma_{ref1} = 0.4$ ***vs.*** $\sigma_{ref2} = 1.2$ | 41704.04 | 34285.55 | 32861.17 | 29006.81 | 27025.36 |
| $\sigma_{ref1} = 0.8$ ***vs.*** $\sigma_{ref2} = 1.2$ | 52362.40 | 49329.08 | 44572.41 | 39110.81 | 39142.15 |

**Appendix 9-5:** Set of eighteen equations to scale the estimator:

1. $100 = a \cdot 74725^2 + b \cdot 74725$
2. $M = a \cdot 34216^2 + b \cdot 34216$
3. $L = a \cdot 10603^2 + b \cdot 10603$

4. $\frac{M+100}{2} = a \cdot 52362^2 + b \cdot 52362$
5. $\frac{M+100}{2} = a \cdot 49329^2 + b \cdot 49329$
6. $\frac{M+100}{2} = a \cdot 44572^2 + b \cdot 44572$
7. $\frac{M+100}{2} = a \cdot 39111^2 + b \cdot 39111$
8. $\frac{M+100}{2} = a \cdot 39142^2 + b \cdot 39142$

9. $\frac{L+100}{2} = a \cdot 41704^2 + b \cdot 41704$

10. $\frac{L+100}{2} = a \cdot 34285^2 + b \cdot 34285$

11. $\frac{L+100}{2} = a \cdot 32861^2 + b \cdot 32861$

12. $\frac{L+100}{2} = a \cdot 29007^2 + b \cdot 29007$

13. $\frac{L+100}{2} = a \cdot 27025^2 + b \cdot 27025$

14. $\frac{L+M}{2} = a \cdot 26518^2 + b \cdot 26518$

15. $\frac{L+M}{2} = a \cdot 21057^2 + b \cdot 21057$

16. $\frac{L+M}{2} = a \cdot 18610^2 + b \cdot 18610$

17. $\frac{L+M}{2} = a \cdot 20779^2 + b \cdot 20779$

18. $\frac{L+M}{2} = a \cdot 17708^2 + b \cdot 17708$

# THE BIBLIOGRAPHY


Abbadeni, N., Ziou, D., & Wang, S. (2000). Autocovariance-based perceptual textureal features corresponding to human visual perception. *Proceedings 15th IAPR International Conference on Pattern Recognition* , 913-916.

Abbadeni, N., Ziou, D., & Wang, S. (2000). Computational measures corresponding to perceptual textureal features. *IEEE International Conderence on Image Processing* .

Adelson, A. (2001). On seeing stuff: the perception of materials by humans and machines. *SPIE Human Vision Imaging VI , 4299*, 1-12.

Amadasun, M., & King, R. (1989). Textural features corresponding to textural properties. *IEEE Transactions on System, Man and Cybernetics , 19* (5), 1264-1274.

Anderson, R., & Brodley, D. (1998). Perception of three-dimensional structure from motion. *Trends of Congnitive Sciences , 2* (6), 222-228.

Annen, T., Mertens, T., Bekaert, P., Seidel, H., & Kautz, J. (2007). Convolution Shadow Maps. *Rendering Techniques 2007: Eurographics Symposium on Rendering* , 51-60.

Balas, B. (2006). Using Computational Models to Study Texture Representations in the Human Visual System. *Vision Research , 46*, 299-309.

Ballesteros, S., Reales, J., Ponce de Leon, L., & Garcia, B. (2005). The perception of ecological textures by touch: does the perceptual space change under bimodal visual and haptic exploration? *Eurohaptics Conference, 2005 and Symposium on Haptic Interfaces for Virtual Environment and Teleoperator Systems* , 635-638.

Battiato, S., Gallo, G., & Nicotra, S. (2003). Perceptive visual texture classification and retrieval. *Image Analysis and Processing* , 524-529.

Beland, M. C., & Bennett, J. M. (2000). Effect of local microroughness on the gloss uniformity of printed paper surfaces. *Applied Optics , 39*, 2719-2726.

Belhumeur, P. N., Kriegman, D. J., & Yuille, A. L. (1999). The Bas-Relief Ambiguity. *International Journal of Computer Vision , 35* (1), 33-44.

Bensmaia, S. J., & Hollins, M. (2003). The vibrations of texture. *Journal of Somatosens Mot Research , 20*, 33-43.

Benthin, C., Wald, I., & Slusallek, P. (2003). A Scalable Approach to Interactive Global Illumination. *Computer Graphics Forum , 22* (3), 621–630.

Blinn, J. F. (1977). Models of light reflection for computer synthesized pictures. *Computer Graphics Proc. SIGGRAPH'77* , 192-198.

Blinn, J. F. (1978). Simulation of Wrinkled Surfaces. *In Proc. SIGGRAPH 78* , 286-292.

Blume, H., Steven, P., Ho, A., Stevens, F., Abileah, A., Robinson, S., et al. (2003). Characterization of liquid-crystal displays for medical images. *Medical Imaging 2003: Visualization, Image-Guided Procedures, and Display, Proceedings of the SPIE , 5029*, 449-473.

Blunt, L., & Jiang, X. (2003). *Advance techinques for assessment surface topography* . Butterworth Heinemann.

Bovik, A. C., Clark, M., & Geisler, W. S. (1990). Multichannel texture analysis using localized spatial filters. *IEEE Transactions on Pattern Analysis and Machine Intelligence , 12*, 55-73.

Brabec, S., Annen, T., & Seidel, H. P. (2003). Practical Shadow mapping. *Journal of Graphics Tools , 7* (4).

Brodatz, P. (1966). *Textures: A photographic album for artist and designers .* Dover and Greer publishing company.

Brusham, N., Rao, R., & Lohse, G. (1997). The texture lexicon: understanding the categorization of visual texture terms and their relationship to texture images. *Cognitive Science , 21* (2), 219-246.

BS_1134-1:1988. (1988). Assessment of surface texture. *British Standard* .

BS_EN_623-4:2004. (2004). Advanced techinical ceramic - General and textureal properties. *British Standard* .

Cai, Y., & Siegel, M. (2002). Texture characterization of the visual appearance of paintings. *IEEE instrumentation and Measurement* , 21-23.

Campbell, F. W., & G, R. J. (1968). Application of fourier analysis to the visibility of gratings. *Journal of Physiology , 197* (3), 551-566.

Casio, C. J., & Sathian, K. (2001). Temporal cues contribute to tactile perception of roughness. *Journal of Neuroscience , 21*, 5289-5296.

Chantler, M. (1995). Why illuminant direction is fundamental to texture analysis. *IEE Proc. Vision, Image and Signal Processing , 142* (4), 199-206.

Cook, R. (1984). Shade Trees. *ACM in Computer Graphics , 18* (3), 223-231.

Copeland, A., & Trivedi, M. M. (1996). Texture perception in humans and computers: models and psychophysical experiments. *Proc. SPIE , 2742*, 436-446.

Crow, F. (1977). Shadow algorithms for computer graphics. *SIGGRAPH: Proceedings of the 4th Annual Conference on Computer Graphics and Interactive Techniques* , 242-248.

Dalkin, S. C., Willians, C. B., & Hess, R. F. (1999). The interaction of first- and secont-order cues to orientation. *Vision Research , 34*, 2867-2884.

Dana, K., & Nayar, S. (1999). Correlation model for 3d texture. *ICCV99: IEEE International Conference on Computer Vision* , 1061-1067.

Dana, K., & Nayar, S. (1998). Histogram model for 3d textures. *IEEE Conference on Computer Vision and Pattern Recognition* , 618-624.

Dana, K., Nayar, S., Van Ginneken, B., & Koenderink, J. (1997). Reflectance and texture of real-world surfaces. *IEEE Conference on Computer Vision and Pattern Recognition* , 151-157.

Dijkstra, T. M., Cornilleau-Pérès, V., C, G. C., & Droulez, J. (1995). Perception of three-dimensional shape from ego- and object-motion: comparison between small- and large-field stimuli. *Vision Research , 35* (4), 453-4662.

Donnelly, W., & Lauritzen, A. (2006). Variance shadow maps. *Interactive 3D Graphics and Games* , 161-165.

Donnely, W. (2005). *GPU Gems 2.* Addison-Wesley Professional.

Douiri, N., Khoudeir, M., & Olivier, C. (2001). Roughness characterization of an indoor environment. *Image and Analysis Stereology* , 225-229.

Ehrenstein, W., Ehrenstein, E., Windhorst, V., & Johansson, H. (1999). *Modern Techniques in Neuroscience Research.* Berlin: Springer.

Engelena, L., Wijka, R., Van der Biltb, A., J, P., Janssena, A., & Bosma, F. (2005). Relating particles and texture perception. *Physiology and Behavior* , 111-117.

Everitt, C., Rege, A., & Cebenoyan, C. (2002). Hardware shadow mapping. *Technical Report NVIDIA* .

Fernando, R., Fernandez, S., Bala, K., & Greenberg, D. P. (2001). Adaptive shadow maps. *SIGGRAPH: Proceedings of the 28th Annual Conference on Computer graphics and Interactive Techniques* , 387-390.

Fujii, K., Suji, S., & Ando, Y. (2003). Textural properties corresponding to visual perception based on the correlation mechanism in the visual system. *Psychological Research , 67* (3), 197-208.

Gamzu, E., & Ahissar, E. (2001). Importance of temporal cues for tactile spatial-frequency discrimination. *Journal of Neuroscience , 21*, 7416-7427.

Gerasimov, P., Randima, F., & Green, S. (2005). Shader Model 3.0, Using Vertex Textures. *NVIDIA whitepaper - developer.nvidia.com* .

Geusebroek, J., & Smeulders, A. W. (2005). A six-stimulus theory for stochastic texture. *International Journal of Computer Vision , 62* (1/2), 7-16.

Gibson, E. J., Gibson, J. J., Smith, O. W., & Flock, A. (1959). Motion parallax as a determinant of perceived depth. *Journal of Experimental Psychology , 54*, 40-51.

Gibson, G. O., & Craig, J. C. (2002). Relative roles of spatial and intensive cues in the discrimination of spatial tactile stimuli. *Perception & Psychophysics , 64* (7), 1095-1107.

Gilchrist, A., & Jacobsen, A. (1984). Perception of lightness and illunimation in a world of one reflectance. *Perception , 13*, 5-19.

Graham, N., Sutter, A., & Venkatesan, C. (1993). Spatial-frequency- and orientation-selectivity of simple and complex channels in region segmentation. *Vision Research , 33*, 1893-1911.

Gurnsey, R., & Fleet, D. (2001). Texture space. *Vision Research , 41* (6), 745-757.

Harvey, L., & Gervais, M. (1981). Internal representation of visual texture as the basis for the judgement of similarity. *Journal of Experimental Psychology: Human Perception and Performance , 7* (4), 741-753.

Hasenfratx, J. M., Lapierre, N., Holzschuch, N., & Sillion, F. (2003). A survey of real-time soft shadows algorithms. *Computer Graphics Forum , 22* (4), 753-774.

Heaps, C., & Handel, S. (1999). Similarity and features of natural textures. *Journal of Experimental Psychology: Human Perception and Performance , 25* (2), 229-320.

Hinckley, K., Tullio, J., Pausch, R., Proffitt, D., & Kassell, N. (1997). Usability Analysis of 3D Rotation Techniques. *Symposium on User Interface Software and Technology* , 1-10.

Hirche, J., Ehlert, A., Guthe, S., & Doggett, M. (2004). Hardware accelerated per-pixel displacement mapping. *Proceedings of Graphics Interface 2004 - ACM International Conference Proceeding Series , 64*, 153-158.

Ho, Y.-X., Landy, M. S., & Maloney, L. T. (2008). Conjoint measurement of gloss and surface texture. *In Press: Psychological Science* .

Ho, Y.-X., Maloney, L. T., & Landy, M. S. (2006). How direction of illumination affects visually perceived surface roughness. *Journal of vision , 6(5):8*, 634-648.

Ho, Y.-X., Maloney, L. T., & Landy, M. S. (2007). The effect of viewpoint on perceived visual roughness. *Journal of vision , 7(1):1*, 1-16.

Hollins, M., & Risner, S. R. (2000). Evidence for the duplex thory of tactile texture perception. *Perception Psychophysics , 62*, 695-705.

Hollins, M., Faldowski, R., Rao, S., & Young, F. (1993). Perceptual dimensions of tactile surface texture - a mulitdimensional-scaling analysis. *Perception Psychophysics , 54*, 697-705.

Hyslip, J. P., & Vallejo, L. (1997). Fractal analysis of the roughness and size distribution of granular materials. *Engineering Geology , 48*, 231-244.

Ichikawa, M., Nishida, S., & Ono, H. (2004). Depth perception from second-roder-motion stimulus yoked to head movement. *Vision Research , 44* (25), 2945-2954.

ISO_11562:1998. (1998). Geometric Product Specifications (GPS) - Surface texture: Profile method - Metrological characteristics of phase correct filters. *International Standard Organization* .

ISO_12085:1998. (1998). Geometric Product Specification (GPS) - Surface texture: Profile Method- Motif parameters. *International Standard Organization* .

ISO_2632/2-1985. (1985). Roughnesss Comparison Specimens. *International Stanadard Organization* .

ISO_4287:1997. (1997). Geometrical Product Specification (GPS) - Surface texture: Profile method - Terms, definitions and surface texture parameters. *International Standards Organization* .

ISO_4287:1998. (1998). Geometrical Product Specifications(GPS) - Surface texture: Profile method - Terms, definitions and surface texture parameters. *International Standards Organizations* .

ISO_4288:1998. (1998). Geometric Product Specification (GPS) - Surface Texture - Profile Method: Rules and Procedures for the assesment of surface texture. *International Standard Organization* .

ISO_RC_213_Workgroup_16. (2005). Geometric product specification (GPS) - Surface Texture: Areal. *Standard Proposal - International Standard Organization* .

Jahn, R., & Truckenbroth, H. (2003). A simple fractal analysis method of the surface roughness. *Journal of Materials Processing Technology , 145*, 40-45.

Julesz, B. (1987). Textons, the elements of texture perception, and their interactions. *Nature , 290*, 91-97.

Kaneko, T., Takahei, T., Inami, M., N, K., Yonaguida, Y., T, M., et al. (2001). Detailed shape representation with parallax mapping. *Interational Conference of Artificial Real Telexistence , 11*, 205-208.

Kilgard, M. J. (2000). A practical and robust bump-mapping techique for today's GPUs. *Game Developers Conference 2000* .

Koenderink, J. J. (1986). Optic Flow. *Vision Research , 26* (1), 161-179.

Koenderink, J. J., & Van Doorn, A. J. (2004). Light direction from shad(ow)ed random Gaussian surfaces. *Perception , 33* (12), 1405–1420.

Koenderink, J. J., Van Doorn, A., Kappers, A. M., te Pas, S. F., & Pont, S. C. (2003). Illumination direction from texture shading. *Journal of the Optical Society of America , 20* (6), 987-995.

Kozlov, S. (2004). *Perspective shadow maps.* Addison-Wesley.

Landy, M. S., & Bergen, J. R. (1991). Texture segregation and orientation gradient. *Vision Research , 31*, 679-691.

Landy, M. S., & N, G. (2004). Visual perception of texture. *The Visual Neurosciences* , 1106-1118.

Landy, M. S., & Oruç, I. (2002). Properties of 2nd-order spatial frequency channels. *Vision Research* , 2311-2329.

Landy, M. S., & Oruc, I. (2002). Properties of second-order spatial frequency channels. *Vision Research , 42*, 2311-2329.

Lederman, S. J., & Abbott, S. G. (1981). Texture perception: studies of intersensory organization using a discrepency paradigm, and visual versus tactual psychophysics. *Journal of Experimental Psychology and Human Perception Performance , 7* (4), 902-915.

Lederman, S. J., Thorne, G., & Jones, B. (1986). Perception of texture by vision and touch: multidimensionality and intersensory integration. *Journal of Experimental Psychology Human Perception and Performance , 12* (2), 169-180.

Lee, A., Moreton, H., & Hoppe, H. (2000). Displaced subdivision surfaces. *SIGGRAPH 2000* , 85-94.

Lee, W., & Sato, M. (2001). Visual perception of texture of textiles. *Color Research & Application , 26* (6), 69-477.

Leung, T., & Malik, J. (2001). Representing and recognizing the visual appearance of materials using three-dimensional textons. *International Journal of Computer Vision , 43* (1), 29-44.

Lipp, M. (2005). A survey of real-time shadow mapping techiques. *Vienna University of Technology* .

Liu, B., & Todd, J. T. (2004). Perceptual biases in the interpretation of 3D shape from shading. *Vision Research , 44*, 2135-2145.

Long, H., & Leow, W. K. (2002). A hybrid model for invariant and perceptual texture mapping. *Proceedings ICPR* .

Long, H., & Leow, W. K. (2001). Perceptual texture space improves perceptual consistency of computational features. *Proceedings IJCAI* , 1391-1396.

M, W., Scherzer, D., & Purgathofer, W. (2004). Light space perspective shadow maps. *Eurographics Symposium on Rendering 2004* , 143-152.

Madison, C., Thomson, W., Kersten, D., & Shirley, P. (2001). Use of interreflections and shadows for surface contact. *Perception and Psychophysics , 63*, 187-194.

Malik, J., & Perona, P. (1990). Preattentive texture discrimination with early vision mechanims. *Journal of the Optical Society of America A , 7*, 923-932.

Mannos, J. L., & Sakrison, D. J. (1974). The effects of a visual fidelity criterion on the encoding of images. *IEEE Trasactions on Information Theory , 20* (4).

Martin, T., & Tan, T. (2004). Anti-aliasing and continuity with trapeziodal shadow maps. *Eurographics Symposium on Rendering 2004* , 153-160.

Meftah, E., L, B., & E, C. C. (2000). Relative effects of the spatial and temporal characteristics of scanned surfaces on human perception of tactile roughness using passive touch. *Experimental Brain Research , 132*, 351-361.

Moule, K., & McCool, M. D. (2002). Efficient Bounded Adaptive Tessellation of Displacement Maps. *Graphics Interface* , 171-180.

Newman, S. D., Klatzky, R. L., Lederman, S. J., & Just, M. A. (2005). Imaging material versus geometry properties of objects: an fMRI study. *Cognitive Brain Research , 23*, 235-246.

NVIDIA, & authors, V. (2005). NVIDIA GPU Programming Guide. *developer.nvidia.com* .

Oliveira, M. M., & Policarpo, F. (2005). An Efficient Representation for Surface Details. *UFRGS Technical Report RP-351* .

Olshausen, B. (2005). How close are we to understanding V1? *Neural Computation , 17*, 1665-1699.

Ontrup, J., Ritter, H., & Wersing, H. (2004). A computational feature binding model of human texture perception. *Cognitive Processing , 5*, 31-44.

Opik, E. (1924). Photometric measures of the moon and the earth-shine. *L'Observatorie Astronomical de L'Université de Tartu* .

Oppenheim, A. V., Schafer, R. W., & Buck, J. R. (1999). *Discrete-Time Signal Processing.* Prentice Hall.

Oren, M., & Nayar, S. (1994). Generalization of Lambert's reflectance model. *Proceedings of the 21st annual conference on Computer graphics and interactive techniques* , 239-246.

Payne, J., & Stonham, T. J. (2001). Can texture and image content retrieval methods match human perception? *Intelligent Multimedia, Video and Speech Processing* , 154-157.

Payne, J., Hepplewhite, L., & Stonham, T. J. (1999). Evaluating content-based image retrieval techniques using perceptual based metrics. *Electronic Imaging '99 , TR-696*.

Payne, J., Hepplewhite, L., & Stonham, T. J. (2000). Texture, human perception and information retrieval measures. *SIGIR2000 , TR-706*.

Petrou, M., & Talebpour, A. K. (2007). Reverse engineering the way humans rank textures. *Pattern Analysis and Applications , 10* (2), 101-114.

Phillips, J. R., Johansson, R. S., & Johnson, K. O. (1992). Responses of human mechanoreceptive afferentt to embossed dot arrays scanned across fingerpad skin. *Journal of Neuroscience , 12*, 827-839.

Phong, B. T. (1975). Illumination for computer generated pictures. *Communications of the ACM , 8*, 311–317.

Picard, D., Dacremont, C., Valentin, D., & Giboreau, A. (2003). Perceptual dimensions of tactile textures. *Acta Psychologica , 114*, 165-184.

Picard, D., Narcon, S., Egoroff, C., & Kirsche, L. (2006). Partial perceptual equivalence between vision and touch for texture information. *Acta Psychologica , 121* (3), 227-248.

Policarpo, F., Oliveira, M., & Comba, J. L. (2005). Real-Time Relief Mapping on Arbitrary Polygonal Surfaces. *ACM Transactions on Graphics , 24* (3), 935-943.

Portilla, J., & Simoncelli, E. P. (2000). A Parametric Texture Model based on Joint Statistics of Complex Wavelet Coefficients. *International Journal of Computer Vision , 40* (1), 49-71.

Pourdeyhimi, P., & Sobus, J. (1993). Evaluating carpet appearance loss: surface intensity and roughness. *Textile Research Journal , 63* (9), 523-535.

Randen, T., & Husoy, J. H. (1999). Filtering for texture classification: a comparative study. *IEEE Transactions on Pattern Analysis and Machine Intelligence , 21* (4), 291-310.

Rao, A. R., & Lohse, G. L. (1993). Identifying high level features of texture perception. *GVGIP: Graphical Models and Image Processing , 55* (3), 218-233.

Rao, A. R., & Lohse, G. L. (1993). Towards a texture naming system: Identifying relevant dimensions of texture. *IEEE Conference on Visualization, Proceedings of Visualization '93* , 220-227.

Rao, A. R., & Lohse, G. L. (1996). Towards a texture naming system: Identifying relevant dimensions of texture. *Vision Research , 36*, 1649-1669.

Rees, W. G. (1990). *Physical Principles of Remote Sensing.* Cambridge, England: Cambridge University Pres.

Roehrig, H., Chawla, A. S., Krupinski, E. A., Fan, J., & Gandhi, K. (2004). Why should you calibraste your display? *The International Society for Optical Engineering , 5199*, 181-192.

Russ, J. C. (1994). *Fractal Surfaces.* New York: Plenum.

Scheers, J., Vermeulen, M., De Mare, C., & Meseure, K. (1998). Assesment of steel surface roughness and waviness in relation with paint appearance. *International Journal of Machine Tools and Manufacture , 38* (5), 647-656.

Schmahling, J., Hamprecht, F. A., & Hoffmann, D. M. (2006). A three-dimensional measure of surface roughness based on mathematical morphology. *International Journal of Machine Tools and Manufacture , 46* (14), 1764-1769.

Shirado, H., & Maeno, T. (2005). Modeling of human texture perception for tactile displays and sensors. *Eurohaptics Conference, 2005 and Symposium on Haptic Interfaces for Virtual Environment and Teleoperator Systems* , 629 - 630.

Shoemake, K. (1985). Animating rotation with quaternion curves. *ACM SIGGRAPH 1985 Computer Graphics , 19* (3), 245-254.

Shreiner, D., Woo, M., Neider, J., & Davis, T. (2003). *OpenGL Programming Guide: The Official Guide to Learning OpenGL Version 1.4.* Addison Wesley.

Sloan, P. P., & Cohen, M. (2000). Interactive horizon mapping. *Europgraphics* , 281-286.

Smith, A. M., Chapman, C. E., Deslandes, M., Langlais, J. S., & Thibodeau, M. P. (2002). Role of friction and tangential force variation in the subjective scaling of tactile roughness. *Experimental Brain Research , 144*, 211-223.

Stamminger, M., & Drettakis, G. (n.d.). Perspective shadow maps. *SIGGRAPH: 2002* , 557-562.

Tamura, H., Mori, S., & Yamawaka, T. (1978). Textural features corresponding to Visual Perception. *IEEE Transactions Systems Man and Cybernetics* (8), 460-473.

Thomson, D. (2005). VA testing in optometric practice Part 1 - The Snellen chart. *Optometry Today , 45* (7).

Torrance, K. E., & Sparrow, E. M. (1967). Theory for Off-Specular Reflection From Roughness Surfaces. *Journal of the Optical Society of America , 57* (9), 1105-114.

Van Ginneken, B., Koenderink, J., & Dana, K. (1999). Texture histograms as a function of irradiation and viewing direction. *International Journal of Computer Vision , 31* (2), 169-184.

Vanrell, M., & J, V. (1997). A four-dimensional texture representation space. *Pattern Recognition and Image Analysis , 1*, 245-250.

Wald, I., Friedrich, H., Marmitt, G., Slusallek, P., & Seidel, H. P. (2005). Faster Isosurface Ray Tracing using Implicit KD-Trees. *IEEE Transactions on Visualization and Computer Graphics , 11* (5), 562-572.

Wald, I., Kollig, T., Benthin, C., Keller, A., & Slusallek, P. (2002). Interactive Global Illumination using Fast Ray Tracing. *Proceedings of the 13th Eurographics Workshop on Rendering* , 15–24.

Wang, L., Tong, X., Lin, S., Hu, S., Guo, B., & Shum, H. Y. (2004). Generalized displacement maps. *In Eurographics Symposium on Rendering 2004* , 227–234.

Wang, L., Wang, X., Tong, X., Lin, S., Hu, S., Guo, B., et al. (2003). View-dependent displacement mapping. *Proceedings of ACM SIGGRAPH 2003 , 22* (3), 334-339.

Weisenberger, J., & Poling, G. L. (2004). Multisensory roughness perception of vistual surfaces: effects of correlated cues. *International Symposium on Haptic Interfaces for Virtual Environment and Teleoperator Systems , 27*, 161-168.

Weiskopt, D., & Ertl, T. (2003). Shadow mapping based on dual depth layers. *Eurographics 2003 Short Papers* , 53-60.

Willians, L. (1978). Casting curved shadows on curved surfaces. *SIGGRAPH: Proceedings of the 5th Annual Conference on Computer Graphics and Interactive Techniques* , 270-274.

Wilson, H. R., McFarlane, D. K., & Phillips, G. C. (1983). Spatial frequency tuning of orientation selective units estimated by oblique masking. *Vision Research , 23* (9), 873-882.

Wimmer, M., Shecrzer, D., & Purgathofer, W. (2004). Light space perspective shadow maps. *Rendering Tecniques - Eurographics Symposium on Rendering* , 143-151.

Wu, P., Manjunath, B. S., Newsam, S. D., & Shin, H. D. (1999). A texture descriptor for image retrieval and browsing. *Computer Vision and Pattern Recognition Workshop* .

Yashida, T., Gibb, B., Dorsch, A. K., Hsiao, S. S., & Johnson, K. O. (2001). Neural coding mechanism underlying perceived roughness of finely textured surfaces. *The Journal of Neuroscience , 21* (17), 6905-6916.

Yuille, A., Coughlan, J., & Konishi, S. (2003). The KGBR viewpoint–lighting ambiguity. *Journal of Optical Society of America , 20* (1), 24-31.